

INSTITUTE
FOR
COSMIC RAY RESEARCH
THE UNIVERSITY OF TOKYO

ANNUAL REPORT
(APRIL 2016 – MARCH 2017)



Editorial Board

MIYOKI, Shinji

YOSHIKOSHI, Takanori

TAKENAGA, Yumiko

FUKUDA, Hironobu

©Institute for Cosmic Ray Research, The University of Tokyo

5-1-5, Kashiwanoha, Kashiwa, Chiba 277-8582, Japan

Telephone: (81) 4-7136-3102

Facsimile: (81) 4-7136-3115

WWW URL: <http://www.icrr.u-tokyo.ac.jp/>

TABLE OF CONTENTS

Preface	
Research Divisions	1
Neutrino and Astroparticle Division	2
High Energy Cosmic Ray Division	28
Astrophysics and Gravity Division	52
Observatories and a Research Center	65
Norikura Observatory	66
Akeno Observatory	72
Kamioka Observatory	75
Kagra Observatory	76
Research Center for Cosmic Neutrinos	77
Appendix A. ICRR Workshops and Ceremonies	79
Appendix B. ICRR Seminars	82
Appendix C. List of Publications	82
(a) Papers Published in Journals	
(b) Conference Papers	
(c) ICRR Reports	
Appendix D. Doctoral Theses	89
Appendix E. Public Relations	89
(a) ICRR News	
(b) Public Lectures	
(c) Visitors	
Appendix F. Inter-University Researches	97
Appendix G. List of Committee Members	101
(a) Board of Councillors	
(b) Advisory Committee	
(c) Inter-University Research Advisory Committee	
Appendix H. List of Personnel	102

PREFACE

This report summarizes the scientific activities of the Institute for Cosmic Ray Research (ICRR) of the University of Tokyo in the Japanese FY 2016.

ICRR is an inter-university research institute for studies of cosmic rays. The headquarters of ICRR is located in Kashiwa, Chiba prefecture, Japan. In order to promote various cosmic-ray-related studies efficiently, ICRR has three research divisions; Neutrino and Astroparticle division, High Energy Cosmic Ray division, and Astrophysics and Gravity division. Before April 2016, ICRR had three observatories in Japan; Kamioka Observatory (Kamioka underground, Gifu prefecture), Norikura Observatory (2770 meters above sea level, Mt. Norikura, Gifu prefecture), and Akeno Observatory (Yamanashi prefecture), together with 1 research center; Research Center for Cosmic Neutrinos (Kashiwa, Chiba prefecture). On April 1, 2016, KAGRA Observatory (Kamioka underground, Gifu prefecture) has been established in order to operate the KAGRA gravitational wave detector and to carry out various studies with it. In addition, there are two major experimental facilities outside of Japan. They are located in Utah in USA, and Yangbajing in Tibet, China. The La Palma island in Spain is also recognized as an important site for the ICRR's activities.

Many researchers from various Japanese institutions as well as those from overseas are involved in the research programs of ICRR. It should be noted that most of the scientific outputs from this institute are the results of the collaborative efforts by many scientists from various institutions. In order to produce outstanding results, it is very important to carry out an experiment by an international collaboration composed of top-level researchers all over the world. Hence, most of the experimental collaborations that ICRR is involved are international ones. For example, the number of collaborators in the Super-Kamiokande experiment is about 160; about a half of them are from abroad (USA, Korea, China, Poland, Spain, Canada, Italy, France and United Kingdom).

Many exciting scientific activities of ICRR are described in this report. For example, the Super-Kamiokande and T2K (which uses Super-Kamiokande as the far detector) experiments have been continuously producing impressive results on neutrino oscillation physics. The neutrino oscillation studies by the Super-Kamiokande experiment were recognized by the 2015 Nobel Prize in Physics.

Some of the other recent highlights are mentioned here: The gravitational wave telescope (KAGRA) had the initial operation in March-April 2016. KAGRA plans to begin operating the interferometer with cryogenic mirrors in the spring of 2018. The highest energy cosmic ray experiment TA (Telescope Array) has observed indication that the highest energy cosmic rays arrive from a particular direction of the sky, which may suggest the birth of a new research field, the highest energy cosmic ray astronomy.

As an inter-university research institute, ICRR is reviewed by the top-level researchers in the field. Furthermore, future projects of ICRR are evaluated by a committee composed of top-level researchers from various nearby fields. The report from the ICRR Future Project Evaluation Committee was released in September 2013. The Committee evaluated various possible future projects of ICRR. Several projects have been recommended highly. Among them, joining the CTA project, which is a global TeV gamma ray astronomy project, has been recommended as the top priority ICRR future project. The review report from the External Review Committee, which was released in May 2013 (please see the 2013 Annual Review), also supported joining CTA. ICRR is going to contribute to construct and operate the CTA observatory and carry out various researches with it as an important international partner of this project. Because the CTA project has been approved partially by the Japanese government and there are new developments in the planning of future projects, a new ICRR Future Project Evaluation Committee has been formed in 2016.

We hope that this report is useful for the understanding of the current research activities of ICRR. Finally, we appreciate the strong support of our colleagues in this research field, the University of Tokyo and the Japanese Ministry of Education, Culture, Sports, Science and Technology. They are indispensable for the continuing, and exciting scientific outcome of ICRR.



Takaaki Kajita,

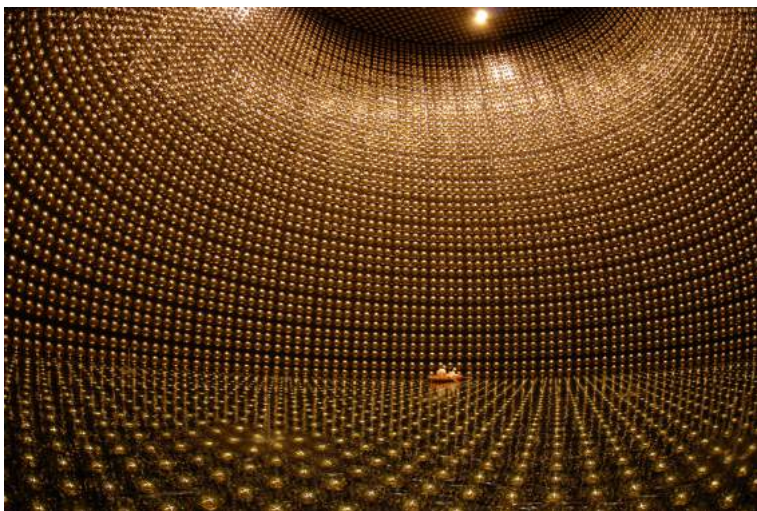
Director,

Institute for Cosmic Ray Research,

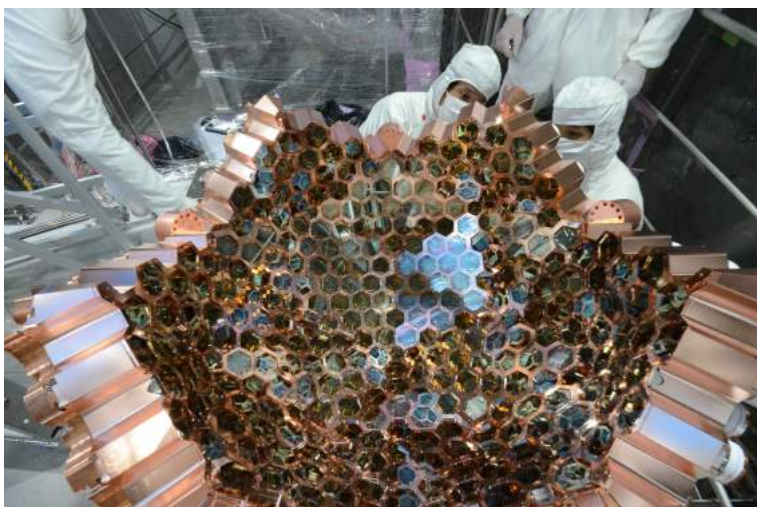
The University of Tokyo



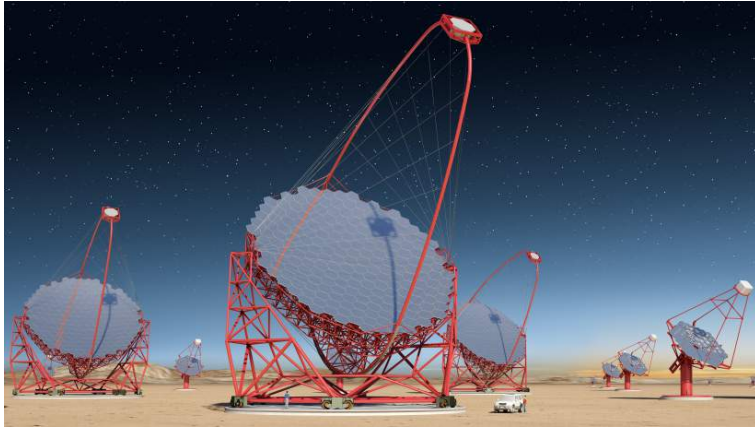
The ICRR building at Kashiwa, Chiba, Japan.



The Super-Kamiokande detector (the photo was taken during pure water fill in 2006).



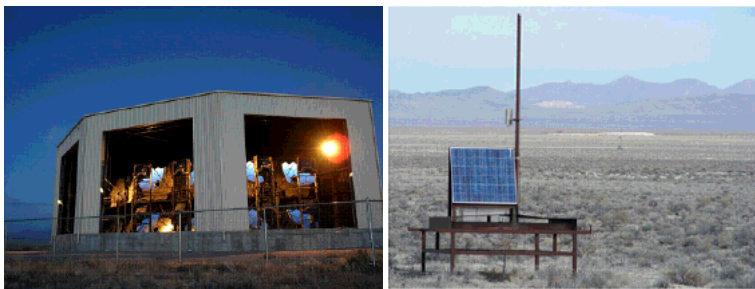
The XMASS detector (the photo was taken during the refurbishment work in 2013).



Artist view of the CTA observatory. CTA consists of three types of telescopes, Large Size Telescopes (23m diameter), Mid Size Telescopes (12m) and Small Size Telescopes (4m), and covers the broad energy band from 20GeV to 100TeV.



Tibet-III air shower array (37000 m²) at Yangbajing, Tibet (4300 m in altitude).



Air fluorescence telescopes (left) and a scintillator surface detector (right) of the Telescope Array experiment in Utah, USA to explore the origin of extremely high energy cosmic rays.

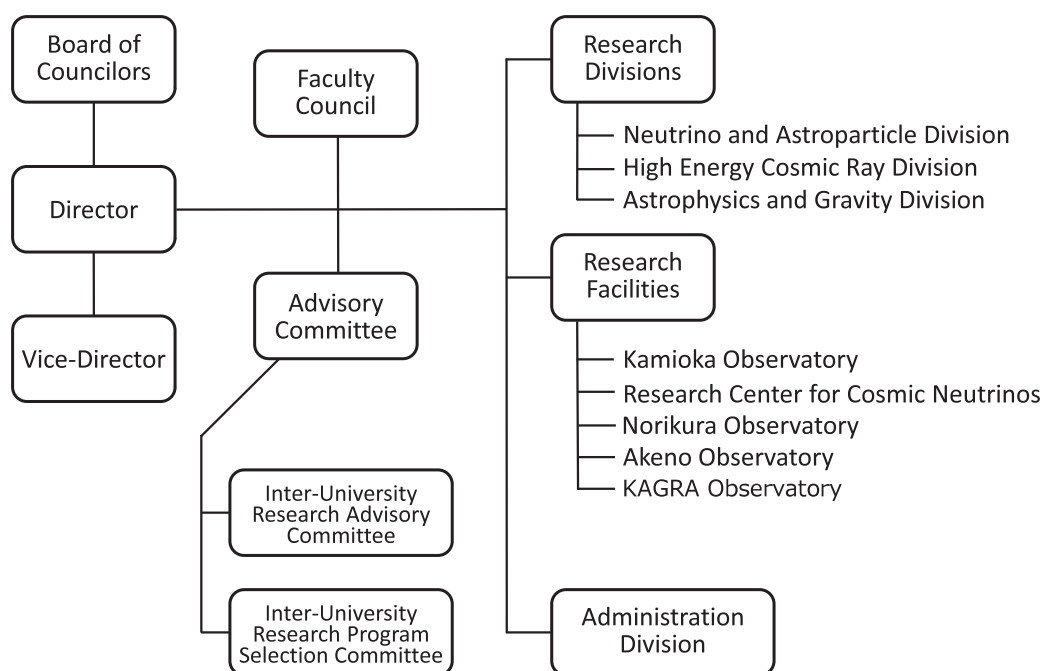


KAGRA X-arm tunnel.



A public lecture co-organized by the Public Relation Office and Research Center for Neutrino (RCCN).

Organization



Number of Staff Members (As of May 1, 2016)

	Scientific Staff	Technical Staff	Research Fellows	Administrators and Secretaries	Total
Neutrino and Astroparticle Div.	24	4	3	17	48
High Energy Cosmic Ray Div.	16	9	4	2	31
Astrophysics and Gravity Div.	14	3	4	10	31
Administration	0	0	0	16	16
Total	54	16	11	45	126

FY 2010-2016 Budget

	2010	2011	2012	2013	2014	2015	2016
Personnel expenses	576 000	653 000	658 000	687 000	706 000	684 000	683 000
Non-personnel expenses	1 048 000	1 400 000	1 172 000	1 095 000	1 282 000	1 595 000	1 288 000
Total	1 624 000	2 053 000	1 830 000	1 782 000	1 988 000	2 279 000	1 971 000

(in 1 000 yen)

RESEARCH DIVISIONS

Neutrino and Astroparticle Division

Overview

Super-Kamiokande

T2K Experiment

XMASS Experiment

Hyper-Kamiokande

High Energy Cosmic Ray Division

Overview

Cherenkov Cosmic Gamma-Ray Group

TA: Telescope Array Experiment

Tibet AS γ Project

High Energy Astrophysics Group

Other Activities

Astrophysics and Gravity Division

Overview

Gravitational Wave Group

KAGRA Project

Observational Cosmology Group

Theory Group

Particle Phenomenology

Particle Cosmology

NEUTRINO AND ASTROPARTICLE DIVISION

Overview

This division aims to study particle physics with prime interests in physics of neutrinos and proton decay, and astroparticle physics with the use of underground experimental facilities.

The Super-Kamiokande (SK) detector is a 50 kton water Cherenkov detector using 11,129 50 cm-diameter photomultipliers (PMTs) for its inner detector and 1,885 20 cm-diameter PMTs for its outer detector. The data taking of SK started in April 1996 and 20th anniversary was celebrated in 2016. The neutrino oscillations in atmospheric neutrinos were discovered in 1998 and thereby it was demonstrated that neutrinos have a finite mass. In 2001, the accurate measurements of the ^8B solar neutrino flux by SK and SNO discovered that neutrino oscillations are the solution of the solar neutrino problem beyond doubt. These findings became the research achievement for which the Nobel Prize in Physics was awarded in 2015. After the epoch-making discoveries, precise measurements of atmospheric neutrinos and solar neutrinos have been performed and they unraveled various phenomena of neutrino oscillations. The evidence of tau neutrino appearance in atmospheric neutrinos was confirmed in 2013 and atmospheric neutrino anomaly has been finally concluded. The indication of day-night asymmetry of the solar neutrino flux, which is expected from the matter effect of neutrino oscillations, was reported in 2014. At present, the most interesting subjects in those observations are the determination of neutrino mass hierarchy using atmospheric neutrinos and the consistency check of solar(ν_e) and reactor($\bar{\nu}_e$) oscillations.

A high intensity neutrino beam experiment using the J-PARC accelerator (T2K) was started in 2009. The T2K experiment uses the SK detector as the far detector. Electron neutrino appearance (the effect of the mixing angle θ_{13}) and the high precision measurement of oscillation parameters are main physics subjects in T2K. An indication of electron neutrino appearance was found in June 2011, and later the electron appearance has been established with greatly improved significance. Since 2014, anti-neutrino beam data also have been taken in order to search for CP violation.

The search for nucleon decay is another important subject at SK because it gives a direct evidence for the Grand Unified Theories (GUTs). SK gives the current best limit which strongly constrains various GUT models.

If a supernova happens in our galaxy, thousands of neutrino interactions are expected at SK and they will reveal detailed mechanism of the supernova explosion. SK is the only detector in the world which can identify the direction of the supernova neutrinos. So, SK has been running almost all the time with small dead time and if a supernova is observed at SK, we will send burst information to astronomers as soon as it is detected. In addition, SK aims to observe supernova relic neutrinos, which is an accumulated supernova burst neutrinos from the beginning of the universe. For this purpose, it

is planned to add 0.1% of gadolinium into the Super-K tank (called SK-Gd project) in order to tag neutrons for $\bar{\nu}_e$ detection. A feasibility study for the SK-Gd project is being performed using a 200 ton tank which mimics the Super-K detector.

Another activity of the Neutrino and Astroparticle division is a multi-purpose experiment using liquid xenon aiming at the detection of cold dark matter, neutrino absolute mass using neutrinoless double beta decay, and low energy solar neutrinos. A 800 kg liquid xenon detector was constructed in an experimental hall near the SK site, and searches for dark matter interactions and rare phenomena in liquid xenon have been running in the last several years.

The Hyper-Kamiokande (Hyper-K or HK) experiment is proposed as a joint project of the university of Tokyo and KEK by combining a next generation underground water Cherenkov detector and upgraded J-PARC neutrino beam. The Hyper-K detector is an order of magnitude larger in detector mass than Super-K and has discovery potential of leptonic CP violation and proton decays. The detector construction has been endorsed by the ICRR future project committee's report in March 2017.

SUPER-KAMIOKANDE

[Spokesperson : Masayuki Nakahata
(Kamioka Observatory, ICRR, The University of Tokyo)]

Search for nucleon decay

Proton decays and bound neutron decays (nucleon decays in general) is the most dramatic prediction of Grand Unified Theories (GUTs) in which three fundamental forces of elementary particles are unified into a single force. Super-Kamiokande (SK) is the world's largest detector to search for nucleon decays. Various nucleon decay modes have been looked for, but we have found no significant signal excess so far.

A proton decay into one charged lepton and one neutral pion ($p \rightarrow e^+\pi^0$, $p \rightarrow \mu^+\pi^0$) is one of the benchmark decay modes which have large detection efficiency. The results with neutron tagging and two box analysis separated by total momentum described in the previous annual report have been published [1].

Not only π^0 , but also several decay modes which a proton decays into an anti-charged lepton (e^+ , μ^+) and a meson (η , ρ^0 , ω) and a neutron decays into an anti-charged lepton and a meson (π^- , ρ^-) have been studied systematically. They are predicted by several GUT models with different branching ratio. Thus, studies of these modes may give us hint which model is correct. Selection criteria for these modes are somehow similar to $p \rightarrow e^+\pi^0$ and reconstructed meson mass ex-

cept π^- is used to extract signal. To reconstruct meson mass, all decayed particles should be visible in Water Cherenkov detector. Thus, following decay modes of mesons are used this analysis: $\eta \rightarrow 2\gamma, \eta \rightarrow 3\pi^0, \rho^0 \rightarrow \pi^+ + \pi^0, \omega \rightarrow \pi^0 + \gamma, \omega \rightarrow \pi^+ + \pi^- + \pi^0, \rho^- \rightarrow \pi^- + \pi^0$. Figure 1 shows reconstructed η mass distributions from SK-I to SK-IV which shows η mass could be reconstructed with same quality for all period.

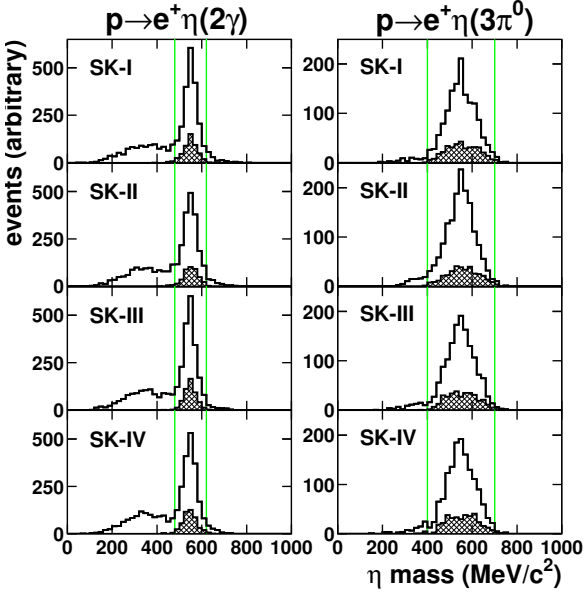


Fig. 1. Reconstructed η mass distribution for signal MC. Left figures show $p \rightarrow e^+ + \eta, \eta \rightarrow 2\gamma$ and right figures are $\eta \rightarrow 3\pi^0$ case. Green lines show selected area. Hatched histograms show free proton decay case. η mass can be reconstructed for all period.

Then total invariant mass and total momentum are reconstructed to separate signal from background. Cut for total mass is $800 < M_{tot} < 1050 \text{ MeV}/c^2$ except for $p \rightarrow e^+ + \omega(\pi^+ \pi^- \pi^0)$ ($600 \sim 800 \text{ MeV}/c^2$) and $p \rightarrow \mu^+ + \omega(\pi^+ \pi^- \pi^0)$ ($450 \sim 700 \text{ MeV}/c^2$). The signal region for total momentum is less than $250 \text{ MeV}/c^2$ except for $p \rightarrow e^+ + \eta(3\pi^0), e^+ + \rho^0, e^+ + \omega(\pi^0 \gamma)$ to reduce background. Figure 2 shows scatter plots of total mass vs total momentum for $p \rightarrow e^+/\mu^+ + \eta$ modes. In $\eta \rightarrow 2\gamma$ case, two box analysis is applied as same as $p \rightarrow e^+ + \pi^0$ case. As seen in the most left bottom figure, there are some candidates in some nucleon decay mode. However, they are consistent with expected background. Table 1 shows summary of expected background, observed data, probability to observe candidates greater than or equal actual observed number assuming Poisson statistics with expected background events as mean value, and obtained lower limits of nucleon lifetime with 90% confidence level.

Figure 3 shows summary of lifetime limits for a nucleon decays into an anti-lepton and a meson. Most of them gives the stringent limits in the world and they are improved by factor 2~3 since the previous publication [2]. Also these results show capability of water Cherenkov detector for various nucleon decay modes.

New reconstruction algorithm, fitQun, is developing for atmospheric ν analysis. $p \rightarrow e^+ + \pi^0$ and $p \rightarrow \nu + K^+$ were also studied with fitQun. Even though fitQun has better performance, it doesn't improve efficiency and background for $p \rightarrow e^+ + \pi^0$ much because inefficiency comes from π^0 interaction in nucleus. However, fitQun has better performance in vertex finding even region close to wall and it may be helpful to enlarge fiducial volume for nucleon decay searches.

Bibliography

- [1] K. Abe *et al.* [Super-Kamiokande Collaboration], Phys. Rev. D **95**, 012004 (2017).
- [2] H. Nishino *et al.* [Super-Kamiokande Collaboration], Phys. Rev. D **85**, 112001 (2012).
- [3] C. McGrew *et al.* [IMB Collaboration], Phys. Rev. D **59**, 052004 (1999).
- [4] K. S. Hirata *et al.* [Kamiokande Collaboration], Phys. Lett. B **220**, 308-316 (1989).
- [5] C. Berger *et al.* [Frejus Collaboration], Z.Phys. C **50**, 385-394 (1991).

Atmospheric neutrinos

Atmospheric neutrinos are decay products of secondary cosmic rays which are product of the air shower induced by primary cosmic rays high in the atmosphere. Atmospheric neutrinos have several remarkable features:

- The flavor ratio, $(\nu_\mu + \bar{\nu}_\mu)/(\nu_e + \bar{\nu}_e)$ is 2 (> 2 for above few GeV)
- Zenith angle distribution is up/down symmetry above a few GeV

These features are realized without neutrino oscillations, and provide a useful constraint in the study of these neutrinos. Super-Kamiokande has been observing atmospheric neutrinos since 1996 and has accordingly made several important measurements, including the discovery of neutrino oscillations [1, 2].

Three flavor oscillations and the neutrino mass hierarchy

The SK atmospheric neutrino data are described at leading order by two-flavor $\nu_\mu \rightarrow \nu_\tau$ oscillations with maximal mixing ($\theta_{23}=\pi/4$). However, sub-leading contributions via $\nu_\mu \rightarrow \nu_e$ oscillations induced by the mixing angle θ_{13} as well as the "solar" mixing parameters ($\Delta m_{12}^2, \theta_{12}$) provide the ability to probe currently unknown aspects of the standard neutrino oscillation paradigm, such as the existence of leptonic CP violation and the neutrino mass ordering (hierarchy). Understanding these open questions may bring important insight into larger questions, such as the origin and evolution of today's matter-dominated universe.

Several sub-leading oscillation effects are expected to appear in atmospheric neutrinos:

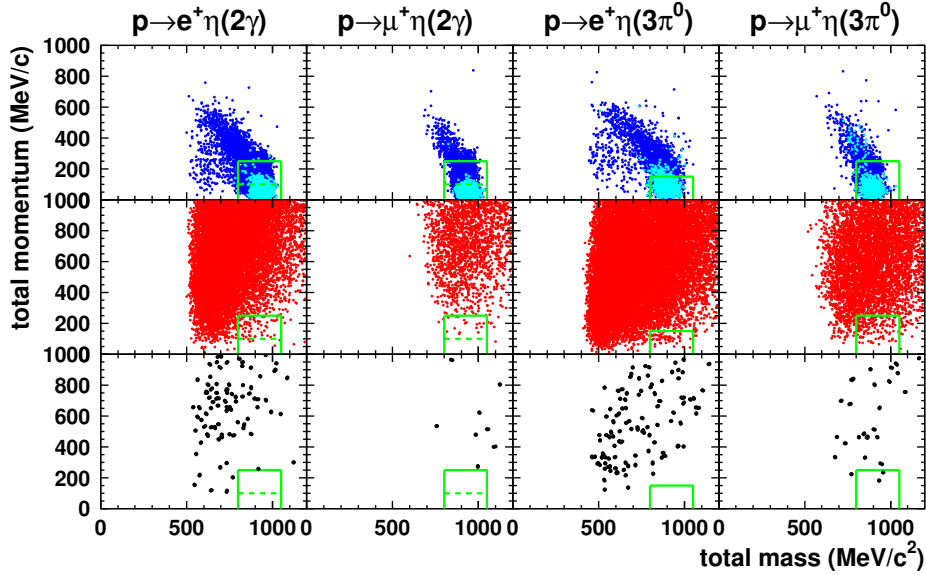


Fig. 2. Total invariant mass and total momentum for $p \rightarrow l^+ \eta$ MC (top, cyan for free proton and blue for bound proton), atmospheric neutrino background MC corresponding to about 2000 years live time of SK (middle), and data (bottom) for $p \rightarrow e^+ \eta$ ($\eta \rightarrow 2\gamma$), $p \rightarrow \mu^+ \eta$ ($\eta \rightarrow 2\gamma$), $p \rightarrow e^+ \eta$ ($\eta \rightarrow 3\pi^0$), and $p \rightarrow \mu^+ \eta$ ($\eta \rightarrow 3\pi^0$) searches from left to right. The results from SK-I to SK-IV are combined. The signal box is shown as a green box. For the $p \rightarrow l^+ \eta$ (2γ) searches, the total momentum is separated at the horizontal dashed line in the signal box.

Modes	Background (events)	Candidate (events)	Probability (%)	Lifetime Limit ($\times 10^{33}$ years) at 90% CL
$p \rightarrow e^+ \eta$	0.78 ± 0.30	0	-	10.
$p \rightarrow \mu^+ \eta$	0.85 ± 0.23	2	20.9	4.7
$p \rightarrow e^+ \rho^0$	0.64 ± 0.17	2	13.5	0.72
$p \rightarrow \mu^+ \rho^0$	1.30 ± 0.33	1	72.7	0.57
$p \rightarrow e^+ \omega$	1.35 ± 0.43	1	74.1	1.6
$p \rightarrow \mu^+ \omega$	1.09 ± 0.52	0	-	2.8
$n \rightarrow e^+ \pi^-$	0.41 ± 0.13	0	-	5.3
$n \rightarrow \mu^+ \pi^-$	0.77 ± 0.20	1	53.7	3.5
$n \rightarrow e^+ \rho^-$	0.87 ± 0.26	4	1.2	0.03
$n \rightarrow \mu^+ \rho^-$	0.96 ± 0.28	1	61.7	0.06
total	8.6	12	15.7	-

Table 1. Summary of the nucleon decay searches. The number of events are summed from SK-I to SK-IV and for all the meson decay modes for each nucleon decay search. The events in the total signal box are shown for $p \rightarrow l^+ \eta$ search. The number of the expected atmospheric backgrounds with the systematic errors are shown in the second column. The Poisson probability to observe events greater than or equal to the number of data candidates, without considering the systematic uncertainty in the background, is shown in the fourth column.

- Resonant enhancement of $\nu_\mu \rightarrow \nu_e$ oscillations due to the effects of matter occur at energies between 2 and 10 GeV and will manifest as an excess of upward-going electron-like events (e-like) in the atmospheric sample.
- This enhancement exists for either ν_e or $\bar{\nu}_e$ depending on the mass hierarchy. Therefore the mass hierarchy can be probed by understanding the relative amount of neutrino and antineutrino interactions in the detector.
- The combination of the solar oscillation parameters and the octant of $\sin^2 \theta_{23}$, may enhance or suppress the event rate, and to some extent alter the spectral shape, of Sub-GeV electron-like data due to $\nu_\mu \leftrightarrow \nu_e$ oscillations they induce.
- The CP violating term, δ_{cp} , induces several sub-dominant oscillation effects which are predicted to appear across many of the SK atmospheric neutrino samples.

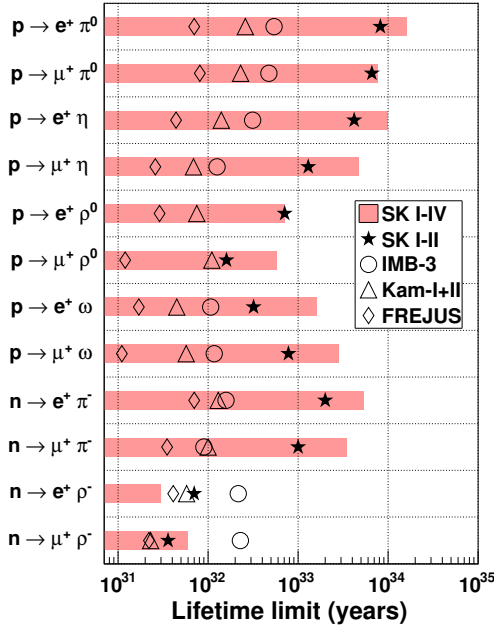


Fig. 3. Explored ranges and lower limits of nucleon partial lifetime with the results of the other experiments ([3]-[5]) and the previous SK analysis [2]. The $p \rightarrow l^+ \pi^0$ results [1] are also included.

Super-Kamiokande has studied the effects of these oscillations on atmospheric neutrino data separated into fully-contained (FC) events, partially-contained (PC) events, and upward-going muon topologies. Fully-contained events are characterized by a primary interaction vertex that is located inside the 22.5 kton fiducial volume of the detector and whose visible particles stop within the inner detector. On the other hand, though the primary vertex position of PC events is within the fiducial volume, they are characterized by having at least one charged particle escaping the inner detector and depositing light in the outer detector. In most cases the escaping particle is a muon. Upward-going muons originate from high energy muon-neutrino interactions in the rock surrounding the detector. Since all other particles are lost to interactions in the rock, only the muon is penetrating enough to reach the detector and be identified. The FC sample is separated into electron-like and muon-like (μ -like) subsamples by applying a particle identification algorithm to the most energetic Cherenkov ring of each event. Since PC and upward-going events are predominantly produced by muon neutrinos, no particle identification is applied. Though SK cannot distinguish on an event-by-event basis neutrino and antineutrino interactions, since the effect of the mass hierarchy lies in the difference of their oscillations, statistical separation of multi-GeV electron-like subsamples is performed. A likelihood method designed to enhance the kinematic differences between neutrino and antineutrino interactions is applied to separate the events into ν_e -like and $\bar{\nu}_e$ -like subsamples.

The atmospheric neutrino data accumulated in four period of Super-Kamiokande (totally 5326days) are analyzed.

Zenith angle distributions for six data subsamples are shown in Figure 4. An oscillation analysis considering all mixing parameters from the PMNS framework, including the CP violating term, δ_{cp} , and the effects of the earth's matter on neutrino propagation, has been performed assuming that θ_{13} is constrained to the measured value from reactor neutrino experiments, $\sin^2 \theta_{13} = 0.0238$, and its uncertainty is included as systematic error in the analysis. Figure 5 shows the $\Delta\chi^2$ distribution as a function of neutrino mixing parameters, θ_{23} , δ_{cp} , and mass squared difference (Δm_{32}^2 or Δm_{13}^2). Comparing the minimum absolute χ^2 values between fits to the normal and inverted hierarchy hypotheses indicate that the Super-K data have a weak preference for the normal mass hierarchy, $\Delta\chi^2 = \chi_{NH}^2 - \chi_{IH}^2 = -4.2$. In order to improve sensitivity to the mass hierarchy the analysis has been extended to include external constraints from the T2K experiment. We generated a mimic T2K data using atmospheric neutrino MC reweighted to the beam spectrum and incorporates publicly available data and systematic error information for the analysis [4, 5]. The T2K mimic data samples are analyzed simultaneously with the atmospheric neutrino data including relevant systematic error correlations. In this fit the normal hierarchy preference is strengthened to $\Delta\chi^2 = -5.3$. The best fit oscillation parameters and minimum χ^2 values from these analyses are shown in Table 2.

Tau neutrino appearance search

The deficit of the muon neutrino is dominantly explained by the change of the muon neutrinos to tau neutrinos. A direct detection of tau neutrinos is important for a confirmation of the three-flavor neutrino oscillation scheme.

Super-Kamiokande collaboration previously published a measurement of atmospheric tau neutrino appearance consistent with three-flavor neutrino oscillation with data collected in SK-I through SK-III [6]. This time we updated the analysis method and added new SK-IV data taken between 2008 and 2016.

Background events mainly comes from multi-hadronic productions induced by CC ν_μ and ν_e interactions. We employ a neural network (NN) technique to separate CC tau neutrino events and background events. We used seven kinematic variables and trained a NN by Monte Carlo simulation events to separate the signals and backgrounds.

To estimate the amount of tau neutrino events, we employ a two-dimensional un-binned maximum likelihood fit. Two dimensional probability density functions (PDFs) are constructed for signal and background as a function of NN output and cosine of the zenith angle of event direction. PDFs for each events is a combination of that for background and signal:

$$PDF_s = PDF_{s_{bg}} + \alpha \times PDF_{s_{tau}} + \sum_i \epsilon_i \cdot PDF_{s_{sys}},$$

where the last term represents the change of PDFs due to systematic error effects. The likelihood is calculated as a production of PDFs for each events and the parameters α and ϵ_i 's are adjusted to maximize the likelihood.

Figure 6 shows the zenith angle distribution of tau-like (NN output > 0.5) and non-tau-like (NN output < 0.5) sam-

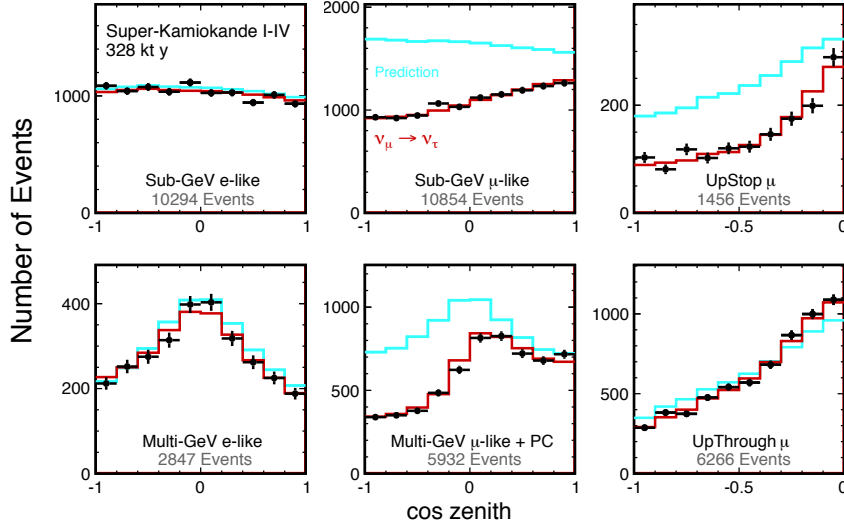


Fig. 4. Zenith angle distributions of SK atmospheric neutrino data. The horizontal axis indicates the cosine of the reconstructed zenith angle ($\cos \theta = -1$ corresponds to the upward-going direction). The data are shown by the black points with error bars and the MC predictions without oscillations and with two flavor $\nu_\mu \rightarrow \nu_\tau$ oscillations are shown by the blue and red lines, respectively.

	δ_{CP}	$\sin^2 \theta_{23}$	$\Delta m_{32}^2 (\times 10^{-3})$	χ^2
SK only (NH)	4.19	0.587	2.5	571.74
SK only (IH)	4.19	0.575	2.5	576.08
SK+T2K (NH)	4.89	0.550	2.4	639.61
SK+T2K (IH)	4.54	0.550	2.5	644.82

Table 2. Best fit oscillation parameters obtained by the three flavor oscillation analysis. Fits are conducted for both the normal (NH) and inverted (IH) hierarchy assumptions for the atmospheric neutrino data (“SK only”) and including constraints from the T2K experiment (“SK+T2K”). All fits are performed assuming $\sin^2 \theta_{13}=0.0238$, which is taken from PDG.

ples after fitting (left side). NN output distribution for upward ($\cos(\Theta) < -0.2$) and downward ($\cos(\Theta) > 0.2$) events are also shown in right side. Estimated relative normalization to expectation from standard three-flavor neutrino oscillation is $\alpha = 1.47 \pm 0.32(\text{stat}+\text{syst.})$, and a significance level of 4.6σ of rejection the hypothesis of no-tau-appearance.

Indirect WIMP searches

Weakly Interacting Massive Particles (WIMPs), GeV/c^2 -scale particles which have only gravitational and weak interactions, are a favored candidate of dark matter. Though direct dark matter detection experiments search for the elastic scattering interactions of these proposed particles with ordinary baryonic matter, it is also possible that WIMPs decay or annihilate into Standard Model particles which can then be detected to give indirect evidence for WIMPs. If WIMPs become trapped in the gravitational potential of a massive system, such as the center of the Milky Way, the earth, or the sun, their density may become sufficient for large numbers of these particles to annihilate into particles which then decay into neutrinos. This neutrinos pass undeflected through the

universe and would be detected in SK.

The atmospheric neutrino data are binned in both lepton momentum and the reconstructed angle to the galactic center, the earth core, or to the sun to search for the presence of an extra neutrino signal from those directions. The analysis proceeds by separately assuming annihilation into each of $\nu\bar{\nu}$, $b\bar{b}$, $t\bar{t}$, and W^+W^- with 100% branching fraction. For each assumed WIMP mass the expected neutrino energy distribution emerging from the decay chains of these particles is computed and used to define the signal spectrum at Super-K. Super-Kamiokande collaboration previously published the results from the sun [7], and this time we update analysis to the galactic center and the earth core. No evidence for a neutrino signal on top of the atmospheric neutrino background has been found in both case. Limits on the product of self-annihilation cross section and relative velocity, and WIMP-nucleon scattering cross sections are shown in Figure 7.

Bibliography

- [1] Y. Fukuda *et al.* [Super-Kamiokande Collaboration], Phys. Rev. Lett. **81** 1562 (1998).

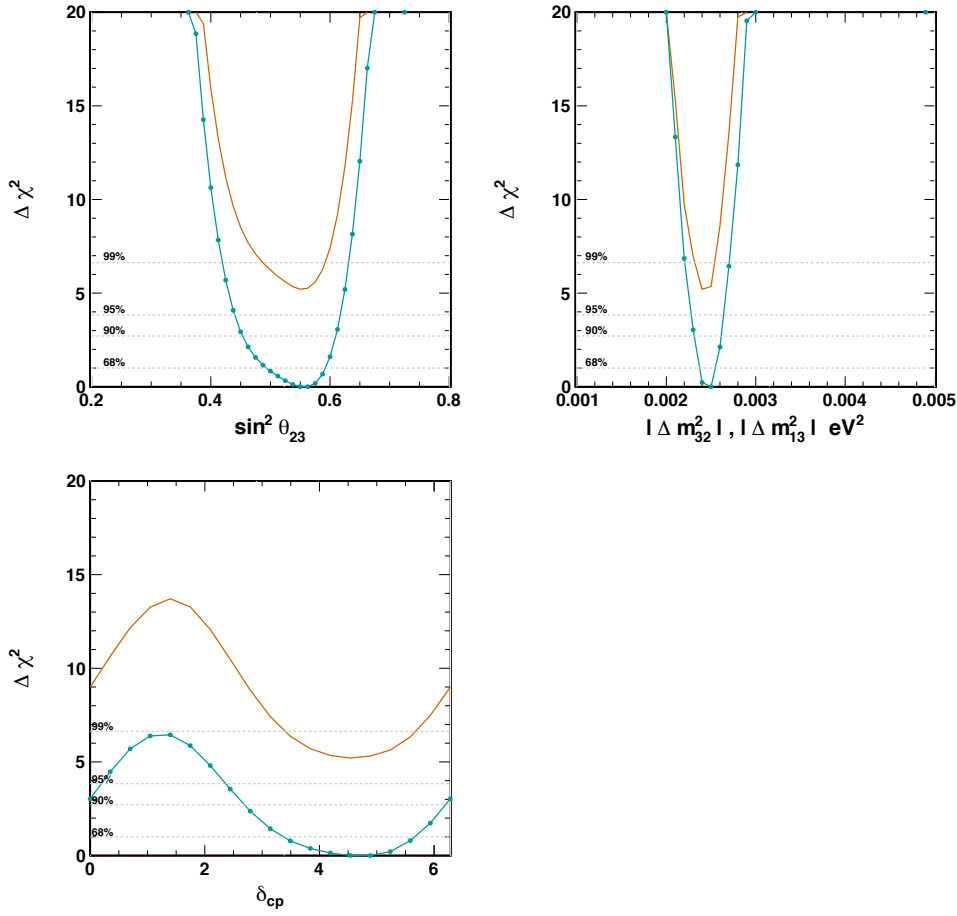


Fig. 5. The $\Delta\chi^2$ as a function of $\Delta m_{23,31}^2$, $\sin^2 \theta_{23}$, and δ_{cp} . Fits to the normal (blue) and inverted (orange) hierarchy hypotheses are shown.

- [2] Y. Fukuda *et al.* [Super-Kamiokande Collaboration], Phys. Rev. Lett. **81**, 1562 (1998) [arXiv:9807003 [hep-ex]].
- [3] P. Adamson *et al.* [MINOS Collaboration], Phys. Rev. Lett. **112**, 191801 (2014) [arXiv:1403.0867 [hep-ex]].
- [4] K. Abe *et al.* [T2K Collaboration], Phys. Rev. Lett. **112**, 181801 (2014) [arXiv:1403.1532 [hep-ex]].
- [5] K. Abe *et al.* [T2K Collaboration], Phys. Rev. Lett. **112**, 061802 (2014) [arXiv:1311.4750 [hep-ex]].
- [6] K. Abe *et al.* [Super-Kamiokande Collaboration], Phys.Rev.Lett **110**, 181802 (2013), [arXiv:1206.0328 [hep-ex]].
- [7] K. Choi *et al.* [Super-Kamiokande Collaboration], Phys. Rev. Lett. **114**, no. 14, 141301 (2015) [arXiv:1503.04858 [hep-ex]].
- [8] M.G. Aartsen *et al.* [IceCube Collaboration], [arXiv:1705.08103 [hep-ex]].
- [9] R. Bernabei *et al.* [DAMA Collaboration], Eur. Phys. J. C **56**, 333 (2008)
- [10] C. Savage *et al.*, J. Cosmol. Astropart. Phys. **04**, 010 (2009)
- [11] A. Albert *et al.* [ANTARES Collaboration], arXiv:1602.06792 [hep-ex].
- [12] M.G. Aartsen *et al.* [IceCube Collaboration], Eur. Phys. J. C **77**, 82 (2017) [arXiv:1609.01492 [astro-ph.HE]].

Solar Neutrinos

The solar neutrinos are produced by the nuclear fusion reaction, $4p \rightarrow \alpha + 2e^+ + 2\nu_e$, in the core of the Sun. Electron neutrinos (ν_e) produced in the Sun are so called *pp*, *pep*, ${}^7\text{Be}$, ${}^8\text{B}$ and *hep* neutrinos, whose fluxes had been predicted by the standard solar model [1]. Their energy distributes from ~ 0.1 MeV to ~ 20 MeV as shown in the left of Figure 8.

Solar neutrino flux measurements from Super-Kamiokande (SK) [2] and the Sudbury Neutrino Observatory (SNO) [3] have provided direct evidence for solar neutrino flavor conversion. However, there is still no clear evidence that this solar

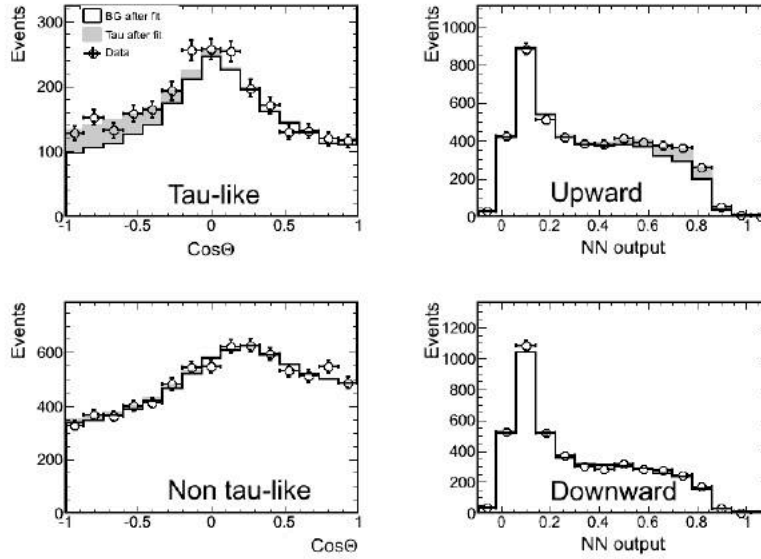


Fig. 6. (Left) Zenith angle distribution of tau-like (NN output < 0.5) and non-tau-like (NN output > 0.5) samples after fitting. (Right) NN output distribution for upward ($\cos(\Theta) < -0.2$) and downward ($\cos(\Theta) > 0.2$) events. Shaded histograms show CC tau events components for best fitted parameters.

neutrino flavor conversion is indeed due to neutrino oscillations and not caused by any other mechanism.

The current interesting physics motivation of the solar neutrino observation with the Super-Kamiokande (SK) detector [4] is to search for the Mikheyev-Smirnov-Wolfenstein (MSW) effect [5, 6]. The MSW effect leads to a resonant conversion of the higher energy solar neutrinos within the Sun and results in an about 30% level of the survival probability above a few MeV as shown in the left of Figure 8, which is so called “Up-turn”. Since the energy spectrum reflects the survival probability of the electron neutrinos, SK searches for the “Spectrum up-turn” by measuring the recoil electron energy spectrum. In addition, due to the matter effect in the interior of the Earth, the electron flavor neutrinos are regenerated as shown in the right of Figure 8. It is expected that the neutrino flux in night is larger than that in day by about a few % level depending on the neutrino oscillation parameters. In 2014, SK reported an indication of the terrestrial matter effects by about 2.7σ [7].

In 2016, the Super-Kamiokande Collaboration released a paper about the solar neutrino analysis results [8]. In this annual report, the updated results, expect for the day/night flux asymmetry measurement, are presented using data taken through the end of March, 2016 (SK-IV 2365 days data set). The total livetime throughout the difference phases of SK [2, 9, 10] is 5,200 days. On May 2015, the trigger threshold was changed from 34 observed PMT signals within 200 nsec to 31 hits [11, 12]. Because of this lower threshold, the detection efficiency between 3.5 MeV and 4.0 MeV was improved from $\sim 86\%$ to $\sim 100\%$.

The SK detector observes solar neutrino via the elastic scattering between the solar neutrino and the electron in pure

water. In the case of ν - e interaction, the direction of the recoil electron is highly correlated with the direction of the incident neutrino. Figure 9 shows the distribution of cosine between the reconstructed direction of observed recoil electrons and the direction of the Sun. Using 5,200 days data, more than 84,000 events are observed so far. Based on this data, the ^8B solar neutrino flux is determined to be $(2.355 \pm 0.033) \times 10^6 / \text{cm}^2 / \text{sec}$ assuming a pure electron neutrino flavor content. The ratio between the SK result and the SNO NC current flux [13] becomes 0.4486 ± 0.0062 .

The solar activity cycle is the 11 years periodic change of sun spots releasing the magnetic flux at the surface of the Sun. The number of the sun spots strongly correlated with the solar activity cycle. SK has observed solar neutrinos for about 19 years, this long term observation covers more than 1.5 solar activity cycles. Figure 10 shows the SK yearly flux measured throughout the different phases of SK together with the corresponding sun spot number (Source: WDC-SILSO, Royal Observatory of Belgium, Brussels [14]). Using the present data, the χ^2 is calculated with the total experimental uncertainties as $\chi^2 = 15.52/19$ d.o.f., which corresponds to a probability of 68.9%. The SK solar rate measurements are fully consistent with a constant solar neutrino flux emitted by the Sun.

The energy spectrum of the recoil electrons are extracted using an extended maximum likelihood fit [8]. Figure 11 shows the energy spectrum obtained in SK-IV. The total number of energy bins is 23, where 20 bins of 0.5 MeV width between 3.5 MeV and 13.5 MeV, and two bins of 1 MeV between 13.5 MeV and 15.5 MeV, and one bin between 15.5 and 19.5 MeV. Figure 12 shows the combined energy spectrum from SK-I to SK-IV with the predictions assuming the MSW effect. Comparing χ^2 between the data (black) and the

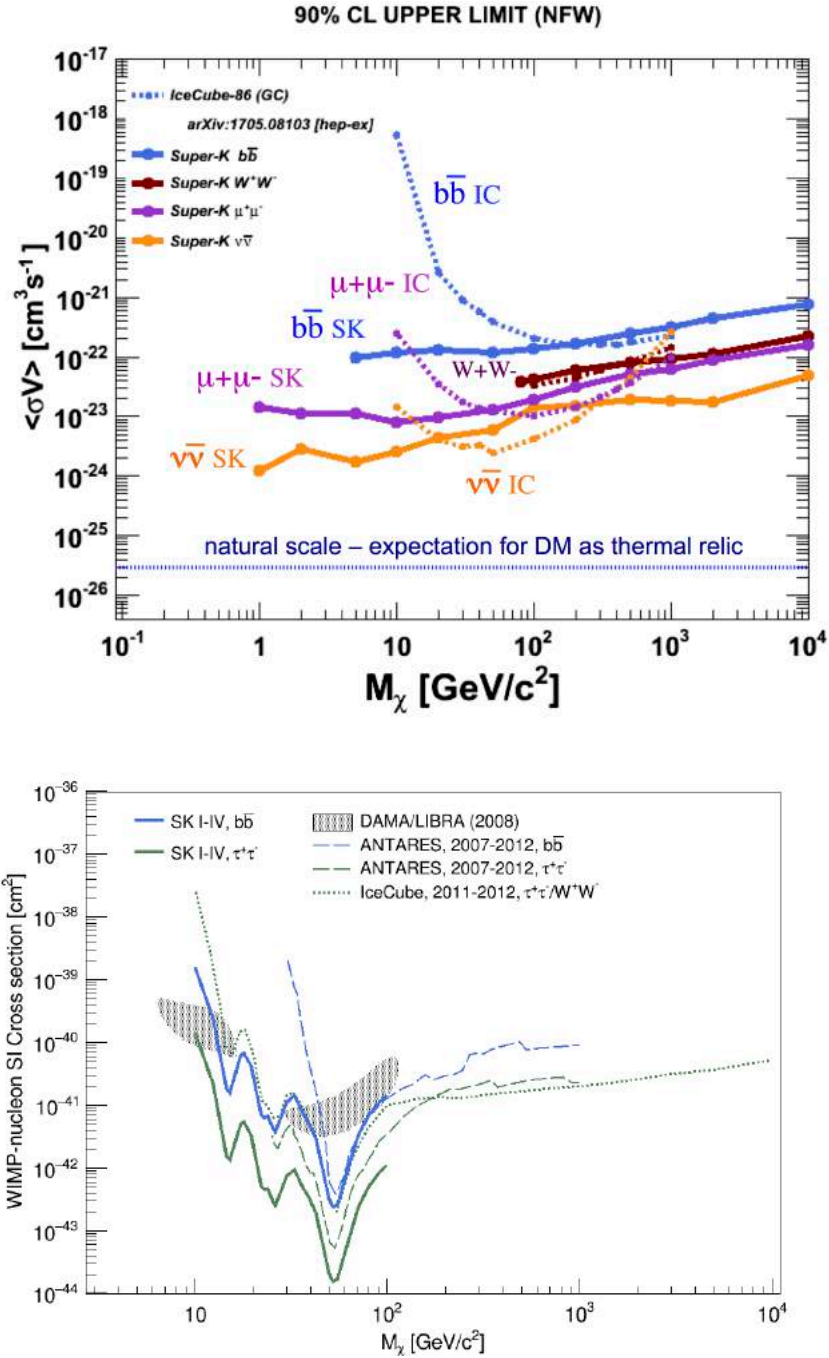


Fig. 7. The 90% C.L. upper limits on the product of dark matter self-annihilation cross section and the relative velocity of the dark matter particles in the galactic center (upper) and the 90% C.L. upper limit on the WIMP-nucleon spin independent cross section in the earth core (lower). These limits are calculated assuming WIMP annihilation into $\tau^+\tau^-$, $b\bar{b}$, and W^+W^- each with 100% branching fraction. Limits and allowed regions from other experiments are also shown [8, 9, 10, 11, 12].

predictions (green and blue), the MSW prediction drawn in blue is disfavored by $\sim 2\sigma$ level.

Neutrino energy spectrum is de-convoluted from the recoil electron energy spectrum. Figure 12 shows the result of the survival probability ($P_{ee}(E_\nu)$) with the other experimen-

tal results (pp and CNO neutrino flux constraints from the all solar neutrino data [15, 16, 17, 18], and the ${}^7\text{Be}$, pep and ${}^8\text{B}$ flux measurements of Borexino [19, 20]). The red band shows the allowed region from SK plus SNO [13] combined data as a function of neutrino energy. This analysis result gives the

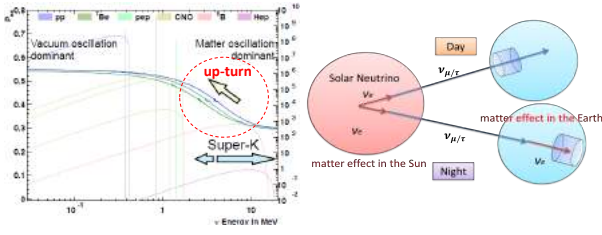


Fig. 8. Left: Several prediction of the survival probability of electron neutrinos emitted from the Sun as well as the fluxes of each solar neutrino; Right: The visual explanation of the day/night flux asymmetry.

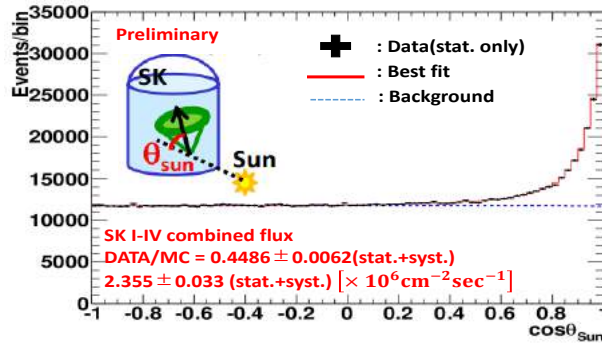


Fig. 9. The solar angle distribution combining for SK-I through SK-IV. The horizontal axis shows the cosine of the solar angle $\cos \theta_{\text{Sun}}$ and the vertical axis shows the number of the observed events. The black points shows the observed data, the red (blue) histogram shows the best-fit (background-shape).

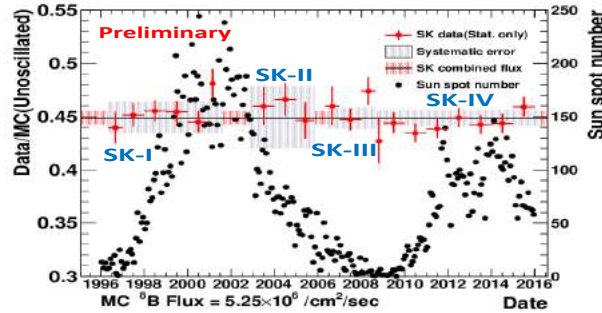


Fig. 10. The result of the solar neutrino flux from 1996 to 2015. The red points show the yearly flux measured by SK (statistical uncertainty only), the gray bands show the systematic uncertainties for each SK phase, the black-horizontal line shows the combined measured flux with the uncertainty drawn as the red horizontal band. The back points show the sun spot number provided by [14].

world's strongest constraints on the shape of the survival probability in the transition region between vacuum oscillation and MSW resonance.

The oscillation analysis was conducted using SK, SNO [13], radiochemical solar neutrino experiments [15, 16, 17] and Borexino [18, 19, 20] as well as the anti-neutrino measurement by KamLAND [21, 22]. Figure 14 shows the allowed contour measured by SK as well as KamLAND. SK uniquely selects the Large Mixing Angle MSW region by more than 3σ and

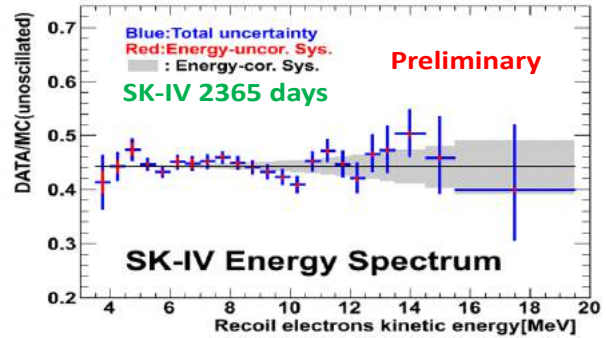


Fig. 11. The energy spectrum of the observed recoil electron in SK-IV as a function of energy. The red (blue) points show the data with the statistical (plus energy un-correlated systematic uncertainties). The energy correlated uncertainties are shown in gray band. The horizontal line shows the average value.

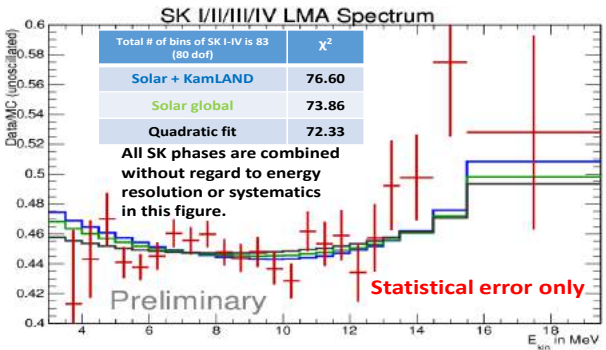


Fig. 12. The energy spectrum combining SK-I through SK-IV as a function of the recoil electron energy. The red points show the ratio of the data to the expected flux using a non-oscillated ^8B solar neutrino spectrum.

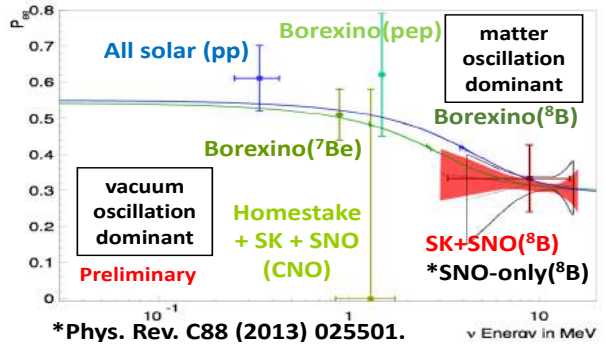


Fig. 13. The 1σ constraint of the survival probability combining SK with SNO [13], which is drawn in red. The colored plots show other measurement results [15, 16, 17, 18, 19, 20]. The blue and green lines show the prediction of the MSW.

SK significantly contributes to the measurement of the solar angle θ_{12} . When combining with SNO data, it gives strongest constraints on $\sin^2 \theta_{12}$ as shown in Figure 15 (green dash-line). On the other hand, The SK spectrum and day/night data favors a lower m_{21}^2 value than KamLAND's by more than 2σ . This parameter is mostly determined by the solar neutrino os-

oscillation fit and further precise measurements are required in future.

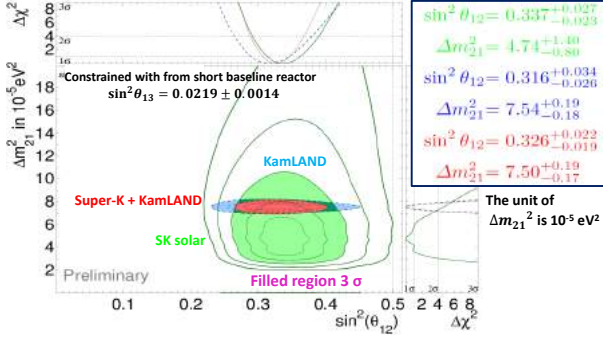


Fig. 14. The allowed contours for Δm_{21}^2 vs. $\sin^2 \theta_{12}$ from the SK combined analysis (green) as well as the allowed region from KamLAND. The combined allowed region is shown in red.

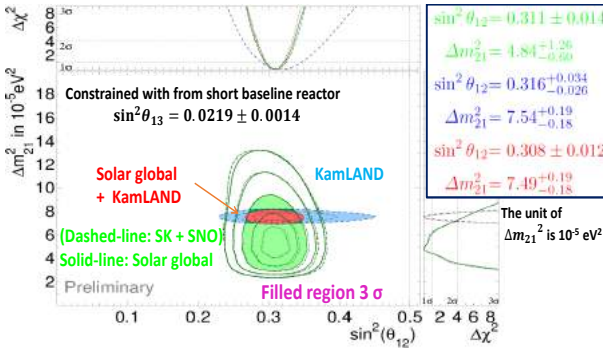


Fig. 15. The allowed contours for Δm_{21}^2 vs. $\sin^2 \theta_{12}$ from the SK plus SNO (green dashed line) as well as the allowed region from all solar neutrino data (solar global, green solid line). The allowed contour from KamLAND is also shown in blue. The combined allowed region is shown in red.

Removing the θ_{13} constraint, oscillation angle θ_{13} can be extracted using the solar neutrino experiments as well as the KamLAND as shown in Figure 16. The measured value is $\sin^2 \theta_{13} = 0.029^{+0.014}_{-0.015}$, which is 2σ level away from zero. The obtained result is consistent with the precise reactor measurement [23, 24, 25].

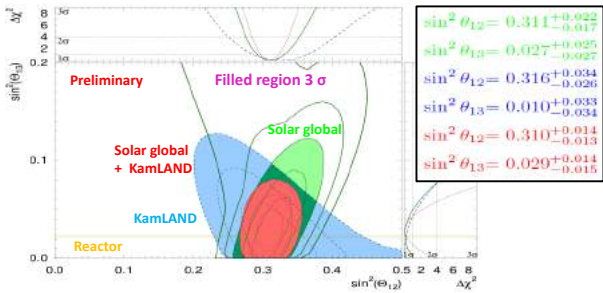


Fig. 16. The allowed contours for $\sin^2 \theta_{13}$ vs. $\sin^2 \theta_{12}$ from solar neutrino data (green) as well as the allowed region from KamLAND (blue). The precise measurement result by reactor experiments is also shown in yellow band.

In summary, Super-Kamiokande has precisely measured the ^8B solar neutrino flux, its time variation and recoil electron spectrum. No significant correlation between the observed solar neutrino flux and the sun spot number is found. In addition, the energy spectrum analysis slightly disfavors the MSW prediction by $\sim 2\sigma$ level. In the solar neutrino oscillation analysis combined with the KamLAND result, oscillation parameters are determined as $\Delta m_{21}^2 = 7.49^{+0.19}_{-0.18} \times 10^{-5} \text{ eV}^2$, $\sin^2 \theta_{12} = 0.308 \pm 0.012$. When the constrain of θ_{13} is removed, solar neutrino experiments and KamLAND measure $\sin^2 \theta_{13} = 0.029^{+0.014}_{-0.015}$, which is good agreement with reactor anti-neutrino measurements.

Bibliography

- [1] John N. Bahcall and Roger K. Ulrich, Rev. mod. Phys. **60**, 297 (1988).
- [2] J. Hosaka *et al.*, Phys. Rev. D **73**, 112001 (2006).
- [3] Q. R. Ahmad *et al.*, Phys. Rev. Lett. **87**, 071301 (2001).
- [4] Y. Fukuda *et al.*, Nucl. Instrum. Meth. A **501**, 418 (2003).
- [5] S. P. Mikheyev and A. Y. Smirnov, Sov. Jour. Nucl. Phys. **42**, 913 (1985).
- [6] L. Wolfenstein, Phys. Rev. D **17**, 2369 (1978).
- [7] A. Renshaw *et al.*, Phys. Rev. Lett. **112**, 091805 (2014).
- [8] K. Abe *et al.*, Phys. Rev. D **94**, 052010 (2016).
- [9] J. P. Cravens *et al.*, Phys. Rev. D **78**, 032002 (2008).
- [10] K. Abe *et al.*, Phys. Rev. D **83**, 052010 (2011).
- [11] S. Yamada *et al.*, IEEE Trans. Nucl. Sci. **57**, 428 (2010).
- [12] Y. Nakano, PhD thesis, The Univ. of Tokyo (2016).
- [13] B. Aharmin *et al.*, Phys. Rev. C **88**, 025501 (2013).
- [14] WDC-SILSO, Royal Observatory of Belgium, Brussels. <http://www.sidc.be/silso/datafiles>
- [15] R. Davis, Jr., D. S. Harmer, and K. C. Hoffman *et al.*, Phys. Rev. Lett. **20**, 1205 (1968).
- [16] J. N. Adburashitov *et al.*, Phys. Rev. C **80**, 015807 (2009).
- [17] M. Altmann *et al.*, Phys. Lett. B **616**, 174 (2005).
- [18] G. Bellini *et al.*, Phys. Rev. Lett. **107**, 141302 (2011).
- [19] Bellini *et al.*, Phys. Rev. D **82**, 033006 (2010).
- [20] Bellini *et al.*, Phys. Rev. Lett. **707**, 051302 (2012).
- [21] S. Abe *et al.*, Phys. Rev. Lett. **100**, 221803 (2008).
- [22] A. Gando *et al.*, Phys. Rev. D **88**, 033001 (2013).
- [23] F. P. An *et al.*, Chin. Phys. C **37**, 011001 (2013).
- [24] J. K. Ahn *et al.*, Phys. Rev. Lett. **108**, 191802 (2012).
- [25] Y. Abe *et al.*, Phys. Rev. D **86**, 052008 (2012).

Supernova neutrinos

In 1987, the observation of supernova 1987a by Kamiokande and IMB etc, opened the neutrino astronomy. This observation confirmed that the energy released by neutrinos is about several $\times 10^{53}$ ergs. However, the core collapse supernova (ccSN) mechanism is not yet fully understood. Super-Kamiokande (SK) would be able to detect several thousand neutrino events if a ccSN happened near the center of our galaxy. Such an observation would enable us to investigate in detail the mechanics of the ccSN explosion.

On average, 1-2 ccSNe per century are expected in our galaxy and therefore we must be prepared for these events. An online program called SNWATCH searches for time clustered events [1]. Events with total energy greater than 7 MeV and vertex position within the 22.5-kton fiducial volume in SK are selected. Cosmic ray muons and their subsequent decay electron events are removed. For each selected event, a 20-second time window is opened backwards in time, and the number of selected events in the window, N_{clus} , is counted. A variable D that identifies the dimension of the vertex distribution is computed. It is an integer number from 0 to 3, corresponding to point-, line-, plane- and volume-like distributions, respectively.

When $N_{clus} \geq 60$ and $D = 3$ a prompt SN warning is generated including automatic phone-calling and emails to experts. Then, the experts check whether it is a real supernova signal or not by looking at various plots which are uploaded to a secured site accessible from the Internet. These alarms are usually due to the accidental coincidence of two cosmic ray induced clusters. We have supernova drills several times per year. So far, no real supernova neutrino burst signal has been observed at SK.

In these drills, SNWATCH conveners and executive committee members meet via TV conference system, and discuss about a prompt announcement to outside researchers and the press. The decision is taken within one hour after the SN warning and these drills are done as if a real supernova may have happened. We also have SN shift training at SK by illuminating with an LD the SK detector a few times every month. SK shift members are notified by a dummy alarm that SNWATCH makes when the LD is illuminated. The shift members then call SNWATCH experts and give a report. The SK collaborators will be ready for the real supernova through the drills and training.

Other searches conducted at SK are those for neutrinos from Supernova Relic Neutrinos (SRNs). The SRN signal is the diffuse supernova neutrino background from all the core collapse supernovae in the past. This signal has never been detected but it is expected to be detectable in the 16-30 MeV energy region, which corresponds to the gap between the spectrum of solar and atmospheric neutrinos. Our published result [2] utilizes SK-I, II and SK-III data with an analysis energy threshold of 16 MeV. A maximum likelihood search was performed in multiple regions of the Cherenkov angle distribution to extract the most accurate flux limit. The obtained flux limit is between 2.7 and 3.0 $\bar{\nu}cm^{-2}s^{-1}$ (positron energy > 16 MeV), which in fact depends on the shape of the neutrino spectrum assumed. This result currently provides the world's best limit on SRN flux (Figure 18).

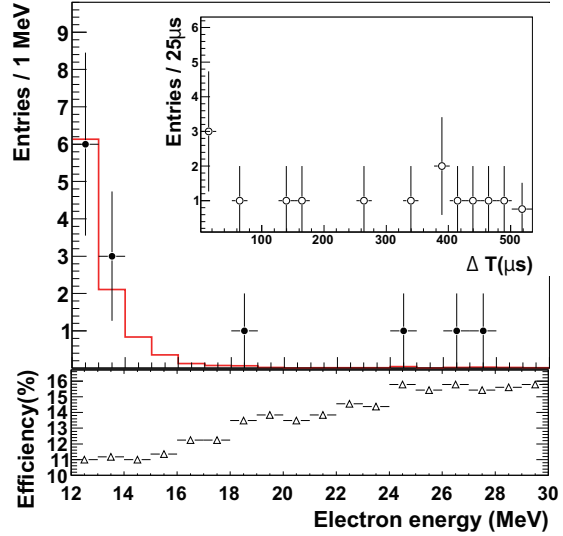


Fig. 17. Energy spectrum of prompt signals (points). The red histogram shows the expected accidental background. The plot embedded in the upper right shows the timing difference for the delayed candidates. The bottom figure shows the detection efficiency of SRN for each energy bin; the jumps at 18 MeV and 24 MeV are due to energy-dependent spallation cuts. Errors are statistical only.

In SK-IV, a new result of the SRN search using the neutron tagging technique was also published [3]. In this analysis, the neutrons captured on hydrogen from SRN reactions ($\bar{\nu}_e, p \rightarrow e^+, n$) are searched. After a neutron is captured, a single 2.2 MeV gamma is emitted. Thus, by detecting the prompt positron signal and the delayed 2.2 MeV gamma signal, we can reduce backgrounds, most of which are not accompanied by neutrons.

Figure 17 shows the energy spectrum of prompt signal, the time difference between a prompt signal and a delayed signal, and the detection efficiency of SRN for each energy bin. Figure 18 shows the obtained flux limit comparing with other results. The neutron detection efficiency is very low because of the low energy of the gamma from the neutron capture on hydrogen (compare the 2.2 MeV gamma with the kinetic energy threshold of 3.5 MeV for solar neutrino analysis). However, with this method we could obtain the world best limit below 16 MeV. This result shows a high potential of neutron tagging techniques, which can be a strong tool for SRN detection.

Bibliography

- [1] Abe, K. et al., *Astropart. Phys.* 81, 39 (2016)
- [2] K.Bays et al., *Phys. Rev. D* 85, 052007 (2012)
- [3] H.Zhang et al., *Astropart. Phys.* 60, 41 (2015)

R&D for the gadolinium project

As mentioned above, although at SK a few SRN events a year are expected, SRNs have not been detected yet because of the large backgrounds that constrain our search. The main goal of our research is to reduce these backgrounds and be able to detect SRNs. The observation of SRNs in general or

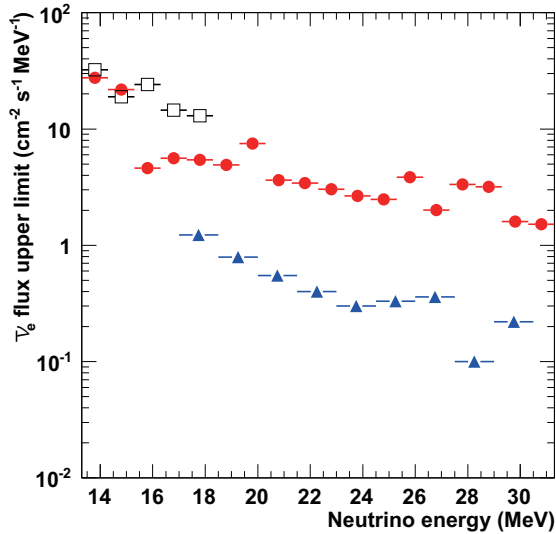


Fig. 18. Model-independent SRN 90% C.L. upper limits as a function of neutrino energy for SK-IV (solid circle). For comparison, both KamLAND result (open square) and previous SK result (solid triangle) are also shown.



Fig. 19. In the new cavern, the 200-ton tank (a) with currently 240 photomultipliers installed, the Gd pre-mixing and pre-treatment 15-ton tank (b), the selective filtration system (d), Gd removal resins (c) for test and a device to measure the water transparency (e) have been installed.

neutrinos from distant supernovae in particular, would give us some information about the universe, for example the core collapse rate from SRNs, and about the neutrino itself too, for example its lifetime.

As shown in the previous section, the current SK detector can only detect positrons efficiently but not neutrons. In order to achieve a high detection efficiency for neutrons, it is proposed to add 0.2% of gadolinium (Gd) sulfate into SK. Since Gd has a neutron capture cross section of 49,000 barns (about 5 orders of magnitude larger than that of protons) and emits a gamma cascade of 8 MeV, neutrons could be easily detected at SK (in space, vertices within tens of cm and in time, with the neutron capture delayed about 20 μ sec).

EGADS (Evaluation Gadolinium's Action on Detector Systems) project was funded in 2009. The main motivation of

EGADS is to show that by adding Gd, SK will be able to detect anti-neutrinos using the delayed coincidence technique, while keeping all its capabilities in the other analyses like solar and atmospheric neutrinos. Since then, a new hall near the SK detector has been excavated and a 200-ton tank with its ancillary equipment has been installed, see Fig.19, to mimic the conditions at SK. Of special importance is the selective water filtration system, that filters out water impurities while keeping the Gd in the water.

From January 2010 to July 2011 we circulated pure water through the 200-ton tank and proved that our water system is stable and achieves a high water quality. In 2013, from February 6th to April 20th, the 200-ton tank has been step-wise loaded with Gd until the final 0.2% concentration was reached. In summer 2013, we installed 240 photomultipliers and the data taking started from September without Gd and with a DAQ based on old SK ATM modules.

After the water quality became good and stable, detector calibrations were performed. In April 2015, we achieved the final concentration of 0.2% $Gd_2(SO_4)_3$ and we have been running the EGADS detector steadily.

Figure 20 shows the time variation of Cherenkov light left after travelling 15 m in Gd loaded water. The blue band in the figure shows typical values for SK-III and SK-IV. As shown in the figure, the transparency of 0.2% $Gd_2(SO_4)_3$ water is within the typical SK range. In addition to the good water transparency, no Gd loss has been detected since the EGADS detector reached the final concentration more than two years ago (black dashed line shows the final expected concentration). By measuring Gd concentration, we confirmed that the Gd sulfate quickly dissolves homogeneously in the 200-ton tank.

Detailed studies have evaluated the impact on current analyses at SK. These studies show that current analyses will be basically unharmed after adding Gd in SK and all other tests and studies conducted have shown no showstoppers. As a consequence, the SK collaboration decided in spring 2015 to approve the SuperK-Gd project. The project has been funded and the actual schedule is being determined together with the T2K collaboration.

In the first half of 2017, EGADS has upgraded its electronics: We installed QBEEs and upgraded our DAQ. Currently, we are conducting an extensive calibration campaign. These efforts have the goal of becoming a detector with instant galactic supernova detection capabilities.

T2K EXPERIMENT

[Spokesperson : Tsuyoshi Nakaya (Kyoto University)]

The T2K (Tokai-to-Kamioka) experiment [1] is a long-baseline neutrino oscillation experiment, employing a high intensity muon neutrino beam produced in the Japan Proton Accelerator Research Complex (J-PARC). T2K uses Super-Kamiokande (SK) [2] as the far detector to measure neutrino rates at a distance of 295 km from the accelerator, and near

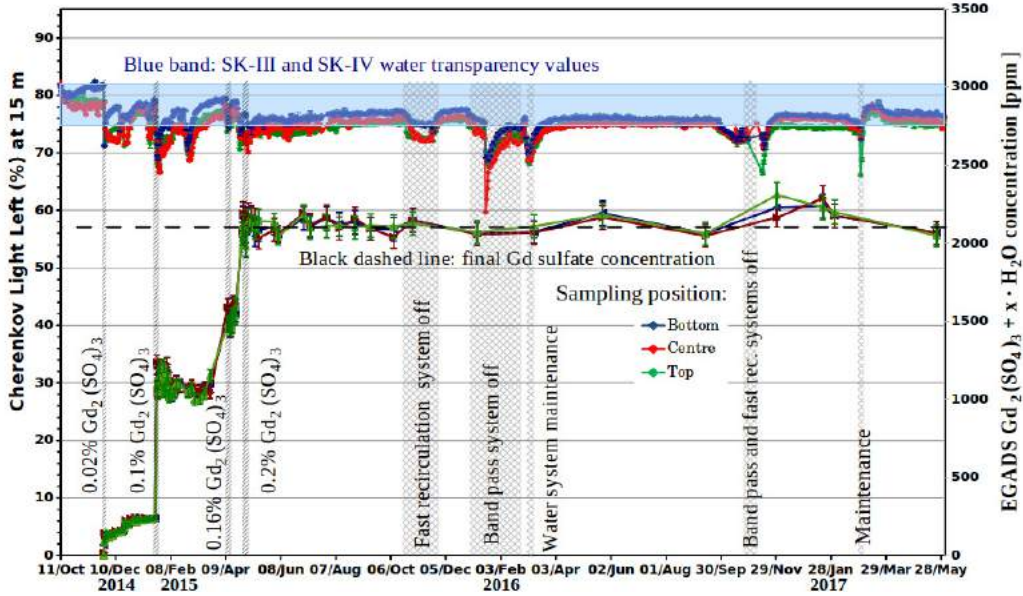


Fig. 20. Cherenkov light left at 15 m for Gd loaded water. The horizontal blue band are the typical values for SK-III and SK-IV. The vertical lines shows the injection dates where we also indicate the concentration (% in mass) in the 200-ton tank. The black dashed line shows the final expected concentration.

detectors to sample the beam just after production. The experiment includes a neutrino beamline and a near detector complex at 280 m (ND280).

T2K's physics goals include the precise measurement of the neutrino oscillation parameters via the muon neutrino disappearance for the atmospheric mass square (Δm_{32}^2) and the mixing angle θ_{23} , and the detection of the electron neutrino appearance from muon neutrino driven by the mixing angle θ_{13} . Now T2K has achieved the most precise measurement in θ_{23} in the world [3, 4, 5, 6] and established the electron neutrino appearance with the significance greater than 5σ [7, 8, 9]. Recently T2K started to produce muon antineutrino beam in $\bar{\nu}$ -mode to study oscillation in antineutrino and the CP symmetry in the lepton sector.

T2K adopts the off-axis method [10] to generate the narrow-band neutrino beam using the MW-class proton synchrotron at J-PARC. In this method the neutrino beam is purposely directed at an angle with respect to the baseline connecting the proton target and the far detector, SK. The off-axis angle is set at 2.5° so that the narrow-band muon neutrino beam generated toward the far detector has a peak energy at ~ 0.6 GeV, which maximizes the effect of the neutrino oscillation at 295 km and minimizes the background to electron-neutrino appearance detection.

The neutrino beam is produced by the interaction of 30 GeV protons from the J-PARC main ring accelerator on a long, 1.9 interaction-length, graphite target. Secondary hadrons, mainly pions and kaons, leaving the target are focused by three electromagnetic horns, which are currently operated at a current of either +250 kA or -250 kA to focus positive or negative particles respectively. The outgoing hadrons are then allowed to decay in a 96 m long decay volume, where a rel-

atively pure beam of muon neutrinos is produced mostly by the decay of positively charged hadrons in positive focusing mode (ν -mode), while more muon antineutrinos are produced in negative focusing mode ($\bar{\nu}$ -mode).

The near detector site at ~ 280 m from the production target houses on-axis and off-axis detectors. The on-axis detector (INGRID) [11], composed of an array of iron/scintillator sandwiches, measures the neutrino beam direction and profile. The off-axis detector, immersed in a magnetic field, measures the muon neutrino flux and energy spectrum, and intrinsic electron neutrino contamination in the beam in the direction of the far detector, along with measuring rates for exclusive neutrino reactions. These measurements are essential in order to characterize signals and backgrounds that are observed in SK. The far detector, SK, is a 50 kton water Cherenkov detector. For recording beam data, SK uses the beam spill information with the GPS timestamp delivered from J-PARC. All PMT hit information within $\pm 500 \mu\text{s}$ from the beam arrival timing are recorded to disk and then fed into offline processing for T2K data analysis.

The T2K neutrino flux at the near and far detectors assuming no neutrino oscillation is predicted by a simulation [12]. Interactions of the primary proton beam, whose profile is measured by a suite of proton beam monitors, as well as subsequently-produced pions and kaons, are simulated within the graphite target. The predicted hadron production rates inside and outside the target are then re-weighted based on the results from the NA61/SHINE experiment [13, 14], as well as other hadron production experiments. Particles which exit the target and subsequently decay are tracked through the horns and decay volume. Neutrino interactions are then simulated based on the flux predictions using NEUT event generator [15]. The

Table 3. T2K data taking periods and integrated numbers of protons on target (POT) after the event selection applied.

Run Period	Dates	$\times 10^{20}$ POT ν	$\bar{\nu}$
Run 1	Jan.2010 - Jun.2010	0.32	–
Run 2	Nov.2010 - Mar.2011	1.11	–
Run 3	Mar.2012 - Jun.2012	1.58	–
Run 4	Oct.2012 - May.2013	3.56	–
Run 5	May.2014 - Jun.2014	0.24	0.51
Run 6	Oct.2014 - Jun.2015	0.19	3.51
Run 7	Feb.2016 - May.2016	0.48	3.46
Run 8	Oct.2016 - Apr.2017		

predicted event rates at both the ND280 and SK are based on parametrized neutrino flux and interaction model. These models are fit to the precisely measured, high statistics data at the ND280, producing both a better central prediction of the SK event rate and reducing the systematic uncertainties associated with the flux and interaction models.

So far T2K has been accumulated neutrino data in the eight run periods (Table 3). Up to Run 7, the total accumulated neutrino data amounts to 14.9×10^{20} protons on target (POT). Among of them, 7.48×10^{20} POT is in ν -mode and 7.47×10^{20} POT is in $\bar{\nu}$ -mode. The intensity of the proton has been continuously increased owing to several improvements in J-PARC and the beam power exceeds 400 kW during the Run 7 period. The Run 8 beam data was taken from October 2016 and continued up to March 2017. The total accumulated POT in T2K from the beginning of the experiment exceeds 2.0×10^{21} during Run 8 period [16].

$\bar{\nu}_\mu$ disappearance measurement: T2K presents the first measurement of muon antineutrino disappearance in 2016 [17]. Observing a significant difference between the disappearance probabilities of neutrinos and antineutrinos would be evidence for new physics [18]. Results from the MINOS [19] and Super-Kamiokande (SK) collaborations [20] indicate no significant difference between muon antineutrino oscillations and muon neutrino oscillations. This analysis allows the dominant antineutrino oscillation parameters for $\bar{\nu}_\mu$ disappearance to vary independently from those describing neutrino oscillations, i.e., $\theta_{23} \neq \bar{\theta}_{23}$ and $\Delta m_{32}^2 \neq \Delta \bar{m}_{32}^2$, where the barred parameters refer to antineutrino oscillations. $\bar{\theta}_{13}$, $\bar{\theta}_{12}$, $\Delta \bar{m}_{21}^2$ are assumed to be identical.

Using a $\bar{\nu}$ -mode beam data set corresponding to 4.01×10^{20} POT up to Run 6, 34 fully contained $\bar{\nu}_\mu$ -like events were observed. The best-fit oscillation parameters are $\sin^2 \bar{\theta}_{23} = 0.45$ and $|\Delta \bar{m}_{32}^2| = 2.51 \times 10^{-3} \text{ eV}^2$ with 68% confidence intervals of 0.38-0.64 and $2.26\text{-}2.80 \times 10^{-3} \text{ eV}^2$, respectively. The fit results are shown in Fig 21. These results are in agreement with existing antineutrino parameter measurements and also with the ν_μ disappearance parameters measured by T2K, providing no indication of new physics.

Combined analysis of ν and $\bar{\nu}$ oscillations: A new source of CP violation beyond the Cabibbo-Kobayashi-Masakawa (CKM) quark mixing matrix is necessary to explain observations of

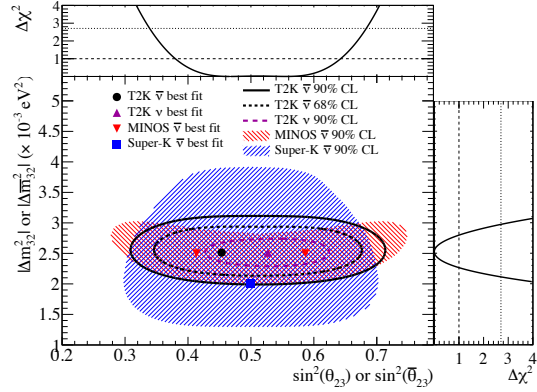


Fig. 21. The 68% and 90% confidence regions for the $\sin^2 \bar{\theta}_{23}$ - $|\Delta \bar{m}_{32}^2|$ plane assuming normal hierarchy, alongside the T2K ν , SK $\bar{\nu}$, and MINOS $\bar{\nu}$ 90% confidence regions. One-dimensional $\delta\chi^2$ profiles for the two parameters are shown at the top and right, overlaid with lines representing the 1D $\delta\chi^2$ values for the 68% and 90% confidence intervals.

baryon asymmetry in the Universe. In the lepton sector the Pontecorvo-Maki-Nakagawa-Sakata (PMNS) framework [21, 22] allows for CP violation. The discovery of $\nu_\mu \rightarrow \nu_e$ oscillation by T2K have opened the possibility to look for CP violation in neutrino oscillation. Comparing electron neutrino and antineutrino appearance probabilities allows a direct measurement of CP violation at T2K. In the paper published in May 2017 May [23], T2K reports its first results in the search for CP violation in neutrino oscillation using appearance disappearance $\nu_\mu \rightarrow \nu_e$ ($\bar{\nu}_\mu \rightarrow \bar{\nu}_e$) and $\nu_\mu \rightarrow \nu_\mu$ ($\bar{\nu}_\mu \rightarrow \bar{\nu}_\mu$) for ν - and $\bar{\nu}$ -mode oscillation.

The analyzed data includes all runs up to Run 7, comprising 7.482×10^{20} POT in ν -mode, which yielded in the far detector 32 ν_e -like and 135 ν_μ -like events, and 7.471×10^{20} POT in $\bar{\nu}$ -mode, which yielded 4 $\bar{\nu}_e$ -like and 66 $\bar{\nu}_\mu$ -like events. The reconstructed neutrino energy spectra for the ν_e and $\bar{\nu}_e$ sample is shown in Fig. 22.

The oscillation parameters $\sin^2 \theta_{23}$, Δm_{32}^2 , $\sin^2 \theta_{13}$, and δ_{CP} are estimated by performing a joint maximum-likelihood fit of the four far-detector samples. A parameter of $-2\Delta \ln L$ is defined as the ratio between the marginal likelihood at the point of the relevant oscillation parameter space and the maximum marginal likelihood. In the fit, reactor measurements of $\sin^2 \theta_{13}$ have been used as an additional constraint. A series of fits are performed where one or two oscillation parameters are determined and the others are marginalized, and then confidence regions are set using the constant $-2\Delta \ln L$ method. Fig. 23 shows the confidence region in $\sin^2 \theta_{23}$ - $|\Delta m_{32}^2|$ plane. The best-fit values are $\sin^2 \theta_{23} = 0.532$ and $|\Delta m_{32}^2| = 2.545 \times 10^{-3} \text{ eV}^2$ ($\sin^2 \theta_{23} = 0.534$ and $|\Delta m_{32}^2| = 2.510 \times 10^{-3} \text{ eV}^2$) for the normal (inverted) ordering. The result is consistent with maximal disappearance. The T2K data weakly prefer the second octant ($\sin^2 \theta_{23} > 0.5$) with a posterior probability of 61%. Confidence regions in the δ_{CP} - $\sin^2 \theta_{13}$ plane are also computed independently for both mass-ordering hypotheses without using the reactor measurement. Confidence intervals for δ_{CP} are obtained using the Feldman-Cousins method

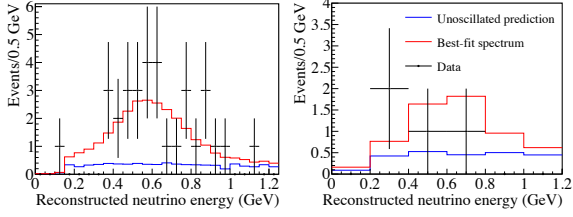


Fig. 22. The reconstructed neutrino energy at SK for the ν_e (left) and $\bar{\nu}_e$ (right) candidate samples is shown together with the expected distribution without oscillation (blue histogram) and the best fit (red histogram).

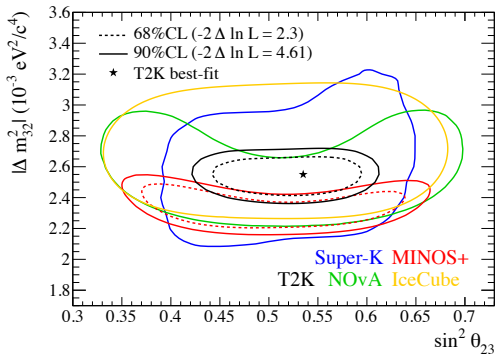


Fig. 23. The 68% (90%) constant $-2\Delta\ln L$ confidence regions for the $\sin^2\theta_{23}$ - $|\Delta m_{32}^2|$ plane assuming normal ordering, alongside confidence regions of other experiments (NOvA, MINOS+, SK, and IceCube).

(Fig. 24). The best-fit value is obtained for the normal ordering and $\delta_{CP} = -1.791$, close to maximal CP violation. The δ_{CP} confidence interval at 90% C.L. spans the range $(-3.13, -0.39)$ for normal mass ordering. The CP conservation hypothesis ($\delta_{CP} = 0, \pi$) is excluded at 90% C.L..

Measurement of double differential cross section of CC interaction: T2K measures muon neutrino charged-current (CC) interactions on carbon without pions in the final state at the T2K beam energy using 5.734×10^{20} POT [24]. For the first time the measurement is reported as a flux-integrated, double-differential cross-section in muon kinematic variables $(\cos\theta_\mu, p_\mu)$, without correcting for events where a pion is produced and then absorbed by final state interactions. Two analyses are performed with different selections, background evaluations and cross-section extraction methods to demonstrate the robustness of the results against biases due to model dependent assumptions. The measurements compare favorably with recent models which include nucleon-nucleon correlations but, given the present precision, the measurement does not solve the degeneracy between different models. The data also agree with Monte Carlo simulations which use effective parameters that are tuned to external data to describe the nuclear effects. The total cross-section in the full phase space is $\sigma = (0.417 \pm 0.047(\text{syst}) \pm 0.005(\text{stat})) \times 10^{-38} \text{ cm}^2 \text{ nucleon}^{-1}$ and the cross-section integrated in the region of phase space

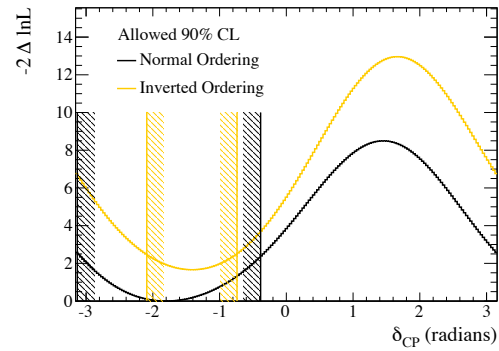
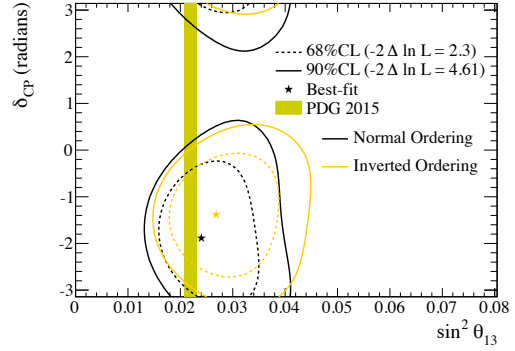


Fig. 24. TOP: The 68% (90%) constant $-2\Delta\ln L$ confidence regions in the δ_{CP} - $\sin^2\theta_{13}$ plane are shown by the dashed (continuous) lines, computed independently for the normal (black) and inverted (yellow) mass ordering. The best-fit point is shown by a star for each mass-ordering hypothesis. The 68% confidence region from reactor experiments on $\sin^2\theta_{13}$ is shown by the yellow vertical band. BOTTOM: $-2\Delta\ln L$ as a function of δ_{CP} for the normal (black) and inverted (yellow) mass ordering. The vertical lines show the corresponding allowed 90% confidence intervals, calculated using the Feldman-Cousins method. $\sin^2\theta_{13}$ is marginalized using the reactor measurement as prior probability.

with largest efficiency and best signal-over-background ratio ($\cos\theta_\mu > 0.6$ and $p_\mu > 200$ MeV) is $\sigma = (0.202 \pm 0.0359(\text{syst}) \pm 0.0026(\text{stat})) \times 10^{-38} \text{ cm}^2 \text{ nucleon}^{-1}$.

Measurement of CC single π^+ production cross section: The T2K off-axis near detector, ND280, is used to make the first differential cross section measurements of muon neutrino charged current single positive pion production on a water target at energies ~ 0.8 GeV [26]. The differential measurements are presented as a function of muon and pion kinematics, in the restricted phase space defined by $p_{\pi^+} > 200 \text{ MeV}/c$, $p_{\mu^-} > 200 \text{ MeV}/c$, $\cos\theta_{\pi^+} > 0.3$ and $\cos\theta_{\mu^-} > 0.3$. The total flux integrated ν_μ charged current single positive pion production cross section on water in the restricted phase-space is measured to be $\langle \sigma \rangle_\phi = 4.25 \pm 0.48(\text{stat}) \pm 1.56(\text{syst}) \times 10^{-40} \text{ cm}^2/\text{nucleon}$. The total cross section is consistent with the NEUT prediction ($5.03 \times 10^{-40} \text{ cm}^2/\text{nucleon}$) and 2σ lower than the GENIE prediction ($7.68 \times 10^{-40} \text{ cm}^2/\text{nucleon}$). The differential cross sections are in good agreement with the NEUT generator. The GENIE simulation reproduces well the shapes of the distributions, but over-estimates the overall cross

section normalization.

Measurement of flux-averaged cross section for CC coherent π^+ production on carbon: T2K reports the first measurement of the flux-averaged cross section for charged current coherent π^+ production on carbon for neutrino energies less than 1.5 GeV, and with a restriction on the final state phase space volume in the T2K near detector, ND280 [27]. Comparisons are made with predictions from the Rein-Sehgal coherent production model [28] and the model by Alvarez-Ruso et al. [29], the latter representing the first implementation of an instance of the new class of microscopic coherent models in a neutrino interaction Monte Carlo event generator. T2K observe a clear event excess above background, disagreeing with the null results reported by K2K and SciBooNE in a similar neutrino energy region. The measured flux-averaged cross sections are below those predicted by both the Rein-Sehgal and Alvarez-Ruso et al. models.

Proposal for an extended run of T2K to 20×10^{21} POT (T2K-II): Measurements by the T2K hint at maximum CP violation with $\delta_{CP} \sim -\pi$ and normal mass hierarchy. With the current approved exposure of 7.8×10^{21} POT, T2K could observe CP violation with 90% C.L. sensitivity around 2020. Meanwhile the next generation of measurements such as Hyper-Kamiokande [30] and DUNE [31] are expected to start from 2026. T2K proposes to extend the run from 7.8×10^{21} POT to 20×10^{21} POT in a five or six year period after the currently approved running to explore CP violation (T2K-II) [32]. According to the anticipated J-PARC Main Ring (MR) beam power upgrade, T2K can expect to accumulate 20×10^{21} POT by JFY2026 (Fig. 25). T2K is also working intensively to increase the effective statistics and sensitivity of the experiment per POT by improving beamline upgrades and analysis improvement by up to 50%. T2K also expect to reduce the systematic error of the predicted number of events at far detector to 4%. With these accelerator and beamline upgrades, as well as analysis improvements, the sensitivity to CP violation reaches 3σ or higher for the the oscillation parameter region favored by current existing result; $\delta_{CP} = -\pi$, $0.43 < \sin^2 \theta_{23} < 0.6$, and normal hierarchy (Fig. 26). In addition the mixing parameters, θ_{23} and Δm_{32}^2 , will be measured with precision of 1.7° and 1%, respectively.

Bibliography

- [1] K. Abe *et al.* (T2K Collaboration), Nucl. Instrum. Meth. A **659**, 106 (2011)
- [2] Y. Fukuda *et al.* (Super-Kamiokande Collaboration), Nucl. Instrum. Meth. A501, 418 (2003).
- [3] K. Abe *et al.* (T2K Collaboration), Phys. Rev. D **85**, 031103 (2012).
- [4] K. Abe *et al.* (T2K Collaboration), Phys. Rev. Lett. **111**, 211803 (2013).
- [5] K. Abe *et al.* (T2K Collaboration), Phys. Rev. Lett. **112**, 181801 (2014).
- [6] K. Abe *et al.* (T2K Collaboration), Phys. Rev. D **91**, 072010 (2015).

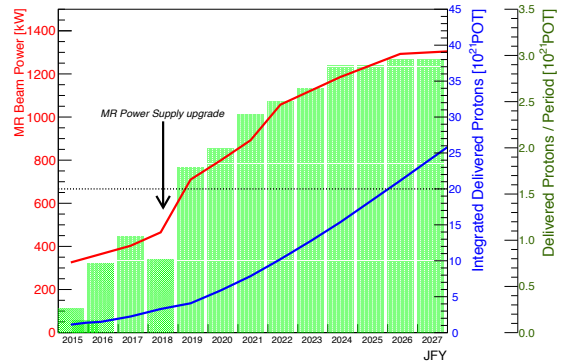


Fig. 25. Anticipated Main Ring (MR) beam power (red) and POT accumulation (blue) as function of Japanese Fiscal Year (JFY) which starts 1 April of the corresponding calendar year.

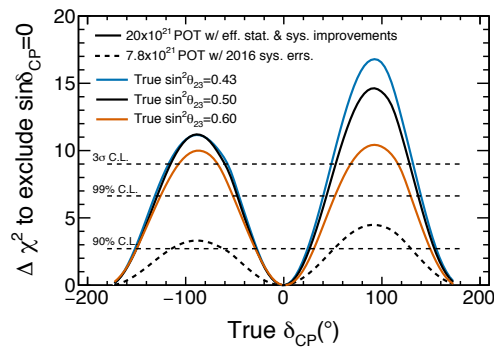


Fig. 26. Sensitivity to CP violation plotted as function of true δ_{CP} with a 50% effectively statistic improvement of full T2K Phase 2 statistic and improved systematic error. The normal mass hierarchy is assumed. Sensitivities at different values of $\sin^2 \theta_{23}$ (0.43, 0.5, 0.63) are compared. Mass hierarchy is assumed to be known.

- [7] K. Abe *et al.* (T2K Collaboration), Phys. Rev. Lett. **107**, 041801 (2011).
- [8] K. Abe *et al.* (T2K Collaboration), Phys. Rev. D **88**, 032002 (2013).
- [9] K. Abe *et al.* (T2K Collaboration), Phys. Rev. Lett. **112**, 061802 (2014).
- [10] D. Beavis, A. Carroll, I. Chiang, *et al.*, Long Baseline Neutrino Oscillation Experiment at the AGS (Proposal E889), 1995. Physics Design Report, BNL 52459.
- [11] M. Otani, N. Nagai, D. Orme, A. Minamino, K. Nitta, O. Drapier, F. Moreau and M. Besnier *et al.*, Nucl. Instrum. Meth. A **623**, 368 (2010).
- [12] K. Abe *et al.* (T2K Collaboration), Phys. Rev. D **87**, 012001 (2013).
- [13] N. Abgrall *et al.* (NA61/SHINE Collaboration), Phys. Rev. C **84**, 034604 (2011).

- [14] N. Abgrall *et al.* (NA61/SHINE Collaboration), Phys. Rev. C **85**, 035210 (2012).
- [15] Y. Hayato, Nucl. Phys. (Proc. Suppl.) B112, 171 (2002).
- [16] <http://t2k-experiment.org/2017/03/j-parc-delivers-2-0e21-protons-on-target/>.
- [17] K. Abe *et al.* (T2K Collaboration), Phys. Rev. Lett. **116**, 181801 (2016).
- [18] J. Beringer *et al.* (Particle Data Group), Phys. Rev. D **86**, 010001 (2012).
- [19] P. Adamson *et al.* (MINOS Collaboration), Phys. Rev. Lett. **108**, 191801 (2012).
- [20] K. Abe *et al.* (Super-Kamiokande Collaboration), Phys. Rev. Lett. **107**, 241801 (2011).
- [21] Z. Maki, M. Nakagawa, and S. Sakata, Prog. Theor. Phys. **28**, 870 (1962).
- [22] B. Pontecorvo, Sov. Phys. JETP **26**, 984 (1968).
- [23] K. Abe *et al.* (T2K Collaboration), Phys. Rev. Lett. **118**, 151801 (2017).
- [24] K. Abe *et al.* (T2K Collaboration), Phys. Rev. D **93**, 112012 (2016).
- [25] K. Abe *et al.* (T2K Collaboration), Phys. Rev. D **91**, 112002 (2015).
- [26] K. Abe *et al.* (T2K Collaboration), Phys. Rev. D **95**, 012010 (2017).
- [27] K. Abe *et al.* (T2K Collaboration), Phys. Rev. Lett. **117**, 192501 (2016).
- [28] D. Rein and L. Sehgal, Nucl. Phys. B **223** (1983).
- [29] L. Alvarez-Ruso, L. S. Geng, S. Hirenzaki, and M. J. Vicente-Vacas, Phys. Rev. C **75**, 055501 (2007).
- [30] K. Abe *et al.* (Hyper-Kamiokande Proto-Collaboration), PTEP 053C02 (2015), arXiv:1502.05199 [hep-ex].
- [31] R. Acciarri *et al.* (DUNE), (2016), arXiv:1601.05471 [physics.ins-det].
- [32] arXiv:1609.04111 [hep-ex]

XMASS EXPERIMENT

[Spokesperson : Yoichiro Suzuki¹ (-Dec. 2016), Shigetaka Moriyama² (Jan. 2017-)]

¹ Kavli IPMU, the University of Tokyo

² ICRR, the University of Tokyo

Introduction

The XMASS project is designed to detect dark matter, neutrinoless double beta decay, and ${}^7\text{Be}/pp$ solar neutrinos using highly-purified liquid xenon scintillator in an ultra-low radioactivity environment [1]. The advantages of using liquid xenon are a large amount of scintillation light yield, scalability of the size of the detector mass, an easy purification to reduce internal radioactive backgrounds, and a high atomic number ($Z = 54$) to shield radiations from outside of the detector. As the first stage of the XMASS project (XMASS-I), the detector with ~ 830 kg of liquid xenon was constructed. Its construction started in April 2007 and completed in September 2010. After completion of the detector, commissioning data was taken from December 2010 to May 2012. We published results from a search for light weekly interacting massive particle (WIMP) dark matter [2] and a search for solar axions [3], both using 6.7 live days of data collected with the full liquid xenon volume and with the lowest energy threshold of 0.3 keV. We also performed searches for inelastic WIMP-nucleon scattering on ${}^{129}\text{Xe}$ [4], bosonic super-WIMPs [5], and two-neutrino double electron capture on ${}^{124}\text{Xe}$ [6], using 165.9 live days of data with a restricted target mass of 41 kg at the central region of the detector. During the commissioning data-taking, we found that a majority of events at low energy originated from radioactive contamination in the aluminum seal of the photomultiplier tube (PMT) window. In order to reduce the backgrounds, detector refurbishment was conducted. The contaminated parts of PMTs were covered by copper rings and plates in order to stop scintillation lights and radiations caused by its contamination. PMTs were cleaned by acid and copper parts were electropolished in order to remove possible surface contamination. After a year of detector refurbishment, data-taking resumed in November 2013 and is continuing for more than three years till now.

The XMASS-I detector

XMASS-I is a single phase liquid xenon scintillator detector located underground (2700 m water equivalent) at the Kamioka Observatory. Fig. 27 shows a schematic drawing of the XMASS-I detector. It contains ~ 830 kg of liquid xenon in an active region. The volume is viewed by 630 hexagonal and 12 cylindrical Hamamatsu R10789 PMTs arranged on an 80 cm diameter pentakis-dodecahedron support structure. A total photocathode coverage of more than 62% is achieved. The spherical arrays of PMTs are arranged in a double wall vessel made of oxygen free high conductivity (OFHC) copper. The waveforms in each PMT are recorded with CAEN V1751 waveform digitizers with 1 GHz sampling rate and 10 bit resolution. The detector is calibrated regularly with a ${}^{57}\text{Co}$ source inserted along the central vertical axis of the detector. By the data taken with the ${}^{57}\text{Co}$ source at the center of the detector volume, the photoelectron yield was determined to be ~ 14 photoelectrons/keV. In order to shield the liquid xenon detector from external gammas, neutrons, and muon-induced backgrounds, the copper vessel was placed at the center of a $\phi 10 \text{ m} \times 10.5 \text{ m}$ cylindrical tank filled with pure water. The water tank is equipped with 72 Hamamatsu R3600 20-inch PMTs to provide both an active muon veto and passive shielding against these backgrounds. XMASS-I

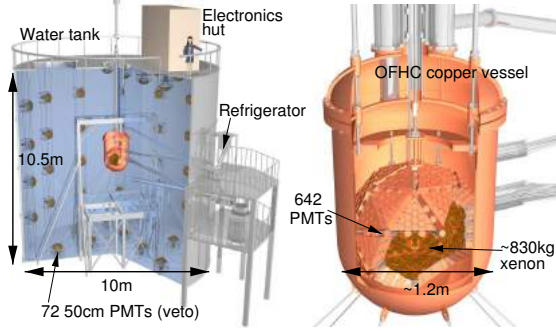


Fig. 27. Schematic drawing of the XMASS-I detector.

is the first direct detection dark matter experiment equipped with such an active water Cherenkov shield. The liquid xenon and water Cherenkov detectors are hence called an Inner Detector (ID) and an Outer Detector (OD), respectively. More details are described in Ref. [7].

Dark matter search by annual modulation [8]

The count rate of dark matter signal is expected to modulate annually due to the relative motion of the Earth around the Sun. The relative velocity of the Earth to the dark matter distribution becomes maximal in June and minimal in December. The amplitude of the modulation can be changed from positive (i.e. higher rate in June than in December) to negative at a cross-over energy and it is possible to observe this effect if the detector threshold is lower than that energy. The annual modulation would be a strong signature for dark matter.

We conducted a search for an annual modulation signal using 359.2 live days of data accumulated between November 2013 and March 2015. This analysis used the full 832 kg liquid xenon volume. Two different energy scales were used: keV_{ee} represents an electron equivalent energy, and keV_{nr} denotes the nuclear recoil energy. The energy threshold in this analysis was $1.1 \text{ keV}_{\text{ee}}$ ($=4.8 \text{ keV}_{\text{nr}}$), corresponding to ~ 8 photoelectrons.

To obtain the annual modulation amplitude from the data, the least squares method was used. The data set was divided into 40 time-bins with roughly 10 days of live time each. The data in each time-bin were further divided into energy-bins with a width of $0.5 \text{ keV}_{\text{ee}}$. Fig. 28 shows the observed count rate as a function of time in the energy region between 1.1 and $1.6 \text{ keV}_{\text{ee}}$ ($=4.8$ - $6.8 \text{ keV}_{\text{nr}}$). The expected count rates assuming the spin-independent WIMP-nucleon cross section of $2 \times 10^{-40} \text{ cm}^2$ for WIMP masses of 7 and $8 \text{ GeV}/c^2$ are also shown. This demonstrates the high sensitivity of XMASS to the annual modulation claimed by the DAMA/LIBRA experiment.

Two fitting methods were performed independently: the pull term method and the covariance matrix method to propagate the effects of the systematic errors. Both of them fit all energy- and time-bins simultaneously. We performed two analyses, one assuming WIMP interactions and the other independent of any specific dark matter model.

In the case of the WIMP analysis, the expected count rate

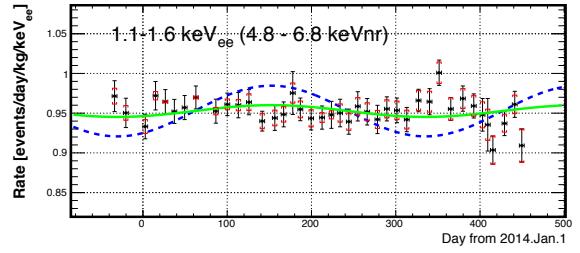


Fig. 28. Observed count rate as a function of time in the 1.1 - $1.6 \text{ keV}_{\text{ee}}$ ($=4.8$ - $6.8 \text{ keV}_{\text{nr}}$) energy range. The error bars show the statistical uncertainty and the square brackets indicate the 1σ systematic error for each time bin. The solid and dashed curves indicate the expected count rates assuming the spin-independent WIMP-nucleon cross section of $2 \times 10^{-40} \text{ cm}^2$ for the 7 and $8 \text{ GeV}/c^2$ WIMPs, respectively.

in the i -th energy and j -th time bin is expressed as:

$$R_{i,j}^{\text{ex}} = \int_{t_j - \frac{1}{2}\Delta t_j}^{t_j + \frac{1}{2}\Delta t_j} \left(C_i + \sigma_{\chi N} \cdot A_i(m_\chi) \cos \frac{2\pi(t - t_0)}{T} \right) dt, \quad (1)$$

where C_i is the unmodulated count rate at i -th energy bin and $\sigma_{\chi N}$ is the WIMP-nucleon cross section. Since the WIMP mass m_χ determines the recoil energy spectrum, the expected modulation amplitudes become a function of the WIMP mass $A_i(m_\chi)$. t_j and Δt_j are the time-bin's center and width, respectively. The modulation period T is fixed to one year and the phase t_0 is fixed to 152.5 days (~ 2 nd of June) when the Earth's velocity relative to the dark matter distribution is expected to be maximal. C_i , $\sigma_{\chi N}$, and m_χ are the free parameters to be determined by the fit. Fig. 29 shows the 90% confidence level exclusion limit on the spin-independent WIMP-nucleon cross section obtained by the pull term method. The $\pm 1\sigma$ and $\pm 2\sigma$ bands represent the expected 90% confidence level exclusion sensitivity estimated using 10,000 dummy samples including systematic uncertainties. The upper limit of $4.3 \times 10^{-41} \text{ cm}^2$ at $8 \text{ GeV}/c^2$ was obtained. The difference between two fitting methods is less than 10%. The result excludes the DAMA/LIBRA allowed region for the WIMP masses higher than $8 \text{ GeV}/c^2$.

For the model independent analysis, the expected count rate is estimated as:

$$R_{i,j}^{\text{ex}} = \int_{t_j - \frac{1}{2}\Delta t_j}^{t_j + \frac{1}{2}\Delta t_j} \left(C_i + A_i \cos \frac{2\pi(t - t_0)}{T} \right) dt, \quad (2)$$

where the free parameters C_i and A_i are the unmodulated count rate and the modulation amplitude at i -th energy bin, respectively. In the fitting procedure, the energy range between 1.1 and $7.6 \text{ keV}_{\text{ee}}$ was used. The modulation period T and phase t_0 were again fixed to one year and 152.5 days, respectively. Fig. 30 shows the best fit amplitude as a function of energy after correcting for the efficiency obtained by the pull term method. The efficiency was evaluated from the simulation of gamma-ray with a flat energy spectrum uniformly distributed in the sensitive volume. Both fitting methods are in good agreement. The $\pm 1\sigma$ and $\pm 2\sigma$ bands represent the expected

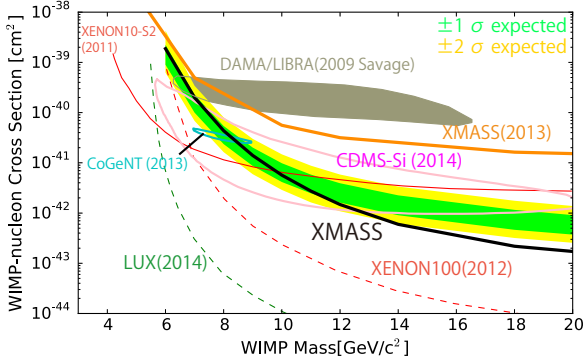


Fig. 29. Limits on the spin-independent WIMP-nucleon cross section as a function of WIMP mass. The solid curve shows the XMASS 90% confidence level exclusion limit from the annual modulation analysis. The $\pm 1\sigma$ and $\pm 2\sigma$ bands represent the expected 90% confidence level exclusion sensitivity.

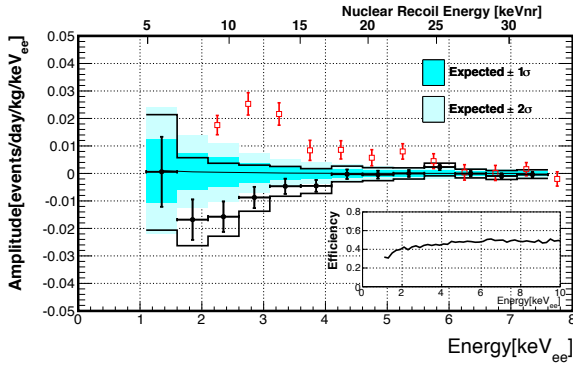


Fig. 30. Observed modulation amplitude as a function of energy for the model independent analysis (circle). The solid lines represent the XMASS 90% positive (negative) upper limits on the modulation amplitude. The $\pm 1\sigma$ and $\pm 2\sigma$ bands represent the expected sensitivity on the amplitude. The DAMA/LIBRA result (square) is also shown.

sensitivity on the modulation amplitude derived from the same dummy samples mentioned above. This test gave a p -value of 0.014 (2.5σ) for the pull term method and of 0.068 (1.8σ) for the covariance matrix method. To be able to test any model of dark matter, we evaluated the constraints on the positive and negative amplitudes separately. The 90% confidence level upper limits on the positive and negative amplitudes a_{up} were calculated by the relations $\int_0^{a_{up}} G(a) da / \int_0^\infty G(a) da = 0.9$ and $\int_{a_{up}}^0 G(a) da / \int_{-\infty}^0 G(a) da = 0.9$, respectively, where $G(a)$ is the Gaussian distribution with the mean and sigma of the amplitude obtained from the fit. We obtained positive (negative) upper limit of 2.1 (-2.1) $\times 10^{-2}$ events/day/kg/keV_{ee} in the energy range between 1.1 and 1.6 keV_{ee}, and the limits become stricter at higher energy.

We make direct comparisons with other experiments not by considering a specific dark matter model but amplitude count rate. DAMA/LIBRA obtained the modulation ampli-

tude of $\sim 2 \times 10^{-2}$ events/day/kg/keV_{ee} in the energy range between 2.0 and 3.5 keV_{ee}. The XENON100 experiment found no statistically significant modulation. Since XENON100 gave the best-fit parameters and uncertainties, we estimated a 90% confidence level upper limit of 3.7×10^{-3} events/day/kg/keV_{ee} between 2.0 and 5.8 keV_{ee} for their result. The XMASS experiment obtained the positive upper limits of $(1.7 - 3.7) \times 10^{-3}$ events/day/kg/keV_{ee} in the same energy region and gave more stringent constraint.

Search for solar Kaluza-Klein axion [9]

In theories of the large extra dimensions, axions could propagate in the extra dimensions beyond the 4-dimensional spacetime, and would acquire Kaluza-Klein (KK) excitations, which could be observed as particles with heavier masses in the standard spacetime. The KK axions can be produced in the Sun via the Primakoff effect ($\gamma Z \rightarrow aZ$) and the photon coalescence mechanism ($\gamma\gamma \rightarrow a$). While most of the produced KK axions escape from the solar system, a small fraction is gravitationally trapped in the orbits around the Sun and accumulated over the age of the Sun. They decay into two photons inside the terrestrial detector.

The expected number density of the trapped KK axions n_a against the distance from the Sun r has been calculated by L. Di Lella and K. Zioutas, and is fitted well by r^{-4} . Here, the number of extra dimensions $n = 2$, the number of extra dimensions axion can propagate $\delta = 2$, and the fundamental scale $M_F = 100$ TeV are assumed. Since the number of trapped KK axions produced by Primakoff effect is three orders of magnitude smaller than those produced by the photon coalescence mechanism, we concentrate on the contribution from the photon coalescence. Fig. 31 shows the expected energy spectra by the trapped solar KK axion at the perihelion and the aphelion. The expected number of events shows annual modulation depending on the distance from the Sun. The shape of spectrum is assumed to be same throughout the year.

We have searched for the decay of these solar KK axions using 832 kg \times 359 days of the XMASS-I data by annual modulation. No significant amplitude excess is found, and therefore a preliminary 90% confidence level exclusion limit is set on the KK axion-photon coupling $g_{a\gamma\gamma}$ as a function of the KK axion number density \bar{n}_a as shown in Fig. 32. As a bench mark, the proposed solar KK axion model ($g_{a\gamma\gamma} = 9.2 \times 10^{-14}$ GeV⁻¹, $\bar{n}_a = 4.07 \times 10^{13}$ m⁻³) is also shown. This is the first experimental constraint for the KK axion.

Detectability of galactic supernova neutrinos [10]

The coherent elastic neutrino-nucleus scattering (CEvNS) is a process in which a neutrino with an energy in the order of MeV interacts with all nucleons in a nucleus coherently,

$$\nu + \text{nucleus} \rightarrow \nu + \text{nucleus}, \quad (3)$$

resulting in a large cross section. However, it has not been observed yet, primarily because the only observable of this interaction is the recoiled nucleus with kinetic energy in the order of keV. The coherent scattering plays a crucial role at the final evolution of stars: it is believed to be the main mechanism for neutrinos to be trapped in the core of a supernova. The CEvNS process has been also proposed as a method to probe

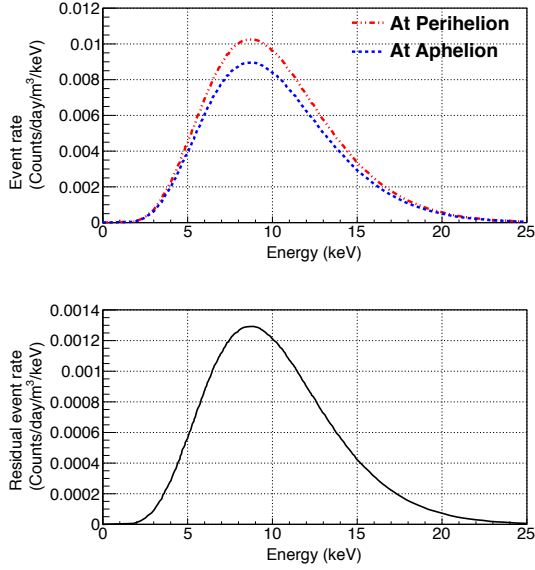


Fig. 31. Expected energy spectra of the sum of the two photons by the decay of the trapped KK axions at the perihelion and the aphelion. The curve in the lower panel shows the expected residual event rate (difference between the perihelion and the aphelion).

non-standard neutrino interactions with quarks, extra heavy neutral gauge bosons, and the neutron part of nuclear form factors. Therefore, the detection of the process would be of importance in both particle and astroparticle physics.

Among all available neutrino sources, galactic supernovae give the highest neutrino flux in the MeV range. It has been pointed out that experiments for direct dark matter search have the potential to detect galactic supernova neutrinos coherently scattered off nuclei. Among all existing experiments, large-volume liquid xenon dark matter detectors seem to be the most practical choice at this moment.

The possibility to detect galactic supernova neutrinos coherently scattered off xenon nuclei in the XMASS detector is calculated. The differential cross section of the coherent scattering as a function of neutrino energy E_ν and nuclear recoil energy E_{nr} is expressed as:

$$\frac{d\sigma}{dE_{nr}}(E_\nu, E_{nr}) = \frac{G_F^2 M}{2\pi} G_V^2 \left[1 + \left(1 - \frac{E_{nr}}{E_\nu}\right)^2 - \frac{ME_{nr}}{E_\nu^2} \right], \quad (4)$$

where G_F is the Fermi constant, M is target nuclear mass, and

$$G_V = \left[\left(\frac{1}{2} - 2\sin^2\theta_W\right)Z - \frac{1}{2}N \right] F(q^2). \quad (5)$$

The axial vector current, leading to a small incoherent contribution to the total neutral current cross section, is ignored. θ_W is the weak mixing angle ($\sin^2\theta_W = 0.23$). Z and N are the numbers of protons and neutrons in the nucleus, respectively. $F(q^2)$ is the nuclear form factor.

Fig. 33 shows energy spectra as a function of true xenon nuclear recoil energy with and without taking into account the

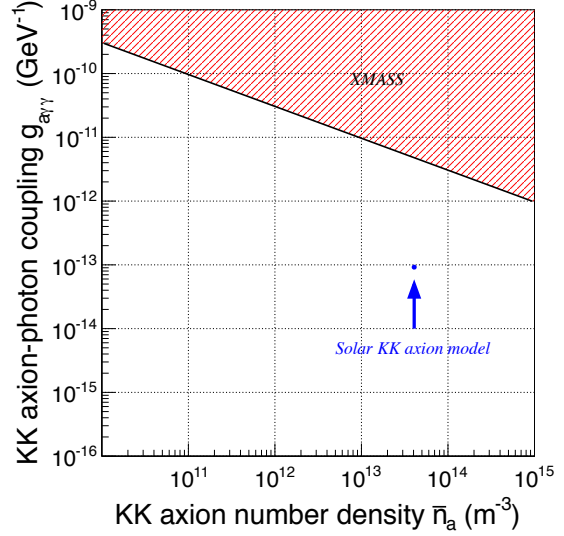


Fig. 32. Preliminary 90% confidence level exclusion limit on the KK axion-photon coupling as a function of the mean KK axion number density.

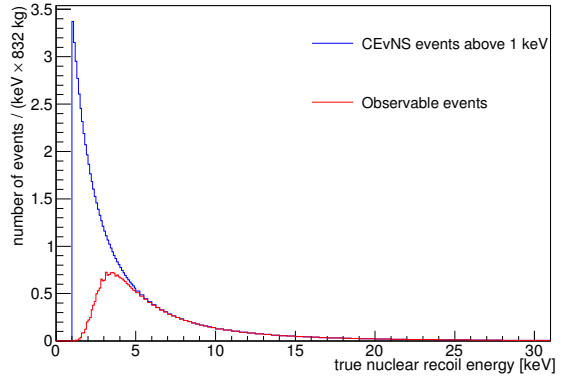


Fig. 33. Energy spectrum as a function of true xenon nuclear recoil energy. The upper and lower curve are the energy spectra with and without taking into account the detection efficiency, respectively. The upper line is calculated above 1 keV. The supernova model used here is the one from Nakazato *et al.* with $M_p = 20 M_\odot$, $Z = 0.02$ and $t_{rev} = 200$ ms. The distance of the supernova from the Earth is assumed to be 10 kpc.

detection efficiency. The total number of observable events from different supernova models are listed in Table 4. Two distances are chosen for comparison, $d = 10$ kpc is roughly the distance from the center of the Milky Way to the Earth, $d = 196$ pc is the distance from Betelgeuse to the Earth. The number of observable events predicted by most of the Nakazato models are significantly less than that predicted by the Livermore model. However, one Nakazato model, which forms a black-hole, predicts similar number of observable events as

Table 4. Number of observable supernova events in XMASS. The weakest Nakazato model is the one with $M_p = 20 M_\odot$, $Z = 0.02$ and $t_{\text{rev}} = 100$ ms. The brightest Nakazato model is the one with $M_p = 30 M_\odot$, $Z = 0.02$ and $t_{\text{rev}} = 300$ ms. The black-hole-forming model is the one with $M_p = 30 M_\odot$, $Z = 0.004$. Neutrino energy spectra used in the calculation are all integrated from core collapse till about 18 seconds later.

Supernova model	$d = 10$ kpc	$d = 196$ pc
Livermore	15.2	3.9×10^4
Nakazato (weakest)	3.5	0.9×10^4
Nakazato (brightest)	8.7	2.3×10^4
Nakazato (black hole)	21.1	5.5×10^4

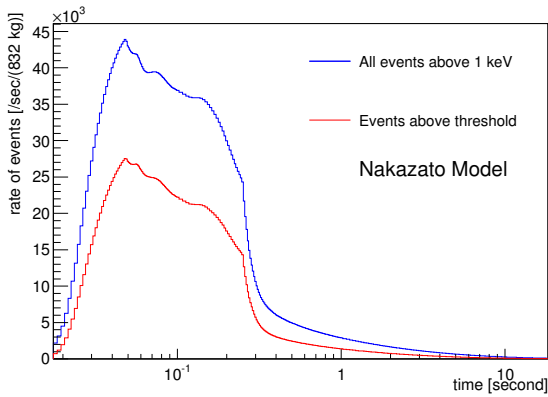


Fig. 34. Rate of CEvNS events in XMASS for a supernova 196 pc away from the Earth predicted by the Nakazato model with $M_p = 20 M_\odot$, $Z = 0.02$ and $t_{\text{rev}} = 200$ ms. The upper lines correspond to all the CEvNS events above 1 keV nuclear recoil energy predicted by models; the lower lines corresponds to all events that can be detected in XMASS.

the Livermore model. This points out the possibility to detect failed supernovae with no optical signal. In case of a supernova as close as Betelgeuse, all the models predict a definitely possible observation.

Fig. 34 shows the rate of CEvNS events in XMASS in about 18 second for a supernova 196 pc away from the Earth predicted by the Nakazato model with $M_p = 20 M_\odot$, $Z = 0.02$ and $t_{\text{rev}} = 200$ ms, assuming without any DAQ loss. Given such a high rate, it is possible to study in detail the supernova explosion mechanism by examining the time evolution of the event rate, since the flux and energy of the neutrinos predicted by different models vary in different phases of the explosion. Possible optimization of XMASS electronic system is under investigation to cope with such a high event rate.

There are three detectors in the Kamioka Underground Observatory which are capable of detecting supernova neutrinos: Super-Kamiokande, KamLAND, and XMASS. They cover each other's dead time, are sensitive to different neutrino interactions and may provide comprehensive understanding of the supernova neutrino burst in case of a simultaneous observation.

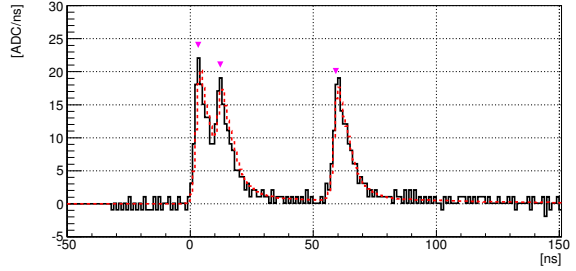


Fig. 35. Typical raw waveform in a PMT (solid line) overlaid with the reconstructed waveform as the sum of 1 PE pulses (dashed curve) for the 122 keV gamma-ray from the ^{57}Co source. The triangle markers indicate timings of the decoupled 1 PE pulses.

Measurement of liquid xenon scintillation time profile [11]

There are two scintillation processes in liquid xenon, the direct scintillation and the recombination processes. The direct scintillation proceeds through two states, singlet excitation and triplet excitation. The decay time constants of singlet and triplet states are a few ns and ~ 20 ns, respectively. The recombination process has a longer decay time constant of ~ 30 ns or more. The scintillation time profile can be used to discriminate between nuclear recoil events and electron events since the ratio of singlet to triplet excitations as well as the recombination time depend on ionization density. In addition, timing information is important for vertex reconstruction.

The time profile of scintillation in liquid xenon has been measured with the XMASS-I detector. The measurement was conducted in a wide energy range, between 5.9 keV and 122 keV for gamma-ray energy, with various radioactive sources, ^{55}Fe , ^{241}Am and ^{57}Co . The waveform data are fitted with a convolution of 1PE pulse waveform obtained from LED calibration data. Fig. 35 shows a typical raw waveform in a PMT overlaid with the reconstructed waveform as the sum of the 1PE pulses for the 122 keV gamma-ray from the ^{57}Co source placed at the center of the detector. It corresponds to 3PE incident and the observed waveform can be clearly reconstructed as the sum of the three 1PE pulses.

The scintillation time profile is evaluated by comparing the reconstructed pulse timing distributions over all PMTs of data and simulated samples with various timing parameters. Scintillation time profile is modeled as

$$f(t) = \frac{F_1}{\tau_1} \exp\left(-\frac{t}{\tau_1}\right) + \frac{1-F_1}{\tau_2} \exp\left(-\frac{t}{\tau_2}\right) \quad (6)$$

where τ_1 and τ_2 are the fast and slow decay time constants, respectively. F_1 defines the fraction of photons following the fast decay time constant τ_1 in an event. The fast decay component corresponds to the singlet excitation process, and here $\tau_1 = 2.2$ ns is assumed. The slow decay component corresponds to the convolution of triplet excitation and recombination processes. In the simulation, the effects of scattering and absorption of scintillation photons in liquid xenon as well as responses of PMT and readout electronics are taken into account.

Fig. 36 shows the pulse timing distribution of the observed

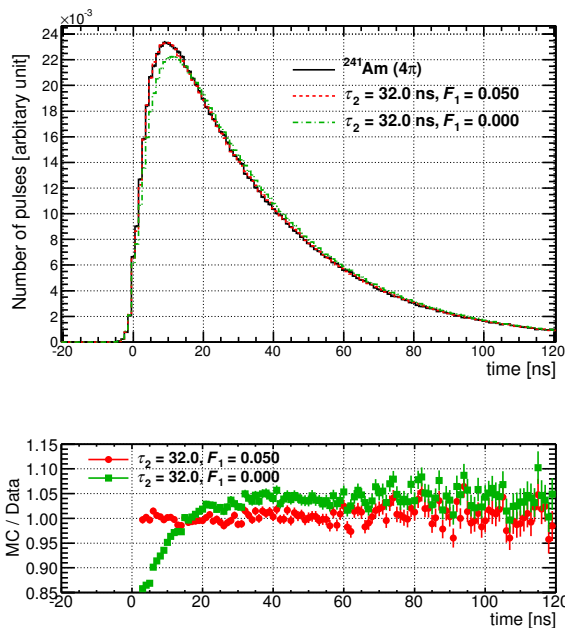


Fig. 36. (Top) Pulse timing distribution of the observed data overlaid with those of the best fit simulated samples with and without a fast decay component. The fourth earliest pulse timing is shifted to $T = 0$ ns for event-by-event timing adjustment. (Bottom) Monte Carlo simulation over a data ratio of the pulse timing distributions.

data overlaid with those of the best fit simulated samples with and without a fast decay component for the 59.5 keV gamma-ray from the ²⁴¹Am source placed at the center of the detector. It is clearly seen that a fast decay component with $\tau_1 = 2.2$ ns, which corresponds to singlet excitation, is necessary to reproduce data.

Energy dependencies of τ_2 and F_1 are studied as a function of the kinetic energy of electrons induced by gamma-rays. The mean kinetic energy of the electrons E_{electron} is evaluated from a Monte Carlo simulation. Fig. 37 shows the decay time constant τ_2 as a function of the electron kinetic energy E_{electron} . τ_2 increased from 27.9 ns to 37.0 ns as the gamma-ray energy increased from 5.9 keV to 122 keV. The accuracy of the measurement is better than 1.5 ns at all energy levels. This analysis gives consistent results with Akimov et al. and extends them to the lower energy region relevant to direct dark matter searches. In addition, the fraction of the fast component F_1 relatively decreased as incident particle energy increased. The ratio changes from 0.15 to 0.05 at the measured energy region.

Identification of ²¹⁰Pb and ²¹⁰Po in the copper bulk with a low-background alpha-ray counter [12]

Oxygen free copper (OFC) is readily available commercial material of low radio isotope (RI) content, and thus it is used in recent low-background experiments. There are multiple methods to measure the RI contaminations in material. The ²³⁸U and ²³²Th contaminations can be investigated by Inductively Coupled Plasma Mass Spectrometry (ICP-MS) or

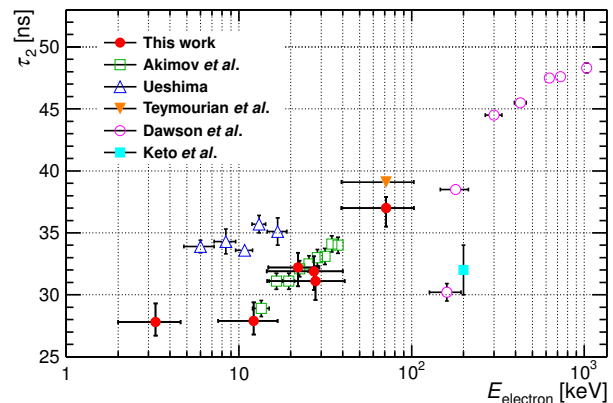


Fig. 37. Decay time constant τ_2 as a function of incident electron energy E_{electron} .

Glow Discharge Mass Spectrometry (GD-MS) with high precision. However, if the radioactive equilibrium is broken, inferred ²²⁶Ra or ²¹⁰Pb contaminations will be wrong. With a high purity germanium detector (HPGe), ²²⁶Ra can be measured down to O(10) mBq/kg while the sensitivity for the ²¹⁰Pb contamination is limited to O(100) mBq/kg. Moreover, HPGe cannot distinguish the surface from bulk contamination. A low-background alpha-ray counter is commonly used to measure the surface RI contamination.

Here, we have established a new method to measure the ²¹⁰Po and ²¹⁰Pb contaminations in the copper bulk with the low-background alpha-ray counter (XIA Ultra-Lo1800). The simulated energy distribution of the alpha-rays from ²¹⁰Po generated uniformly in the copper bulk is shown in Fig. 38. The distribution is continuous since alpha-rays emerging from the bulk lose part of their energy before reaching the surface. The contribution of the bulk ²¹⁰Po alpha-ray comes from within 10 μm from the surface of the copper sample. To be able to measure the ²¹⁰Po contamination in the bulk, the following points are important: (1) Background from the alpha-ray counter itself should be small. (2) Pollution of the sample surface should be minimized. (3) The sample surface roughness should be small. (4) Alpha-rays from other radioactive nuclei should be negligible. In order to minimize the residual surface contamination and to make the surface flat, all the copper samples are electro-polished.

Fig. 39 shows the energy distribution of a coarse copper sample overlaid with the simulated samples for the bulk and surface ²¹⁰Po. Coarse copper is the quality of copper before the electrolysis process and its purity is about 99%. Since the threshold of the data acquisition is not implemented in the simulation, the simulated distribution at energies below 2.5 MeV do not match the data. Events in $2.5 < E < 4.8$ MeV are used to estimate the ²¹⁰Po contamination in the bulk. The emissivity, the efficiency corrected alpha-ray event rate from a unit area, in this energy range is converted to the ²¹⁰Po contamination by comparing the data and simulated samples. The conversion factor is obtained as 272 (Bq/kg)/(alpha/cm²/hr).

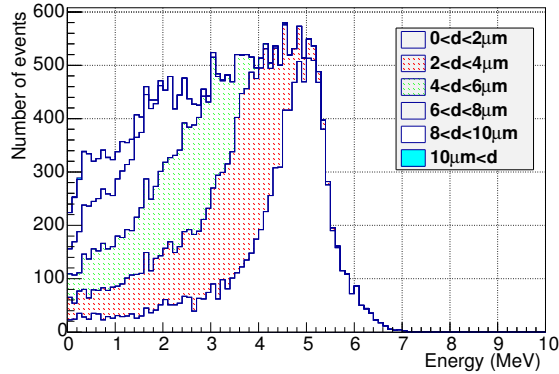


Fig. 38. Simulated energy distribution of alpha-rays from the ^{210}Po decay produced in the bulk copper. Stacked histograms are separated by the distance between the generated point and the copper surface.

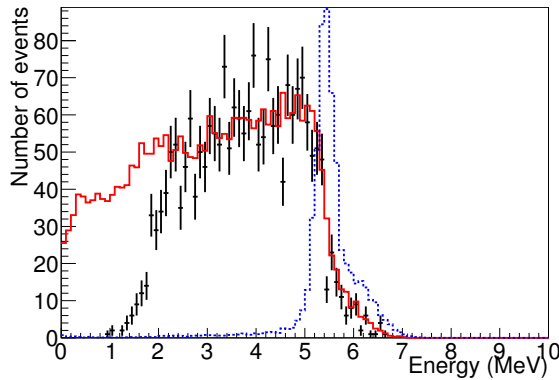


Fig. 39. Preliminary energy distribution of the coarse copper sample (black points) overlaid with the simulated samples for the bulk (solid) and surface (dashed) ^{210}Po . The bulk simulation is normalized by the number of events in $2.5 < E < 4.8$ MeV. Note that the energy threshold of the data acquisition is not implemented in the simulation.

In order to determine the ^{210}Pb contamination, we measure ^{210}Po several times over different periods since the ^{210}Pb and ^{210}Po decay equilibrium maybe broken. Fig. 40 shows the time variation of the ^{210}Po contaminations in the bulk for the measured OFC samples. As a preliminary result of the fitting, the ^{210}Pb contamination in all the samples are estimated to be within 17 – 30 mBq/kg, though ^{210}Po contamination varies widely. This is the first identification of a ^{210}Pb contamination in OFC. This ^{210}Pb is interpreted as a small residual from the electrolysis process based on the investigation of the coppers in each production step.

To find the copper least contaminated with ^{210}Pb , we investigated 6N (>99.9999% purity) copper. 6N copper is made from bare copper with an additional electrolysis in a clean environment. Another very low ^{210}Pb contamination sample was electroformed copper. The electro-formed copper we measured was accumulated on a stainless steel base about 500 μm in thickness. The measured event rates from both samples are consistent with the background. Therefore we

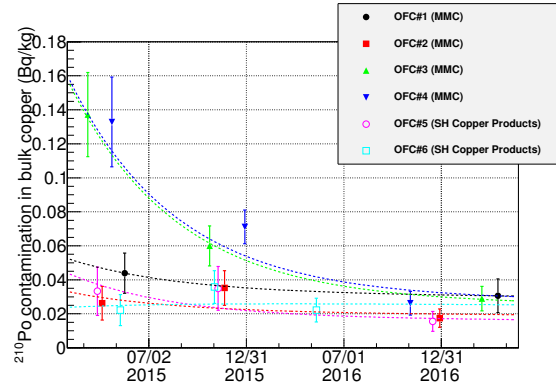


Fig. 40. Preliminary time variation of the ^{210}Po bulk contamination in OFC samples. Error bars show the statistical error only.

derive the preliminary 90% confidence level upper limits for the ^{210}Pb contamination to be <4.1 mBq/kg in the 6N copper and <5.3 mBq/kg in the electro-formed copper.

Bibliography

- [1] Y. Suzuki *et al.*, hep-ph/0008296.
- [2] K. Abe *et al.* (XMASS Collaboration), Phys. Lett. B **719** (2013) 78.
- [3] K. Abe *et al.* (XMASS Collaboration), Phys. Lett. B **724** (2013) 46.
- [4] H. Uchida *et al.* (XMASS Collaboration), Prog. Theor. Exp. Phys. (2014) 063C01.
- [5] K. Abe *et al.* (XMASS Collaboration), Phys. Rev. Lett. **113** (2014) 121301.
- [6] K. Abe *et al.* (XMASS Collaboration), Phys. Lett. B **759** (2016) 64.
- [7] K. Abe *et al.* (XMASS Collaboration), Nucl. Instrum. Meth. A **716** (2013) 78.
- [8] K. Abe *et al.* (XMASS Collaboration), Phys. Lett. B **759** (2016) 272.
- [9] N. Oka *et al.* (XMASS Collaboration), in preparation.
- [10] K. Abe *et al.* (XMASS Collaboration), Astropart. Phys. **89** (2017) 51.
- [11] H. Takiya *et al.* [XMASS Collaboration], Nucl. Instrum. Meth. A **834** (2016) 192.
- [12] K. Abe *et al.* (XMASS Collaboration), in preparation.

HYPER-KAMIOKANDE

[Project Leader: Masato Shiozawa
(Kamioka Observatory, ICRR, The University of Tokyo)]

Introduction

The Hyper-Kamiokande (Hyper-K or HK) experiment is proposed as a joint project of the university of Tokyo and KEK by combining a next generation underground water Cherenkov detector and upgraded J-PARC (Japan Proton Accelerator Research Complex, Ibaraki, Japan) neutrino beam. In FY2016 ICRR and KEK have set first priority to the Hyper-K and upgrade of J-PARC for the project. This project is selected as one of top 28 important large research projects in the “Masterplan 2017” by the Science Council of Japan.

Figure 41 shows a schematic view of the Hyper-K cylindrical detector with 60 m in height and 74 m in diameter. The water mass is 0.258 million metric tons, with an order of magnitude larger fiducial mass of 0.187 million metric tons than Super-K. It provides an enormous potential to discover leptonic charge-parity (CP) violation by observing neutrino and anti-neutrino beams from J-PARC. A search for nucleon decays is an important subject to explore new paradigm beyond the standard model of particle physics. Hyper-K will also have far better capabilities to observe atmospheric neutrinos, solar neutrinos, and neutrinos from other astronomical sources than those of predecessor experiments.

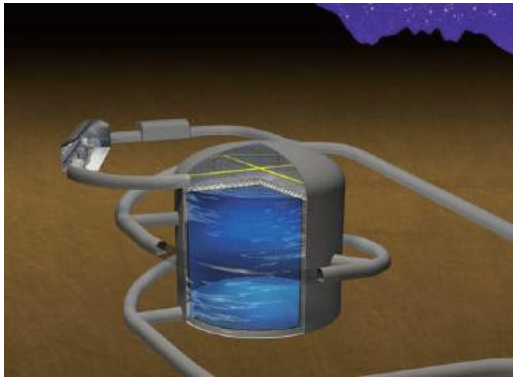


Fig. 41. Schematic view of the Hyper-K water tank.

The Hyper-K international proto-collaboration consists of about 300 researchers from 77 institutes in 15 countries. Technical details were published as a design report in October 2016 with various physics reaches[1]. The detector technology has been developed based upon the successful Super-K experiment. The candidate site has been pinned down by geological surveys. In conclusion the feasibility study has been completed and the project is technically ready to start construction. The international group aims to start the detector construction in 2018 and to start its operation in 2026.

Photosensors

A Cherenkov light in a ultra pure water is detected by 40,000 newly developed photomultiplier tubes (PMTs), R12860 by Hamamatsu Photonics K.K., with 40% photo-coverage. It was significantly upgraded from the R3600 PMT used in Super-K due to an improved dynode structure using a box-and-line type and optimized curvature glass as shown in Fig. 42.

The peak quantum efficiency is about 30%, that is 1.4 times higher than that of the Super-K PMT. In total, the new



Fig. 42. New 50 cm photomultiplier tube with a box-and-line dynode (R12860, Hamamatsu Photonics K.K.).

PMT achieved twice higher single photon detection efficiency because the photoelectron collection efficiency was also greatly improved. The timing and charge resolutions at single photoelectron also becomes much better as 1.1 ns and 35% which can be compared with 2.1 ns and 53% of the Super-K PMT, respectively. These outstanding improvements enhance Hyper-K detector performance and its physics reaches.

Moreover, pressure tolerance was improved up to the 125 m water depth in order to fit the 60 m depth of the detector water. New PMT cover which consists of a stainless steel vessel and an UV transparent acrylic cap was established by an implosion test at 80 m water depth.

Location

One of technical challenges of the project is to realize a gigantic underground cavern for the Hyper-K detector. In order to pin down the candidate place, seismic prospecting by using artificially generated elastic wave was performed at the area of (400 m)³. Receivers or sensors, called ‘geophones,’ which detect the elastic wave, were installed in six tunnels at 111 locations with three geophones to capture triaxial components of the elastic wave for each. A seismic source is set in the tunnels and generated the elastic wave at 738 points.

The data obtained in the seismic survey were analyzed with two methods, seismic tomography and reflection imaging. Figure 43 shows the results of reflection imaging overlaid with known faults and fracture zones. The study identified the known faults as expected, while there was no new faults found at the central region. Figure 44 is rock class distribution made by combining the results of seismic tomography, reflection imaging, and the past geological survey. In both figures, the red dashed rectangle denotes a region which has the best rock quality and the least uneven rock over the entire Hyper-K candidate site. We successfully found the candidate place that is suitable for the gigantic cavern construction.

Physics

Hyper-K will be able to measure the magnitude of the CP violation with high precision, which could explain the baryon asymmetry in the Universe. Figure 45 shows an expected significance of the CP violation discovery by ten years operation. Hyper-K covers the 76% of δ_{CP} parameter space with 3σ or more significance, and 57% of the parameter space with 5σ or more. Hyper-K will go beyond 7σ significance if $\delta_{CP} = -90^\circ$ as suggested by T2K[2] and NOvA[3] results.

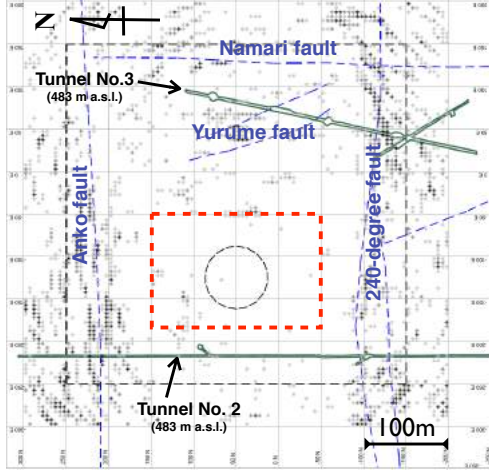


Fig. 43. Top view of reflection imaging by seismic prospecting at altitude of 483 m above sea level. Asterisks (*) indicate the reflection positions where reflection happens which indicate faults, fracture zone, and open cracks in the bedrock. Blue dashed lines indicate the location of known faults. The red dashed rectangles denotes a selected candidate region for Hyper-K cavern. Dashed circle indicates the size of the Hyper-K cavern.

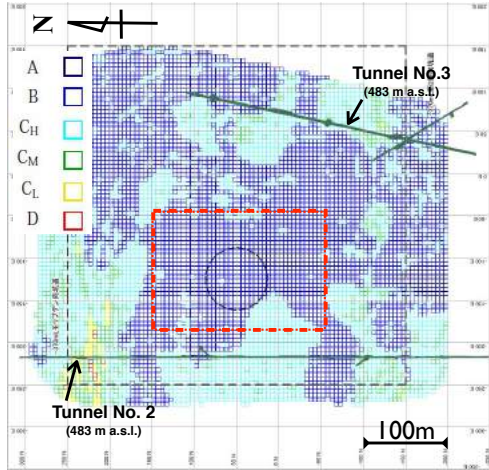


Fig. 44. Rock class distribution obtained by combining the results of seismic tomography, reflection imaging and the geological survey results with bore-hole and the existing tunnels. The red dashed rectangles and dashed black circle are same manners as in Fig. 43.

Figure 46 shows the discovery significance for the case of $\delta_{CP} = -90^\circ$ as a function of year. The US-based program LBNF/DUNE [6] plans to start its beam in 2026 and it is critical for Hyper-K to start its construction and operation on time.

A proton decay $p \rightarrow e^+ \pi^0$ is an important signal favored by many Grand Unified Theory models with a prediction close to the current limit of the proton decay life time. Figure 47 shows the 3σ discovery potential for the $p \rightarrow e^+ \pi^0$ mode as a function of year. Hyper-K is an only realistic proposal which

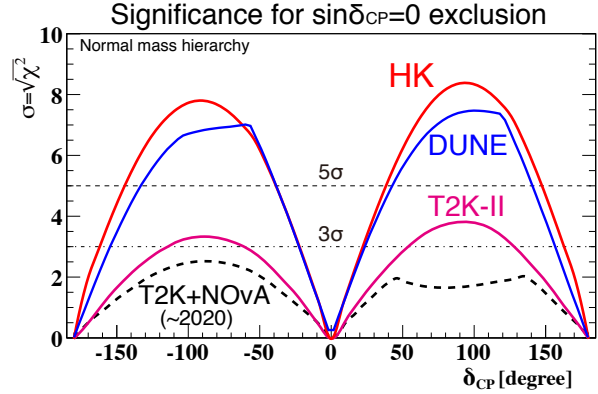


Fig. 45. Significance of the CP violation discovery in lepton sector with a 10-year observation in Hyper-K (HK) as a function of the unknown CP phase. The normal neutrino mass hierarchy is assumed. Ongoing and planned long baseline experiments are superimposed [4, 5].

CPV significance for $\delta_{CP} = -90^\circ$, normal hierarchy

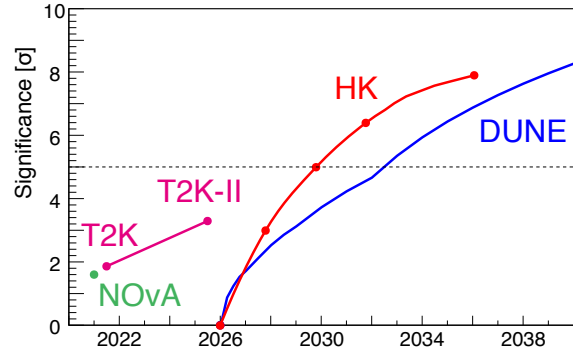


Fig. 46. Discovery potential of the CP violation in lepton sector as a function year. The normal neutrino mass hierarchy is assumed. Ongoing and planned long baseline experiments are superimposed [4, 5].

can go beyond the proton lifetime of 1×10^{35} years.

As well as the supernova burst neutrino that was successfully observed in Kamiokande at once, undiscovered supernova relic neutrinos, accumulated by past all supernovae since the beginning of the universe, are interesting events to explore the history of heavy elements and the onset of stellar formation. Figure 48 shows the expected number of events as a function of year.

Community support and Organization

The Hyper-K project has been supported by both the Japan Association of High Energy Physicists (JAHEP) and the Cosmic Ray Researchers Congress (CRC) in Japan. In January 2015, ICRR and KEK-IPNS signed a memorandum of understanding (MoU) for cooperation on the Hyper-K project. In June 2016, KEK Project Implementation Plan (KEK-PIP) has been released [11], where the first priority was given to upgrade of the J-PARC accelerator for the Hyper-K experiment. Finally the ICRR released report by the future project committee in March 2017 and Hyper-K is recognized as a ICRR's

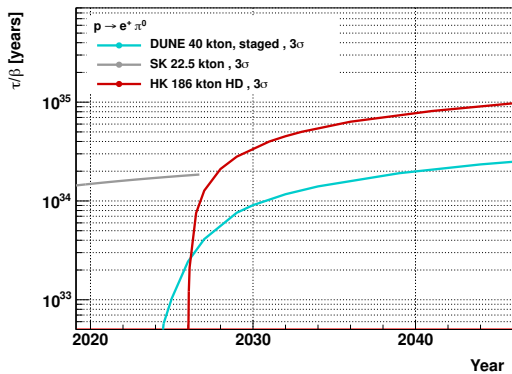


Fig. 47. The $p \rightarrow e^+ \pi^0$ discovery reach in proton lifetime with 3σ significance as a function of year. It shows Hyper-K (HK) planning to start in 2026, superimposed with the ongoing Super-K (SK) and planned DUNE experiments. The DUNE project assumes 10 kton operation from 2024, toward full 40 kton by increasing 10 kton every year[6].

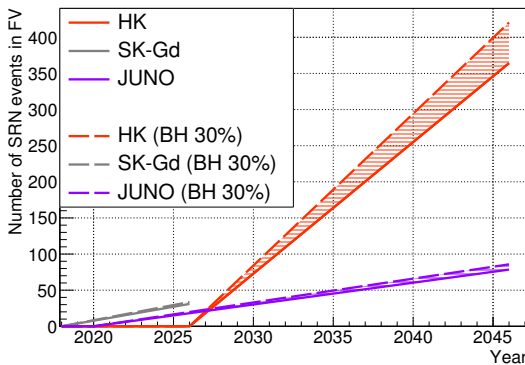


Fig. 48. The accumulated number of supernova relic neutrino events as a function of year. The JUNO experiment and SK-Gd are also plotted [7, 8, 9, 10]. Effective temperature of neutrinos inside supernova is assumed to be 6 MeV. The solid line assumes no black hole formation while the dashed line assumes that 30% of core-collapse stars form a black hole.

next main project.

In addition, a new institute of “Next-generation Neutrino Science Organization” will be formed in October 2017 in the University of Tokyo in order to promote the project. At the beginning, it will consist of around 25 leading researchers in the neutrino physics field, from ICRR, Kavli Institute for the Physics and Mathematics of the Universe (IPMU) and Graduate School of Science in the University of Tokyo.

In conclusion, Hyper-K is a promising experiment to bring unique and leading results in near future as an important Roadmap of the future neutrino program in Japan, and essential for the progress of particle physics and astronomy.

Bibliography

- [1] “Hyper-Kamiokande Design Report,”
KEK Preprint 2016-21 / ICRR-Report-701-2016-1

- [2] K. Abe *et al.* [T2K Collaboration],
Phys. Rev. Lett. 118, 151801.
- [3] P. Adamson *et al.* [NOvA Collaboration],
Phys. Rev. Lett. 118, 231801.
- [4] K. Abe *et al.* [The T2K Collaboration],
arXiv:1609.04111 [physics.ins-det].
- [5] K. Abe *et al.* [The T2K Collaboration],
PTEP **2015**, no. 4, 043C01 (2015).
- [6] R. Acciarri *et al.* [The DUNE Collaboration],
arXiv:1601.05471 [physics.ins-det].
- [7] H. Sekiya [Super-K Collaboration],
PoS(ICHEP2016) 982 (2016).
- [8] ICRR News (2016), <http://www.icrr.u-tokyo.ac.jp/2016/06/30101400.html>.
- [9] F. An *et al.* [JUNO Collaboration],
J. Phys. G **43**, no. 3, 030401 (2016).
- [10] Yu-Feng LI, Presentation at “Workshop on Supernova at Hyper-Kamiokande” (2017).
- [11] KEK Roadmap (Project Implementation Plan),
<https://www.kek.jp/ja/About/Organization/Overview/Assessment/Roadmap/KEK-PIP.pdf> (2016).

HIGH ENERGY COSMIC RAY DIVISION

Overview

There are three major experimental research activities in the High Energy Cosmic Ray Division, the study of high energy gamma rays and the development of the next generation gamma-ray telescopes by the Cherenkov Cosmic Gamma Ray group, the study of extremely high energy cosmic rays by the Telescope Array (TA) group, and the study of very high energy cosmic rays and gamma rays by the Tibet AS γ group.

Other activities, such as experiments utilizing the Akeno observatory, the Norikura observatory, the Mt. Chacaltaya observatory (jointly operated with Bolivia) are closely related to inter-university joint research programs. Also an all-sky high resolution air-shower detector (Ashra) is in partial operation on the Hawaii island. The High Energy Astrophysics group created in the fiscal year 2009 aims to explore various high energy astrophysical phenomena, through theoretical and observational approaches.

The CANGAROO telescopes had been in operation in South Australia since 1992, with a 3.8 m small telescope and then with four 10 m telescopes. The major scientific objective was the study of Very High Energy (VHE) gamma-ray sources in our galaxy in the southern hemisphere. The mission of these telescopes was completed and the CANGAROO observation site was closed in 2011.

For further development of VHE gamma-ray astronomy, the Cherenkov Cosmic Gamma Ray group is working on the design study and development of the next generation international ground-based gamma-ray observatory CTA which will offer an order of magnitude better sensitivity than currently running Cherenkov telescopes, three times better angular resolution, and wider energy coverage from 20 GeV to 100 TeV or higher.

At the Akeno observatory, a series of air shower arrays of increasing geometrical sizes were constructed and operated to observe extremely high energy cosmic rays (EHECRs). The Akeno Giant Air Shower Array (AGASA) was operated from 1991 to January 2004 and covered the ground area of 100 km² as the world largest air shower array. In 13 years of operation, AGASA observed a handful of cosmic rays exceeding the theoretical energy end of the extra-galactic cosmic rays (GZK cutoff) at 10²⁰ eV.

The Telescope Array (TA), a large plastic scintillator array with air fluorescence telescopes, has been constructed in Utah, USA, which succeeds AGASA and measures the EHECRs with an order of magnitude larger aperture than that of AGASA for the further study of EHECRs. The full-scale TA is accumulating data as the largest array viewing the northern sky and observed the energy spectrum with high statistics, which is in good agreement with the GZK suppression.

An air shower experiment aiming to search for celestial gamma-ray point sources started in 1990 with Chinese physicists at Yangbajing (Tibet, 4,300 m a.s.l.). This international collaboration is called the Tibet AS γ Collaboration. An ex-

tension of the air shower array was completed in 1995 and an emulsion chamber has been combined with this air shower array since 1996 to study the primary cosmic rays around the knee energy region. After successive extensions carried out in 1999, 2002 and 2003, the total area of the air shower array amounts to 37,000 m². The sun's shadow in cosmic rays affected by the solar magnetic field was observed for the first time in 1992, utilizing its good angular resolution at multi-TeV energy region.

The High Energy Astrophysics group is conducting theoretical researches on fundamental processes responsible for non-thermal particle acceleration in various astrophysical environments, including first-order diffusive shock acceleration, second-order stochastic acceleration in shock downstream regions, modification of shock structure by pick-up interstellar neutrals, as well as injection processes of suprathermal particles. In addition to these theoretical works, R/D studies for radio observations of pulsars and cosmic ray air showers are also being made.

Cherenkov Cosmic Gamma-Ray Group

CTA Project (Cherenkov Telescope Array)

CTA-Japan Consortium

[Spokespersons : M.Teshima and H.Kubo]

Collaboration list:

Institute for Cosmic Ray Research, The University of Tokyo, Chiba, Japan; Department of Physics, Aoyama Gakuin University, Tokyo, Japan; Department of Physics, Hiroshima University, Hiroshima, Japan; Hiroshima Astrophysical Science Center, Hiroshima University, Hiroshima, Japan; Faculty of Science, Ibaraki University, Ibaraki, Japan; Institute of Particle and Nuclear Studies, High Energy Accelerator Research Organization (KEK), Ibaraki, Japan; Department of Physics, Konan University, Hyogo, Japan; Faculty of Medical Engineering and Technology, Kitasato University, Kanagawa, Japan; Graduate School of Science and Technology, Kumamoto University, Kumamoto, Japan; Department of Physics, Kyoto University, Kyoto, Japan; Department of Applied Physics, University of Miyazaki, Miyazaki, Japan; Department of Physics, Nagoya University, Aichi, Japan; Institute for Space-Earth Environmental Research, Nagoya University, Aichi, Japan; Kobayashi-Maskawa Institute, Nagoya University, Aichi, Japan; Department of Earth and Space Science, Osaka University, Japan; Department of Physics, Kinki University, Osaka, Japan; Astrophysical Big Bang laboratory, RIKEN, Wako, Japan; Department of Physics, Rikkyo University, Tokyo, Japan; Department of Physics, Saitama University, Saitama, Japan; Institute of Space and Astronautical Science, JAXA, Kanagawa,

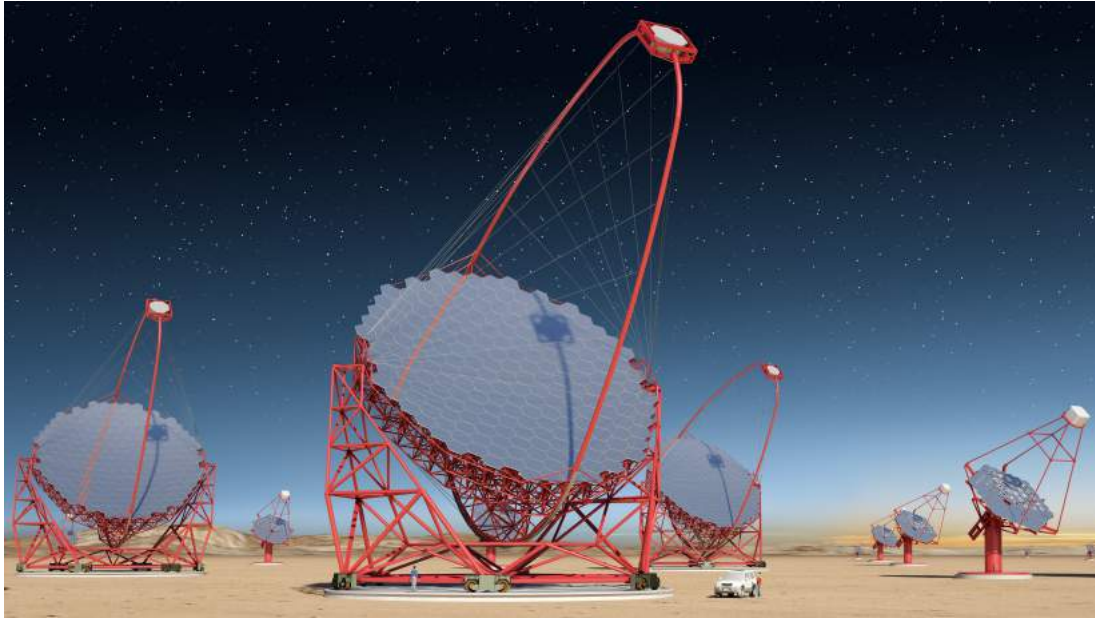


Fig. 1. Artist view of the CTA observatory. CTA consists of three types of telescopes, Large Size Telescopes (23m diameter), Mid Size Telescopes (12m) and Small Size Telescopes (4m), and covers the broad energy band from 20GeV to 100TeV.

Japan; Department of Physics, Tokai University, Kanagawa, Japan; Faculty of Integrated Arts and Sciences, The University of Tokushima, Tokushima, Japan; Department of Astronomy, The University of Tokyo, Tokyo, Japan; Department of Physics, The University of Tokyo, Tokyo, Japan; Faculty of Science and Engineering, Waseda University, Tokyo, Japan; Department of Physics, Yamagata University, Yamagata, Japan; Faculty of Management Information, Yamanashi Gakuin University, Yamanashi, Japan [1].

CTA Project

During the past several years, Very High Energy (VHE) gamma-ray astronomy has made spectacular progress and has established itself as a vital branch of astrophysics. To advance this field even further, we propose the Cherenkov Telescope Array (CTA) [5], the next generation VHE gamma ray observatory, in the framework of a worldwide, international collaboration. CTA is the ultimate VHE gamma ray observatory, whose sensitivity and broad energy coverage will attain an order of magnitude improvement above those of current Imaging Atmospheric Cherenkov Telescopes (IACTs). By observing the highest energy photons known, CTA will clarify many aspects of the extreme Universe, including the origin of the highest energy cosmic rays in our Galaxy and beyond, the physics of energetic particle generation in neutron stars and black holes, as well as the star formation history of the Universe. CTA will also address critical issues in fundamental physics, such as the identity of dark matter particles and the nature of space and time.

VHE gamma rays from 100GeV to 10TeV can be observed with ground-based IACTs. The history of VHE gamma ray astronomy began with the discovery of VHE gamma rays from the Crab Nebula by the Whipple Observatory in 1989. To

date, the current generation IACTs featuring new technologies, such as H.E.S.S., MAGIC, VERITAS, and CANGAROO, have discovered more than 200 Galactic and extragalactic sources of various types.

CTA is designed to achieve superior sensitivity and performance, utilizing established technologies and experience gained from the current IACTs. The project is presently in its pre-construction (prototyping) phase, with international efforts from Japan, US, and EU countries. It will consist of several 10s of IACTs of three different sizes (Large Size Telescopes, Mid Size Telescopes, and Small Size Telescopes). With a factor of 10 increase in sensitivity ($1\text{m Crab} \sim 10^{-14}\text{ergs}^{-1}\text{cm}^{-2}$), together with a much broader energy coverage from 20GeV up to 100TeV, CTA will bring forth further dramatic advances for VHE gamma ray astronomy. The discovery of more than 1000 Galactic and extragalactic sources is anticipated with CTA.

CTA will allow us to explore numerous diverse topics in physics and astrophysics. The century-old question of the origin of cosmic rays is expected to be finally settled through detailed observations of supernova remnants and other Galactic objects along with the diffuse Galactic gamma ray emission, which will also shed light on the physics of the interstellar medium. Observing pulsars and associated pulsar wind nebulae will clarify physical processes in the vicinity of neutron stars and extreme magnetic fields. The physics of accretion onto supermassive black holes, the long-standing puzzle of the origin of ultrarelativistic jets emanating from them, as well as their cosmological evolution, will be addressed by extensive studies of active galactic nuclei (AGN). Through dedicated observing strategies, CTA will also elucidate many aspects of the mysterious nature of gamma ray bursts (GRBs), the most energetic explosions in the Universe. Detailed studies of both

AGNs and GRBs can also reveal the origin of the highest energy cosmic rays in the Universe, probe the cosmic history of star formation including the very first stars, as well as provide high precision tests of theories of quantum gravity. Finally, CTA will search for signatures from elementary particles constituting dark matter with the highest sensitivity yet. Realisation of the rich scientific potential of CTA is very much feasible, thanks to the positive experience gained from the current IACTs.

The CTA-Japan consortium [1] is aiming at contributing in particularly to the construction of the Large Size Telescopes (LSTs) and is involved in their development. The LST covers the low energy domain from 20GeV to 1000GeV and is especially important for studies of high redshift AGNs and GRBs. The diameter and area of the mirror are 23m and 400m², respectively, in order to achieve the lowest possible energy threshold of 20GeV. All optical elements/detectors require high specifications, for example, high reflectivity, high collection efficiency, high quantum efficiency and ultra fast digitisation of signal, etc. For this purpose, CTA-Japan is developing high quantum efficiency photomultipliers, ultrafast readout electronics and high precision segmented mirrors. On the strength of their experience gained from construction of the MAGIC telescope, the Max-Planck-Institute for Physics in Munich is responsible for the design of the 23m diameter telescope structure, based on a carbon fiber tube space frame. The LSTs require very fast rotation (180 degrees/20seconds) for promptly observing GRBs. The first LST will be built in the CTA North, La Palma, Spain in 2017 and three more LSTs will be built during 2018 to 2020, then four more LSTs in the CTA South will be built in the ESO site in Paranal, Chile. The location of the LST array in the CTA North will overlap with MAGIC telescopes, which will allow us to operate CTA-LSTs and MAGIC telescopes together in the early phase of the construction.

The Cherenkov Cosmic Gamma Ray group is also operating the MAGIC Telescopes [9] on La Palma, Canary Islands. This facility is used not only for scientific observations but also for technological development toward the future observatory CTA.

Bibliography

- [1] CTA Consortium website: <http://www.cta-observatory.jp/> and <http://www.cta-observatory.org/>.
- [2] The Cherenkov Telescope Array potential for the study of young supernova remnants, *Astropart. Phys.* 62 (2015) 152-164.
- [3] Introducing the CTA concept, The CTA Consortium, *Astropart. Phys.* 43 (2013) 3-18.
- [4] Gamma-ray burst science in the era of the Cherenkov Telescope Array, S. Inoue et al., *Astropart. Phys.* 43 (2013) 252-275.
- [5] Design Concepts for The Cherenkov Telescope Array, The CTA Consortium, *Exper. Astron.* 32 (2011) 193-316.

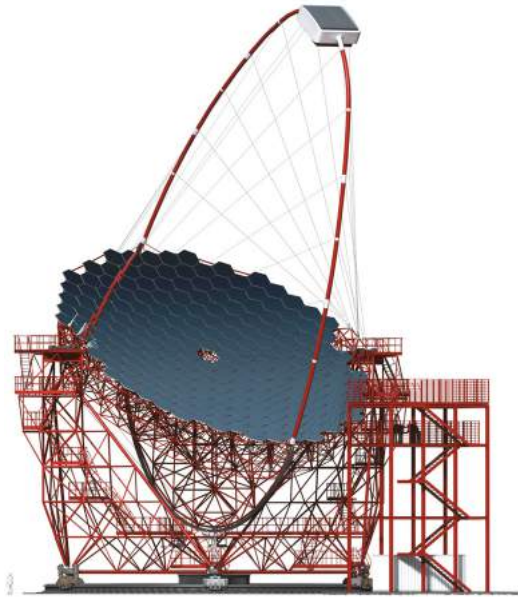


Fig. 2. Large Size Telescope (23m diameter) designed by Max-Planck-Institute for Physics. CTA Japan is contributing to the design and prototyping of the imaging camera at the focal plane, ultrafast readout electronics, and high precision segmented mirrors.



Fig. 3. Camera cluster for the Large Size Telescope (LST) developed by CTA-Japan. This cluster consists of seven high quantum efficiency photomultipliers (R11920-100), CW High Voltages, pre-amplifier, Slow Control Board, DRS4 Ultra fast waveform recording system and Trigger. The LST camera can be assembled with 265 of these clusters, cooling plates and camera housing.

- [6] Status of Very High Energy Gamma Ray Astronomy and Future Prospects, M. Teshima, *The Astronomical Herald*, 104 (2011) 333-342.
- [7] Design Study of a CTA Large Size Telescope, Proc. of ICRC2012 at Beijing China, M. Teshima, arXiv:1111.2183.
- [8] Introducing the CTA Concept, B. Acharya et al., *Astroparticle Physics*, 34 (2013) 3.
- [9] MAGIC Collaboration website: <http://magic.mppmu.mpg.de/>.



Fig. 4. The high precision segmented mirrors for the Large Size Telescope (LST) developed by CTA-Japan in cooperation with Sanko Co.LTD. The mirror is made of a 60mm thick aluminum honeycomb sandwiched by 3mm thin glass on both sides. A surface protection coat consisting of the materials SiO₂ and HfO₂ is applied to enhance the reflectivity and to elongate the lifetime.

MAGIC

The MAGIC Collaboration has built in 2002 / 2003 a first large atmospheric imaging Cherenkov telescope, MAGIC-I, with a mirror surface of 236 sq.m. and equipped with photomultiplier tubes of optimal efficiency. In 2009, a second telescope of essentially the same characteristics was added; MAGIC-II was installed at a distance of 85m from MAGIC-I. With the accent of these instruments on large mirror surface and best light collection, cosmic gamma-rays at an energy threshold lower than any existing or planned terrestrial gamma-ray telescope have become accessible. So far achieved has been a threshold of 25 GeV. The Japanese group has joined the MAGIC collaboration since 2010, and contributed to the operation, observations and data analysis. The MAGIC telescopes are upgraded with new cameras, electronics and partially new mirrors in 2012, and are now operated with an unprecedented sensitivity by an international collaboration of 17 institutes from 8 countries.

The recent highlights from MAGIC are, 1) the successful observation of pulsed gamma ray signal from the Crab pulsar up to TeV regime [1], 2) the discoveries of the most distant blazars 3S 0218 + 35 with the redshift of 0.944 [2] and PKS 1441 + 25 with the redshift of 0.939 [3], 3) the observation of the very fast flare of 1min time scale from the blazar inside Perseus cluster, IC310 [4]. These results brought new questions on the pulsar emission mechanism, the EBL energy density, and gamma ray emission mechanism from the supermassive blackholes or vicinity of them.

Bibliography

- [1] Phase-resolved energy spectra of the Crab pulsar in the range of 50-400 GeV measured with the MAGIC telescopes, the MAGIC Collaboration, Aleksić et al. *A&A* 540 (2012) A69.
- [2] ATEL 6349.
- [3] ATEL 7416.
- [4] Black hole lightning due to particle acceleration at sub-horizon scales, the MAGIC collaboration, *Science* 346 (2014) 1080-1084.



Fig. 5. MAGIC Stereo System with two Cherenkov telescopes of 17m diameters, so far achieved the threshold energy of 25GeV. It locates near the mountain top of the Roque de los Muchachos on the Canary Island of La Palma. Two telescopes are located with the distance of 85 meters.



Fig. 6. Akeno atmospheric Cherenkov telescope of 3 m diameter, located in the Akeno Observatory.

Other Activities

As a test bench for domestic R & D activities of future ground-based gamma-ray observatory projects, an old atmospheric Cherenkov telescope of 3 m diameter was repaired and then placed at the Akeno Observatory in November 2010. This telescope shown in Figure 6 (Akeno telescope, hereafter) is currently the only atmospheric Cherenkov telescope located in Japan [1]. We have developed an R & D imaging camera system with the Akeno telescope since 2009, of which the purpose is to make a battery-powered data acquisition system for a future mobile imaging atmospheric Cherenkov telescope array [2]. In the fiscal year 2016, test observations of atmospheric Cherenkov light events with the R & D system were successfully carried out at Akeno. An example of a recorded atmospheric Cherenkov light image is shown in Figure 7. Observed data are currently under analysis for estimating basic system performance. We are going to try to detect gamma-ray events from the Crab Nebula using this system in the next fiscal year.

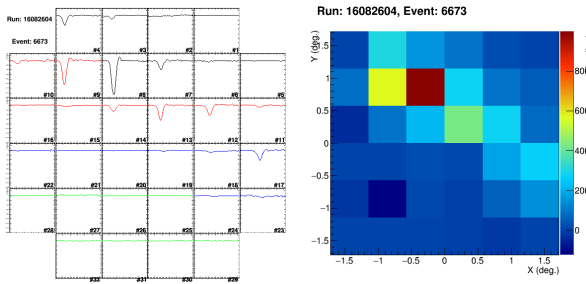


Fig. 7. Example of an atmospheric Cherenkov light image recorded by the R & D imaging camera system installed in the Akeno telescope. The left: atmospheric Cherenkov light pulse profiles recorded with individual 32 pixels (PMTs). The width of each box corresponds to 64 ns. The right: color map of atmospheric Cherenkov light brightness (integrations of the left pulses).

Bibliography

- [1] M. Ohishi et al., Proc. of 33rd Internat. Cosmic Ray Conf. (Rio de Janeiro), 587 (2013).
- [2] T. Yoshikoshi et al., Proc. of 34th Internat. Cosmic Ray Conf. (The Hague), 887 (2015).

TA: Telescope Array Experiment

[Spokespersons: H. Sagawa¹, G. B.Thomson²]

1 : ICRR, The Univ. of Tokyo, Kashiwa, Chiba 277-8582

2 : Dept. of Physics, University of Utah

Collaborating Institutions:

Chiba Univ., Chiba, Japan; Chubu Univ., Kasugai, Japan; Earthquake Research Institute, Univ. of Tokyo, Tokyo, Japan; Ehime Univ., Matsuyama, Japan; Ewha W. Univ., Seoul, Korea; Hiroshima City Univ., Hiroshima, Japan; Hanyang Univ., Seoul, Korea; ICRR, Univ. of Tokyo, Kashiwa, Japan; INR, Moscow, Russia; IPMU, Univ. of Tokyo, Kashiwa, Japan; Kanagawa Univ., Yokohama, Japan; KEK/ IPNS, Tsukuba, Japan; Kinki Univ., Higashi-Osaka, Japan; Kochi Univ., Kochi, Japan; Kyushu Univ., Fukuoka, Japan; Moscow M.V. Lomonosov State University; Nat. Inst. of Rad. Sci., Chiba, Japan; Osaka City Univ., Osaka, Japan; RIKEN, Wako, Japan; Ritsumeikan Univ., Kusatsu, Japan; Rutgers Univ., Piscataway, NJ, USA; Saitama Univ., Saitama, Japan; Shinshu Univ., Nagano, Japan; SKKU, Suwon, Korea; Tokyo City Univ., Tokyo, Japan; Tokyo Inst. of Tech., Tokyo, Japan; Tokyo Univ. of Science, Noda, Japan; ULB, Brussels, Belgium; UNIST, Ulsan, Korea; Univ. of Utah, Salt Lake City, USA; Univ. of Yamanashi, Kofu, Japan; Waseda Univ., Tokyo, Japan; Yonsei Univ., Seoul, Korea

Overview and Status of TA, Tax4 and TALE

TA

The Telescope Array (TA) is the largest Ultra-High-Energy Cosmic-Ray (UHECR) observatory in the Northern Hemis-

phere, located in the West Desert in Utah, the USA (latitude 39.3° N, longitude 112.9° W, altitude ~1400 m) [1]. TA is designed to observe extensive air showers (EAS) induced by UHECRs above 10^{18} eV, and measures the energy spectrum, mass composition, and arrival direction distribution of UHECRs. The aim of these measurements is to explore the origin, propagation and interaction of UHECRs. The TA detector consists of an air shower surface detector (SD) array of plastic scintillation counters to measure the lateral distribution of secondary particles on the ground, and fluorescence detectors (FDs) to measure the longitudinal development of the EAS in the atmosphere. The SD array consists of 507 counters each with an area of 3 m², which were deployed on a square grid with 1.2-km spacing between each, covering an area of approximately 700 km². Three FD stations are located at the periphery, looking inward over the SD array. The Middle Drum (MD) FD site is located to the north of the SD array, and is instrumented with 14 refurbished telescopes that were used at the High-Resolution Fly's Eye (HiRes) [2]. The Black Rock Mesa (BRM) and Long Ridge (LR) FD sites are located to the southeast and southwest of the SD array, respectively. They are each instrumented with 12 new telescopes. The TA detector is operated by an international collaboration of researchers from Japan, the USA, Korea, Russia, and Belgium. Hybrid observations using both SDs and FDs commenced in March 2008.

TAx4

TA found evidence for intermediate-scale anisotropy of the highest-energy cosmic rays ($E > 5.7 \times 10^{19}$ eV). With enhanced statistics, we expect to observe the structure of the hotspot along with other possible excesses, point sources along with the correlations with extreme phenomena in the nearby universe. Based on this picture, we proposed to quadruple the area of the TA SD aperture. We plan to install additional 500 counters of the current TA SD design, which will be deployed on a square grid with wider, 2.08-km spacing between each [3]. Including the existing TA SD array, we will extend the aperture of the surface detector array in total to approximately 3,000 km². The new array would need two FD stations overlooking it to confirm the energy scale and to increase the number of hybrid events for the measurement of the depth of shower maximum X_{\max} . These FDs will be formed using additional refurbished HiRes telescopes. This TA extension, which we call Tax4, will greatly accelerate the pace at which we will reach the goals. The layout of Tax4 is shown in Figure 8.

The proposal of the SD part of Tax4 that was applied to the Japan Society for the Promotion of Science through Grant-in-Aid for Scientific Research on Specially Promoted Research (PI: H. Sagawa of ICRR) was approved in Japan in 2015. It is in effect over a period of five years. Recorded data will clarify anisotropy of arrival directions of highest-energy cosmic rays, which can be originated from the matter structure or extreme phenomena in the nearby universe. The FD part of Tax4 was approved by NSF in the USA in 2016.

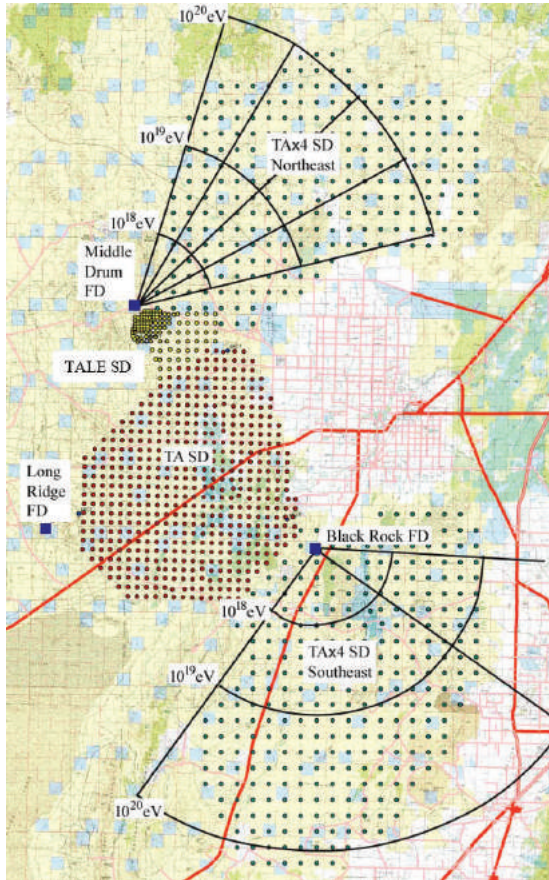


Fig. 8. The layout of the proposed TAX4. The array of 507 SDs (red filled circles) is the current TA SD array. There are three TA FD stations (MD to the north, LR to the west, and BRM to the east of the TA SD array). The array of surface detectors to the north of the TA SD array is the TALE SD array (yellow filled circles). Additional two sub-arrays of 500 surface detectors in total (green filled circles) for TAX4 are located to the northeast and southeast of the TA SD array. Additional two FD stations with refurbished HiRes telescopes for the TAX4 are located at the MD and BRM FD sites (blue filled squares) and view to the northeast and southeast as denoted each by a fan.

TALE

The TA Low Energy Extension (TALE) enables detailed studies of the energy spectrum and composition from $\sim 10^{16}$ eV upwards. Previous experiments reported the second knee in the cosmic-ray spectrum around the 10^{17} -eV decade. The energy scales of these detectors differed by about a factor of two, so the energy at which this spectral break occurred was quite uncertain. The transition from galactic cosmic rays to extragalactic cosmic rays may take place around this energy region. Thus we expect to observe the transition from heavy to light composition. A 14-TeV center-of-mass collision at the LHC corresponds to a proton of approximately 10^{17} eV colliding with another proton at rest. The cosmic-ray data observed by the TALE could be compared with the air shower Monte Carlo (MC) simulation tuned by the results of the LHC experiments.

The TALE detector is located north of the TA site. Ten ad-

ditional TALE FDs view 31° – 59° in elevation, and have been operational using refurbished HiRes-II telescopes. The TALE infill SD array consists of approximately 100 plastic scintillation counters, which are identical to those of the TA SD array. These counters have graded spacings, ranging from 400 m near the FD to 600 m further away, which merge into the TA SD array with 1200-m spacing at its northwestern corner. The TALE FD operation was commenced in the spring of 2013. The 35 TALE surface detectors were deployed at that time, and 16 surface detectors have been running.

We saw two clear breaks at around $10^{16.3}$ eV and $10^{17.2}$ eV in the energy spectrum measured with the TALE FD as shown in Figure 9. It is of importance to measure X_{\max} precisely adding timing information of surface detectors near the shower core on the ground. Therefore we proposed to complete the TALE surface detectors by adding remaining surface detectors. The proposal of adding remaining SDs in the TALE SD array was applied for the Japan Society for the Promotion of Science through Grant-in-Aid for Scientific Research (S) (PI: S. Ogio of Osaka City University) and was approved in Japan in 2015. It is in effect over a period of five years.

The permission of the TAX4 SD deployment has not yet been obtained from BLM (Bureau of Land Management). As a test of new data acquisition system of surface detectors, 68 SDs were deployed in February of 2017. The full 103 TALE SDs will be tuned for full operation.

We are also proposing the observation of cosmic rays with energies further down to 10^{15} eV, which we call the Non-Imaging Cherenkov (NICHE) array [4]. The plan is to install an array of simple Cherenkov counters of PMTs each three inches in diameter on the ground looking upwards, deployed with 100-, 200-, and 400-meter spacings within the TALE infill array. We use counter timing to reconstruct the shower geometry, counter pulse heights to reconstruct the shower energy, and counter signal widths to reconstruct X_{\max} . The part of the NICHE with 15 PMTs that we call jNICHE has been approved in Japan in 2014 and supported by the Japan Society for the Promotion of Science through Grant-in-Aid for Young Scientists (A) (PI: Y. Tsunesada of Osaka City University). It is being constructed. The full NICHE will be proposed to the NSF in the USA.

Energy Spectrum

The preliminary result of cosmic-ray spectra from TA was presented at UHECR2016 [5]. Figure 9a shows TA cosmic-ray fluxes multiplied by E^3 using the TA SD data, TA monocular FD data and TALE FD data.

The energy spectrum for four years of the TA SD data with zenith angles less than 45° has been published [6]. Here, we update the energy spectrum of cosmic rays above $10^{18.2}$ eV using the SD data for the first seven years of observations with an exposure of $6300 \text{ km}^2 \text{ sr yr}$. The MC data were generated by a CORSIKA air shower simulation with the QGSJET II-03 model. A GEANT4 simulation was used for the detector simulation. We use the correlation of S_{800} , which is the charge density at a distance of 800 m from the shower core, and zenith angle with primary energy from the MC study for the first estimation of the cosmic-ray energy. The energy scale uncertainty in the SD MC simulation can be large, mainly due

to the modeling of hadronic interactions. The energy scale uncertainty is experimentally controlled by the FD because the energy measurement is calorimetric. We correct our energy scale to the TA FD using events detected by both the FD and SD. The observed differences between the FD and SD events are well described by a simple proportionality relationship, where the SD energy must be reduced by 27% to agree with the FD energy. The red filled triangles correspond to the flux using TA SD data.

Two energy spectra measured by monocular analysis of the TA FD data are shown: one is obtained using cosmic-ray data above $10^{17.2}$ eV collected during the first seven years with the BRM and LR FDs (blue filled downward triangles) [7] and the other is obtained using cosmic-ray data above $10^{18.2}$ eV collected during the first five years with the MD FD (blue filled upward triangles) [8].

The energy spectrum using the TALE FD data is shown above $10^{15.5}$ eV with red filled circles [9]. The events observed with the TALE FD are placed into three subsets: Cherenkov dominated events, fluorescence dominated events, and mixed signal events. Different appropriate event selection criteria and quality cuts are applied to each set.

The resulting combined cosmic-ray flux multiplied by E^3 is shown together with a broken power-law fit in Figure 9b. TA confirmed the ankle at $10^{18.7}$ eV and the flux suppression above $10^{19.8}$ eV. The statistical significance of having the same spectral index above the ankle (no suppression) is $\sim 6\sigma$. And we see two clear breaks at around $10^{16.3}$ eV and $10^{17.2}$ eV in the energy region measured with the TALE FD. We possibly see the knee feature at around $10^{15.6}$ eV.

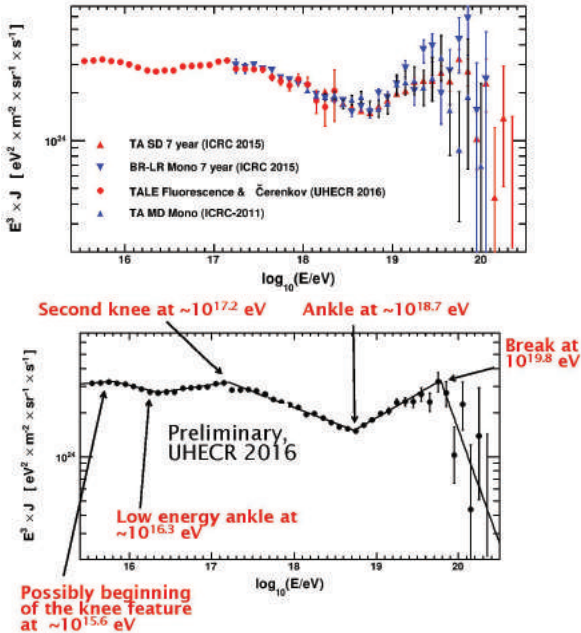


Fig. 9. The preliminary TA cosmic-ray fluxes multiplied by E^3 a) for TA SD data, TA monocular FD data and TALE telescope data. b) TA cosmic-ray combined flux multiplied by E^3 . The solid line shows the fit of the TA data to a broken power law.

Figure 10 is the TA and Auger energy spectra after Auger energies are rescaled by +10% as of ICRC2015. We see significant discrepancy with Auger above around 25 EeV, whereas we see good agreement everywhere below 25 EeV.

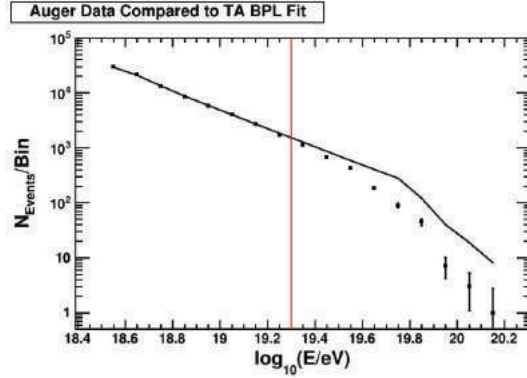


Fig. 10. The TA and Auger energy spectra after Auger energies were rescaled by +10% (as of ICRC2015). The solid line represents the broken power-law fit to the TA data. The dots represent the Auger data.

Figure 11 shows TA energy spectra of UHECR events with zenith angles up to 55° for the declination angle below 26° and greater than 26° . The positions of the break points of highest-energy suppression appear to be dependent on the declination. The effect of the difference is approximately 3.9σ .

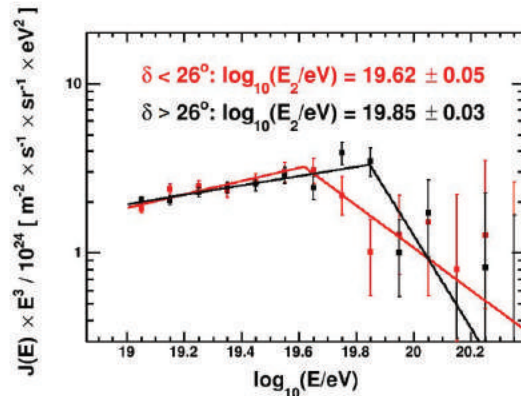


Fig. 11. The TA spectra of UHECR events with declination angles below 26° in red and above 26° in black

Mass Composition

The dependence of shower maximum depth, X_{\max} , on the primary energy is used to determine the mass composition. The HiRes result is consistent with proton-dominated composition for $E > 10^{18}$ eV [10], whereas the Auger result is compatible with mixed composition [11].

The X_{\max} result using the events observed with the MD FD and SDs (hybrid events) from May 2008 through May 2013 has been presented [12]. In this analysis, an updated version of the pattern recognition analysis (PRA) method, which

selects events that have a clear rise and fall in shower profile signal, is used. Using an updated version of the PRA method [13], a result of X_{\max} using the MD hybrid events in the seven year period is presented. Figure 12 shows the evolution of the average X_{\max} with energy together with the MC simulation for the MD hybrid data, BRM/LR hybrid data, and MD/BRM/LR stereo data. These three TA results are in agreement with light composition within systematic uncertainty.

The TA and Auger composition working group reported on a comparison of X_{\max} distributions measured by the Auger and TA observatories [14]. A direct comparison of the measured X_{\max} distributions is not correct due to different detector acceptances and resolutions as well as different analysis techniques. A set of showers compatible to the composition measured by the Auger detectors was simulated and reconstructed using the official TA software chain. This procedure simulates an energy-dependent composition mixture, which presents a good fit to Auger X_{\max} distributions, exposed through the detector acceptance, resolution and analysis procedure of the TA experiment. The TA data is within the systematics uncertainties compatible to a mixed composition as the one measured by the Auger detectors.

TA muon studies

The number of muons in inclined air showers observed with water Cherenkov surface detectors at the Pierre Auger Observatory is approximately 1.8 times that of the MC prediction with QGSJET II-03 hadronic model assuming proton primaries at 10^{19} eV [15]. We studied muons in air showers using the TA 7-years SD data [16]. Air shower events are classified using θ , ϕ and R parameters to search for the condition of high purity of muons. Here θ is the zenith angle of the shower axis, ϕ is the azimuthal angle of the location of a surface detector around the shower core on the ground, and R is the distance of the location of the surface detector from the shower axis. The direction of zero degrees of ϕ is opposite to the cosmic-ray incident direction projected onto the ground. The counterclockwise direction is positive. We compared the charge density from air shower signals of the data with that of the MC on the high-muon-purity condition ($30^\circ < \theta < 45^\circ$ and $150^\circ < |\phi| < 180^\circ$ (the older side in an inclined shower), $2000 \text{ m} < R < 4000 \text{ m}$) at $E \sim 10 \text{ EeV}$. This condition gives muon purity of $\sim 65\%$ from the MC expectation. Typical ratios of charge densities of the data to those of the MC are 1.72 ± 0.10 (stat) ± 0.40 (syst) at $1910 \text{ m} < R < 2160 \text{ m}$ and 3.14 ± 0.36 (stat) ± 0.72 (syst) at $2760 \text{ m} < R < 3120 \text{ m}$ as shown in Figure 13. The charge density of the data at larger R is larger than that of the MC.

In order to make direct comparisons between the SD detection techniques used by Auger and TA, we deployed and operate two Auger water Cherenkov surface detectors (one Auger-North type and one Auger-South type) at the TA Central Laser Facility (CLF) site [17]. At the CLF site, the TA muon detector project consisting of scintillators with concrete blocks and the detector with a lead sheet sandwiched between two scintillator plates is also ongoing. We took data of single muon signals from Auger SDs for calibration purpose and observed signals from Auger SDs that coincided with the air-

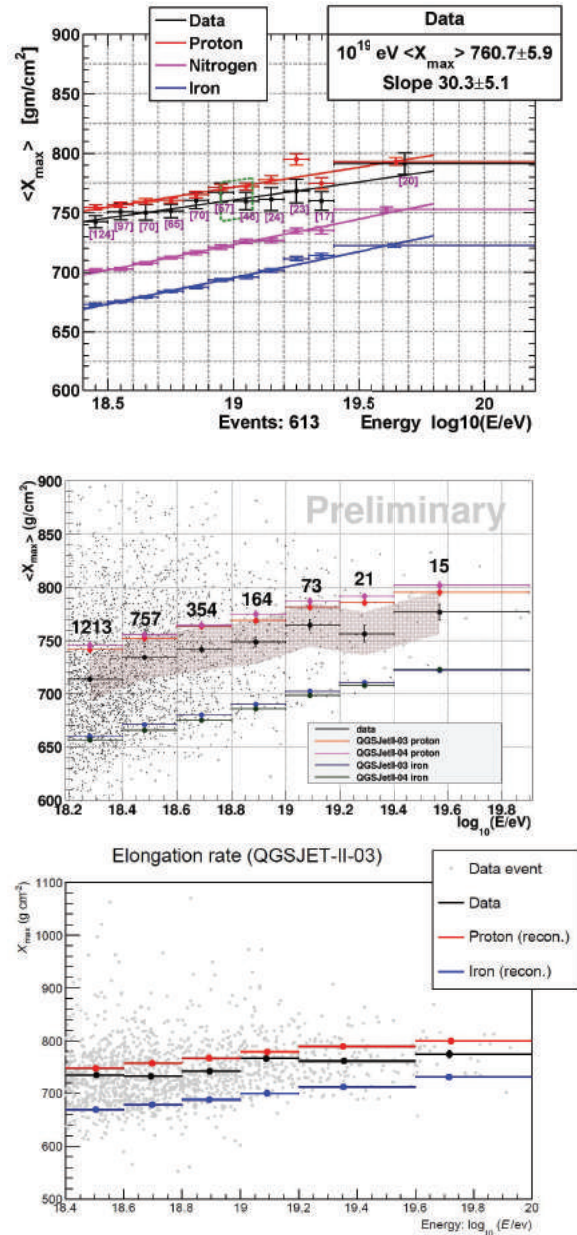


Fig. 12. The average reconstructed X_{\max} (black points) as a function of energy for a) the TA MD hybrid data, b) the TA BRM/LR hybrid data, and c) the TA stereo data. The black, red and blue colors denote the data, pure proton and iron predictions respectively. In a), the purple color corresponds to nitrogen prediction. In b), the red and purple colors denote QGSJET II-03 and QGSJET II-04 models, respectively, for proton prediction. The blue and green colors denote QGSJET II-03 and QGSJET II-04 models, respectively, for iron prediction.

shower events observed by the TA surface detectors.

Anisotropy in Arrival Directions of UHECRs

TA hotspot for the highest-energy cosmic rays

We have searched for intermediate-scale anisotropy of cosmic-ray events with energy greater than 5.7×10^{19} eV using five

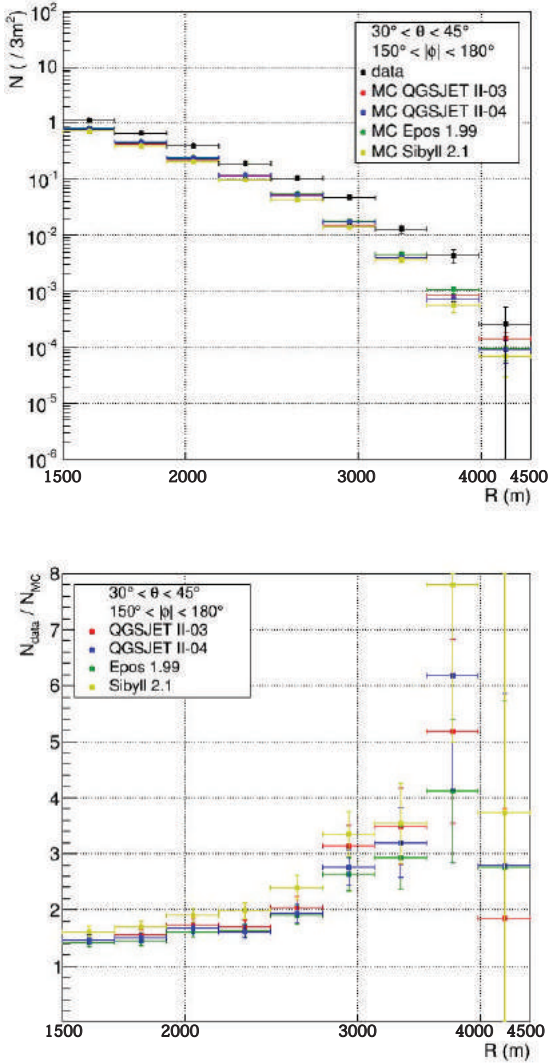


Fig. 13. The lateral distribution of air showers of the data together with those of the MC for $30^\circ < \theta < 45^\circ$, $150^\circ < |\phi| < 180^\circ$ and $1500 \text{ m} < R < 4500 \text{ m}$. (a) The lateral distribution of the average charge densities. The black, red, blue, green and yellow represent the data, QGSJET II-03, QGSJET II-04, EPOS 1.99 and Sibyll 2.1 models, respectively. (b) The average ratio of the data to the MC. The color corresponds to MC hadronic models described in (a).

years of the TA SD data [18]. Here we use the event selection somewhat looser than the TA standard anisotropy analysis [19] in order to increase the number of events with maintaining reasonable energy and angular resolution. We obtain 109 cosmic-ray events for seven years of TA SD data. In order to estimate the significance of this hotspot, we use oversampling with circles 20° in radius. The maximum excess in our Field-of-View (FoV) appears as a hotspot centered at right ascension of 148.4° and declination of 44.5° with a statistical significance of 5.1σ (the number of observed events = 24, and the number of events expected in an isotropic cosmic-ray sky = 6.88). The probability of such a hotspot appearing

by chance in an isotropic cosmic-ray sky is estimated to be 3.7×10^{-4} (3.4σ).

Hot/cold spot

An energy dependent intermediate-scale anisotropy was studied in the arrival directions of UHECRs above $10^{19.2} \text{ eV}$ in the northern hemisphere, using seven years of the TA SD data [20]. The energy distributions inside oversampled circles are compared to that outside using the Poisson Likelihood Ratio test. The maximum pre-trial significance was obtained to be 6.71σ at right ascension of 139° and declination of 45° . The energy distribution within the circle at the center of maximum significance shows a deficit of events below $10^{19.75} \text{ eV}$ and an excess above as shown in Figure 14. The post-trial probability of this energy anisotropy, appearing by chance anywhere on isotropic sky, is found by MC simulation to be 9×10^{-5} (3.74σ).

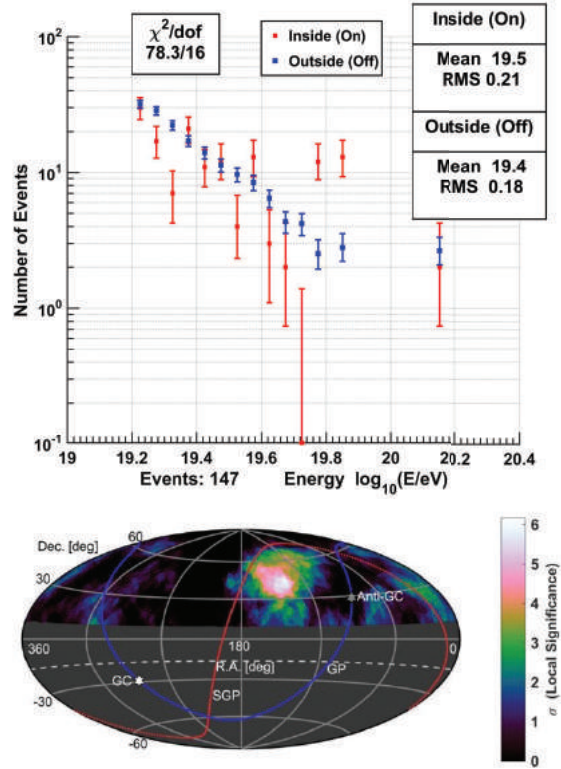


Fig. 14. a) The histogram of energies of events inside the spherical cap bin of radius 28.43° (red) at the maximum pre-trial significance. It's compared to the histogram of expected (normalized outside) energies (blue). b) The pre-trial energy spectrum anisotropy significance, for each spherical cap bin of radius 30° and $E \geq 10^{19.2} \text{ eV}$. The dashed curve at declination of -16° defines the TA FoV. Blue and red solid curves indicate the galactic plane (GP) and supergalactic plane (SGP), respectively. White and grey hexagrams indicate the galactic center (GC) and anti-galactic center (Anti-GC), respectively.

Spectrum anisotropy with respect to the supergalactic plane

In the cosmic-ray energy region above 10 EeV, the shape of cosmic-ray energy spectrum may carry an imprint of the

distribution of the cosmic-ray source density. The Super-Galactic anticenter direction is found. Using these data, we obtain an upper limit on the fraction of EeV cosmic rays of galactic origin at 1.3% at 95% confidence level.

The Super-Galactic plane (SGP) consists of local galactic clusters containing more nearby objects. By considering the effect of the loss of UHECRs due to attenuation during the propagation in the universe, the energy spectrum of UHECRs in the area near the SGP (On-source area) is expected to be different from that in the area far from the SGP (Off-source area) containing less nearby objects. Here the On-source area is defined as the area within $\pm 30^\circ$ from the SGP latitude of 0° and the Off-source area is defined as the area that is the rest in the sky. As shown in Figure 15, we find that the Off-source spectrum has a break at lower energy. The chance probability of obtaining such or larger difference in statistically equivalent distributions is estimated to be $6.2 \pm 1.1 \times 10^{-4}$ (3.2σ) by a MC simulation [21]. The observed difference in the spectra is in a reasonable quantitative agreement with a simplified model assuming that the UHECR sources trace the galaxy distribution from the 2MRS catalogue [22], primary particles are protons and the magnetic deflections are neglected.

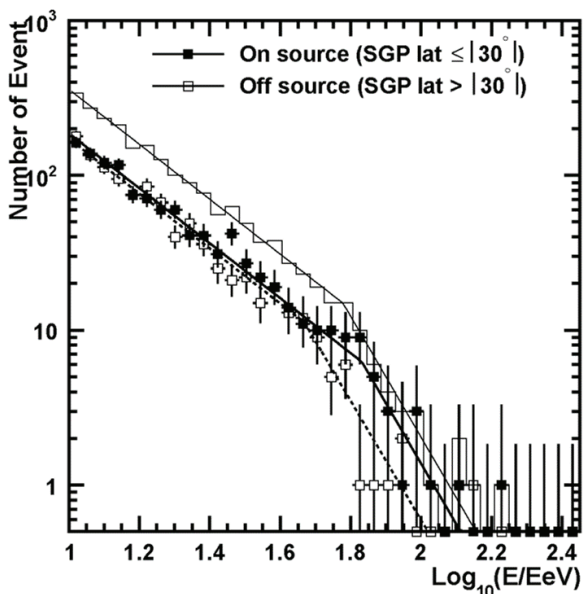


Fig. 15. The energy distributions of UHECR events observed with the TA surface detectors. The histogram shows the distribution of all events. Closed and open symbols show energy distributions observed in On- and Off-source areas respectively.

Search for EeV protons of galactic origin

To study the origin of EeV cosmic rays one can search for anisotropy in their arrival directions. Galactic cosmic rays of this type should be seen mostly along the galactic plane, and there should be a shortage of events coming from directions near the galactic anticenter. Guided by models of the galactic magnetic field that indicate that the enhancement along the galactic plane should have a standard deviation of about 20° in galactic latitude, and the deficit in the galactic anticenter direction should have a standard deviation of about 50° , we use the TA data to search for these effects [23]. Neither an enhancement along the galactic plane nor a deficit in the galactic

R&D for future detectors

To collect much better statistics at the highest energies, significantly larger detectors are needed to identify sources via anisotropy studies. Because of the prohibitive cost, it may be difficult to build a sufficiently large detector using existing technologies. Hence, it is important to develop new detectors.

The JEM-EUSO is a new type of observatory that will utilize very large volumes of the earth's atmosphere as a detector of the highest-energy cosmic rays from the universe. K-EUSO represents the ultimate effort towards a full JEM-EUSO mission and will be mounted to the International Space Station (ISS) at an altitude of approximately 400 km. The light sensor is a very wide-field, fast, and large telescope, and observes brief UV flashes in the earth's atmosphere caused by the highest-energy cosmic rays. EUSO-TA, which is a EUSO prototype installed at the TA BRM FD site in 2013, has been tested occasionally. In September of 2016, EUSO-TA observed laser shots, star images, meteors and UHECRs in association with those observed with the BRM FD. In parallel, preliminary test of the main detector of EUSO-SPB (EUSO on a Super Pressure Balloon) was performed at the BRM FD site before its launching. These results were reported at UHECR2016 [24].

A Fluorescence detector Array of Single-pixel Telescopes (FAST) was proposed for large area and low-cost detection of ultra-high energy cosmic rays for the next generation of UHECR experiments [25]. One FAST telescope was constructed for the test at the BRM FD site, and the observation of cosmic rays is being performed.

Summary

TA confirmed the ankle at $10^{18.7}$ eV and the flux suppression above $10^{19.8}$ eV. The statistical significance of having the same spectral index above the ankle (no suppression) is $\sim 6\sigma$. We confirmed the breaks at $10^{16.3}$ eV and $10^{17.2}$ eV in the energy spectrum measured with the TALE FD. The preliminary X_{\max} measurement above $10^{18.2}$ eV is consistent with light composition. We found an indication of a cluster of cosmic rays with energy greater than 5.7×10^{19} eV (TA hotspot) by oversampling using 20° -radius circles. Its significance appearing in an isotropic cosmic-ray sky is 3.7×10^{-4} (3.4σ).

In order to confirm the TA hotspot and understand its feature, TA proposed TAx4, which would quadruple the TA SD aperture and would add two FD stations. We are constructing the TAx4, which is in addition expected to explore spectrum anisotropy that TA currently sees at a level of 3σ . And we will measure energy spectrum and X_{\max} at around or above the cutoff with much more events.

The TALE SDs were fully deployed at the TALE site, and the data acquisition system is been checked. In addition to TA and TALE, TAx4 and NICHE will provide important measurements of energy spectrum, composition, and arrival directions of UHECRs from the knee region up to the highest-energy region of over five to six decades in energy with crosscheck of energy scale between different detectors.

The TA BRM FD site is used for R&D of future detectors with larger aperture. The prototype (EUSO-TA) of JEM-EUSO for the observation of UV UHECR showers from the space has been tested occasionally since 2013. In 2016, the main detector of EUSO-SPB for the first UV UHECR shower observation from the sky was tested before launching. FAST, a new type of fluorescence telescope consisting of small-sized reflective mirrors and four PMTs, aims at a future large and low-cost observatory of UHECRs, and its test with CR observation has started.

Bibliography

- [1] K. Kawai *et al.*, J. Phys. Soc. Jpn. Suppl. A 78 (2009) 108.
- [2] G. Thomson *et al.*, Nucl. Phys. B 36 (2004) 28.
- [3] H. Sagawa *et al.*, 34th International Cosmic Ray Conference (ICRC2015), The Hague, The Netherlands, July 30 - August 6, 2015, #1022.
- [4] Y. Tsunesada *et al.*, 2016 International Conference on Ultra-High Energy Cosmic Rays (UHECR2016), Kyoto Research Park, Japan, October 11-14, 2016. <https://indico.cern.ch/event/504078/>.
- [5] D. Ivanov *et al.*, UHECR2016.
- [6] T. Abu-Zayyad *et al.*, Astrophys. J. Lett. 768 (2013) L1 (5pp).
- [7] R.U. Abbasi *et al.*, Astropart. Phys. 80 (2016) 131.
- [8] D. Bergman *et al.*, ICRC2011, Beijing, China, August 11-18, 2011.
- [9] T. Abu-Zayyad *et al.*, UHECR2016.
- [10] R.U. Abbasi *et al.*, Phys. Rev. Lett. 104 (2010) 161101.
- [11] A. Aab *et al.*, Astrophys. J. 794 (2014) 172 (15pp).
- [12] R.U. Abbasi *et al.*, Astropart. Phys. 64 (2015) 49-62.
- [13] J.P. Lundquist for the TA collaboration, in proceedings of ICRC2015.
- [14] W.Hanlon *et al.*, UHECR2016.
- [15] A. Aab *et al.*, Phys. Rev. D91, 032003 (2015).
- [16] R. Takeishi *et al.*, JPS meeting, Osaka University, March 17-20, 2017.
- [17] S. Quinn for the Auger and TA collaborations, UHECR2016.
- [18] R.U. Abbasi *et al.*, Astrophys. J. Lett. 790 (2014) 21.
- [19] T. Abu-Zayyad *et al.*, Astrophys. J. 757 (2012) 26 (11pp).
- [20] P. Tinyakov *et al.*, UHECR2016.
- [21] T. Nonaka *et al.*, UHECR2016.
- [22] J. P. Huchra, L. M. Macri, K. L. Masters, T. H. Jarrett, P. Berlind, M. Calkins, A. C. Crook, R. Cutri, P. Erdodu, E. Falco, T. George, C. M. Hutcheson, O. Lahav, J. Mader, J. D. Mink, N. Martimbeau, S. Schneider, M. Skrutskie, S. Tokarz, and M. Westover, The Astrophysical Journal Supplement Series 199, 26 (2012).
- [23] R.U. Abbasi *et al.*, Astropart. Phys. 86 (2017) 21.
- [24] M. Casolino *et al.* UHECR 2016.
- [25] T. Fujii *et al.*, JPS meeting, Osaka University, March 17-20, 2017.

Tibet AS γ Project

[Spokespersons : M. Takita]

ICRR, The Univ. of Tokyo, Kashiwa, Chiba 277-8582

Experiment

The Tibet air shower experiment has been successfully operated at Yangbajing (90°31' E, 30°06' N; 4300 m above sea level) in Tibet, China since 1990. It has continuously made a wide field-of-view (approximately 2 steradian) observation of cosmic rays and gamma rays in the northern sky.

The Tibet I array was constructed in 1990 and it was gradually upgraded to the Tibet II by 1994 which consisted of 185 fast-timing (FT) scintillation counters placed on a 15 m square grid covering 36,900 m², and 36 density (D) counters around the FT-counter array. Each counter has a plastic scintillator plate of 0.5 m² in area and 3 cm in thickness. All the FT counters are equipped with a fast-timing 2-inch-in-diameter photomultiplier tube (FT-PMT), and 52 out of 185 FT counters are also equipped with a wide dynamic range 1.5-inch-in-diameter PMT (D-PMT) by which we measure up to 500 particles which saturates FT-PMT output, and all the D-counters have a D-PMT. A 0.5 cm thick lead plate is put on the top of each counter in order to increase the counter sensitivity by converting gamma rays into electron-positron pairs in an electromagnetic shower. The mode energy of the triggered events in Tibet II is 10 TeV.

In 1996, we added 77 FT counters with a 7.5 m lattice interval to a 5,200 m² area inside the northern part of the Tibet II array. We called this high-density array Tibet HD. The mode energy of the triggered events in Tibet HD is a few TeV.

In the late fall of 1999, the array was further upgraded by adding 235 FT-counters so as to enlarge the high-density area from 5,200 m² to 22,050 m², and we call this array and further upgraded one Tibet III. In 2002, all of the 36,900 m² area was covered by the high-density array by adding 200 FT-counters more. Finally we set up 56 FT-counters around the 36,900 m² high density array and equipped 8 D-counters with FT-PMT in 2003. At present, the Tibet air shower array consists of 761 FT-counters (249 of which have a D-PMT) and 28 D-counters as in Fig. 16.

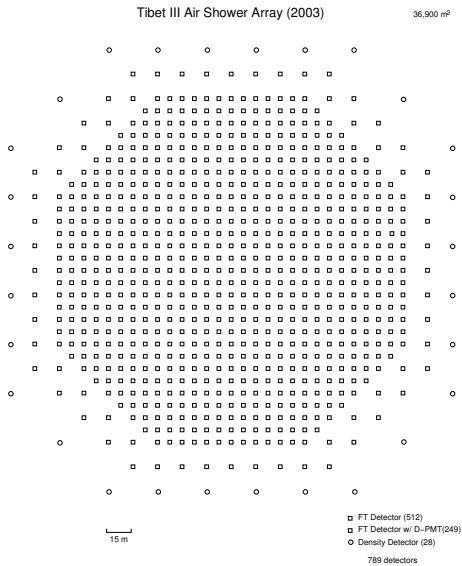


Fig. 16. Schematic view of Tibet III.

The performance of the Tibet air shower array has been well examined by observing the Moon's shadow (approximately 0.5 degrees in diameter) in cosmic rays. The deficit map of cosmic rays around the Moon demonstrates the angular resolution to be around 0.9° at a few TeV for the Tibet III array. The pointing error is estimated to be better than $\sim 0.01^\circ$, as shown in Fig. 17, by displacement of the shadow center from the apparent center in the north-south direction, as the east-west component of the geomagnetic field is very small at the experimental site. On the other hand, the shadow center displacement in the east-west direction due to the geomagnetic field enables us to spectroscopically estimate the energy scale uncertainty at $\pm 12\%$ level, as shown in Fig. 18. Thus, the Tibet air shower experiment introduces a new method for energy scale calibration other than the conventional estimation by the difference between the measured cosmic-ray flux by an air shower experiment and the higher-energy extrapolation of cosmic-ray flux measured by direct measurements by balloon-borne or satellite experiments.

Physics Results

Our current research theme is classified into 4 categories:

- (1) TeV celestial gamma-ray point/diffuse sources,
- (2) Chemical composition and energy spectrum of primary cosmic rays in the knee energy region,
- (3) Cosmic-ray anisotropy in the multi-TeV region with high precision,
- (4) Global 3-dimensional structure of the solar and interplane-

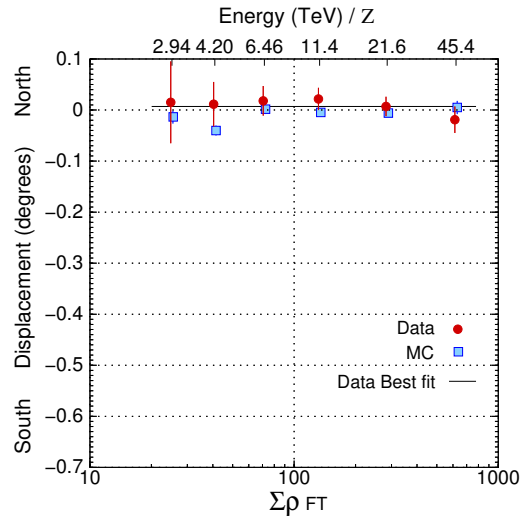


Fig. 17. From [1]. The Moon's shadow center displacement from the apparent position in the north-south direction as a function of energy, observed by Tibet III.

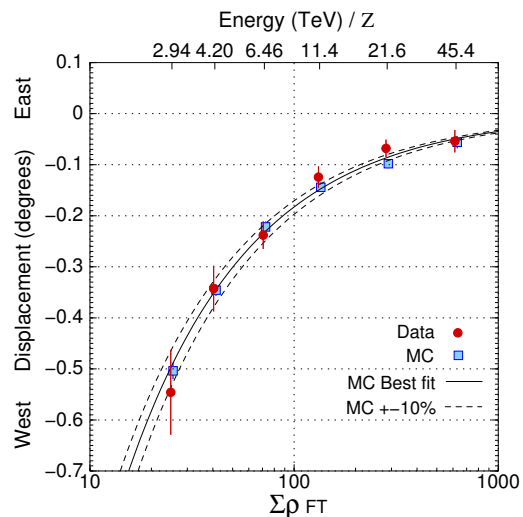


Fig. 18. From [1]. The Moon's shadow center displacement from the apparent position in the east-west direction as a function of energy, observed by Tibet III.

tary magnetic fields by observing the Sun's shadow in cosmic rays.

We will introduce a part of the results obtained in this fiscal year.

The galactic cosmic rays arrive at Earth almost isotropically, as they are mostly charged particles and deflected in the galactic magnetic field. Very small anisotropy ($\sim 0.1\%$) is expected from the diffusion and/or drift effects in the galactic magnetic field. However, the variation of the amplitude with energy observed by many air shower experiments seems to be difficult to interpret in terms of the conventional galactic cosmic-ray diffusion model in the galaxy. Hence, study of galactic cosmic-ray anisotropy is important to understand the

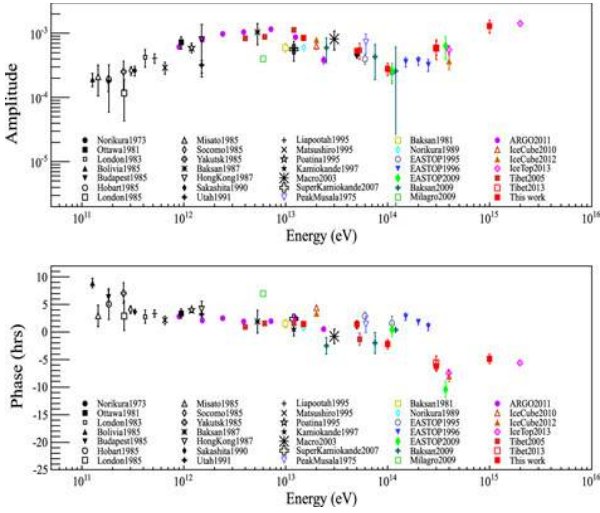


Fig. 19. From Ref. [2] and the references therein. The energy dependences of amplitude (top) and phase (bottom) of the first harmonics of the CRs anisotropy obtained in this work, and reported from previous measurements.

origin and propagation of galactic cosmic rays.

As is shown in Fig. 19, several results of the galactic cosmic-ray anisotropy in the energy range from hundreds of TeV up to ~ 10 PeV have been reported, due to the low statistics of cosmic rays in this energy range. EAS-TOP reported for the first time a detection of anisotropy at ~ 200 TeV in 1996. They improved their statistics later and reported a sharp increase of the anisotropy amplitude at primary energies around ~ 370 TeV in 2009. At the PeV energy region, the Akeno experiment reported an increase of the cosmic-ray anisotropy amplitude in 1986. No hint of the anisotropy, on the other hand, has been found in the KASCADE data at higher energies between 0.7 and 6 PeV in 2004. Recently, IceCube reported the anisotropy observed in the southern sky, showing a new phenomenon different from that obtained by EAS-TOP in 2012. A clear deficit with a post-trial significance of -6.3σ at 400 TeV was detected, which was then confirmed by the result from Ice-Top in 2013. The Ice-Top data further revealed the existence of anisotropy at energies up to 1 PeV in 2013.

The Tibet air shower array presented the first two-dimensional anisotropy measurements at TeV energies in 2005. The anisotropy features, known as the "tail-in" and "loss-cone" features, were observed with very high significances. A new component anisotropy at multi-TeV energies from the Cygnus direction was also reported in 2006. It has been shown that the amplitude of the first order anisotropy decreases above a few hundred TeV, indicating the co-rotation of GCRs around the Galactic center. The anisotropy feature above ~ 300 TeV observed in this work was found to be different from those in lower energy regions and in agreement with IceCube's result at 400 TeV. Combining with IceCube's results, we present a full-sky anisotropy observed at hundreds of TeV. By improving the reconstruction of primary energy, we will also extend the analyzed energy range to two decades between 10 TeV and 1 PeV, which is also the widest coverage of such works.

Analysis of the 10 - 1000 TeV large-scale sidereal anisotropy

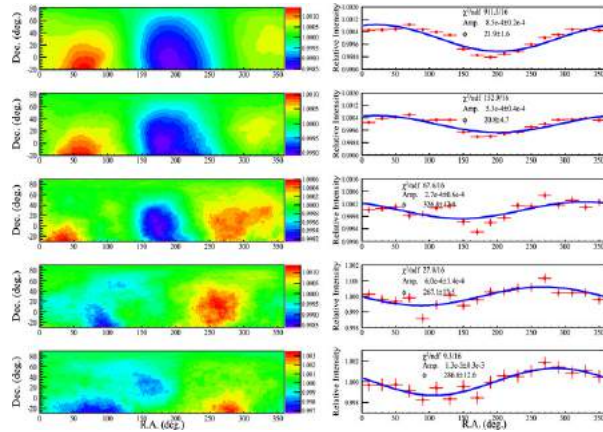


Fig. 20. From Ref. [2]. 2D anisotropy maps in five energy samples (15, 50, 100, 300, and 1000 TeV, from top to bottom). Left panels show the relative intensity maps (with 30° smoothing), while right panels show the 1D projections. The blue curve shows the first harmonic fitting to the data.

of galactic cosmic rays was made with the data collected by the Tibet air shower array from 1995 October to 2010 February [2]. In this analysis, we improve the energy estimate and extend the declination range down to -30° . Our result is shown in Fig. 20. We find that the anisotropy maps above 100 TeV are distinct from that at a multi-TeV band. The so-called tail-in and loss-cone features identified at low energies get less significant, and a new component appears at ~ 100 TeV. The spatial distribution of the galactic cosmic-ray intensity with an excess (7.2σ pre-trial, 5.2σ post-trial) and a deficit (-5.8σ pre-trial) are observed in the 300 TeV anisotropy map, consistent with IceCube's results at 400 TeV. Combining our results in the northern sky with IceCube's results in the southern sky, we establish a full-sky picture of the anisotropy in hundreds of TeV band. We further find that the amplitude of the first order anisotropy increases sharply above ~ 100 TeV, indicating a new component of the anisotropy. These results will make significant contribution to understanding the origin and propagation of galactic cosmic rays.

Another result is related to MC study on improvement of energy estimation for a gamma-ray induced air shower event.

A primary cosmic ray bombarding nuclei, such as nitrogen and oxygen in the atmosphere, produces a number of secondary particles which cascade toward the ground level. We call the phenomenon an extensive air shower. A charged primary cosmic ray, such as proton, helium, etc., induces an air shower (cosmic-ray shower) consisting of three components, *i.e.*, the electro-magnetic, the nucleonic, and the muonic components. On the other hand, a primary gamma-ray induced air shower (gamma-ray shower) is dominated by the electro-magnetic component alone. The secondary particles spread in the lateral direction due to multiple Coulomb scatterings. The number of particles in the air shower reaches its maximum and then rapidly attenuates due to the ionization losses by the electrons in the air. The air shower induced by a 10 TeV primary gamma ray includes approximately 6,000 electrons/positrons at 4,300 m above sea level. These secondary particles are sampled by a ground air shower array, which consists of a number

of scintillation counters deployed with uniform spacing.

The present/past air shower arrays, such as the Tibet air shower array, the ARGO-YBJ and the Milagro, have observed several gamma-ray sources with wider field of view and higher energy threshold than the Cherenkov telescopes. Recently, the Tibet water-Cherenkov-type muon detector (MD) array ($\sim 4,000 \text{ m}^2$) was added underground beneath the Tibet air shower (AS) array to observe gamma rays above 10-1000 TeV from energetic celestial sources with low cosmic-ray background and high gamma-ray sensitivity, and the data taking in the AS+MD configuration was started in 2014. This AS+MD array significantly improves gamma-ray sensitivity in the 10-1000 TeV region by means of separation between gamma rays and hadronic cosmic rays based on counting number of muons accompanying an air shower. Above 100 TeV, pure gamma-ray showers dominated by the electro-magnetic component are observed with the AS+MD array.

Under these circumstances, we study the energy determination of gamma-ray showers in the 10-1000 TeV energy region based on the lateral distribution of air showers by Monte Carlo (MC) simulation assuming the present Tibet AS array.

We study the performance of the AS array based on a full MC simulation using the CORSIKA version 7.4 code for air shower event generation and the GEANT4 code for response of each scintillation counter, respectively. The air showers are generated by the CORSIKA with EPOS LHC, as a hadronic interaction model assuming the following energy spectra of primary particles. A spectrum with a power-law index of -2.0 is assumed for the primary gamma-ray spectrum above 0.3 TeV. A primary cosmic-ray spectrum and its mass composition are sampled mainly from the direct observational data above 0.3 TeV. The core locations of generated air showers are uniformly distributed within a 300 m in-radius circle centered at the array. Subsequently, generated secondary particles in the air shower are fed into the detector simulation based on the GEANT4 code, and are analyzed in the same way as the experimental data to reconstruct the energy and the arrival direction.

The reconstructed core location of an air shower on the AS array is estimated by the density weighted position as follows,

$$(X_{\text{core}}, Y_{\text{core}}) = \left(\frac{\sum_i \rho_i^2 x_i}{\sum_i \rho_i^2}, \frac{\sum_i \rho_i^2 y_i}{\sum_i \rho_i^2} \right), \quad (7)$$

where (x_i, y_i) and ρ_i are the coordinates and the number density (m^{-2}) of detected particles, respectively, of the i -th counter. The errors of core location at 10 TeV and 100 TeV are estimated to be 10.0 m and 4.7 m, respectively, corresponding to 68% confidence level.

The primary gamma-ray energy can be estimated from the lateral distribution of particle density from the air shower core location determined by Eq.7. To estimate air shower size (the total number of particles in an air shower at the altitude of the site), we fit the lateral distribution of particle density measured by the AS array using the following Nishimura-Kamata-Greisen (NKG) function.

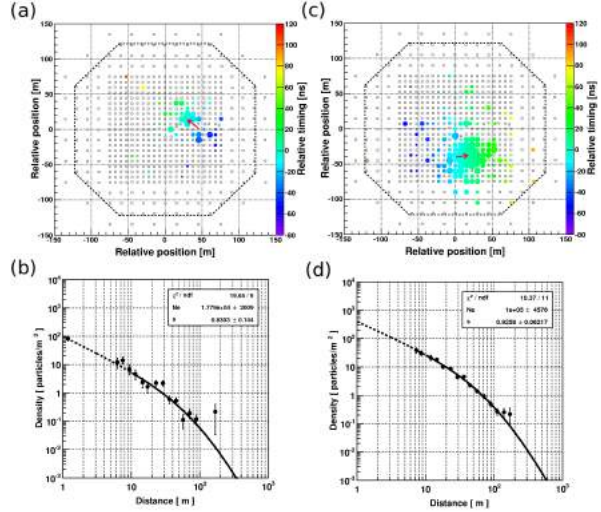


Fig. 21. From Ref. [3]. Upper figures : Event displays of typical MC gamma-ray events assuming the Tibet AS array. The small open squares indicate the positions of the scintillation counters with an area of 0.5 m^2 . Circle size is proportional to the logarithms of the number of particles detected in each counter. The circle colors represent the relative timings of signal detected by the counter. The red arrow indicates the arrival direction of each shower toward the shower core location identified at the arrow head. The selected air shower cores are located within the enclosed region with the dashed line. Lower figures : The lateral distribution of MC gamma-ray events. The solid curves show the NKG functions fitted to the data with $r > 10 \text{ m}$. The dashed curves display the extrapolations of the fitted NKG functions to $r < 10 \text{ m}$. The generated energies and zenith angles of these events are 21 TeV and 19.0° for (a)(b), and 102 TeV and 15.8° for (c)(d), respectively.

$$\rho_{\text{NKG}}(r) = \frac{N_e}{r_m^2} \frac{\Gamma(4.5-s)}{2\pi\Gamma(s)\Gamma(4.5-2s)} \left(\frac{r}{r_m}\right)^{s-2} \left(1 + \frac{r}{r_m}\right)^{s-4.5}, \quad (8)$$

where r is the distance from air shower axis, N_e (the total number of particles in an air shower observed at an altitude) and s are free parameters denoting the air shower size and the age of the air shower, respectively, and r_m (Moliere unit) is a fixed parameter set to be 130 m. The counters located closer than 10 m from the air shower axis are not used for this fitting because of a small number of counters in this area and a large fluctuation of particle density due to the error in core location determination. Also FT (D) counters detecting more than 15 (5,000) particles are not used, because the PMT linearity fails for such high particle density. Figure 21 shows typical event display maps, and lateral distributions of gamma-ray events generated by the MC simulation. Each point in Fig. 21 (b)(d) is the averaged particle density by counters within a circular ring of Δr width including “silent” counters.

The primary cosmic-ray energy has been traditionally estimated from the reconstructed air shower size N_e using the NKG function or simply the sum of detected particle density. In the analysis of the ultra-high-energy cosmic rays with $E > \sim 10^{16} \text{ eV}$ observed by a widely spread array ($> 1 \text{ km}$ spacing), the particle density at only a specific distance from the shower axis has been used as a well established energy

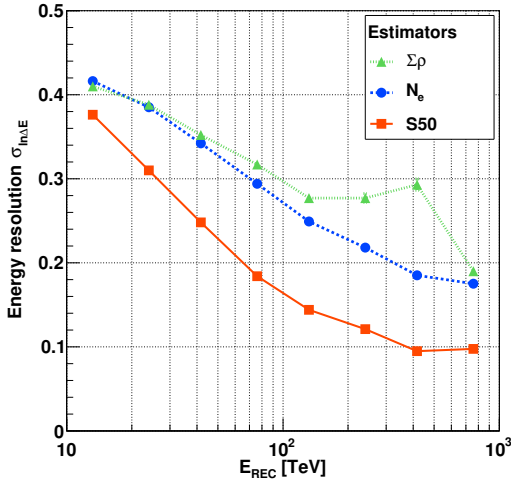


Fig. 22. From Ref. [3]. Energy resolution ($\sigma_{\text{in}\Delta E}$) vs the reconstructed energy using different three estimators, S50 (red squares), N_e (blue circles) and $\Sigma\rho$ (green triangles). $\sigma_{\text{in}\Delta E}$ is the standard deviation of the logarithmic Gaussian function. All results assume the case of the zenith angle $\theta < 20^\circ$.

estimator, which depends weakly on the interaction models, fluctuation in shower development, and the primary mass. For example, the Telescope Array experiment has adopted S800, which is the particle density at a lateral distance of 800 m from the core, as an energy estimator. Following this parameter, we define an air shower parameter S50, which is the particle density at 50 m from the air shower axis, namely $\rho_{\text{NKG}}(50)$ in Eq.8, as a new energy estimator.

Using the new energy estimator S50, the energy resolutions for the gamma rays are estimated to be approximately 40% at 10 TeV and 16% at 100 TeV with the zenith angle $\theta < 20^\circ$. The new energy estimator S50 shows better energy resolution than the air shower size (N_e) and the sum of detected particles density ($\Sigma\rho$) used so far, as is shown in Fig. 22. A hump seen in the energy resolution of $\Sigma\rho$ between 200 TeV and 600 TeV, which corresponds to $\Sigma\rho$ between 1,000 and 3,000 particles, is due to a counter directly hit by an air shower core. When a counter is directly hit by the air shower core, the counter accidentally records a large number of particles because secondary particles highly concentrate on the center of core ($\Sigma\rho$ is the sum of particle density including the counters located closer than 10 m from the air shower axis). As a result, the reconstructed energy is significantly overestimated. Above 600 TeV, the energy resolution is recovered, because the number of observed particles in a direct hit counter is saturated around 5,000 particles.

We also investigate different Sr parameters, which are $\rho_{\text{NKG}}(r)$ shown in Fig. 24, and started data-taking in 2014. YAC2 aims at mainly studying the energy spectra of proton and helium components in the knee energy region.

We also investigate different Sr parameters, which are $\rho_{\text{NKG}}(r)$ shown in Fig. 24, and started data-taking in 2014. YAC2 aims at mainly studying the energy spectra of proton and helium components in the knee energy region.

Therefore, we employ S50 in the middle of plateau region between S40 and S60.

Other Activities

The emulsion-pouring facilities can meet the demands for making any kind of nuclear emulsion plates which are used

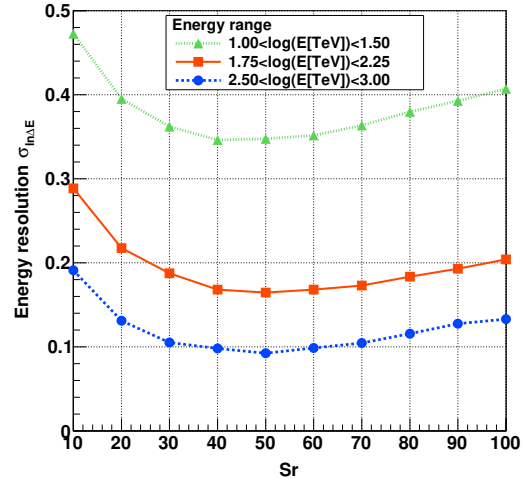


Fig. 23. From Ref. [3]. Energy resolution ($\sigma_{\text{in}\Delta E}$) vs the Sr parameter, which is $\rho_{\text{NKG}}(r)$ in Eq.8 at different three energy ranges, $1.0 < \log(E[\text{TeV}]) < 1.5$ (green triangles), $1.75 < \log(E[\text{TeV}]) < 2.25$ (red squares) and $2.5 < \log(E[\text{TeV}]) < 3.0$ (blue circles). $\sigma_{\text{in}\Delta E}$ is the standard deviation of the logarithmic Gaussian function. All results assume the case of the zenith angle $\theta < 20^\circ$.

for cosmic ray or accelerator experiments. The thermostatic emulsion-processing facilities are operated in order to develop nuclear emulsion plates or X-ray films. Using these facilities, it is also possible to make and develop emulsion pelticle in 600-micron thickness each. In this way, these facilities have been open to all the qualified scientists who want to carry out joint research programs successfully. Of recent, however, the shrinking demand for the facilities let us decide that we should suspend calls for joint research programs to utilize the emulsion-pouring facilities, starting from 2012.

Ongoing Plans

(1) Chemical composition of primary cosmic rays making the knee in the all-particle energy spectrum

We have measured the energy spectra of primary cosmic-ray protons, helium, all particles around the knee energy region. The main component responsible for making the knee structure in the all particle energy spectrum is heavier nuclei than helium. The next step is to identify the chemical component making the knee in the all particle energy spectrum. We have a plan to install an Yangbajing Air shower Core detector array (YAC) near the center of Tibet III to distinguish the chemical component making the knee. We completed construction of YAC2 (124 detectors over $\sim 500\text{m}^2$ in area), as is shown in Fig. 24, and started data-taking in 2014. YAC2 aims at mainly studying the energy spectra of proton and helium components in the knee energy region.

(2) Gamma-ray astronomy in the 100 TeV region

For the purpose of detecting high-energy cosmic gamma rays with an air shower array, a large underground muon detector [4] is very effective to reduce cosmic-ray background.



Fig. 24. YAC2 set up at Yangbajing.

We decided to add a large ($\sim 4,000 \text{ m}^2 \times 1.5 \text{ m}$ deep) underground ($\sim 2.5 \text{ m}$ soil+concrete overburden) water Cherenkov muon detector array (Tibet MD) under the present Tibet air shower array (Tibet AS). By Tibet AS + MD, we aim at background-free detection of celestial point-source gamma rays around 100 TeV with the world-best sensitivity and at locating the origins (PeVatrons) of cosmic rays accelerated up to the knee (PeV) energy region in the northern sky. The measurement of cut off energies in the energy spectra of such gamma rays in the 100 TeV region may contribute significantly to understanding of the cosmic-ray acceleration limit at SNRs. Search for extremely diffuse gamma-ray sources by Tibet AS + MD, for example, from the galactic plane or from the Cygnus region may be very intriguing as well. Above 100 TeV, the angular resolution of Tibet AS with 2-steradian wide field of view is 0.2° and the hadron rejection power of Tibet MD is 1/1000.

In addition to unknown point-like sources, we expect to detect established sources in the 100 TeV region: TeV J2032+4130, HESS J1837-069, Crab, MGRO J2019+37, MGRO J1908+06, Milagro candidate sources, Mrk421, Mrk501 are sufficiently detectable and Cas A, HESS J1834-087, LS I+63 303, IC443 and M87 are marginal.

Furthermore, our integral flux sensitivity to diffuse gamma rays will be very high. We hope that the diffuse gamma rays from the Cygnus region reported by the Milagro group and also diffuse gamma-rays from the galactic plane will be detected. Diffuse gamma-rays of extragalactic origin may be an interesting target as well.

In 2007, a prototype 100-m^2 underground water Cherenkov muon detector was successfully constructed in Tibet to demonstrate the technical feasibility, cost estimate, validity of our Monte Carlo simulation. Data analyses demonstrate that our MC simulation reproduces real data quite reasonably.

In 2014, construction of the $\sim 4,000 \text{ m}^2$ MD, as is shown in Fig. 25, was successfully completed and data-taking started. We have accumulated approximately three-year data. One of the detector cell filled with water is demonstrated in Fig. 26.

Development of Monte Carlo simulation is under way for comparison with real data. Various analysis tools are also extensively being developed. According to the simulation, the

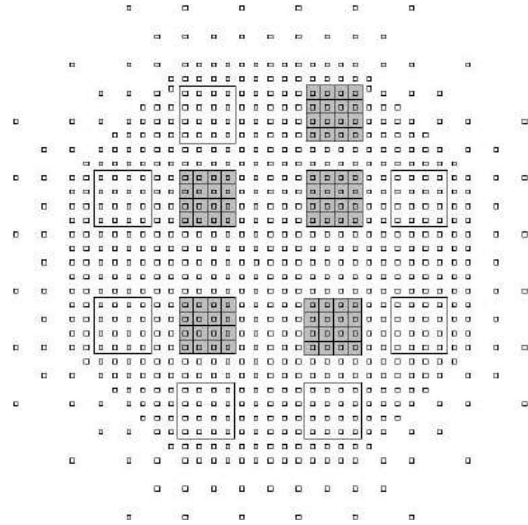


Fig. 25. The 5 shaded squares represent the constructed 5 MD pools.



Fig. 26. PMTs mounted in a MD cell filled with water.

sensitivity of the current configuration (Tibet AS + MD) is demonstrated in Fig. 27.

Bibliography

Papers in refereed journals

- [1] “Multi-TeV Gamma-Ray Observation from the Crab Nebula Using the Tibet-III Air Shower Array Finely Tuned by the Cosmic-Ray Moon’s Shadow”, M. Amenomori *et al.*, *Astrophysical Journal*, **692**, 61-72 (2009).
- [2] “Northern sky Galactic Cosmic Ray anisotropy between 10-1000 TeV with the Tibet Air Shower Array”, M. Amenomori *et al.*, *THE ASTROPHYSICAL JOURNAL*, **836**, 153-1-7 (2016).
- [3] “Energy Determination of Gamma-Ray Induced Air Showers Observed by An Extensive Air Shower Array”, K. Kawata *et al.*, *Experimental Astronomy*, online 03 March 2017, (2016), DOI:10.1007/s10686-017-9530-9.

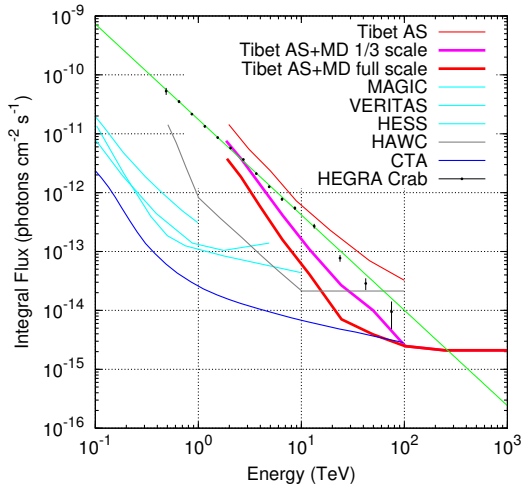


Fig. 27. Sensitivity to point-like gamma-ray sources with Tibet AS+MD (see, Tibet AS+MD 1/3 scale) by pink curve.

- [4] “Exploration of a 100 TeV gamma-ray northern sky using the Tibet air-shower array combined with an underground water-Cherenkov muon-detector array”, T.K. Sako *et al.*, *Astroparticle Physics*, **32**, 177-184 (2009).

The Tibet AS γ Collaboration

M. Amenomori,¹ X. J. Bi,² D. Chen,³ T. L. Chen,⁴ W. Y. Chen,² S. W. Cui,⁵ Danzengluobu,⁴ L. K. Ding,² C. F. Feng,⁶ Zhaoyang Feng,² Z. Y. Feng,⁷ Q. B. Gou,² Y. Q. Guo,² H. H. He,² Z. T. He,⁵ K. Hibino,⁸ N. Hotta,⁹ Haibing Hu,⁴ H. B. Hu,² J. Huang,² H. Y. Jia,⁷ L. Jiang,² F. Kajino,¹⁰ K. Kasahara,¹¹ Y. Katayose,¹² C. Kato,¹³ K. Kawata,¹⁴ M. Kozai,¹³ Labaciren,⁴ G. M. Le,¹⁵ A. F. Li,^{16,6,2} H. J. Li,⁴ W. J. Li,^{2,7} C. Liu,² J. S. Liu,² M. Y. Liu,⁴ H. Lu,² X. R. Meng,⁴ T. Miyazaki,¹³ K. Mizutani,^{11,17} K. Munakata,¹³ T. Nakajima,¹³ Y. Nakamura,¹³ H. Nanjo,¹ M. Nishizawa,¹⁸ T. Niwa,¹³ M. Ohnishi,¹⁴ I. Ohta,¹⁹ S. Ozawa,¹¹ X. L. Qian,^{6,2} X. B. Qu,² T. Saito,²⁰ T. Y. Saito,²¹ M. Sakata,¹⁰ T. K. Sako,¹⁴ J. Shao,^{2,6} M. Shibata,¹² A. Shiomi,²² T. Shirai,⁸ H. Sugimoto,²³ M. Takita,¹⁴ Y. H. Tan,² N. Tateyama,⁸ S. Torii,¹¹ H. Tsuchiya,²⁴ S. Udo,⁸ H. Wang,² H. R. Wu,² L. Xue,⁶ Y. Yamamoto,¹⁰ K. Yamauchi,¹² Z. Yang,² A. F. Yuan,⁴ T. Yuda,^{14,25} L. M. Zhai,² H. M. Zhang,² J. L. Zhang,² X. Y. Zhang,⁶ Y. Zhang,² Yi Zhang,² Ying Zhang,² Zhaxisangzhu,⁴ X. X. Zhou⁷

¹Department of Physics, Hirosaki University, Hirosaki 036-8561, Japan

²Key Laboratory of Particle Astrophysics, Institute of High Energy Physics, Chinese Academy of Sciences, Beijing 100049, China

³National Astronomical Observatories, Chinese Academy of Sciences, Beijing 100012, China

⁴Department of Mathematics and Physics, Tibet University, Lhasa 850000, China

⁵Department of Physics, Hebei Normal University, Shijiazhuang 050016, China

⁶Department of Physics, Shandong University, Jinan 250100, China

⁷Institute of Modern Physics, SouthWest Jiaotong University, Chengdu 610031, China

⁸Faculty of Engineering, Kanagawa University, Yokohama 221-8686, Japan

⁹Faculty of Education, Utsunomiya University, Utsunomiya 321-8505, Japan

¹⁰Department of Physics, Konan University, Kobe 658-8501, Japan

¹¹Research Institute for Science and Engineering, Waseda University, Tokyo 169-8555, Japan

¹²Faculty of Engineering, Yokohama National University, Yokohama 240-8501, Japan

¹³Department of Physics, Shinshu University, Matsumoto 390-8621, Japan

¹⁴Institute for Cosmic Ray Research, University of Tokyo, Kashiwa 277-8582, Japan

¹⁵National Center for Space Weather, China Meteorological Administration, Beijing 100081, China

¹⁶School of Information Science and Engineering, Shandong Agriculture University, Taian 271018, China

¹⁷Saitama University, Saitama 338-8570, Japan

¹⁸National Institute of Informatics, Tokyo 101-8430, Japan

¹⁹Sakushin Gakuin University, Utsunomiya 321-3295, Japan

²⁰Tokyo Metropolitan College of Industrial Technology, Tokyo 116-8523, Japan

²¹Max-Planck-Institut für Physik, München D-80805, Deutschland

²²College of Industrial Technology, Nihon University, Narashino 275-8576, Japan

²³Shonan Institute of Technology, Fujisawa 251-8511, Japan

²⁴Japan Atomic Energy Agency, Tokai-mura 319-1195, Japan

²⁵Deceased

High Energy Astrophysics Group

[Spokesperson: K. Asano]

ICRR, Univ. of Tokyo, Kashiwa, Chiba 277-8582

Overview

The high energy astrophysics group has been making theoretical and observational studies of violent astrophysical phenomena, in which nonthermal cosmic ray particles are being accelerated. Targets of the group's study include high energy astrophysical objects such as supernova remnants/pulsar magnetospheres, giant flares and repeating bursts of magnetars, a giant galactic explosion called ‘Fermi bubble’, black hole/neutron star merger events, fast radio bursts (FRBs), jets from active galactic nuclei (AGN), as well as mysterious gamma ray bursts (GRBs). Research works on the origin of ultra high energy cosmic rays (UHECRs) are also within the coverage of the group.

Research Topic 1: UHECR Production in GRB Jets

We revisit GRBs as UHECR sources, although the GRB hypothesis has been considered to have disadvantages. The prompt emission of GRBs is believed to be emitted from collimated ultrarelativistic outflows. In most of the GRB UHECR models, the internal shocks formed in the GRB outflows are supposed to be the UHECR acceleration site. However, the observed GRB rate is so low that the required cosmic-ray luminosity to agree with the observed UHECR flux is 30–100 times the gamma-ray luminosity or more.

We propose a novel model to produce UHECRs in GRB jets. After the prompt gamma-ray emission, hydrodynamical turbulence is excited in the GRB jets at or before the afterglow phase. The mildly relativistic turbulence stochastically accelerates protons. This acceleration mechanism can produce harder UHECR spectra than the spectra the shock acceleration yields. The acceleration rate is much slower than the usual first-order shock acceleration rate, but in this case it can be energy independent. As shown in Figure 28, our models can reproduce the observed spectra of UHECRs obtained with Telescope Array or AUGER experiments. The resultant UHECR spectrum is so hard that the bulk energy is concentrated in the highest energy range, resulting in a moderate requirement for the typical cosmic-ray luminosity of $10^{53.5}$ erg s⁻¹. In this model, the secondary gamma-ray and neutrino emissions initiated by photopion production are significantly suppressed. Although the UHECR spectrum at injection shows a curved feature, this does not conflict with the observed UHECR spectral shape. The cosmogenic neutrino spectrum in the 10^{17} – 10^{18} eV range (see thin solid lines in Figure 28) becomes distinctively hard in this model, which may be verified by future observations.

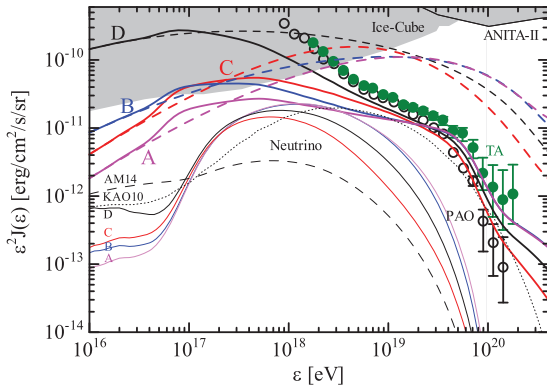


Fig. 28. The diffuse UHECR spectra in our models (A–D, thick solid lines). The thick dashed lines are spectra neglecting the effects of photomeson production and Bethe-Heitler pair production during intergalactic propagation. The thin lines show the all-flavor cosmogenic neutrino intensities, which are below the upper limits (gray shaded area) by IceCube.

Research Topic 2: Population Studies for Compact Binary Mergers

Advanced LIGO has detected signals of gravitational waves from the mergers of massive black hole binaries ($> \sim 30M_{\odot}$).

The origin of such massive binaries is not understood yet. In general, very massive stars are produced in low metallicity environment. To avoid the mass loss due to the strong stellar wind, the low metallicity is favorable. One of candidates for the origin of the detected massive binaries is very massive stars born in very early universe before the metal pollution. They are called Population III stars. If we detect many Population III binary black hole (BBH) mergers, it may be possible to constrain the Population III binary evolution paths not only by the mass distribution but also by the spin distribution.

The final part of gravitational waves from merging BBHs is called the ringdown phase. The detection of the ringdown not only gives a precise estimation of the BH's mass and spin, but also tests Einstein's general relativity. Using the recent population synthesis results of Population III massive BBHs, we extensively examine BBH binary formations. Then, we calculate the remnant BH's mass and the spin, and the event rate. The results are shown in Figure 29. Future observations such as KAGRA may reveal the mass and spin distributions, which will constrain the models of the progenitors of BBHs.

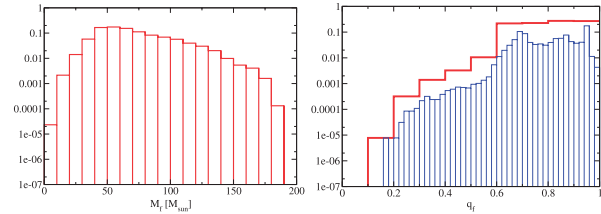


Fig. 29. The remnant mass (left) and spin (right) distributions for our standard model.

On the other hand, the detections of the mergers of neutron star (NS)–BH binaries are also expected. We estimate the future detection rate of the NS–BH mergers originated in Pop III stars. The merger rate depends on the kick velocity of NSs at the supernova explosion. Changing the kick velocity, we estimate the chirp mass distributions of NS–BH (see Figure 30). The chirp mass distributions for the Pop III case are clearly different from those for the Pop I and II cases. The reasons are the difference of BH progenitor evolution and the supernova mass ejection effect. Pop III stars do not lose mass by the stellar wind and the less binary interaction such as the common envelope phase. We find that the event rate of Pop III NS–BH merger rate is ~ 1 Gpc⁻³ yr⁻¹. This suggests that there is a good chance of detecting Pop III NS–BH mergers in future observations.

Research Topic 3: Afterglow of BH–BH Merger

The Fermi Gamma-ray Burst Monitor reported the possible detection of the gamma-ray counterpart of a binary black hole merger event, GW150914, though the detection significance is not high enough. If the energy source of the gamma-ray emission is the gravitational energy of accreting matter, the required mass is so tiny compared to the BH mass. We assume that a huge energy release in the localized region around the BH leads to an optically thick radiation-dominated plasma, whose components are photons, electrons, and positrons.

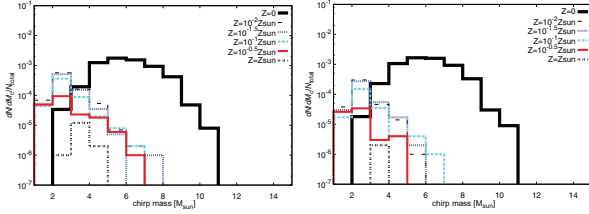


Fig. 30. The chirp mass distributions of NS–BH for each metallicity. The left and right panels are the models for the dispersion of the kick velocity of 265 km/s and 500 km/s, respectively.

The plasma expansion evolves to a relativistic outflow of baryons, which may emit gamma-rays at the outer radius via internal shock. To make photons escape from the emission site without $\gamma\gamma$ -absorption, a relativistic outflow with Lorentz factor larger than 10 is required. Subsequently, debris outflow pushes the ambient gas to form a shock, which is responsible for the afterglow synchrotron emission. As shown in Figure 31, we find that the 1.4 GHz radio flux peaks at $\sim 10^5$ s after the burst trigger. If the ambient matter is dense enough, with density larger than 10^{-2} cm $^{-3}$, then the peak radio flux is ~ 0.1 mJy, which is detectable with radio telescopes such as the Very Large Array. The optical afterglow peaks earlier than the radio, and if the ambient matter density is larger than 0.1 cm $^{-3}$, the optical flux is detectable with large telescopes such as the Subaru Hyper Suprime-Cam. To reveal the currently unknown mechanisms of the outflow and its gamma-ray emission associated with the binary black hole merger event, follow-up electromagnetic observations of afterglows are important. Detection of the afterglow will localize the sky position of the gravitational wave and gamma-ray emissions, and it will support the physical association between them.

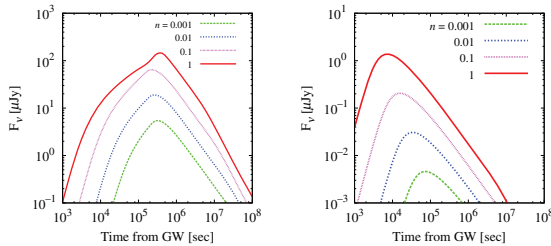


Fig. 31. Radio (left) and optical (right) afterglow light curves from the BH–BH Merger for various ambient densities.

Research Topic 4: Pulsar Polar Cap

Recent γ -ray observations suggest that particle acceleration occurs at the outer region of the pulsar magnetosphere. The magnetic field lines in the outer acceleration region (OAR) are connected to the neutron star surface (NSS). If copious electron–positron pairs are produced near the NSS, such pairs flow into the OAR and screen the electric field there. To activate the OAR, the electromagnetic cascade due to the electric field near the NSS should be suppressed. However, since a return current is expected along the field lines through the OAR (see Figure 32), the outflow extracted from the NSS alone can-

not screen the electric field just above the NSS.

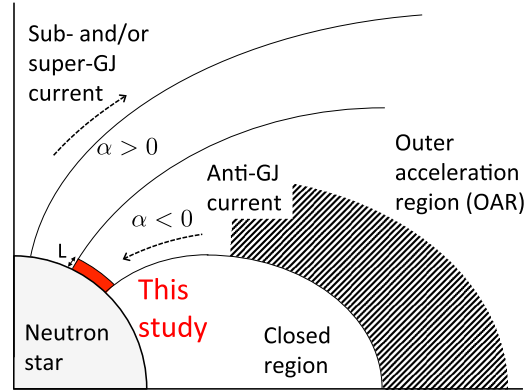


Fig. 32. Schematic picture of the current closure in the pulsar magnetosphere. The shaded area denotes the OAR. The length scale L is our calculation domain.

We analytically and numerically study the electric field screening at the NSS, taking into account the effects of the backflowing particles from the OAR. In certain limited cases, the electric field is screened without significant pair cascade if only ultra-relativistic particles flow back to the NSS. On the other hand, if electron–positron pairs with a significant number density and mildly relativistic temperature, expected to distribute in a wide region of the magnetosphere, flow back to the NSS, these particles adjust the current and charge densities so that the electric field can be screened without pair cascade. We obtain the condition needed for the number density of particles to screen the electric field at the NSS. We also find that in the ion-extracted case from the NSS, bunches of particles are ejected to the outer region quasi-periodically (see Figure 33), which is a possible mechanism of observed radio emission.

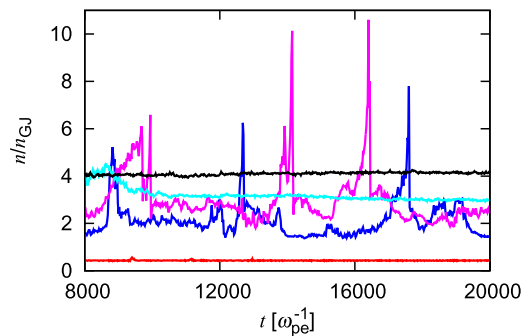


Fig. 33. Number density of particles except for the beam component from the OAR at the outer boundary in our models as a function of time.

Research Topic 5: Spectra of Giant Radio Pulses from the Crab Pulsar

Pulsar radio emission cannot be explained by a simple emission mechanism in the pulsar magnetosphere, and may be

attributed to a coherent process such as the bunching mechanism of plasma or maser process. Many theoretical models have been proposed, but the question how the radio emission is produced has not been solved yet. From several pulsars, sporadic intense radio pulses that are much brighter than the normal pulse ux, called giant radio pulses (GRPs) are observed.

Radio observation of GRPs from the Crab pulsar has been our major subject since the birth of our group in 2009. Our group has developed the analysis method of the large set of the radio data to probe the unknown mechanism of the radio emission in close collaboration with radio astronomers in Japan. Based on a campaign of multi-frequency observations of the Crab pulsar from P (325MHz) to X (8GHz) bands, we study the broad-band GRP spectrum. In the frequency range from 0.3 to 2.2 GHz, we find that about 70% or more of the GRP spectra are consistent with single power laws and their spectral indices are distributed from -4 to -1 . We also find that a significant number of GRPs have such a hard spectral index (approximately -1) that the fluence at 0.3 GHz is below the detection limit (“dim-hard” GRPs). Stacking light curves of such dim-hard GRPs at 0.3 GHz, we detect consistent enhancement compared to the off-GRP light curve (see Figure 34).

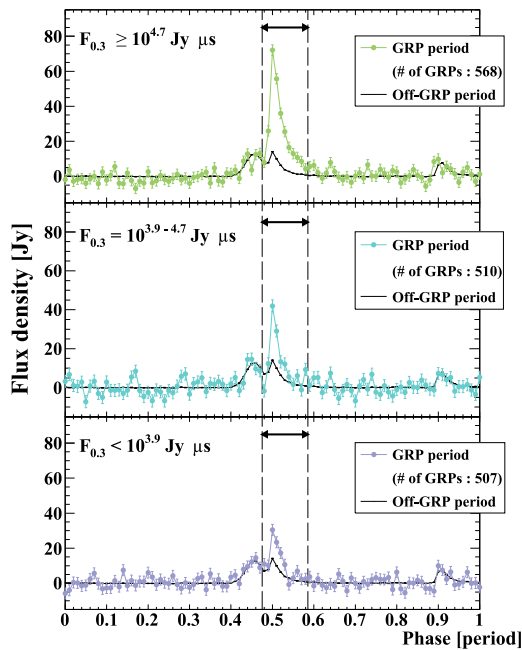


Fig. 34. Average pulse profiles at 0.3 GHz, when GRPs occurred above 1.4 GHz. The samples are divided into sub-groups according to the expected fluence, obtained extrapolating the spectrum above 1.4 GHz. We also show the average profile for the off-GRP periods.

A positive correlation between the L/S band fluence and Our results suggest an anti-correlation between the total energy release and hardness. Our Monte Carlo simulations to reproduce the distributions of the fluences and spectral index show that the typical spectral index is as hard as -1 , differ-

ently from the previous reports. Our comprehensive studies on the GRP spectra are useful materials to verify the GRP model of FRB in future observations.

Research Topic 6: CALET Project

We have joined CALET, CALorimetric Electron Telescope, which is a mission for the Japanese Experiment Module-Exposed Facility (JEM-EF) on the International Space Station. The CALET mission aims at revealing unsolved problems in high energy phenomena of the Universe by carrying out accurate measurements of high energy spectra of electrons, gamma-rays and nuclei. HTV5 equipped with CALET was successfully launched by the H-IIB at 8:50:49 p.m. on August 19 2015 (JST) from the Tanegashima Space Center, and CALET is observing cosmic rays without apparent problems.

Major scientific objectives are to search nearby cosmic ray sources and dark matter signatures by carrying out accurate measurements of cosmic ray electrons in 1 GeV - 20 TeV and gamma-rays in 4 GeV - 10 TeV. Since proton background is very large, high proton rejection power is mandatory for high energy electron and gamma-ray measurements. CALET has an imaging and deep calorimeter with 30 radiation length for electromagnetic particles, which provides high proton rejection and excellent energy resolution.

Our team is successfully operating the observation. Some of our group joins to calibration task for one of the instruments on CALET, gamma-ray burst monitor (CGBM), which already detected several GRBs. The calibrated spectra of those GRBs will be published in near future.

Using the instruments onboard CALET, we set upper-limits of the gamma-ray fluxes for the gravitational-wave signal GW151226 detected by by LIGO (see Figure 35), which is significantly dimmer than usual short GRBs.

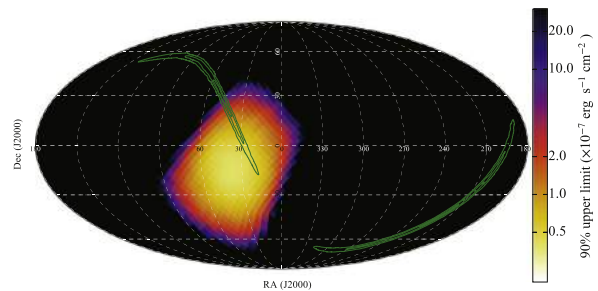


Fig. 35. Sky map of the 90% upper limit for CAL in the 1–100 GeV band. A power-law model with a photon index of -2 is used to calculate the upper limit. The GW151226 probability map is shown as green contours.

Bibliography

Papers in refereed journals

1. Ryo Yamazaki, Katsuaki Asano, Yutaka Ohira “Electromagnetic Afterglows Associated with Gamma-ray Emission Coincident with Binary Black Hole Merger Event GW150914”, Prog. Theor. Exp. Phys., 2016, 051E01(7pp) (2016).

2. M. Ackermann, R. Anantua, K. Asano, et al. “Minute-timescale > 100 MeV γ -ray Variability during the Giant Outburst of Quasar 3C 279 Observed by Fermi-LAT in 2015 June”, *Astrophys. J.*, 824, L20(8pp) (2016).
3. Katsuaki Asano, Peter Mészáros “Ultra-high-energy Cosmic Ray Production by Turbulence in Gamma-ray Burst Jets and Cosmogenic Neutrinos”, *Phys. Rev. D*, 94, 023005(10pp) (2016).
4. Kazuhiro Takefuji, Toshio Terasawa, Tetsuro Kondo, Ryo Mikami, Hiroshi Takeuchi, Hiroaki Misawa, Fuminori Tsuchiya, Hajime Kita, Mamoru Sekido “Very Long Baseline Interferometry Experiment on Giant Radio Pulses of Crab Pulsar toward Fast Radio Burst Detection”, *Pub. Astron. Soc. Pacific*, 128, 084502(6pp) (2016).
5. O. Adriani, Y. Akaike, K. Asano, et al. “CALET Upper Limits on X-ray and Gamma-ray Counterparts of GW 151226”, *Astrophys. J.*, 829, L20(5pp) (2016).
6. Takashi Nakamura, Masaki Ando, Tomoya Kinugawa, Hiroyuki Nakano, Kazunari Eda, Shuichi Sato, Mitsuru Musha, Tomotada Akutsu, Takahiro Tanaka, Naoki Seto, Nobuyuki Kanda, Yousuke Itoh “Pre-DECIGO can Get the Smoking Gun to Decide the Astrophysical or Cosmological Origin of GW150914-like Binary Black Holes”, *Prog. Theor. Exp. Phys.*, 2016, 093E01(16pp) (2016).
7. Shota Kisaka, Katsuaki Asano, Toshio Terasawa “Electric Field Screening with Backflow at Pulsar Polar Cap”, *Astrophys. J.*, 829, 12(14pp) (2016).
8. Tomoya Kinugawa, Hiroyuki Nakano, Takashi Nakamura “Gravitational Wave Quasinormal Mode from Population III Massive Black Hole Binaries in Various Models of Population Synthesis”, *Prog. Theor. Exp. Phys.*, 2016, 103E01(21pp) (2016).
9. S. Guiriec, C. Kouveliotou, D. H. Hartmann, J. Granot, K. Asano, P. Meszaros, R. Gill, N. Gehrels, J. McEnery “A Unified Model for GRB Prompt Emission from Optical to γ -rays; Exploring GRBs as Standard Candles”, *Astrophys. J.*, 831, L8(6pp) (2016).
10. Ryo Mikami, Katsuaki Asano, Shota J. Tanaka, Shota Kisaka, Mamoru Sekido, Kazuhiro Takefuji, Hiroshi Takeuchi, Hiroaki Misawa, Fuminori Tsuchiya, Hajime Kita, Yoshinori Yonekura, Toshio Terasawa “Wide-band Spectra of Giant Radio Pulses from the Crab Pulsar”, *Astrophys. J.*, 832, 212(25pp) (2016).
11. Makoto Arimoto, Katsuaki Asano, Masanori Ohno, Peter Veres, Magnus Axelsson, Elisabetta Bissaldi, Yutaro Tachibana, Nobuyuki Kawai “High-energy Non-thermal and Thermal Emission from GRB 141207A Detected by Fermi”, *Astrophys. J.*, 833, 139(13pp) (2016).
12. Tomoya Kinugawa, Takashi Nakamura, Hiroyuki Nakano “The Possible Existence of Pop III NS–BH Binary and its Detectability”, *Prog. Theor. Exp. Phys.*, 2017, 021E01(9pp) (2017).
13. Y. Asaoka, Y. Akaike, Y. Komiya, R. Miyata, S. Torii, O. Adriani, K. Asano, et al. “Energy Calibration of CALET Onboard the International Space Station”, *Astropart. Phys.*, 91, 1-10 (2017).
14. Kohei Inayoshi, Ryosuke Hirai, Tomoya Kinugawa, Kenta Hotokezaka “Formation Pathway of Population III Coalescing Binary Black Holes through Stable Mass Transfer”, *Mon. Not. R. Astron. Soc.*, 468, 5020-5032 (2017).

Other Activities

Ashra NTA

[Spokesperson: Makoto Sasaki]

ICRR, Univ. of Tokyo, Kashiwa, Chiba 277-8582

Pevatron Identification with PeV ν 's and γ 's

IceCube reported the detection of PeV scale astrophysical neutrinos (ν 's). The origin (Pevatron) has not been revealed [1]. The ν 's are expected to be produced in reactions: $p + \gamma \rightarrow \Delta^+ \rightarrow \pi^0 + p$, $\pi^+ + n$; $p + \text{nucleus} \rightarrow \pi^{\pm,0} + X$, where gamma(γ)-rays are also produced. HESS also reported deep γ observations with arcminute angular resolution of the region surrounding the supermassive black hole Sgr A* at the Galactic Center [2], with the hard power-law γ spectra indicating a candidate of Pevatron. Combined detection of PeV ν 's and γ 's from an accelerator provides indispensable identification of the location and the physics mechanism. Such a “multi-particle” paradigm [3] can be performed by Ashra NTA with a single unique detector system [4].

Imaging ν_τ and γ Air-showers

The Earth-skimming tau ν (ES- ν_τ) technique [5] enjoys a large target mass by detecting air-showers (ASs) produced by τ decays in the air. The τ 's, produced by ν_τ 's that interact with the Earth matter, traverse, and emerge out of a mountain or the ground decaying and generating ASs. Adding to the good detection sensitivity for ν 's, the advantages are perfect shielding of cosmic ray secondaries, precise arrival direction determination, and negligible background from atmospheric ν 's [6]. The Ashra detector can efficiently image AS Cherenkov (CE) and fluorescence (FL) light generated from ES- ν_τ and γ ASs in the effective volume of air in the field of view (FOV) (Figure 36). The unique point is the resolution better than 0.1° yielding strong hadron rejection as selecting γ 's both with FL and CE light.

From Ashra-1 to Ashra NTA

The Ashra Phase 1 (Ashra-1) [7] light collector (LC) (Figure 37) achieves the total resolution of ~ 3 arcminutes covering 42° FOV. The key feature is the use of electrostatic rather than optical lenses to generate convergent beams with the 20 inch Photoelectric Lens Imaging tube (PLI) [8] (Figure 37)

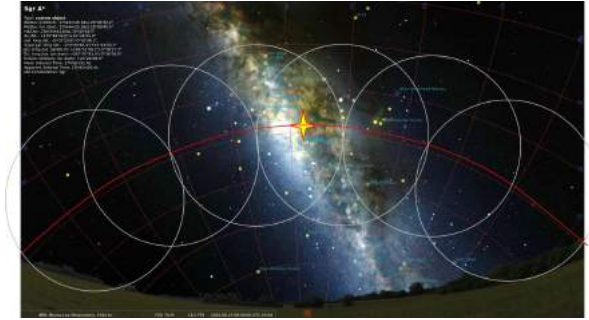


Fig. 40. Simulated southern sky at the Mauna Loa site at 0:00 on June 23, 2019. The cross star indicates the location of the galactic center(GC). The track of GC (arc) and the FOV of the rearranged Ashra-1 light collectors (circles) are also shown.

corresponds to the distance to the shower max larger than 9 km (26 km) and the threshold energies higher than 16 TeV (240 TeV). This situation is useful to check the cut-off energy in the γ -ray spectrum in the galactic bulge or central region. Once the northward NTA units detect ν 's from the same direction as γ -rays, we can discuss the physics of the occurrence of γ -rays and ν 's more concretely than ever.

Bibliography

- [1] M. Aartsen *et al.*, PRL **113**, 101101 (2014).
- [2] HESS Collaboration, Nature **531**, 476 (2016).
- [3] M. Sasaki, ICRR2000 Sat. Sympo., 109 (2000).
- [4] M. Sasaki, G. Hou, arXiv:1408.6244 (2014).
- [5] M. Sasaki, *et al.*, Astropart. Phys. **19**, 37 (2003).
- [6] Y. Asaoka, M. Sasaki, Astropart. Phys. **41**, 7 (2013).
- [7] M. Sasaki, Prog. Theo. Phys. Suppl. **151**, 192 (2003).
- [8] Y. Asaoka, M. Sasaki, NIMA **647**, 34 (2011).
- [9] M. Sasaki, *et al.*, NIMA **492**, 49 (2002).
- [10] M. Sasaki *et al.*, NIMA **501**, 359 (2003).
- [11] Y. Aita *et al.*, ApJ Lett. **736**, L12 (2011).

γ I Project

γ I Consortium
[Spokesperson : R.Enomoto]

Collaboration list:

ICRR, The University of Tokyo, Chiba, Japan; College of Science, Ibaraki University, Ibaraki, Japan; Faculty of Medical Engineering and Technology, Kitasato University, Kanagawa, Japan; Department of Radiological Sciences, Tokyo Metropolitan University, Tokyo, Japan; IPNS, High Energy Accelerator Research Organization, Ibaraki, Japan; National Cancer Center, East, Chiba, Japan; Fuji Electric Co, Tokyo, Japan

Introduction

γ I is a gamma-ray imager for sub-MeV gamma-rays. This device uses Compton scatterings in order to identify the gamma-ray's incident direction (i.e., "Compton Camera"). Last year we had developed an all-sky camera for such low-dose-rate as 0.01–30 μ Sv/h [1].

This year, we have developed an all-sky camera for high-dose-rate area of less than 1 mSv/h and greater than 1 μ Sv/h.

Detector

The main changes are reduction of the crystal cube size (from 3.5cm to half-inch), the crystal configuration to octahedron, and the scintillator from CsI(Tl) to NaI(Tl) in order to achieve faster responses. The test was carried out at the high-dose facility of Fuji Electric Co. as shown in Figure 41. We successfully obtained the



Fig. 41. Test at the high-dose facility of Fuji Electric Co. The detector was located at left and RI was located inside the heavy shield (light green, left).

maximum dose limit of 1mSv/h. Also from the field work in Iidate (Fukushima), we obtained the minimum detection limit of 1 μ Sv/h for this detector.

Gamma-ray Images at Fukushima Daiichi Nuclear Power Station (1F)

In order to show actual performance, we carried out the measurement in 1F on September 2016. The detailed report can be found in [2]. At first, we took images of the known hotspot of 1mSv/h at the surface as shown in Figure 42. The distance between the hotspot

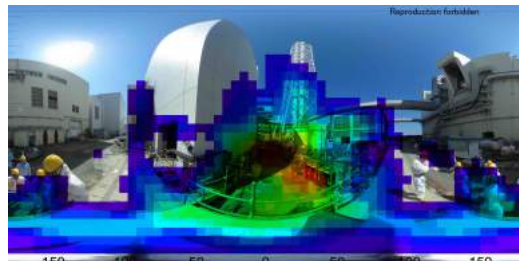


Fig. 42. A shot of 20-m from a hotspot (1 mSv/h at surface) somewhere.

and the detector was 20m. The optical image was taken using RI-COH THETA camera which is known as all-sky camera. The figures are plotted using Mercator projection showing all of the solid angle at once. The gamma-ray's image is superimposed with the rainbow color map. The hotspot was well seen, with other hotspots too. The observation period was 30-min, although 5-min of data could show the similar image which was checked by the offline analysis.

The next shot was taken at the 100-m west of Unit 3, which was the most damaged unit as shown in Figure 43. The Unit 3 was masked with the white square. The dose rate at the detector was 200 μ Sv/h. The maximum radiation was detected from Unit 3 itself. The other known hotspot was located left. The minimum time of 15-min was enough to obtain the similar image.

The last shot was taken from 150m west of Unit 2 as shown in Figure 44. Stronger radiation was found from sky above the Unit 2 ("Skyshine"). The mean-free-path of the air for 662-keV gamma-rays is approximately 100m. From the distance of 150m, most of

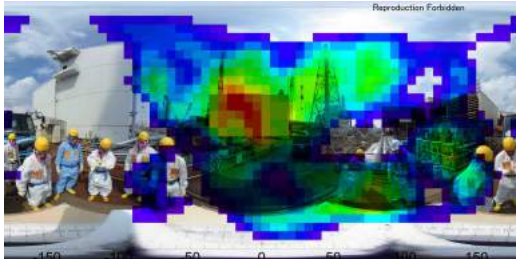


Fig. 43. A shot of 100-m west from the Unit 3.

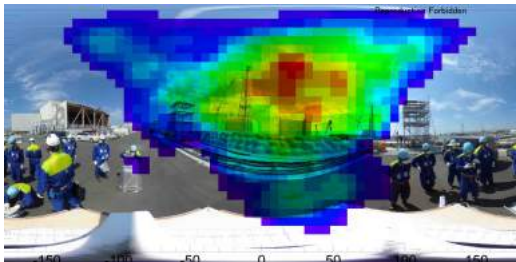


Fig. 44. A shot of 150-m west from the Unit 2.

gamma-rays were scattered more than once in the air from upper direction and absorbed in the soil (concrete) from the lower direction. The images, therefore, looked like “mirage”. The most of dose at the detector position was due to the scattered gamma-rays from Unit 2, therefore, they all came from the upper direction. The observed energy spectrum was consistent with this assumption. The same effect is seen in Figure 43.

Conclusion

We have demonstrated that the γ I detector is able to obtain images of gamma-rays from the all-sky direction simultaneously. A wide field of view helps to reduce the total observation time. The detector can be operated at such high-dose area as 1mSv/h. It also works at low level of $1\mu\text{Sv/h}$. In future, we will test this detector inside the accelerator tunnel of JPARC which aimed at the highest intensity hadron beam. The beam loss is one of reasons to limit beam intensity and the components near these losses become radio-active to emit sub-MeV gamma-rays. “To know where beam is lost” may help to increase the beam intensity. The ν -beam intensity is one of big interests of our laboratory.

Acknowledgement

We appreciate Tokyo Electric Power Company Holdings, Inc. for cooperation.

Bibliography

- [1] T.Watanabe et al., submitted for publication.
- [2] H.Katagiri et al., submitted for publication.

ASTROPHYSICS AND GRAVITY DIVISION

Overview

Astrophysics and Gravity Division consists of Gravitational Wave Group, The Observational Cosmology Group, Primary Cosmic Ray Group and Theory Group.

The Gravitational Wave Group conducts experimental research of gravitational wave with researchers of gravitational wave experiment and theory in Japan. The main items are the construction of the large scale cryogenic interferometer(KAGRA) at Kamioka underground and the operation of CLIO. For this purpose, KAGRA observatory was established at the beginning of the fiscal year of 2016 to assist the construction of KAGRA gravitational wave telescope.

The Observational Cosmology Group studies the cosmic history based on deep multi-wavelength observations in collaboration with worldwide researchers. This group has started a new optical deep survey project with the wide-field imager of Hyper Suprime-Cam mounted on the Subaru telescope.

Theory Group conducts both theoretical study of the Universe and astroparticle physics.

Gravitational Wave Group

KAGRA Project Status

[Spokesperson : Takashi UCHIYAMA]

ICRR, The Univ. of Tokyo, Hida, Gifu 506-1205

Overview

KAGRA, Large-scale Cryogenic Gravitational wave Telescope, aims at detecting gravitational waves and developing gravitational wave astronomy, which was established by the first detection of gravitational waves by LIGO. KAGRA employs a 3 km L-shaped laser interferometer with a cryogenic mirror system placed underground at Kamioka. The KAGRA development is divided into two stages: the initial KAGRA (iKAGRA) and baseline KAGRA (bKAGRA). The iKAGRA detector is a simple Michelson interferometer with a 2-Watt laser, room-temperature mirrors, and a simple seismic isolation system. We completed the iKAGRA detector with a test run in March 2016. Then we proceed to bKAGRA. The bKAGRA detector will employ a Resonant Sideband Extraction (RSE) interferometer with 180-Watt laser, cryogenic Sapphire mirrors, and an advanced Seismic Attenuation System (SAS). The bKAGRA detector should attain the sensitivity high enough for the detection of gravitational waves with the help of the high power laser and RSE interferometer to reduce the quantum noise, the cryogenic Sapphire mirrors to reduce the thermal noise, and the SAS to reduce the seismic noise. We plan to operate the cryogenic 3 km Michelson interferometer by the end of March 2018, and then install other necessary bKAGRA subsystems to attain the target sensitivity.

Figure 1 shows the estimated ultimate sensitivity limits of KAGRA, where incoherent sum of the fundamental noise sources is assumed. The observation range for an in-spiral and merger of neutron-star binary with the ultimate sensitivity limit of KAGRA is about 173 Mpc with the same definition of the observation range as LIGO and Virgo.

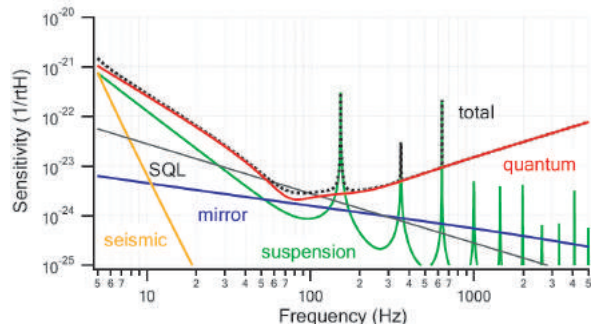


Fig. 1. Ultimate sensitivity limit of KAGRA.

In the end of FY2015 we performed the first half of test run between Mar. 25 and Mar. 31, 2016. The details of the iKAGRA interferometer and the test run were described in the last annual report. In the beginning of FY 2016 we stopped the test run and improved the interferometer to reduce noise level and enhance stability. After the improvements, we performed the second half of test run from Apr. 11 to Apr. 25. Typical noise level at 100 Hz was improved from $3 \times 10^{-15} \text{ Hz}^{-1/2}$ to $7 \times 10^{-16} \text{ Hz}^{-1/2}$ and an observation range of gravitational waves from binary coalescences of Neutron stars with 1.4 solar mass was extended from 0.77 pc to 4.2 pc. The duty cycle of the interferometer was increased from 85.2 % to 90.4 % even though Kumamoto earthquakes on Apr. 14 and 16 hit the test run. The longest lock of the interferometer reached 21.3 hours instead of 3.6 hours in the first half of the test run.

The scimon shift we took during the test run was the following. Each day was divided into three shift: 1:00 to 9:00, 9:00 to 17:00, and 17:00 to 1:00. In each shift slot one expert from ICRR, NAOJ, and KEK and two researchers from other universities/institutes were allocated. These scimons registered what happened as well as unusual events that they noticed during the shift. The scimon shift worked pretty smoothly. Finally, total of 65 people and cumulative total of 186 people from 35 institutes participated the shift works.

All the data that was taken during the test run was stored and transferred to ICRR Kashiwa and Osaka City University in real time. The delayed mirroring of raw data was performed by Academia Sinica, Taiwan. KISTI, Korea was also copying the data. The transfer time from the KAGRA site to surface, ICRR Kashiwa, and Osaka City University was 0.3 sec, 2.5 sec, and 3 sec, respectively. The data management system worked very well.

We started upgrading the interferometer from iKAGRA to bKAGRA after the test run, because we plan to operate the cryogenic 3 km Michelson interferometer by the end of March 2018. The upgrading works are on going by many sub-groups. We give reports in the following sections from the vacuum sub-group, the input and output optics sub-group, the cryogenic sub-group, the digital control system sub-group, the detector characterization sub-group, and the mirror subgroup.

We also enhanced the international collaborations with the Einstein Telescope (ET) project, LIGO, Virgo, Korean and other Asian groups mainly based on the JSPS core-to-core program.

The rapidly progressing status of KAGRA were presented in

many international conferences. Many papers about the progress of KAGRA were also published [1], [2], [3], [4], [5], [6]. We also presented activities on our web-page.[7]

Bibliography

- [1] "Circular Polarizations of Gravitational Waves from Core-Collapse Supernovae: A Clear Indication of Rapid Rotation", Kazuhiro Hayama, Takami Kuroda, Ko Nakamura, and Shoichi Yamada, *Phys. Rev. Lett.* 116, 151102 (2016)
- [2] "Characterization of non-Gaussianity in gravitational wave detector noise", Takahiro Yamamoto, Kazuhiro Hayama, Shuhei Mano, Yousuke Itoh, and Nobuyuki Kanda, *Phys. Rev. D* 93, 082005 (2016)
- [3] "Observation of reduction of radiation-pressure-induced rotational anti-spring effect on a 23 mg mirror in a Fabry-Perot cavity", Yutaro Enomoto, Koji Nagano, Masayuki Nakano, Akira Furusawa and Seiji Kawamura, *Class. Quantum Grav.*, 33 (2016) 145002 (2016)
- [4] "Standard quantum limit of angular motion of a suspended mirror and homodyne detection of ponderomotively squeezed vacuum field", Yutaro Enomoto, Koji Nagano, and Seiji Kawamura, *Phys. Rev. A* 94, 012115 (2016)
- [5] "Unveiling linearly and nonlinearly correlated signals between gravitational wave detectors and environmental monitors", Hirotaka Yuzurihara, Kazuhiro Hayama, Shuhei Mano, Didier Verkindt, and Nobuyuki Kanda, *Phys. Rev. D* 94, 042004 (2016)
- [6] "Mitigation of radiation-pressure-induced angular instability of a Fabry-Perot cavity consisting of suspended mirrors", Koji Nagano, Yutaro Enomoto, Masayuki Nakano, Akira Furusawa and Seiji Kawamura, *Phys. Lett. A* 380 3871-3875 (2016)
- [7] <http://gwcenter.icrr.u-tokyo.ac.jp/en/>

Vacuum system for KAGRA

[Spokesperson : Takashi UCHIYAMA]

ICRR, The Univ. of Tokyo, Hida, Gifu 506-1205

The vacuum sub-group of the KAGRA project has been designed and fabricated two vacuum chambers for BRT (Beam Reducing Telescope) in 2016. Both chambers have already placed at the both end experiment rooms. The BRT chamber is made of SUS304 and dimensions are diameter of 1200 mm, height of 2400 mm, and weight of 1990 kg.

We procured 16 sets of Turbo Molecular Pumps (TMP), 17 sets of root pumps, and 10 sets of ion pumps. Evacuation speed of the TMPs, the root pumps, and the ion pumps are larger than 2000 L/s for N₂ and H₂, 600 L/s for N₂ and H₂, and 800 L/s for N₂ and 1200 L/s for H₂, respectively. Finally, KAGRA has 17 sets of TMP pumping units consisting of a TMP and a root pump and 10 sets of TMP and ION pumping units consisting of a TMP, a root pump, and an ion pump. We placed 15 sets of the TMP pumping units in the center experiment room, 1 set of the TMP pumping unit in the both end experiment rooms, and 5 sets of the TMP and ION pumping units in the both arm ducts.

Input and Output Optics

[Spokesperson : Seiji KAWAMURA] ICRR, The Univ. of Tokyo, Hida, Gifu 506-1205

The input and output optics of KAGRA consists of the pre-stabilization system for the laser, auxiliary locking system, input optics

chain, output optics chain, and detectors. The pre-stabilization system includes the frequency stabilization system, intensity stabilization system, pre-mode cleaner, and modulation system for the main interferometer. The auxiliary locking system includes the phase locking system for the green beam, the fiber system, and the locking system for the arm cavity. The input optics chain includes the input mode cleaner, input Faraday isolator, and input mode matching telescope. The output optics chain includes the output mode matching telescope, output Faraday isolator, and output mode cleaner. The detectors are for the symmetric, antisymmetric, and pick-off ports.

At the beginning of the fiscal year 2016, the second test run of initial KAGRA (iKAGRA) was conducted between Apr. 11 and Apr. 25, 2016. Between the first test run conducted at the end of fiscal year 2015 and this second test run, the length control system of the input mode cleaner was improved. The crossover frequency between the path to the laser and the path to the mode cleaner was reduced from 30 Hz to 10 Hz, which provided larger frequency stabilization net gain. The dither alignment system was also implemented instead of the optical lever DC control system, which ensured the optimal alignment of the mode cleaner with respect to the incident laser beam. In addition, during the commissioning break on Apr. 12, the feedback path to the input mirror of the input mode cleaner was added to improve the robustness of the main interferometer control system, and the feedback path to the laser piezoelectric actuator was optimized in the input mode cleaner control system. As a result the input and output optics for iKAGRA worked extremely well during the second test run. The duty factor of the input mode cleaner during the second test run was 98.5 %, which was significantly better than the duty factor during the first test run, 94.4 %. The longest locking time of the input mode cleaner during the second test run was also improved from 12 hours during the first test run to 23.5 hours.

After the second test run, some broken systems were repaired. The magnets attached to the output mirror of the input mode cleaner, which were knocked off the mirror during the installation of the input mode cleaner, were re-glued to the mirror. Also the input and output optics, which was only for iKAGRA, was disassembled and removed for the installation of the input and output optics for bKAGRA. For example the pre-stabilization system were completely disassembled and the small optical table was replaced with a large optical table for bKAGRA, on which pre-stabilization system have been being installed mainly by Institute for Cosmic Ray Research. The input mode matching telescope, which was a pair of fixed mirrors for iKAGRA, was replaced by a pair of the suspended mode matching mirrors mainly by National Astronomical Observatory of Japan. The input and output optics, which did not exist for iKAGRA but is necessary for bKAGRA, has been being installed. For example the wavefront sensing system for the input mode cleaner has been being installed by the University of Tokyo and Niigata University. The tilt sensor, which had been developed by Sogang University, was temporarily installed to monitor the orientation of the end mirror of the input mode cleaner for a test. It worked very well.

The electro-optical modulator for the high power laser was developed and completed by National Defense Academy and Tokyo Institute of Technology as a collaboration work with University of Florida. The experiments to develop the intensity stabilization system and the auxiliary locking system have been being performed by University of Toyama. The design of the output optics chain also has been being developed by Tokyo Institute of Technology as a collaboration work with University of Western Australia.

Cryogenic payload

[Spokesperson : Kazuhiro YAMAMOTO]

ICRR, The Univ. of Tokyo, Kashiwa, Chiba 277-8582

Outlines A key feature of KAGRA is the operation of the interferometer which consists of mirrors made from sapphire at cryogenic temperature. These mirrors are suspended by sapphire fibers (sapphire lop-eared suspension). They are a part of cryogenic payloads which is functions to control mirror position and direction, for vibration isolation and so on.

The cryogenic payload is developed by ICRR and KEK. Here, the activities of members of ICRR in fiscal year 2016 are focused; development of cryogenic payload and sapphire lop-eared suspension, radiation vibration measurement, magnetic field measurement. Outlines of ELITES (this European grant was over in this fiscal year) are also reported.

Cryogenic payload The cooled sapphire mirror is at the bottom of the cryogenic payload. This payload (Fig. 2) is in the radiation shield for cooling and suspended from the Type A vibration isolation system in vacuum but at room temperature. The cryocoolers and payload are connected by heat links made from pure aluminum for cooling. The payload is necessary to control the position and angle of the mirror (otherwise, the interference of the light can never be realized), and for the vibration isolation (especially, the vibration via heat links) and so on.

Takahiro Miyamoto and Tomohiro Yamada develop cryogenic payload at KEK. One of the largest missions for KAGRA at KEK is performance test of cryogenic payload. Takahiro Miyamoto et al., were preparing this test; for example, items to control cryogenic payload (design of coil magnet actuator, preparation of digital system and control model), cryostat for this test at KEK, assembly of payload. Now (June 2017), cooling test starts soon.

Tomohiro Yamada investigates CuBe material properties at cryogenic temperature for design of blade springs (vertical vibration isolation). He also studies pure Aluminum wires as heat links to cool down cryo payload (evaluation of thermal conductivity and so on).

Takafumi Ushiba, who is a postdoc of Japan Society or the Promotion of Science, worked in ICRR in fiscal year 2016(from fiscal year 2017, he is the ICRR fellow). He investigated performance of light emitting diodes and photo diodes which could work at cryogenic temperature. His experiment shows what kinds of diodes are appropriate for position sensor at cryogenic temperature.

Sapphire lop-eared suspension The cooled mirror is suspended by four sapphire fibers. We call this system sapphire lop-eared suspension(Fig. 3). This sapphire suspension consists of a mirror, fibers with nail heads, ears for connection between fibers and a mirror, blade springs to compensate the length differences between four fibers. All of them are made from sapphire. Two joint techniques are adopted. Between the ears and mirror, Hydroxide Catalysis Bonding is applied. This technique is also adopted in Advanced LIGO and Advanced Virgo. On the nail heads of the fibers, indium is applied for joint with the ear or blade spring. When fibers are broken, heat is applied to melt indium (melting point is 157 degree Celsius) and the broken fibers are removed.

Now we proceed with procurement of sapphire parts except for mirrors. In fiscal year 2016, we purchase sapphire parts for two sapphire suspensions. Then, all sapphire parts for all four sapphire mirrors in KAGRA are ready because we have purchased parts for two sapphire suspensions in fiscal year 2015. We asked Kazuhiro Enami(KEK) and Akitoshi Ueda (NAOJ) to check specification of sapphire parts (geometrical shape and flatness of bonding surface), respectively.

We (especially, Kieran Craig) are preparing jig to assembly. Helios Vocca (INFN Perugia, he is a KAGRA collaborator) and mechanical workshop of INFN Perugia supports development of assembly jig based on Advanced Virgo expertise. In summer of 2016,

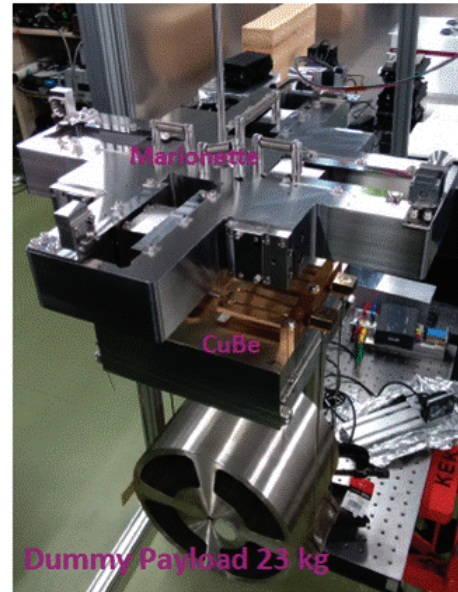


Fig. 2. Assembled prototype of KAGRA cryogenic payload

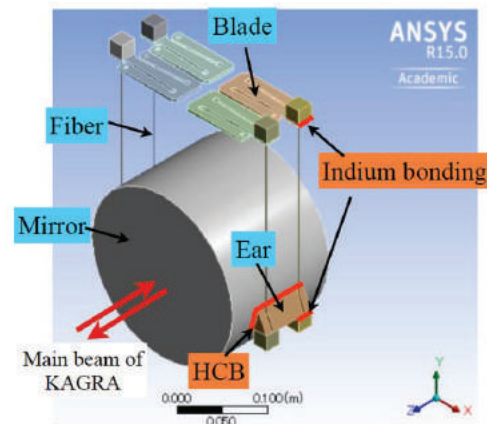


Fig. 3. KAGRA sapphire suspension

we apply HCB between sapphire ears and blank sapphire bulk (geometrical dimension is similar to KAGRA sapphire mirror, but without polish and coating) in jig developed by us. Now, this bulk with ears (Fig. 4) is used in KEK as a part of sapphire suspension prototype. In this mission, Advanced Technology Center (ATC) of National Astronomical Japan (NAOJ) supported us strongly. We used their clean booth. We appreciate efforts of Kenji Mitui (ATC, NAOJ), Naoatsu Hirata(NAOJ), Tomotada Akutsu (NAOJ), Sakae Araki (KEK), Kazuhiro Enami(KEK) and Kennichi Shimizu (SK servies). Since we found some issues in HCB jigs, we continue development. Another sapphire blank bulk is prepared. We were preparing HCB for this sapphire blank bulk in clean room of University of Toyama (Kazuhiro Yamamoto left ICRR on end of February 2017. He now belongs to University of Toyama).

We have manufactured simpler prototype, one fiber prototype.

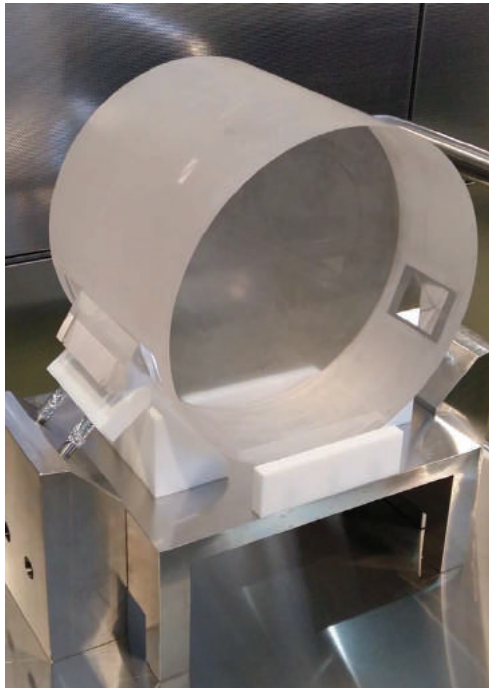


Fig. 4. Sapphire blank bulk (its dimensions are similar to KAGRA sapphire mirror without polish and coating) with sapphire ears. They are connected by Hydroxide Catalysis Bonding as KAGRA sapphire mirror

Only one sapphire fiber suspends a sapphire mass whose weight is a quarter of that of a KAGRA mirror. We need not to take care of balance between fibers during assembly. The stress in suspension is comparable with that in actual sapphire suspension. As like actual suspension, Hydroxide Catalysis Bonding and indium bonding are adopted in this one fiber prototype. We (mainly, Hiroki Tanaka) conducted cooling test to evaluate relation between heat load and temperature of mirror.

Takafumi Ushiba and Tomohiro Yamada checked mechanical properties of Q-values of sapphire blade spring, a part of sapphire suspension.

Radiation shield vibration measurement Cryogenic payload is in radiation shield to avoid attack of room temperature radiation. Vibration of this shield could noise of gravitational wave detector (vibration of sapphire mirror and scattered light). Although we have already measured shield vibration before delivery of cryostat, we repeat measurement because seismic motion in previous measurement (Toshiba Keihin Product Operations) is larger than that at KAGRA site. Luca Naticchioni (INFN Rome) again brought his vertical accelerometer. Toshiro Ochi recovered our old horizontal accelerometer. We installed our accelerometer on November 2016 in cryostat at a KAGRA center room (IXC). This cryostat was cooled down and we measured vibration. Data analysis is in progress. We have plan second cooling test in summer 2017.

Magnetic field measurement Coil magnet actuators are adopted to control cryogenic payload. Fluctuation of magnetic field around payload can shake this payload. We (mainly, Hiroki Tanaka) proceed with measurement of fluctuation of magnetic field.

ELiTES ELiTES (ET-LCGT interferometric Telescope Exchange of Scientists) is a European grant (European 7th Framework Programme Marie Curie action between Mar. 2012 and Feb. 2017) for the collaboration between KAGRA and Einstein Telescope (European future project). This grant supports people in Europe to visit Japan for KAGRA. This grant ended on February 2017. This was quite useful to develop cryogenic payload. The last ELiTES workshop was held on February 2017 and we organized tour in KAGRA and Super Kamiokande. One paper about work with ELiTES was published (K. Haughian et al., *Mechanical loss of a hydroxide catalysis bond between sapphire substrates and its effect on the sensitivity of future gravitational wave detectors*, Physical Review D 94(2016082003))

Master theses One Master thesis by Junko Katayama (*Research of mechanical loss of mirror coating of KAGRA gravitational wave detector*) was accepted.

Acknowledgement Mechanical workshops of Institute for Solid State Physics (The University of Tokyo, Kashiwa campus) and Mechanical Engineering Center of KEK provided many products for our research.

Integrated DAQ/control system using real time computers and analog electronic

[Spokesperson : Osamu MIYAKAWA]

ICRR, The Univ. of Tokyo, Hida, Gifu 506-1205

KAGRA DiGital control System (DGS) is designed to control and operate KAGRA as an interferometer for gravitational wave detection. This DGS system made a very important role during iKAGRA observation, not only to control the interferometer but also as a monitoring system, diagnosis system, human interfaces and so on.

A control room at the surface building, that is a part of DGS system and located 7km away from the mine by the length optical fiber cable, remotely controls the whole KAGRA through the real-time operated computers and related circuits. Each Circuit works as a driver connected subsystem and it also works as a bridge between each subsystem and users at the remote control room. We prepared 6 field racks in the laboratory area during the term of iKAGRA. Each field rack includes an IO chassis with several ADC/DAC cards, anti alias/anti image filters, and the circuits above. Each IO chassis is connected to a real time control PC (RTPC) in the computer room in the mine, and all the RTPCs are controlled or managed from the remote control room. The number of field racks is now 11, and it will be 30 at the final stage of bKAGRA.

After some experiences during test run, we realized the importance of stable operation of the system itself. Once the control system started running and when the observation or even the commissioning started, it was getting much more difficult to test the system or update the system. Then we decided to develop a test bench at the surface building to test new things or to fix troubles without stopping the real system. This test bench has basically the same function as the real DGS system such as data acquisition (DAQ) system and real time control system, but the number of computers are limited to avoid some excess redundancy and it has no circuits to control subsystems. It means that it can not test the redundancy related things of stable operation or connection to subsystems, but it can test the new software/hardware or update the system etc. For example we checked CPU performance with some load on the real time models on this test bench, and found one of the causes of delay of real time control loop.

Recently many young students or young researchers are joining for developing the real time control models. Brushing up the real

time models (software site) can extract the potential function of sub-systems (hardware site). They are experiencing and learning such a developing stage through this DGS system at KAGRA. The controls room is now a good communication area among them. Some original methods or tools have been produced. For example, data streaming method from Geo Physics interferometer to KAGRA DAQ system has been developed. The data of distortion of the mine is being shown on the big monitor in the control room.

This DGS system will keep being developed and updated to establish stable operations for commissioning and observations toward the bKAGRA.

Detector Characterization for KAGRA

[Spokesperson : Kazuhiro Hayama]

ICRR, The Univ. of Tokyo, Hida, Gifu 506-1205

Overview The scope of the detector characterization in 2016 is divided into three parts:

- to The system of the detector diagnostics. The system provides computational environment to understand the detector condition, to find noise sources which limit the sensitivity of the detector. The system includes software to analyze observation data and sensors to know environment around the detector.
- to Data quality information. The data quality information is defined by the evaluation of detector condition. The quality information used to judge that the observed data is satisfied to provide scientific results, the data can be used to inspect the detector and so on.
- to Veto analysis. The veto analysis is performed in order to reject gravitational wave candidates triggered by search pipelines.

During the iKAGRA run, daily summary pages were provided as a detector diagnostics. The daily summary pages were to display a series of plots which showed the detector condition by analyzing ~ 40 important auxiliary channels including the gravitational wave channel. The pages were generated automatically in servers which the detector characterization subsystem managed. Besides daily summary pages, web-based diagnostics tools were provided in the same web site so that they can use them directly through the web page. Fig.5 shows the screenshot of the daily summary page and the diagnostics tools. In regard to the environmental monitors, seismometers were set at the locations of the center, X-end, Y-end of KAGRA to monitor the earthquake(Fig.6).

Environmental monitor The design of the locations of the environmental monitor sensors were discussed with mainly GIF subsystem and other subsystems. Fig.7 shows the locations of environmental sensors on the cartoon of KAGRA. Seismometers, magnetometers, barometers, hygrometers, and thermometers are located in each main station. The locations of microphones, which are important to know acoustic activities, are being under discussion.

Noise modeling In the KAGRA site, it has been observed water flow. In Fig.8 shows the amount of the water flow obtained by the Kamioka mining and smelting company. The typical velocity of the water flow is 0.5 ~ 2m/s. If the fluctuation of a water surface goes with a velocity, the Newtonian gravity noise will be generated. This water Newtonian gravity noise might affect the sensitivity of KAGRA. In order to estimate the effect of the water Newtonian noise,

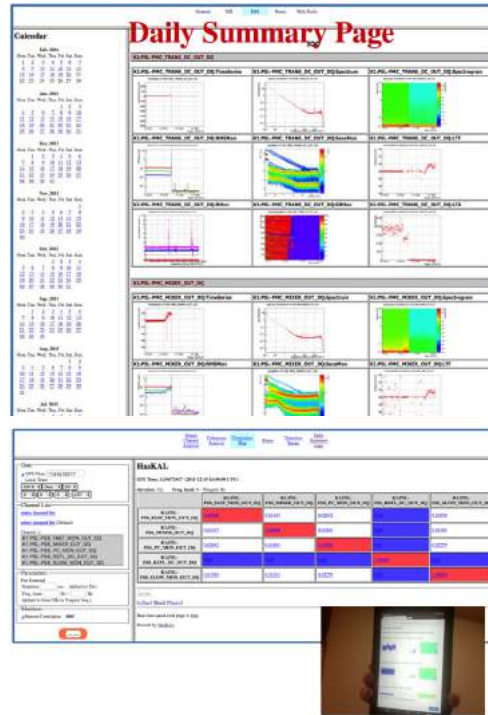


Fig. 5. Daily summary page and web-based diagnostics tools during iKAGRA run

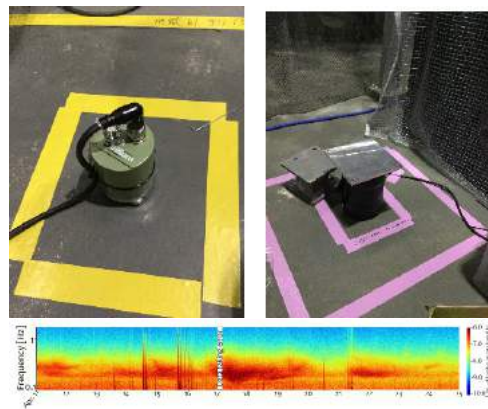


Fig. 6. Seismometer running during iKAGRA run and the spectrogram

we started to model the water flow and the Newtonian noise. the result will be reported in annual report in 2017.

Education In the KAGRA F2F meeting taking place at the U Tokyo on 7,8 in December, we had a bootcamp for diagnostics tools.

Publications

- T Yamamoto, K Hayama, S Mano, Y Itoh, and N Kanda, "Characterization of non-Gaussianity in gravitational wave detector noise", Phys. Rev. D 93, 082005 (2016)
- H Yuzurihara, K Hayama, S Mano, D Verkindt, and N Kanda "Unveiling linearly and non-linearly correlated signals between

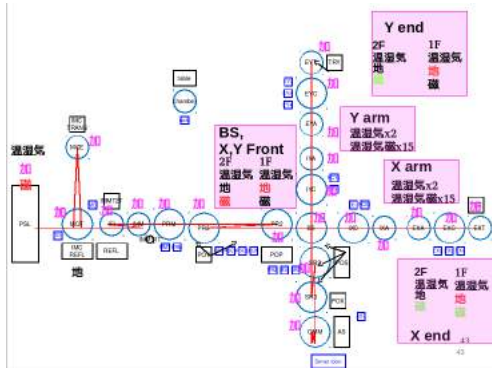


Fig. 7. Proposed locations of environmental monitor sensors around KAGRA

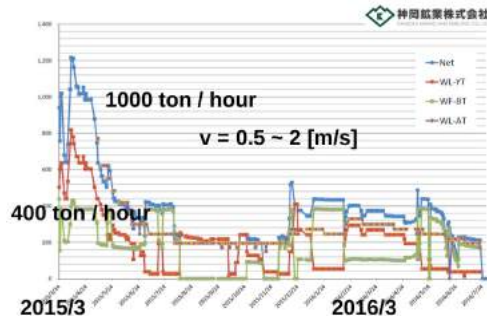


Fig. 8. water flow at the KAGRA site

gravitational wave detectors and environmental monitors” Phys. Rev. D 94, 042004 (2016)

Core Optics for KAGRA

[Spokesperson : Eiichi HIROSE]

ICRR, The Univ. of Tokyo, Kashiwa, Chiba, 277-8582

In the KAGRA detector, two types of materials are used for substrates of core optics. One is sapphire used for the test mass mirrors, and the other is fused silica used for the rest of core optics. These materials are shaped in certain dimensions, polished, and finally coated to become mirrors.

The sapphire mirrors form two Fabry-Perot cavities along the L-shaped 3 km arms (X and Y arms). Two sapphire mirrors placed at the end of each arm are called the ETMs (ETMX and ETMY), and the other two sapphire mirrors near the corner are called the ITMs (ITMX and ITMY). ETM (ITM) stands for End (Input) Test Mass. So far, we have polished the ETMs, and they are currently being coated. The ITMs are being polished and will be coated by the end of this fiscal year. Sapphire is a very hard material. However, thanks to a polishing vendors state-of-the-art technologies, all specifications are satisfied. The expected round trip loss inside the cavity is less than 100 ppm. In order to cool the sapphire mirrors, both sapphire crystal and coating must have very low absorption at the laser wavelength 1064 nm. Especially, the absorption coefficient required to the ITMs is less than 50 ppm/cm. We should point out that we have successfully found such crystals with a domestic crystal maker. The mirrors diameter is 220 mm, and thickness is 150 mm. Each mirror

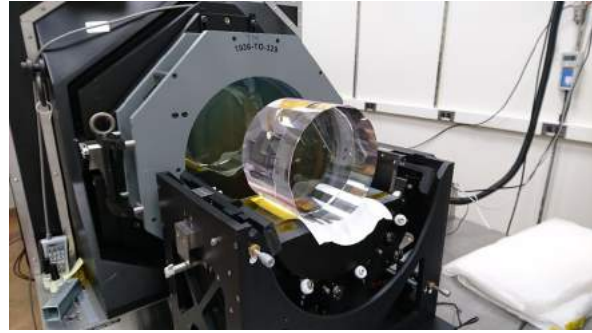


Fig. 9. Sapphire ETM mirror during characterization.

weighs 23 kg. To the best of our knowledge, the KAGRA detector employs the biggest sapphire mirrors in the world with ultra-low loss quality.

Fabrication of all fused silica mirrors were completed by the end of 2016. These include the beam splitter (BS), mirrors in the Power Recycling Cavity (PRM, PR2, and PR3), mirrors in the Signal Recycling Cavity (SRM, SR2, and SR3), mirrors in the Mode Cleaner (MCe, MCI, and MCo), and mirrors for the Input Mode Matching Telescope (IMMT1 and IMMT2). Currently, some fabrication which was not initially planned is under way such as for a replacement of a damaged mirror during installation at the Kamioka site, and mirrors in the Output Mode Matching Telescope (OMMT1 and OMMT2).

Observational Cosmology Group

[Spokesperson : Yoshiaki Ono]

ICRR, The Univ. of Tokyo, Kashiwa, Chiba 277-8582

Morphologies of $\sim 190,000$ Galaxies at $z = 0 - 10$ Revealed with HST Legacy Data **II. Evolution of Clumpy Galaxies [1]**

We investigate the evolution of clumpy galaxies with *Hubble Space Telescope (HST)* samples of $\sim 17,000$ photo- z and Lyman break galaxies at $z \simeq 0 - 8$. We detect clumpy galaxies with off-center clumps in a self-consistent algorithm that is well tested with previous study results, and we measure the number fraction of clumpy galaxies at the rest-frame UV, $f_{\text{clumpy}}^{\text{UV}}$. We identify an evolutionary trend of $f_{\text{clumpy}}^{\text{UV}}$ over $z \simeq 0 - 8$ for the first time: $f_{\text{clumpy}}^{\text{UV}}$ increases from $z \simeq 8$ to $z \simeq 1 - 3$ and subsequently decreases from $z \simeq 1$ to $z \simeq 0$, which follows the trend of the Madau-Lilly plot. A low average Sérsic index of $n \simeq 1$ is found in the underlining components of our clumpy galaxies at $z \simeq 0 - 2$, indicating that typical clumpy galaxies have disk-like surface brightness profiles. Our $f_{\text{clumpy}}^{\text{UV}}$ values correlate with physical quantities related to star formation activities for star-forming galaxies at $z \simeq 0 - 7$. We find that clump colors tend to be red at a small galactocentric distance for massive galaxies with $\log M_*/M_\odot \gtrsim 11$. All of these results are consistent with the picture that a majority of clumps form in the violent disk instability and migrate into the galactic centers.

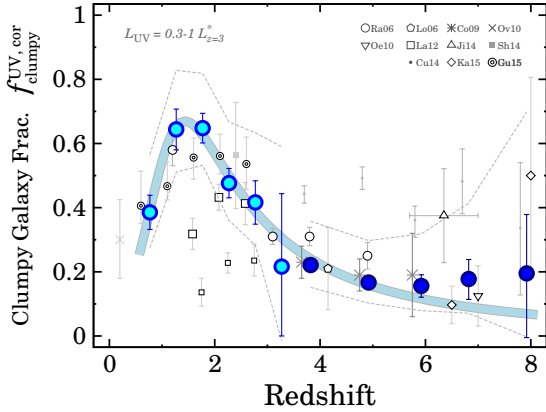


Fig. 10. Redshift evolution of the clumpy galaxy fraction, $f_{\text{clumpy}}^{\text{UV,cor}}$, at $z \sim 0 - 8$ for the star-forming galaxies with $L_{\text{UV}} = 0.3 - 1 L_{z=3}^*$. The filled cyan and blue circles denote the SFGs and the LBGs, respectively. The error bars are given by Poisson statistics from the galaxy number counts. The cyan solid curve denotes the best-fit function. The gray dashed lines present the upper and lower limits of $f_{\text{clumpy}}^{\text{UV,cor}}$ derived by changing F_c in a range of $0.5 \times F_c^{\text{fid}} - 2 \times F_c^{\text{fid}}$, where F_c^{fid} is the fiducial F_c value for each redshift. The gray symbols show LBAs and LBGs with clumps or irregular morphologies in the literature. The small and large open squares are based on the selection of clumpy galaxies with the GM_{20} and A indices, respectively. The double circles represent $f_{\text{clumpy}}^{\text{UV,cor}}$ for SFGs with $\log M_*/M_\odot = 9.6 - 10.4$ in previous work. The error bars are given by Poisson statistics from the number of sample galaxies, if no error bar has been presented in the literature. This figure is reproduced by permission of the AAS.

Bibliography

- [1] Shibuya, T., Ouchi, M., Kubo, M., & Harikane, Y. 2016, *The Astrophysical Journal*, 821, 72

Evolution of Stellar-to-Halo Mass Ratio at $z = 0 - 7$ Identified by Clustering Analysis with the Hubble Legacy Imaging and Early Subaru/Hyper Suprime-Cam Survey Data [2]

In collaboration with the members of Kavli Institute for the Physics and Mathematics of the Universe, Academia Sinica, University of Geneva, The University of Tokyo, Princeton University, and National Astronomical Observatory of Japan.

We present clustering analysis results from 10,381 Lyman break galaxies (LBGs) at $z \sim 4 - 7$, identified in the Hubble legacy deep imaging and new complimentary large-area Subaru/Hyper Suprime-Cam data. We measure the angular correlation functions of these LBGs at $z \sim 4, 5, 6$, and 7 , and fit these measurements using halo occupation distribution (HOD) models that provide an estimate of halo masses, $M_h \sim (1 - 20) \times 10^{11} M_\odot$. Our M_h estimates agree with those obtained by previous clustering studies in a UV-magnitude versus M_h plane and allow us to calculate stellar-to-halo mass ratios (SHMRs) of LBGs. By comparison with the $z \sim 0$ SHMR, we identify evolution of the SHMR from $z \sim 0$ to $z \sim 4$, and $z \sim 4$ to $z \sim 7$ at the $> 98\%$ confidence levels. The SHMR decreases by a factor of ~ 2 from $z \sim 0$ to 4 , and increases by a factor of ~ 4 from $z \sim 4$ to 7 at the dark matter halo mass of $M_h \sim 10^{11} M_\odot$. We compare our SHMRs with results of a hydrodynamic simulation and a semi-analytic model and find that these theoretical studies do not predict the SHMR increase from $z \sim 4$ to 7 . We obtain the baryon conversion efficiency (BCE) of LBGs at

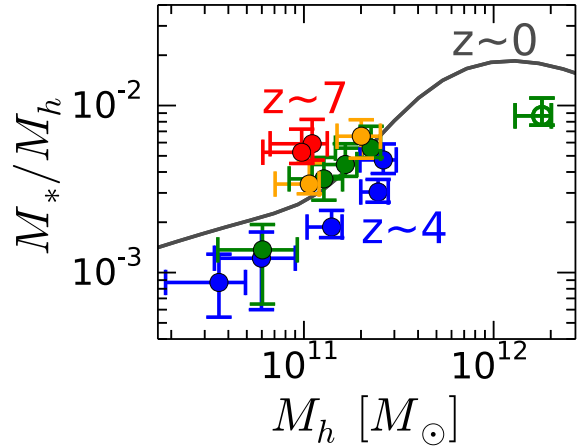


Fig. 11. SHMR of central galaxies as a function of dark matter halo mass at $z \sim 4, 5, 6$, and 7 . The blue, green, orange, and red circles represent the SHMR of our Hubble subsample at $z \sim 4, 5, 6$, and 7 , respectively. The open green circle denotes the SHMR of our subsample constructed from the HSC data. The gray solid curve is the SHMR at $z \sim 0$ obtained in the literature, which is computed by P. Behroozi with the same cosmological parameters and halo mass definition as in our analysis. This figure is reproduced by permission of the AAS.

$z \sim 4$ and find that the BCE increases with increasing dark matter halo mass. Finally, we compare our clustering+HOD estimates with results from abundance matching techniques and conclude that the M_h estimates of the clustering+HOD analyses agree with those of the simple abundance matching within a factor of 3, and that the agreement improves when using more sophisticated abundance matching techniques that include subhalos, incompleteness, and/or evolution in the star formation and stellar mass functions.

Bibliography

- [2] Harikane Y., Ouchi, M., Ono, Y., More, S., Saito, S., Lin, Y.-T., Coupon, J., Shimasaku, K., Shibuya, T., Price, P., Lin, L., Hsieh, B.-C., Ishigaki, M., Komiyama, Y., Silverman, J., Takata, T., Tamazawa, H., & Toshikawa, J. 2016, *The Astrophysical Journal*, 821, 123

Very Compact Dense Galaxy Overdensity with $\delta \simeq 130$ Identified at $z \sim 8$: Implications for Early Protocluster and Cluster-Core Formation [3]

We report the first identification of a compact dense galaxy overdensity at $z \sim 8$ called A2744z8OD. A2744z8OD consists of eight Y -dropout galaxies behind Abell 2744 that were originally pinpointed by Hubble Frontier Fields studies. However, so far, no studies have derived the basic physical quantities of structure formation or made comparisons with theoretical models. We obtain a homogeneous sample of dropout galaxies at $z \sim 8$ from eight field data of Hubble legacy images that are as deep as the A2744z8OD data. Using the sample, we find that a galaxy surface overdensity value of A2744z8OD is very high $\delta \simeq 130$, where δ is defined by an overdensity in a small circle of $6''$ ($\simeq 30$ physical kpc) radius. Because there is no such large δ value reported for high- z overdensities to

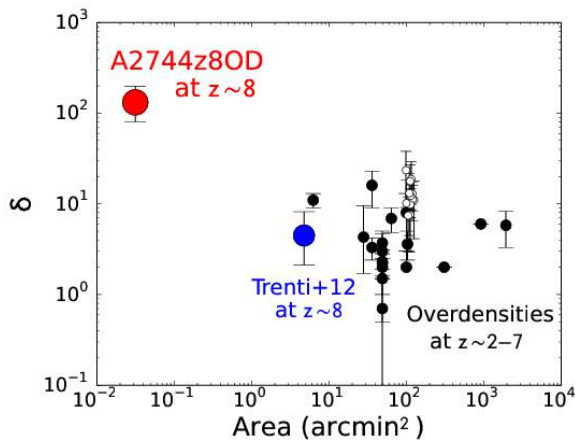


Fig. 12. Galaxy surface overdensity δ as a function of area. The area is the one used for the δ measurements. The red circle represents A2744z8OD at $z \sim 8$, while the blue circle denotes the overdensity at $z \sim 8$ reported by previous work. The black filled and open circles indicate the overdensities at $z \sim 2-7$ obtained in the literature. This figure is reproduced by permission of the AAS.

date, A2744z8OD is a system that is clearly different from those found in previous high- z overdensity studies. In the galaxy+structure formation models of Henriques et al., there exist a very similar overdensity, Modelz8OD, that is made of eight model dropout galaxies at $z \sim 8$ in a $6''$ -radius circle. Modelz8OD is a progenitor of a today's $10^{14}M_{\odot}$ cluster, and more than half of the seven Modelz8OD galaxies are merged into the brightest cluster galaxy of the cluster. If Modelz8OD is a counterpart to A2744z8OD, the models suggest that A2744z8OD would be part of a cluster core forming from a $10^{14}M_{\odot}$ cluster that began star formation at $z > 12$.

Bibliography

[3] Ishigaki, M., Ouchi, M., & Harikane, Y. 2016, *The Astrophysical Journal*, 822, 5

Bright and Faint Ends of Ly α Luminosity Functions at $z = 2$ Determined by the Subaru Survey: Implications for AGN, Magnification Bias, and ISM H I Evolution [4]

In collaboration with the members of Observatoire de Genève and The University of Tokyo.

We present the Ly α luminosity functions (LFs) derived by our deep Subaru narrowband survey that identifies a total of 3,137 Ly α emitters (LAEs) at $z = 2.2$ in five independent blank fields. This sample of LAEs is the largest to date and covers a very wide Ly α luminosity range of $\log L_{\text{Ly}\alpha} = 41.7 - 44.4 \text{ erg s}^{-1}$. We determine the Ly α LF at $z = 2.2$ with unprecedented accuracy and obtain the best-fit Schechter parameters of $L_{\text{Ly}\alpha}^* = 5.29^{+1.67}_{-1.13} \times 10^{42} \text{ erg s}^{-1}$, $\phi_{\text{Ly}\alpha}^* = 6.32^{+3.08}_{-2.31} \times 10^{-4} \text{ Mpc}^{-3}$, and $\alpha = -1.75^{+0.10}_{-0.09}$, showing a steep faint-end slope. We identify a significant hump at the LF bright end ($\log L_{\text{Ly}\alpha} > 43.4 \text{ erg s}^{-1}$). Because all of the LAEs in the bright-end hump have a bright counterpart(s) in either the X-ray, UV, or radio data, this bright-end hump is not made by gravitational lensing magnification bias but by AGNs. These AGNs allow us to derive the AGN UV LF at $z \sim 2$ down to the faint magnitude limit of $M_{\text{UV}} \simeq -22.5$ and to constrain the faint-end slope of AGN UV LF,

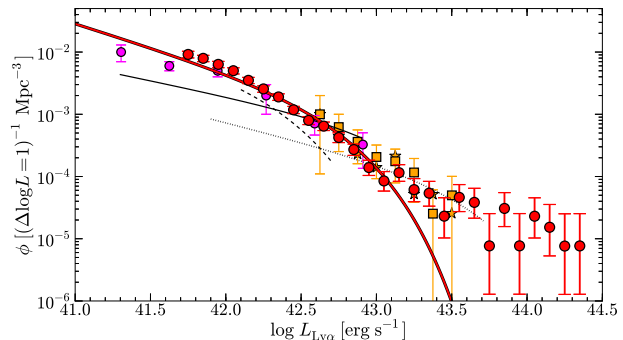


Fig. 13. Comparison of our $z = 2.2$ Ly α LF with the previous measurements of Ly α LF at $z \sim 2$. The red filled circles denote our Ly α LF and the red solid curve is the best-fit Schechter function. The magenta filled circles represent the Ly α LF given by previous work at $2 < z < 3.2$. The orange stars and squares show the LFs in the literature based on the spectroscopic surveys of LAEs at $1.9 < z < 2.8$ and $1.9 < z < 3.8$, respectively. The black solid, dashed, and dotted lines are the best-fit Schechter functions obtained by previous studies. Since the previous Ly α LF estimates are limited in the ranges of $\log L_{\text{Ly}\alpha} = 41.3 - 42.9 \text{ erg s}^{-1}$, $42.1 - 42.7 \text{ erg s}^{-1}$, and $41.9 - 43.7 \text{ erg s}^{-1}$, we show the black lines within these ranges. This figure is reproduced by permission of the AAS.

$\alpha_{\text{AGN}} = -1.2 \pm 0.1$, which is flatter than those at $z > 4$. Based on the Ly α and UV LFs from our and previous studies, we find an increase of Ly α escape fraction $f_{\text{esc}}^{\text{Ly}\alpha}$ from $z \sim 0$ to 6 by two orders of magnitude. This large $f_{\text{esc}}^{\text{Ly}\alpha}$ increase can be explained neither by the evolution of stellar population nor by outflow alone, but the evolution of neutral hydrogen H I density in interstellar medium that enhances dust attenuation for Ly α by resonance scattering. Our uniform expanding shell models suggest that the typical H I column density decreases from $N_{\text{HI}} \sim 7 \times 10^{19}$ ($z \sim 0$) to $\sim 1 \times 10^{18} \text{ cm}^{-2}$ ($z \sim 6$) to explain the large $f_{\text{esc}}^{\text{Ly}\alpha}$ increase.

Bibliography

[4] Konno, A., Ouchi, M., Nakajima, K., Duval, F., Kusakabe, H., Ono, Y., & Shimasaku, K. 2016, *The Astrophysical Journal*, 823, 20

Cosmic Galaxy-IGM H I Relation at $z \sim 2-3$ Probed in the COSMOS/UltraVISTA 1.6 Deg 2 Field [5]

In collaboration with the members of University College London, Kavli Institute for the Physics and Mathematics of the Universe, University of California Santa Cruz, Osaka Sangyo University, University of Texas at Austin, and National Astronomical Observatory of Japan.

We present spatial correlations of galaxies and IGM neutral hydrogen H I in the COSMOS/UltraVISTA 1.62 deg 2 field. Our data consist of 13,415 photo- z galaxies at $z \sim 2-3$ with $K_s < 23.4$ and the Ly α forest absorption lines in the background quasar spectra selected from SDSS data with no signature of damped Ly α system contamination. We estimate a galaxy overdensity δ_{gal} in an impact parameter of 2.5 (proper) Mpc, and calculate the Ly α forest fluctuations $\delta_{(F)}$ whose negative values correspond to the strong Ly α forest absorption lines. We identify weak evidence of an anti-correlation between δ_{gal} and $\delta_{(F)}$ with a Spearman's rank correlation coefficient of -0.39 suggesting that the galaxy overdensities and the Ly α forest absorption lines positively correlate in space at the $\sim 90\%$ con-

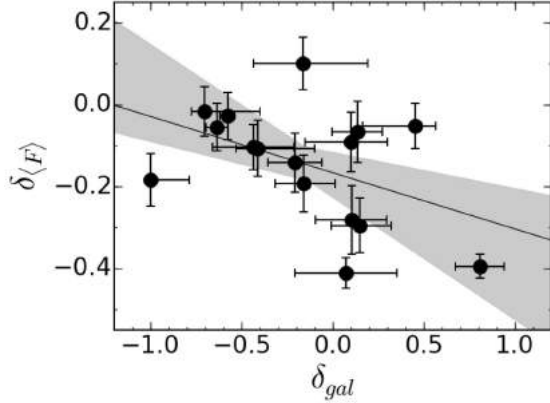


Fig. 14. Ly α forest fluctuation $\delta_{(F)}$ as a function of the galaxy overdensity δ_{gal} . The circles with the error bars represent the galaxy-HI properties of the cylinders. The best-fit linear model is represented by a solid line, with the shaded region indicating the 1σ uncertainty range that is calculated by the perturbation method. This figure is reproduced by permission of the AAS.

fidence level. This positive correlation indicates that high- z galaxies exist around an excess of HI gas in the Ly α forest. We find four cosmic volumes, dubbed A_{obs}, B_{obs}, C_{obs}, and D_{obs}, that have extremely large (small) values of $\delta_{gal} \simeq 0.8$ (-1) and $\delta_{(F)} \simeq 0.1$ (-0.4), three out of which, B_{obs}–D_{obs}, significantly depart from the δ_{gal} – $\delta_{(F)}$ correlation, and weaken the correlation signal. We perform cosmological hydrodynamical simulations and compare with our observational results. Our simulations reproduce the δ_{gal} – $\delta_{(F)}$ correlation, agreeing with the observational results. Moreover, our simulations have model counterparts of A_{obs}–D_{obs}, and suggest that the observations pinpoint, by chance, a galaxy overdensity like a proto-cluster, gas filaments lying on the quasar sightline, a large void, and orthogonal low-density filaments. Our simulations indicate that the significant departures of B_{obs}–D_{obs} are produced by the filamentary large-scale structures and the observation sightline effects.

Bibliography

- [5] Mukae, S., Ouchi, M., Kakiichi, K., Suzuki, N., Ono, Y., Cai, Z., Inoue, A., Chiang, Y.-K., Shibuya, T., & Matsuda, Y. 2017, *The Astrophysical Journal*, 835, 281

Theory Group

Overview

The theory group is active in elementary particle physics focusing on particle phenomenology, and in astroparticle physics focusing on particle cosmology. In particle physics, the main topics are theoretical studies of dark matter, inflation and extensions of the standard model. In astroparticle physics, the main topics are theoretical studies of inflation, thermal history of the early universe, dark matter, baryogenesis and big-bang nucleosynthesis.

In this year, the LHC accumulated around 40 fb^{-1} at the center of mass energy of 13 TeV. Many of the intriguing anomalies observed last year turned out to be statistical fluctuations. However, a large part of the results with 13TeV data will be released in the coming year, which may include interesting anomalies.

In June, the LIGO detectors announced a second robust signal from a black hole merger. In November, they began the second observation run called O2. The sensitivity is upgraded so that it can detect signals from about 20% further away. The results will come in the next year. If they continue to find heavy black holes, their origin becomes one of the most interesting topics.

The supersymmetric (SUSY) extension of the standard model (SM) in the particle physics is considered to be one of the most promising models beyond the standard model. It solves the naturalness problem for the Higgs boson mass term in the standard model, and it is also compatible with the grand unified theories (GUTs). Our group has been studying phenomenological and cosmological aspects of the SUSY models.

Recent cosmological observations including the Planck data determine precisely the mean densities of matter and baryon in the Universe, and existence of non-baryonic dark matter is established. Weakly interacting massive particles (WIMPs) are considered to be good candidates of the dark matter. They act as the cold dark matter in the structure formation of the universe. Our group has been studying model building for dark matter and detectability in direct and indirect search experiments.

For understanding of the early universe, a role of the elementary particle physics is crucial. Recent progress in the particle physics such as grand unification theories and supersymmetry leads us to a more deeper insight into the fundamental aspects of the early universe. In the inflationary universe, the quantum fluctuations of the scalar field which drives the inflation become the density fluctuations and lead to formation of the structure observed in the present universe. On the other hand cosmology and astrophysics are used to test new theories in particle physics. Such particle cosmology is one of main subjects of our group.

Big Bang Nucleosynthesis (BBN) is one of the most important subjects in modern cosmology. Predicted abundances of the light elements are very sensitive to the cosmological scenario. On the other hand, physics beyond the standard model predicts the new particles which would have existed at the BBN epoch. Such particles may spoil the success of BBN, which leads to constraints on the new particles and the particle physics models.

The grand unified theories predict that our universe undergoes several vacuum phase transitions. In the course of phase transitions topological defects (monopoles, cosmic strings and domain walls) are generally produced depending on symmetries of the vacua. Our group has studied evolution of various topological defects.

Particle Phenomenology

[Spokesperson : M. Ibe]

ICRR, The Univ. of Tokyo, Kashiwa, Chiba 277-8582

Dark Matter, Inflation

- Revisiting gravitino dark matter in thermal leptogenesis

In collaboration with the members of ICRR and Kavli IPMU.

In this paper, we revisit the gravitino dark matter scenario in the presence of the bilinear R -parity violating interaction. In particular, we discuss a consistency with the thermal leptogenesis. For a high reheating temperature required for the thermal leptogenesis, the gravitino dark matter tends to be overproduced, which puts a severe upper limit on the gluino mass. As we will show, a large portion of parameter space of the gravitino dark matter scenario has been excluded by combining the constraints from the gravitino abundance and the null results of the searches for the superparticles at the LHC experiments.

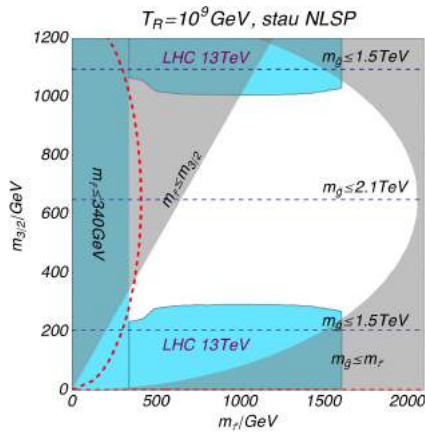


Fig. 15. Combined constraints for the stau NLSP. The reheating temperature is assumed to be $T_R = 10^9$ GeV. The gray shaded regions are excluded where the gravitino is no more the LSP. The blue shaded regions are excluded by ATLAS and CMS search. The GUT relation of the gaugino mass can be satisfied in the left side of the red dashed line. The horizontal dashed lines show the upper limit on the gluino mass for a given gravitino mass.

In particular, the models with the stau (and other charged slepton) NLSP has been almost excluded by the searches for the long-lived charged particles at the LHC unless the required reheating temperature is somewhat lowered by assuming, for example, a degenerated right-handed neutrino mass spectrum.

Thermal Relic Dark Matter Beyond the Unitarity Limit

In collaboration with the members of ICRR, IPMU, IBS, and University of California, Berkeley

We discuss a simple model of thermal relic dark matter whose mass can be much larger than the so-called unitarity limit on the mass of point-like particle dark matter. The model consists of new strong dynamics with one flavor of fermions in the fundamental representation which is much heavier than the dynamical scale of the new strong dynamics. Dark matter is identified with the lightest baryonic hadron of the new dynamics. The baryonic hadrons annihilate into the mesonic hadrons of the new strong dynamics when they have large radii. Resultantly, thermal relic dark matter with a mass in the PeV range is possible.

Constraints on $L_\mu - L_\tau$ Gauge Interactions from Rare Kaon Decay

In collaboration with the members of ICRR and IPMU

A model with $L_\mu - L_\tau$ gauge symmetry is the least constrained model as a resolution to the disagreement of the muon anomalous magnetic moment between the theoretical predictions and the experimental results. In this paper, we discuss how well the $L_\mu - L_\tau$ model can be constrained by looking for decays of the charged kaon associated with a $L_\mu - L_\tau$ gauge boson. More concretely, we consider searches for single muon tracks from the decays of stopped charged kaon as in the E949 experiment. In our conservative estimation, we find that the favored parameter region for the muon anomalous magnetic moment can be tested by using a 10 times larger number of the stopped charged kaons and about a 100 times better photon rejection rate than the E949 experiment.

Gravitino Problem in Minimal Supergravity Inflation

In collaboration with the members of ICRR, IPMU, Univ. of Tokyo, KIAS and Stanford Univ.

We study non-thermal gravitino production in the minimal supergravity inflation. In this minimal model utilizing orthogonal nilpotent superfields, the particle spectrum includes only graviton, gravitino, inflaton, and goldstino. We find that a substantial fraction of the cosmic energy density can be transferred to the longitudinal gravitino due to non-trivial change of its sound speed. This implies either a breakdown of the effective theory after inflation or a serious gravitino problem.

Bibliography

- [1] M. Ibe, M. Suzuki and T. T. Yanagida, JHEP **1702**, 063 (2017) [arXiv:1609.06834 [hep-ph]].
- [2] K. Harigaya, M. Ibe, K. Kaneta, W. Nakano and M. Suzuki, JHEP **1608**, 151 (2016) doi:10.1007/JHEP08(2016)151 [arXiv:1606.00159 [hep-ph]].
- [3] M. Ibe, W. Nakano and M. Suzuki, Phys. Rev. D **95**, no. 5, 055022 (2017) doi:10.1103/PhysRevD.95.055022 [arXiv:1611.08460 [hep-ph]].
- [4] F. Hasegawa, K. Mukaida, K. Nakayama, T. Terada and Y. Yamada, Phys. Lett. B **767**, 392 (2017) doi:10.1016/j.physletb.2017.02.030 [arXiv:1701.03106 [hep-ph]].

Beyond the Standard Model, Collider Phenomenology

- Lower limit on the gravitino mass in low-scale gauge mediation with $m_H \simeq 125$ GeV

In collaboration with the members of ICRR and IPMU

We revisit low-scale gauge mediation models in light of recent observations of CMB Lensing and Cosmic Shear which put a severe upper limit on the gravitino mass, $m_{3/2} \lesssim 4.7$ eV. With such a stringent constraint, many models of low-scale gauge mediation are disfavored when the squark masses are required to be rather large to explain the observed Higgs boson mass unless the gravitino abundance is diluted by late time entropy production. In this note, we discuss a type of low-scale gauge mediation models which satisfy both the observed Higgs boson mass and the upper limit on the gravitino mass. We also show that the gravitino mass cannot be smaller than about 1eV even in such models, which may be tested in future observations of 21 cm line fluctuations.

- Cracking down on fake photons: Cases of diphoton resonance imposters

In collaboration with the members of ICRR, IPMU, KEK and Tokyo Institute of Technology

The search for high-mass diphoton resonance is ongoing at the LHC, and will provide definite evidence of physics beyond the Standard Model once it is discovered. Along with the diphoton resonance, many theoretical models also predict resonances decaying not into a pair of photons but into a pair of highly collimated photon-jets. In this paper, we study how well we can distinguish such diphoton resonance imposters, i.e. diphoton-jet resonances, from diphoton resonances by examining detector responses to the photon-jets. We

find that the sum of pT of the first e+e pair from the photon conversion provides strong discrimination power. We also discuss determination of the lifetime of the light intermediate particle by measuring the photon conversion points.

• On the Gauge Invariance of the Decay Rate of False Vacuum

In collaboration with the members of IPMU, KEK and the University of Tokyo

We study the gauge invariance of the decay rate of the false vacuum for the model in which the scalar field responsible for the false vacuum decay has gauge quantum number. In order to calculate the decay rate, one should integrate out the field fluctuations around the classical path connecting the false and true vacua (i.e., so-called bounce). Concentrating on the case where the gauge symmetry is broken in the false vacuum, we show a systematic way to perform such an integration and present a manifestly gauge-invariant formula of the decay rate of the false vacuum.

• Dark Matter Candidates in a Visible Heavy QCD Axion Model

In collaboration with the members of ICRR and IPMU

In this paper, we discuss dark matter candidates in a visible heavy QCD axion model. There, a mirror copied sector of the Standard Model with mass scales larger than the Standard Model is introduced. By larger mass scales of the mirrored sector, the QCD axion is made heavy via the axial anomaly in the mirrored sector without spoiling the Peccei-Quinn mechanism to solve the strong CP problem. Since the mirror copied sector possesses the same symmetry structure with the Standard Model sector, the model predicts multiple stable particles. As we will show, the mirrored charged pion and the mirrored electron can be viable candidates for dark matter. They serve as self-interacting dark matter with a long-range force. We also show that the mirrored neutron can be lighter than the mirrored proton in a certain parameter region. There, the mirrored neutron can also be a viable dark matter candidate when its mass is around 100 TeV. It is also shown that the mirrored neutrino can also be a viable candidate for dark matter.

Bibliography

- [1] M. Ibe and T. T. Yanagida, Phys. Lett. B **764**, 260 (2017) doi:10.1016/j.physletb.2016.11.016 [arXiv:1608.01610 [hep-ph]].
- [2] H. Fukuda, M. Ibe, O. Jinnouchi and M. Nojiri, PTEP **2017**, no. 3, 033B05 (2017) doi:10.1093/ptep/ptx019 [arXiv:1607.01936 [hep-ph]].
- [3] M. Endo, T. Moroi, M. M. Nojiri and Y. Shoji, Phys. Lett. B **771**, 281 (2017) doi:10.1016/j.physletb.2017.05.057 [arXiv:1703.09304 [hep-ph]].
- [4] H. Fukuda, M. Ibe and T. T. Yanagida, Phys. Rev. D **95**, no. 9, 095017 (2017) doi:10.1103/PhysRevD.95.095017 [arXiv:1702.00227 [hep-ph]].

Particle Cosmology

[Spokesperson : M. Kawasaki]

ICRR, The Univ. of Tokyo, Kashiwa, Chiba 277-8582

Inflation, Thermal History in the early Universe

• Revisiting constraints on small scale perturbations from big-bang nucleosynthesis

In collaboration with the members of ICRR and KIPMU.

We revisit the constraints on the small scale density perturbations ($10^4 \text{ Mpc}^{-1} \lesssim k \lesssim 10^5 \text{ Mpc}^{-1}$) from the modification of the freeze-out value of the neutron-proton ratio at big-bang nucleosynthesis era. Around the freeze-out temperature $T \sim 0.5 \text{ MeV}$, the universe can be divided into several local patches which have different temperatures since any perturbation which enters the horizon after the neutrino decoupling has not diffused yet. Taking account of this situation, we calculate the freeze-out value in detail. We find that the small scale perturbations decrease the n-p ratio in contrast to previous works. With use of the latest observed ^4He abundance, we obtain the constraint on the power spectrum of the curvature perturbations as $\Delta_{\mathcal{R}}^2 \lesssim 0.018$ on $10^4 \text{ Mpc}^{-1} \lesssim k \lesssim 10^5 \text{ Mpc}^{-1}$.

• Squeezed bispectrum in the δN formalism: local observer effect in field space

In collaboration with the members of ICRR and Portsmouth U., ICG.

The prospects of future galaxy surveys for non-Gaussianity measurements call for the development of robust techniques for computing the bispectrum of primordial cosmological perturbations. In this paper, we propose a novel approach to the calculation of the squeezed bispectrum in multiple-field inflation. With use of the N formalism, our framework sheds new light on the recently pointed out difference between the squeezed bispectrum for global observers and that for local observers, while allowing one to calculate both. For local observers in particular, the squeezed bispectrum is found to vanish in single-field inflation. Furthermore, our framework allows one to go beyond the near-equilateral ('small hierarchy') limit, and to automatically include intrinsic non-Gaussianities that do not need to be calculated separately. The explicit computational programme of our method is given and illustrated with a few examples.

Bibliography

- [1] K. Inomata, M. Kawasaki and Y. Tada, Phys. Rev. D **94**, no. 4, 043527 (2016) doi:10.1103/PhysRevD.94.043527 [arXiv:1605.04646 [astro-ph.CO]].
- [2] Y. Tada and V. Vennin, JCAP **1702**, no. 02, 021 (2017) doi:10.1088/1475-7516/2017/02/021 [arXiv:1609.08876 [astro-ph.CO]].

Dark Matter, Baryogenesis, Big-Bang nucleosynthesis

• Elucidating Dark Energy with Future 21 cm Observations at the Epoch of Reionization

In collaboration with the members of ICRR, KEK, Saga.U and IBS(CTPU).

We investigate how precisely we can determine the nature of dark energy such as the equation of state (EoS) and its time dependence by using future observations of 21 cm fluctuations at the epoch of reionization ($6.8 \lesssim z \lesssim 10$) such as Square Kilometre Array (SKA) and Omniscience in combination with those from cosmic microwave background, baryon acoustic oscillation, type Ia supernovae

and direct measurement of the Hubble constant. We consider several parametrizations for the EoS and find that future 21 cm observations will be powerful in constraining models of dark energy, especially when its EoS varies at high redshifts.

- **Constraining light gravitino mass with 21 cm line observation**

In collaboration with the members of ICRR.

We investigate how well we can constrain the mass of light gravitino $m_{3/2}$ by using future observations of 21 cm line fluctuations such as Square Kilometre Array (SKA) and Omniscope. Models with light gravitino with the mass $m_{3/2} \lesssim \mathcal{O}(10)$ eV are quite interesting because they are free from the cosmological gravitino problem and consistent with many baryogenesis/leptogenesis scenarios. We evaluate expected constraints on the mass of light gravitino from the observations of 21 cm line, and show that the observations are quite useful to prove the mass. If the gravitino mass is $m_{3/2} = 1$ eV, we found expected 1σ errors on $m_{3/2}$ are $\sigma(m_{3/2}) = 0.25$ eV (SKA phase 1), 0.16 eV (SKA phase 2) and 0.067 eV (Omniscope) in combination with Planck + Simons Array + DESI (BAO) + H_0 . Additionally, we also discuss detectability of the effective number of neutrino species by varying the effective number of neutrino species for light gravitino $N_{3/2}$ and constraints on the mass of light gravitino in the presence of massive neutrinos. We show that 21 cm line observations can detect the nonzero value of $N_{3/2}$, and allow us to distinguish the effects of the light gravitino from those of massive neutrino.

- **Cosmology with the Square Kilometre Array by SKA-Japan**

In collaboration with the members of SKA-Japan Consortium Cosmology Science Working Group.

In the past several decades, the standard cosmological model has been established and its parameters have been measured to a high precision, while there are still many of the fundamental questions in cosmology; such as the physics in the very early Universe, the origin of the cosmic acceleration and the nature of the dark matter. The future world's largest radio telescope, Square Kilometre Array (SKA), will be able to open the new frontier of cosmology and will be one of the most powerful tools for cosmology in the next decade. The cosmological surveys conducted by the SKA would have the potential not only to answer these fundamental questions but also deliver the precision cosmology. In this article we briefly review the role of the SKA from the view point of the modern cosmology. The cosmology science led by the SKA-Japan Consortium (SKA-JP) Cosmology Science Working Group is also discussed.

- **Foreground effect on the J -factor estimation of classical dwarf spheroidal galaxies**

In collaboration with the members of ICRR and IPMU

The gamma-ray observation of the dwarf spheroidal galaxies (dSphs) is a promising approach to search for the dark matter annihilation (or decay) signal. The dSphs are the nearby satellite galaxies with a clean environment and dense dark matter halo so that they give stringent constraints on the $\mathcal{O}(1)$ TeV dark matter. However, recent studies have revealed that current estimation of astrophysical factors relevant for the dark matter searches are not conservative, where the various non-negligible systematic uncertainties are not taken into account. Among them, the effect of foreground stars on the astrophysical factors has not been paid much attention, which becomes more

important for deeper and wider stellar surveys in the future. In this article, we assess the effects of the foreground contamination by generating the mock samples of stars and using a model of future spectrographs. We investigate various data cuts to optimize the quality of the data and find that the cuts on the velocity and surface gravity can efficiently eliminate the contamination. We also propose a new likelihood function that includes the foreground distribution function. We apply this likelihood function to the fit of the three types of the mock data (Ursa Minor, Draco with large dark matter halo and Draco with small halo) and three cases of the observation. The likelihood successfully reproduces the input J -factor value while the fit without considering the foreground distribution gives a large deviation from the input value by a factor of 3.

- **Relaxation leptogenesis, isocurvature perturbations, and the cosmic infrared background**

In collaboration with the members of ICRR, Kavli IPMU, UCLA and University of Minnesota

Observations of cosmic infrared background (CIB) radiation exhibit significant fluctuations on small angular scales. A number of explanations have been put forth, but there is currently no consensus on the origin of these large fluctuations. We consider the possibility that small-scale fluctuations in matter-antimatter asymmetry could lead to variations in star formation rates which are responsible for the CIB fluctuations. We show that the recently proposed Higgs relaxation leptogenesis mechanism can produce such small-scale baryonic isocurvature perturbations which can explain the observed excess in the CIB fluctuations.

Bibliography

- [1] K. Kohri, Y. Oyama, T. Sekiguchi and T. Takahashi, JCAP **1702**, no. 02, 024 (2017) doi:10.1088/1475-7516/2017/02/024 [arXiv:1608.01601 [astro-ph.CO]].
- [2] Y. Oyama and M. Kawasaki, arXiv:1605.09191 [astro-ph.CO].
- [3] D. Yamauchi *et al.* [SKA-Japan Consortium Cosmology Science Working Group], PoS DSU **2015**, 004 (2016) [Publ. Astron. Soc. Jap. **68**, no. 6, R2 (2016)] doi:10.1093/pasj/psw098 [arXiv:1603.01959 [astro-ph.CO]].
- [4] K. Ichikawa, M. N. Ishigaki, S. Matsumoto, M. Ibe, H. Sugai, K. Hayashi and S. i. Horigome, Mon. Not. Roy. Astron. Soc. **468**, no. 3, 2884 (2017) doi:10.1093/mnras/stx682 [arXiv:1608.01749 [astro-ph.GA]].
- [5] M. Kawasaki, A. Kusenko, L. Pearce, and L. Yang, Phys. Rev. D **95**, no. 10, 103006 (2017) doi:10.1103/PhysRevD.95.103006 [arXiv:1701.02175 [hep-ph]].

Primordial Black Holes

- **Inflationary primordial black holes for the LIGO gravitational wave events and pulsar timing array experiments**

In collaboration with the members of ICRR and KIPMU.

Primordial black holes (PBHs) are one of the candidates to explain the gravitational wave (GW) signals observed by the LIGO detectors. Among several phenomena in the early Universe, cosmic inflation is a major example to generate PBHs from large primordial density perturbations. In this paper, we discuss the possibility

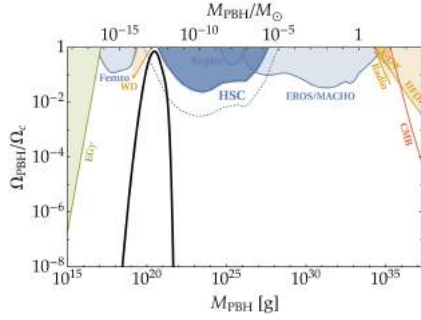


Fig. 16. **Black thick line** shows $\Omega_{\text{PBH}}(M)$. We require the total abundance be equal to the observed DM density, $\Omega_{\text{PBH,tot}} = \Omega_c$. **The solid lines with shades** represent relevant observational constraints on the current PBH mass spectrum [class (a)]: extragalactic gamma-ray (EG γ), femtolensing (Femto), existence of white dwarfs in our local galaxy (WD), Subaru HSC microlensing (HSC), Kepler milli/microlensing (Kepler), EROS/MACHO microlensing (EROS/MACHO), dynamical heating of ultra-faint dwarf galaxies (UFD), and X-ray/radio constraints. **The solid line without shade** illustrates the observational constraints on the past PBH mass spectrum [class (b)]: accretion constraints by CMB. Here we do not show the pulsar timing array constraints on gravitational waves via second order effects because they are indirect and depend on the concrete shape of the scalar power spectrum. Nevertheless, it is noticeable that their constraints are so strong that PBHs with $M \sim 0.75\gamma M_\odot - 75\gamma M_\odot$ are excluded, if they are generated via superhorizon fluctuations. The conservative bound of the new HSC microlensing constraint is shown by the thick blue line with the deep shade, and the dotted one utilizes an extrapolation from the HST PHAT star catalogs in the disk region.

to interpret the observed GW events as mergers of PBHs which are produced by cosmic inflation. The primordial curvature perturbation should be large enough to produce a sizable amount of PBHs and thus we have several other probes to test this scenario. We point out that the current pulsar timing array (PTA) experiments already put severe constraints on GWs generated via the second-order effects, and that the observation of the cosmic microwave background (CMB) puts severe restriction on its μ -distortion. In particular, it is found that the scalar power spectrum should have a very sharp peak at $k \sim 10^6 \text{ Mpc}^{-1}$ to fulfill the required abundance of PBHs while evading constraints from the PTA experiments together with the μ -distortion. We propose a mechanism which can realize such a sharp peak. In the future, simple inflation models that generate PBHs via almost Gaussian fluctuations could be probed/excluded.

• Inflationary Primordial Black Holes as All Dark Matter

In collaboration with the members of ICRR and KIPMU.

Following a new microlensing constraint on primordial black holes (PBHs) with $\sim 10^{20} - 10^{28} \text{ g}$ (Niikura et al. arXiv:1701.02151), we revisit the idea of PBH as all Dark Matter (DM). We have shown that the updated observational constraints suggest the viable mass function for PBHs as all DM to be $\simeq 10^{20} \text{ g}$ with a small width $\sigma \lesssim 0.1$, by imposing observational constraints on an extended mass function in a proper way. We have also provided an inflation model that successfully generates PBHs as all DM by satisfying these requirement.

• Primordial black holes as dark matter in supergravity inflation models

In collaboration with the members of ICRR, KIPMU and UCLA.

We propose a novel scenario to produce abundant primordial black holes (PBHs) in new inflation which is a second phase of a double inflation in the supergravity framework. In our model, some preinflation phase before the new inflation is assumed and it would be responsible for the primordial curvature perturbations on the cosmic microwave background scale, while the new inflation produces only the small scale perturbations. Our new inflation model has linear, quadratic, and cubic terms in its potential and PBH production corresponds with its flat inflection point. The linear term can be interpreted to come from a supersymmetry-breaking sector, and with this assumption, the vanishing cosmological constant condition after inflation and the flatness condition for the inflection point can be consistently satisfied.

Bibliography

- [1] K. Inomata, M. Kawasaki, K. Mukaida, Y. Tada and T. T. Yanagida, Phys. Rev. D **95**, no. 12, 123510 (2017) doi:10.1103/PhysRevD.95.123510 [arXiv:1611.06130 [astro-ph.CO]].
- [2] K. Inomata, M. Kawasaki, K. Mukaida, Y. Tada and T. T. Yanagida, arXiv:1701.02544 [astro-ph.CO].
- [3] M. Kawasaki, A. Kusenko, Y. Tada and T. T. Yanagida, Phys. Rev. D **94**, no. 8, 083523 (2016) doi:10.1103/PhysRevD.94.083523 [arXiv:1606.07631 [astro-ph.CO]].

OBSERVATORIES and A RESEARCH CENTER

Location of the Institute and the Observatories in Japan



Norikura Observatory

Location: Norikuradake, Nyukawa-cho, Takayama-shi, Gifu Prefecture 506-2100
 N 36°06', E 137°33', 2770 m a.s.l.
 Telephone (Fax): +81-50-3730-3809
 Telephone (satellite): +81-90-7721-5674
 Telephone (car): +81-90-7408-6224

Akeno Observatory

Location: 5259 Asao, Akeno-machi, Hokuto-shi, Yamanashi Prefecture 408-0201
 N 35°47', E 138°30', 900 m a.s.l.
 Telephone / Fax: +81-551-25-2301 / +81-551-25-2303

Kamioka Observatory

Location: 456 Higashi-mozumi, Kamioka-cho, Hida-shi, Gifu Prefecture 506-1205
 N 36°25'26", E 137°19'11", 357.5 m a.s.l.
 Telephone / Fax: +81-578-85-2116 / +81-578-85-2121

KAGRA Observatory

Location: 238 Higashi-mozumi, Kamioka-cho, Hida-shi, Gifu Prefecture 506-1205
 N 36°25'26", E 137°19'11", 350 m a.s.l.
 Telephone / Fax: +81-578-85-2343 / +81-578-85-2346

Research Center for Cosmic Neutrinos

Location: 5-1-5 Kashiwanoha, Kashiwa, Chiba Prefecture 277-8582
 Telephone / Fax: +81-4-7136-3138 / +81-4-7136-3115

NORIKURA OBSERVATORY

Introduction

Norikura Observatory (36.10°N and 137.55°E) was founded in 1953 and attached to ICRR in 1976. It is located at 2770 m above sea level, and is the highest altitude manned laboratory in Japan. Experimental facilities of the laboratory are made available to all the qualified scientists in the field of cosmic ray research and associated subjects. The AC electric power is generated by the dynamo and supplied throughout the observatory. In 1996, two dynamos of 70 KVA each were replaced with the new ones. The observatory can be accessed easily by car and public bus in summer (July-September). The 50th anniversary of Norikura Observatory was celebrated in 2003.



Fig. 1. Norikura Observatory.

The feasibility of the automatic operation of Norikura Observatory during winter period has been tested since winter 2004 in order to study the possibilities to reduce maintenance and labor costs without seriously damaging to the use of researches. A long-distance (~40km) wireless LAN system (11M bps) was set up in 2003. Two new easy-to-handle and easy-to-maintain dynamos of 115 KVA each were installed in 2004 as well. The unmanned operation of Norikura Observatory has been mostly successful in winter, during which the battery backed-up solar panels and/or wind power generators kept supplying the electricity to the wireless LAN and on-going cosmic-ray experiments. The 60th anniversary of Norikura Observatory was celebrated in 2013.

Present major scientific interests of the laboratory is focused on the modulation of high energy cosmic rays in the interplanetary space associated with the solar activity and the generation of energetic particles by the solar flares, both of which require long-term monitoring. This research has been carried out by the group of universities, where ICRR provides them with laboratory facility. A part of the facility has been open for the environmental study at high altitude such as aerosol-related mechanism in the atmosphere, observation of total ozone and UV solar radiation, for botanical study in the high-altitude environment, etc.



Fig. 2. A dynamo of 115KV.

Cosmic Ray Physics

A neutron monitor has been continuously operated to study the correlation of solar activities and cosmic ray flux for a long time. It is the only active one in Japan now. The neutron monitor data are open to researchers worldwide as a world observation network point (WDC). In addition, space weather observation is actively made by a 25 m² muon hodoscope at Norikura Observatory [1], [2], [3], [4], [5], [6], [7], [8], [9].

The anisotropy observed with the global muon detector network (GMDN) provides us with a unique information of the spatial gradient of the GCR density which reflects the large-scale magnetic structure in the heliosphere. The solar cycle variation of the gradient gives an important information on the GCR transport in the heliosphere, while the short-term variation of the gradient enables us to deduce the large-scale geometry of the magnetic flux rope and the interplanetary coronal mass ejection (ICME). Real-time monitoring of the precursory anisotropy which has often been observed at the Earth preceding the arrival of the ICME accompanied by a strong shock may provide us with useful tools for forecasting the space weather with a long lead time. By using a self-supporting power system utilizing the solar panels and batteries, we keep a 25 m² muon hodoscope running at the Mt. Norikura Cosmic Ray Observatory as an important component detector of the GMDN. The total power consumption of this detector has been suppressed as low as 36 Watt by replacing all amplifier boards with those using CMOS ICs and by introducing a new recording system using the FPGA. This new system, in which the observation has been automatically carried out by a PC connected with the internet, also enabled us to monitor the data on the real-time basis for the space weather study.

The Sun is the nearest site to the Earth capable of accelerating particles up to high energies. When the Sun becomes active, flares are frequently observed on its surface. The flare accelerates the proton and ion to high energy and they are detected on the Earth soon after the flare. Among the particles generated by the flare, high energy neutrons provide the most direct information about the acceleration mechanism as they come straight from the flare position to the Earth without deflected by the magnetic field.

Observation of solar neutron has been conducted at the Norikura Observatory since 1990. Neutron is used to clarify the acceleration mechanism of high energy particles in association with solar flares, because the neutron is not reflected by the interplanetary magnetic field. The 64m^2 solar neutron telescope was constructed in 1996, which is one of 7 solar neutron telescopes deployed at different longitudes to make up a network of 24 hour observation of solar neutrons. The Norikura 64m^2 solar neutron telescope has been operated by solar batteries and windmills since 2004.

This collaborative work has started since fiscal 2007 succeeding to the previous project titled 'Observation of solar neutrons by using a new method.' Although solar cycle 24 has started since 2008, the solar activity has continued to be inactive, and no new solar neutron event has been detected by the network since 2006. The last solar neutron event was on September 7, 2005. This event is unique because it indicates ions were accelerated or trapped at the acceleration region longer than electrons. The summary of 11 solar neutron events detected until 2005 shows that it may not be probable that a very efficient acceleration such as the shock acceleration works for ions at solar flares. This is given by deriving the energy spectrum of neutrons at the solar surface for each solar neutron event with a power law. Power law indices obtained span from 3 to 7. The energy spectrum of the original ions is softer than that of neutron. Therefore an efficient acceleration has not been detected by the observation of solar neutrons so far. This work continues in solar cycle 24 to accumulate more events to obtain definite results related with particle acceleration at the solar surface.

Another effort aiming at observation of highest-energy solar cosmic rays started at the Norikura Observatory. The Sun is an accelerator of protons and electrons in the universe. In association with large solar flares, protons and electrons are accelerated into high energies. It is known that protons are accelerated over 50 GeV in the largest solar flares[24]. These high energy particles produce the Ground Level Enhancement (GLE).

In order to understand the acceleration mechanism of protons, we have prepared several solar neutron telescopes at the high altitude laboratories in the world. They are located at Gornergrat (3,135m), Mt. Aragats in Armenia (3,200m), Tibet (4,200m), Mauna-Kea in Hawaii (4,200m), Mt. Chacaltaya in Bolivia (5,250m), and at Mt. Sierra Negra in Mexico (4,900m). We have constructed a solar neutron telescopes at Mt. Norikura Cosmic Ray Observatory (2,770m) in 1990 and operated it until 2004[21]. However due to the lack of power supply during the winter time since 2005, the first solar neutron telescope (36m^2) has not been operated.

From 2008 to 2009, we have decided to make a new solar neutron telescope to utilize the large amount of the plastic scintillator (0.5m^3), as shown in Fig.3, left at the observatory.

The new solar neutron telescope with use of the recycled plastic scintillator consists of main target where neutrons are converted into protons and of the anti-counters surrounding the target. The signals of neutrons converted into protons are observed by using one photomultiplier from bottom side to reduce the electric power. Furthermore a lead plate with the thickness of 1cm is located over the target and the lead plate is sandwiched by two layers of the plastic scintillator to identify gamma-rays from neutrons.

The new solar neutron telescope has a function to reject charged particles with an efficiency of 90%. Therefore the new solar neutron telescope has capability of 1/3 of the 64m^2 large solar neutron telescope located at the same place. We are waiting large solar flares over our detectors.



Fig. 3. 0.5-m^2 plastic scintillation counter for a new neutron telescope.

In addition to the long-term cosmic-ray observations mentioned above, various kinds of short-dated experiments are carried out every year taking an advantage of the high altitude of the observatory.

High-energy radiations from thunderstorms have been observed by flight measurement, high-mountain observations and ground-based measurement. There are two types of those radiations associated with thunderstorms. One is short-duration radiations with duration of 1 ms or less. The other is long-duration emissions lasting for a few seconds to a few minutes, or a few tens of minutes on rare occasions. It is believed that both emissions originate from electrons accelerated in strong electric fields formed in lightning and thunderclouds. However, compared with the former, the latter has remained less understood due to lack of a large sample of observations.

To investigate production mechanism of long-duration emissions and the relevant electron acceleration, we installed at Norikura Cosmic-ray Observatory a radiation detection system and environmental sensors to measure light and electric fields during 2008–2010. The radiation system consists of a spherical NaI scintillator and a thin plastic scintillator that is placed just above the NaI counter. During the period, the system detected one long-duration bursts as well as five short-duration events.

Fig. 4 (top) shows the long-duration event observed during thunderstorms on 2008 September 20th [25]. The event lasted for 90 sec. Fig.4 (bottom) represents an observed photon spectrum extending from 10 keV to 10 MeV. This indicates that electrons can be accelerated to at least 10 MeV in a quasi-stable thundercloud electric field. In addition, we compared the observed spectrum with model ones, and concluded that a gamma-ray source is located 60 m–130 m (at 90% confidence level) apart from our detector. Given these results, the observed emission was found to consist of not only gamma rays but also electrons. This was the first simultaneous observation of gamma rays and electrons in long-duration bursts.

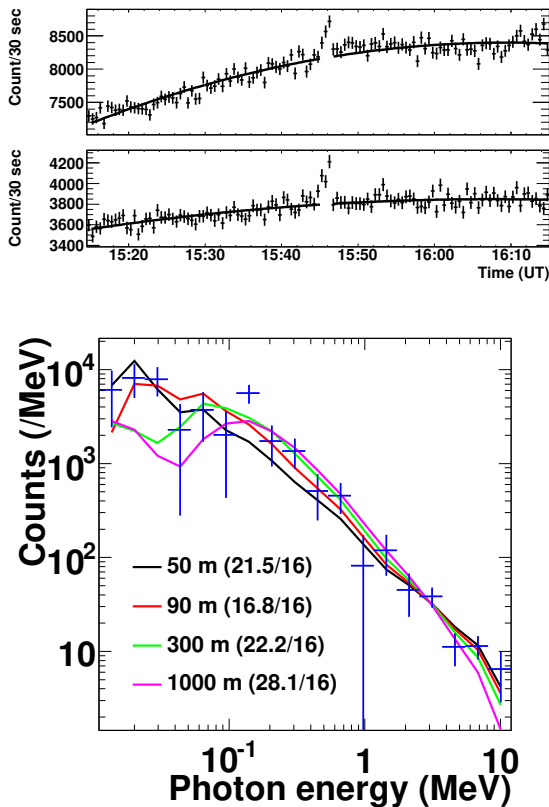


Fig. 4. (Top) Count rates per 30 sec observed by the >10 keV NaI scintillator (upper) and >100 keV plastic one (lower). (Bottom) The photon spectrum observed by the NaI scintillator.

Observation of night sky background is carried out at Mt. Norikura for basic study of ultra high energy cosmic-ray physics.

The JEM-EUSO mission is going on in order to study ultra high energy cosmic rays (UHECRs), especially above 10^{20} eV. A 2.5m telescope with 60° FoV will be attached to the International Space Station in 2017 and detect fluorescence in near UV band from extensive air showers induced by UHECRs. Observation of UHECRs from a satellite orbit has not been done yet, so that the knowledge of background light intensity is important to realize the observation. We have measured it from a balloon altitude, but the opportunity is limited. We started the background measurement at Mt. Norikura. Two 1 inch multi-anode photomultipliers (MAPMTs) developed for EUSO was used with UV filters. The center wavelengths of the filters were 337, 350, 358, 370, 380, 391, 400nm with 10nm band width. In addition BG3 filter was used to detect light in wider range from 330nm to 430nm. The MAPMTs were collimated to 7° FoV. The data was taken with the photon counting method.

We have observed several nights for three years. The intensity at zenith was almost constant at 600-800 photons/ns \sim sr m^2 for BG3 filter. The spectral intensity was about 1.5-2 times larger than those measured at La Palma and Namibia. The estimated portion of star light and zodiacal light was $\sim 30\%$ and artificial light and nightglow at upper atmosphere may be the main components at Mt. Norikura.

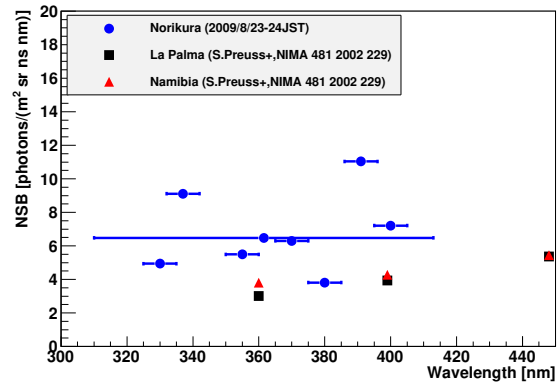


Fig. 5. Spectrum of night sky background measured at Mt. Norikura compared with those at La Palma and Namibia.

Environmental Study

One of the interesting topics is atmospheric environment especially relating with atmospheric aerosol particles and water soluble gases. The cosmic ray observatory at Mt. Norikura provides us very unique opportunity for the observations of atmosphere at free-tropospheric conditions with its high altitude, AC power supply at the site, accommodation facility, and easy accessibility. From year 2000 to 2007, we conducted continuous monitoring (mostly mid-May to mid-October) of meteorological parameters, number-size distribution of aerosols, aerosol chemical composition, ozone and radon concentrations, and column amount of aerosols from sky radiometer and ceilometers. We also collected rain, fog, water-condensed aerosol samples. These samples combined with other observed parameters were used in publications in the following subjects [26, 27, 28]:

- (1) Polluted air pumping effects over central Japanese Alps in summer
- (2) Seasonal variation of aerosol chemistry in free troposphere
- (3) Vertical profiles of aerosols and clouds near the top of the atmospheric boundary layer.

Ceilometer (lidar with small output energy) was installed in summer 2002, and was operated in 6 summer seasons. The aerosol and cloud profiles near the top of the atmospheric boundary layer have been observed. Some events of Asian dust were detected.

Observations of total ozone and UV solar radiation with Brewer spectrophotometer on the Norikura mountains are also made [29, 30, 31].

Aerological Observatory started "Observations of total ozone and UV solar radiation with Brewer spectrophotometer at Norikura mountains" as a joint project with Institute for Cosmic Ray Research (ICRR), University of Tokyo at the Norikura Observatory of ICRR (Brewer site: 36.11 N, 137.56 E, 2,772 m a.s.l.), locating at the Northern Japanese Alps in every summer seasons from 2009 (Ito *et al.*: 2011). Purpose of this study is based on the concept of developing Regional Brewer Calibration Centre in Asia and study of total ozone, total sulfur oxide and global/diffuse UV included solar radiation on the high mountains. Observation results by using Brewer spectrophotometers and other instruments for the observation period of three summer seasons of recent three years between 2009 to 2011 are summarized as follows;

- (1) Daily means of $ds O_3$ (total ozone) at Norikura for the obser-

vation periods were approx. 280 to 290 m atm-cm and were running on the lower values of approx. -3 to -6% compared to the value at Tsukuba (36.06 N, 140.13 E, 39 m a.s.l.) at almost same latitude. Day-to-day variations at Norikura were also small against Tsukuba. On the other hand, daily mean of ds SO₂ (total sulfur oxide) values were not recognized at Norikura.

(2) Absolute calibration of Brewers for ds O₃ and ds SO₂ observations could be carried out within the range of air mass from 7.928 (maximum) to 1.028 (minimum) at Norikura in the clear day. O₃ and SO₂ Extra-Terrestrial Coefficients (=ETC) of Brewers could be produced as about 10 samples satisfying the condition of " $R^2 > 0.9997$ " by the calibrations. As an example of the calibration in 2011, the average of O₃ ETC of Brewers was identical within 1% to the currently used coefficient.

(3) In comparison to the data acquired at Tsukuba, the average of daily total GL_{UV} (global UV, e.g. CIE) for the observation periods indicated the intensities of approx. +23 % in 2009 to -6 % in 2011. The low intensity in 2011 was due to the bad weather on the Norikura Mountain. In the case of clear days, the GL_{UV} at Norikura indicated high intensities of approx. +35 to +52 % against the values at Tsukuba. On the other hand, the GL_{UV} increased in the short wavelength range at Norikura against the average at Tsukuba. The altitudinal increasing rate of GL_{UV} in the clear day indicated the calculated amounts of approx. +13 to +18 % per 1,000 m.

This joint project had been clarifying the low total O₃, high UV in clear day, low turbidity and etc. at Norikura against the value at Tsukuba. Those environmental conditions are useful for the inter-comparison and the absolute calibrations with Brewers. The continuous observations with Brewers and other instrument are very important for the clarification of the seasonal variation and the coefficient trends.

Botanical Study

Effects of snow cover on pine shrub *Pinus pumila* in the alpine region of Mt. Norikura

High mountainous habit is one of the most severe habits for plant life and sometimes dwarf shrubs cannot survive. In the alpine regions of Japan, the dwarf shrub *Pinus pumila* (Japanese name : Haimatsu) forms communities together with small alpine plants, whereas dwarf shrubs occur only in the transition zone between the alpine region and the subalpine forest in Europe and North America. This characteristic of alpine vegetation is considered to be owing to winter heavy snow in the alpine regions of Japan. The purpose of this study is to elucidate how snow cover protects Haimatsu from winter environmental stresses in the alpine region of Mt. Norikura.

Study site

Tree height of Haimatsu and snow depth differ greatly as a result of slight difference in topography. Two site of the study area were selected. (i) site P (wind-protected) and (ii) site E (wind-exposed). At site P, mean tree height was 1.1 m. There was a lot of snow accumulation and Haimatsu was almost entirely covered with snow during the winter. Needle browning and death occurred rarely. At site E, mean tree height was 0.4 m. Snow accumulation was minimal, and Haimatsu was not entirely covered with snow. Needle browning and death was observed frequently.

Winter needle death in Haimatsu[32]

At site E, the browning and death of needles of Haimatsu occurred mainly in early spring at the point where the shoot protrudes from the snowpack. They are thought to be caused by excessive wa-

ter loss due to mechanical damage to the cuticle and/or to a thinner cuticle. However, needle browning and death in Haimatsu were not related to mechanical damage of the cuticle but might be due to changes in the quality and structure of the cuticle wax and resultant increase in water loss from needle cells.

Photosynthetic capacity in Haimatsu[33]

At site E, needles of Haimatsu had lower biomass, nitrogen, Rubisco (enzyme) and cell wall per unit area, and had higher photosynthetic capacity and shorter needle life-span than Haimatsu at site P. These results suggest that Haimatsu at wind-exposed site produces needles at low cost with high productivity to compensate for a short leaf life-span which may be imposed by wind stress when needles appear above the snow surface in winter.

Bibliography

- [1] K. Munakata, S. Yasue, C. Kato, J. Kota, M. Tokumaru, M. Kojima, A. A. Darwish, T. Kuwabara and J. W. Bieber, "On the cross-field diffusion of galactic cosmic rays into the magnetic flux rope of a CME", *Advances in Geosciences*, 2, 115-124, eds. W. H. Ip and M. Duldig (World Scientific Publishing Co., USA), (2006).
- [2] T. Kuwabara, J. W. Bieber, J. Clem, P. Evenson, R. Pyle, K. Munakata, S. Yasue, C. Kato, S. Akahane, M. Koyama, Z. Fujii, M. L. Duldig, J. E. Humble, M. R. Silva, N. B. Trivedi, W. D. Gonzalez and N. J. Schuch, "Real-time cosmic ray monitoring system for space weather", *Space Weather*, 4, S08001-1 10, (2006).
- [3] M. R. Da Silva, A. Dal Lago, E. Echer, A. de Lucas, W. D. Gonzalez, N. J. Schuch, K. Munakata, L. E. A. Vieira, and F. L. Guarnieri, "Muon and neutron observations in connection with the corotating interaction regions", *Adv. Space Res.*, 40, pp348-352, (2007).
- [4] Y. Okazaki, A. Fushishita, T. Narumi, C. Kato, S. Yasue, T. Kuwabara, J. W. Bieber, P. Evenson, M. R. Da Silva, A. Dal Lago, N. J. Schuch, Z. Fujii, M. L. Duldig, J. E. Humble, I. Sabbah, J. Kóta and K. Munakata, "Drift effects and the cosmic ray density gradient in a solar rotation period: First observation with the Global Muon Detector Network (GMDN)", *Astrophys. J.*, 681, 693-707, (2008).
- [5] T. Kuwabara, J. W. Bieber, P. Evenson, K. Munakata, S. Yasue, C. Kato, A. Fushishita, M. Tokumaru, M. L. Duldig, J. E. Humble, M. R. Silva, A. Dal Lago, and N. J. Schuch, "Determination of ICME Geometry and Orientation from Ground Based Observations of Galactic Cosmic Rays", *J. Geophys. Res.*, 114, A05109-1 10, doi:10.1029/2008JA013717, (2009).
- [6] A. Fushishita, T. Kuwabara, C. Kato, S. Yasue, J. W. Bieber, P. Evenson, M. R. Da Silva, A. Dal Lago, N. J. Schuch, M. Tokumaru, M. L. Duldig, J. E. Humble, I. Sabbah, H. K. Al Jassar, M. M. Sharma, and K. Munakata, "Precursors of the Forbush Decrease on 2006 December 14 observed with the Global Muon Detector Network (GMDN)", *Astrophys. J.*, 715, 1239-1247, (2010).
- [7] A. Fushishita, Y. Okazaki, T. Narumi, C. Kato, S. Yasue, T. Kuwabara, J. W. Bieber, P. Evenson, M. R. Da Silva, A. Dal Lago, N. J. Schuch, M. Tokumaru, M. L. Duldig, J. E. Humble, I. Sabbah, J. Kóta, and K. Munakata, "Drift effects and the average features of cosmic ray density gradient in CIRs during successive two solar minimum periods", *Advances in Geosciences*, eds. W. H. Ip and M. Duldig (World Scientific Publishing Co., USA), 21, 199-210, (2010).

- [8] M. Tokumaru, M. Kojima, K. Fujiki, K. Munakata, T. Kuwabara and K. Marubashi, "Relation between loop-shaped interplanetary disturbances and the magnetic flux rope", *Advances in Geosciences*, eds. W. H. Ip and M. Duldig (World Scientific Publishing Co., USA), 21, 21-32, (2010).
- [9] M. Rockenbach, A. Dal Lago, W. D. Gonzalez, K. Munakata, C. Kato, T. Kuwabara, J. W. Bieber, N. J. Schuch, M. L. Duldig, J. E. Humble, H. K. Al Jassar, M. M. Sharma, and I. Sabbah, "Geomagnetic Storms Precursors Observed from 2001 to 2007 with the Global Muon Detector Network GMDN", *Geophys. Res. Lett.*, 38, L16108-1 4, doi:10.1029/2011GL048556, (2011).
- [10] "Solar neutron events of October-November 2003", Watanabe, K. *et al.*, *Astrophys. J.*, **636**, 1135–1144, 2006.
- [11] "Solar neutron events in association with large solar flares in November 2003", Watanabe, K. *et al.*, *Adv. Space Res.*, **38**, 425–430, 2006.
- [12] "Long-lived solar neutron emission in comparison with electron-produced radiation in the 2005 September 7 solar flare", Sako, T. *et al.*, *Astrophys. J.*, **651**, L69–L72, 2006.
- [13] "Highly significant detection of solar neutrons on 2005 September 7", Watanabe, K. *et al.*, *Adv. Space Res.*, **39**, 1462–1466, 2007.
- [14] "A solar neutron telescope in Tibet and its capability examined by the 1998 November 28th event", Muraki, Y. *et al.*, *Astroparticle Phys.*, **28**, 119–131, 2007.
- [15] "Simultaneous detection of high-energy solar neutrons and protons at Chacaltaya observatory on April 15, 2001", Muraki, Y. *et al.*, in Proc. 30th Int. Cosmic Ray Conf, Merida, **1**, 25–28, 2007.
- [16] "Search for solar neutrons associated with series of X-class flares during the declining period of solar cycle 23", Matsubara, Y. *et al.*, in Proc. 30th Int. Cosmic Ray Conf, Merida, **1**, 29–32, 2007.
- [17] "Ion acceleration and neutral emission mechanisms for 2005 September 7 flare", Watanabe, K. *et al.*, in Proc. 30th Int. Cosmic Ray Conf, Merida, **1**, 45–48, 2007.
- [18] "Emission profile of solar neutrons obtained from the ground-based observations for the 7 September 2005 event", Sako, T. *et al.*, in Proc. 30th Int. Cosmic Ray Conf, Merida, **1**, 53–56, 2007.
- [19] "Energy spectrum for the solar neutron event of September 7 2005, derived from the SNT at Sierra Negra", Gonzalez, L. X. *et al.*, in Proc. 30th Int. Cosmic Ray Conf, Merida, **1**, 57–60, 2007.
- [20] "Status of the world-wide network of solar neutron telescopes in solar cycle 24", Matsubara, Y. *et al.*, in Proc. 31st Int. Cosmic Ray Conf, Lodz, **1**, On Conference homepage, 2009.
- [21] "Detection of high-energy solar neutrons and protons by ground level detectors on April 15, 2001", Muraki, Y. *et al.*, *Astropart. Phys.*, **29**, 229–242, 2008.
- [22] "Solar neutron events as a tool to study particle acceleration at the Sun", Valdes-Galicia, J. F. *et al.*, *Adv. Space Res.*, **43**, 565–572, 2009.
- [23] "Physics of ion acceleration in the solar flare on 2005 September 7 determines γ -ray and neutron production", Watanabe, K. *et al.*, *Adv. Space Res.*, **44**, 789–793, 2009.
- [24] "Observation of solar neutrons associated with the large flare on 1991 June 4", Muraki, Y. *et al.*, *ApJ*, **400**, L75-L78, 1992.
- [25] "Observation of an energetic radiation burst from mountain-top thunderclouds", H. Tsuchiya *et al.*, *Phys. Rev. Lett.* **102**, 255003 (2009), Citation Index:13.
- [26] Nishita, C., K. Osada, K. Matsunaga, Y. Iwasaka, e, J. *Geophys. Res.*, **113**, D06202, doi:10.1029/2007JD009302, 2008.
"Nucleation mode particles in up-slope valley winds at Mt. Norikura, Japan: implications for the vertical extent of new particle formation events in the lower troposphere", Nishita, C., K. Osada, K. Matsunaga, Y. Iwasaka, J. *Geophys. Res.*, **113**, D06202, doi:10.1029/2007JD009302, 2008.
- [27] "Temporal variation of water-soluble ions of free tropospheric aerosol particles over central Japan", Osada, K., Kido, M., Nishita, C., Matsunaga, K., Iwasaka, Y., Nagatani, M., Nakada, H., *Tellus*, **59B**, 742-754, 2007.

- [28] “Number-size distributions of free tropospheric aerosol particles at Mt. Norikura, Japan: effects of precipitation and air-mass transportation pathways”, Nishita, C., K. Osada, K. Matsunaga, Y. Iwasaka, *J. Geophys. Res.*, 112, doi:10.1029/2006JD007969, 2007.
- [29] “ Observations of total ozone and UV solar radiation with Brewer spectrophotometers on the Norikura mountains in 2009.”, Ito, M., M. Takano, H. Oguri, M. Takita, H. Shimodaira and H. Ishitsuka, *Jour. of the Aerological Observatory*, **69**, 41-54 2011.
- [30] “ Observations of total ozone and UV solar radiation with Brewer spectrophotometers on the Norikura mountains, Northern Japanese Alps, from 2009.”, Ito, M., S. Shimizu, Y. Noto, T. Shimamura, M. Takano, M. Takita, H. Shimodaira and H. Ishitsuka, *The 13th WMO Biennial Brewer Workshop, Beijing, China in 2011*, 2011.
- [31] “ Total ozone and UV solar radiation with Brewer spectrophotometers at Norikura of Northern Japanese Alps, in recent three years.”, Ito, M., S. Shimizu, Y. Noto, T. Shimamura, M. Takita, H. Shimodaira and H. Ishitsuka, *Jour. of the Aerological Observatory*, **70**, in contribution.
- [32] “Needle browning and death in *Pinus pumila* in the alpine region of central Japan were not related to mechanical damage of cuticle and cuticle thickness.”, Nakamoto A., Ikeda T., Maruta E., *Can. J. For. Res.* 42, 167-178 (2012).
- [33] “Needle traits of an evergreen, coniferous shrub growing at wind-exposed and protected sites in a mountain region: does *Pinus pumila* produce needles with greater mass per area under wind-stress conditions?”, Nagano S., Nakano T., Hikosaka K and Maruta E., *Plant Biology* 11(Suppl.1), 94-100, (2009).

AKENO OBSERVATORY

Introduction

The Akeno Observatory is situated in Akeno of Hokuto-city, 20 km northwest of Kofu and 130 km west of metropolitan Tokyo. The location is at the longitude of 138.5°E and the latitude of 35.8°N. The altitude is ~ 900 m above sea level. It was established in 1977 as a research center for air shower studies in the very high energy region, and it has been administered by the ICRR as a facility of joint-university-use.

Akeno Air Shower Experiments

The Akeno Air Shower Experiment started in 1979 with an array covering 1 km² area (the 1 km² array, see Fig.1). The array was enlarged to 20 km² in 1984 and was gradually expanded to Akeno Giant Air Shower Array (AGASA) of approximately 100 km² area by 1990. The AGASA was built



Fig. 1. Aerial View of Akeno Observatory and 1 km² Array Area

to detect Ultra-High Energy Cosmic Rays (UHECRs) in the energy range of 10²⁰ eV.

One of the distinctive features of Akeno experiments is that the measurements were made over five decades of energies well covering 10¹⁵ eV - 10²⁰ eV by using both the surface detector for electromagnetic component, and the shielded detector for muon component (Fig.2). The wide energy coverage was accomplished by the arrays of scintillation detectors of various inter-detector spacings from 3 m to 1 km and with different triggering conditions. This feature of Akeno air shower measurement is well demonstrated in Fig.3, in which the spectra from Akeno 1 km² array for 10^{14.5} eV - 10^{18.8} eV¹ and AGASA for 10^{18.5} eV - 10^{20.3} eV² are plotted.

*¹ M. Nagano et al., J. Phys. **G10**, 1295 (1984); M. Nagano et al., J. Phys. **G18**, 423 (1992).

*² M. Takeda et al., Astropart. Phys. **19**, 447 (2003).



Fig. 2. One of the muon detector housings with concrete shielding.

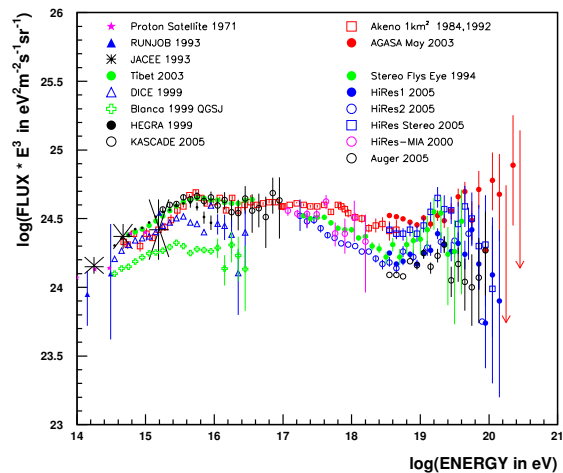


Fig. 3. Akeno energy spectrum measurements for 10¹⁵ eV - 10²⁰ eV.

AGASA

The AGASA was composed of 111 surface detectors, each with plastic scintillator of 2.2 m² area and 5 cm thickness. The counters were deployed with ~ 1 km spacing covering the ground area of about 100 km² in the suburban area of Akeno, outside of the observatory campus. All counters were connected with optical fibers for the timing measurement and digital data transfer to the observatory. The AGASA served as the largest air shower array in the world since its commissioning in 1990 until it stopped data taking in January 2004, when the construction of the succeeding experiment, Telescope Array (TA), started in Utah. The AGASA was dismantled in 2007 together with other Akeno air shower arrays.

An exposure of 5.8×10^{16} m² s sr above 10¹⁹ eV was

accumulated by AGASA in 13 years of operation. Extensive air showers with zenith angles smaller than 45° and with core locations inside the array area were used for the analysis. The AGASA reported an extension of the energy spectrum beyond the predicted Greisen-Zatsepin-Kuzmin (GZK) cutoff in 1998³ and a total of eleven UHECR events were observed above 10^{20} eV by 2003.

Measurement of UHECRs

Since the AGASA measurement in 1998, High Resolution Fly's Eye (HiRes)⁴, Pierre Auger Observatory (PAO)⁵, and Telescope Array (TA)⁶ measured the energy spectra of UHECRs with higher statistics.

The HiRes observed the UHECR using the fluorescence telescope. The PAO and the TA measure the energy spectra using the surface array consisting of either water tanks (PAO) or plastic scintillators (TA), but the energy scale of the array is determined by the fluorescence telescope using a subset of events observed by the fluorescence telescope and surface array at the same time. The adoption of the energy scale by the fluorescence telescopes is based on its small dependence on the air shower simulation.

The energy spectra above 10^{18} eV by AGASA and other experiments are compiled and compared by the working group represented by UHECR experiments in the UHECR2012 symposium held at CERN for Feb. 13th - 16th, 2012⁷. The result is plotted in Fig.4 with the energy scale of each experiment adjusted to a reference energy, which is set halfway between PAO and TA/HiRes. Following factors were applied for the energy scale; $\times 1.10$ for PAO, $\times 0.91$ for TA and HiRes, $\times 0.65$ for AGASA and $\times 0.56$ for Yakutsk.

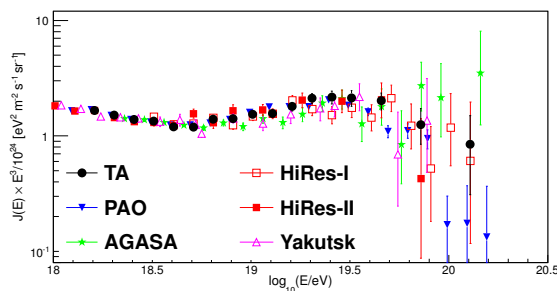


Fig. 4. Compilation of UHECR energy spectra (UHECR2012). The energy scale of each experiment is adjusted as described in the text.

As seen in Fig.4, the overall agreement between experiments is good, and a “dip” structure was seen around $10^{18.7}$ eV by all experiments. The HiRes, PAO and TA confirmed a strong flux suppression above approximately $10^{19.7}$ eV. Although the AGASA spectrum does not demonstrate the cutoff structure, the number of events above 10^{20} eV became only

two after the energy rescaling, making the claim of the extended spectrum statistically insignificant. The estimate of systematic uncertainty of the energy measurement is approximately 20% for all the experiments, and rescalings for the TA/HiRes and PAO are within this limit. Rescaling of the surface array energy, $\times 0.65$ for AGASA and $\times 0.56$ for Yakutsk, indicates that there exist larger systematic uncertainties than originally estimated by running the air shower simulation. This difference of energy scale obtained by the surface array and by the fluorescence telescope remains as a basic question in the understanding of the air shower phenomena. The recent detailed feature of energy spectra by PAO and TA with more statistics are described in the section of TA in this annual report.

Recent Research Activities

The study of UHECRs by AGASA in Akeno was succeeded by the TA experiment in Utah, USA since 2008. After the cessation of AGASA, the Akeno Observatory has been used for small scale cosmic ray experiments, astrophysical observations and as a test and maintenance facility of TA by the ICRR and university researchers. Fig.5 shows a recent photograph of the main site of the Akeno Observatory.



Fig. 5. The main site of the Akeno Observatory. There are the movable tent for a small atmospheric Cherenkov telescope, the large experimental hall, the research building and the lodging facility from the left.

Research and development for the Telescope Array observation in Utah by the TA collaboration

All the TA fluorescence imaging cameras were assembled in the Akeno Observatory by the TA collaboration team. The detectors were tested in Akeno and shipped to the Utah observation site for the installation. All the unit mirrors of the TA fluorescence telescope were tested in Akeno and the atmospheric monitoring lidar of TA using YAG laser was developed in Akeno. In JFY 2015, the R&D of the surface detectors were performed in the large experimental hall of the Akeno Observatory for the TA_{x4} project that quadruples the TA surface detector array in Utah. In August of JFY 2016, 73 scintillator counters were assembled for TA_{x4}.

Research activities in JFY 2016 (April 2016 - March 2017) are described in the following.

*³ M. Takeda et al., Phys. Rev. Lett. **81**, 1163 (1998).

*⁴ R.U. Abbasi et al., Phys. Rev. Lett. **100**, 101101 (2008).

*⁵ J. Abraham et al., Phys. Lett. **B685**, 239 (2010).

*⁶ T. Abu-Zayyad et al., Astrophys. J. **768**, L1 (2013).

*⁷ <http://indico.cern.ch/conferenceDisplay.py?confId=152124>

Observation by the multi-color imager for transients, survey and monstrous explosions (MITSuME) by N. Kawai (Tokyo Institute of Technology) et al.

One of the three MITSuME robotic telescopes was installed in the Akeno Observatory in 2003 (Fig. 6). The telescope has an aperture of 50 cm, an FOV of $28' \times 28'$ and is equipped with a tricolor CCD camera capable of $g'R_C I_C$ -bands photometry (g' :400~550 nm, R_C :570~730 nm, I_C :730~850 nm). It is operated remotely from the Tokyo Tech at the Ookayama Campus using dedicated ADSL connections. Upon receiving a GRB alert from Swift or Fermi satellite, it quickly directs the telescope ($9^\circ/s$ maneuverability) toward the GRB direction, and makes a prompt observation of the GRB and its afterglow.

The limiting magnitudes of 21 GRBs were obtained, in which six were identified with visible light. MiTsuMe joined the campaign of light-infrared astronomy inter-university cooperation research project, and performed follow-up observation of low-mass X-ray binaries. In JFY2015, in order to perform visual follow-up observation of gravitational wave objects, MiTsuMe joined GROWTH that is the worldwide observation network.



Fig. 6. The dome in which the MITSuME telescope was installed in Akeno.

Observation of galactic cosmic rays by large area muon telescope by A. Oshima (Chubu University) et al.

Four layers of proportional counter telescopes, each with 25 m² area, were installed in three muon houses in Akeno and have been continuously measuring the cosmic ray muons since 2003. Fig. 2 shows one of the muon houses. The mode energy of the primary cosmic rays is approximately 2.5 GeV corresponding to 2m thick concrete ceiling of the muon house at the latitude of the Akeno Observatory. The measurement in Akeno is combined with a simultaneous measurement by the GRAPES-3 experiment at Ooty in India, and the modulation effects of galactic cosmic rays by the solar activity such as the Forbush decrease and its precursor have been continuously monitored⁸. In JFY 2016, the preparation for repair of bad proportional counters at one the muon stations (M59) was performed. The networks at two of three muon stations were changed from ADSL service to LTE, and stable connection to the outside was established.

⁸ T. Nonaka et al, Proc. of the 29th ICRC, **1**, 363-366 (2005).

Research and development for a small atmospheric Cherenkov telescope at the Akeno Observatory by T. Yoshikoshi (ICRR) et al.

A small alt-azimuth telescope is being setup in Akeno for various prototype tests with atmospheric Cherenkov observations of gamma rays⁹. This telescope is the only atmospheric Cherenkov telescope from air showers induced by TeV gamma rays in Japan. In JFY2016, an atmospheric cherenkov light event was firstly observed. Relative timing accuracy of DAQ PC in coincide with the GPS receiver was improved down to a level of 50 ns after re-evaluation of software setting. Taking into account temperature dependence, absolute timing accuracy of the system becomes about 1 μ s, by which pulsar observations will be performed.

Other research

A part of the large experimental hall was used for the support for the research on low frequency anti-vibration system of KAGRA: acceptance of devices, temporary storage and partial assembly before the installation in KAGRA.

Other tests using facilities or detectors in the Akeno Observatory were also performed.

⁹ M. Ohishi et al., 33rd ICRC, (Rio de Janeiro), **9**, in press (2013).

KAMIOKA OBSERVATORY

Kamioka observatory is located at 1000 m underground (2700 m water equivalent) in the Kamioka Mine, Gifu prefecture, about 200 km west of Tokyo. The observatory was established in 1995 in order to operate Super-Kamiokande experiment (SK). The underground laboratories are located under Mt.Ikeno-yama and accessible to the experimental site through a 1.7 km horizontal tunnel. The observatory also has surface research buildings and a dormitory located at the distance of 15 minutes drive from the entrance of the underground laboratories.

The Super-Kamiokande experiment had discovered neutrino oscillations through the observations of atmospheric and solar neutrinos (see the section for Neutrino and Astroparticle Division). The atmospheric neutrino oscillation was confirmed by the long baseline neutrino oscillation experiment, K2K, using accelerator neutrino beam, which was conducted between 1999 and 2004. A new long baseline neutrino oscillation experiment (the T2K experiment) using a high intensity beam, 50 times of the K2K neutrino beam, by the J-PARC proton accelerator has started in 2009. In 2011, the experiment has observed 6 ν_e appearance events indicating non-zero θ_{13} which was as yet determined the last neutrino oscillation parameter. Anti-neutrino beam data was taken from 2014 to 2016 in order to search for CP violation. Based on the whole data taken until 2016, T2K presented the first CP violation search result in August 2016.

The low cosmic ray flux and low seismic noise environ-

ment in the underground site enables us to conduct various researches. There is a 100 m long laser interferometer, which is a proto-type of the 3 km gravitational wave antenna (KAGRA). Using the low radioactive background environment in the Kamioka Mine, a dark matter experiment, called XMASS is operated in Lab-C. The XMASS group constructed a 800kg liquid xenon detector and started data taking from 2010. The detector has been improved and searches for dark matter interactions and rare phenomena in liquid xenon have been conducted in the last few years. The R&D study of a tracking type detector for dark matter detection led by the Kobe University group (the NEWAGE experiment) has also been performed in Lab-B. A double beta decay experiment using ^{48}Ca (the CANDLES experiment) led by the Osaka University group has been running in Lab-D. The study to improve the neutrino detection sensitivity by adding gadolinium to Super-Kamiokande (called SK-Gd project) has been performed at Lab-E. A 200 ton test tank dedicated for the R&D study of the SK-Gd project was constructed and a feasibility study has been performed. In order to support those experiments and also related R&D works, the Observatory is equipped with low background Germanium detector in Lab-1 and Lab-A, ICP-MS and so on to measure extremely low radioactive backgrounds. Lab-G area was newly excavated in 2015 and the SK-Gd equipments which include a Gd dissolving system, a pre-treatment system and a Gd-water circulation system were installed in 2016.

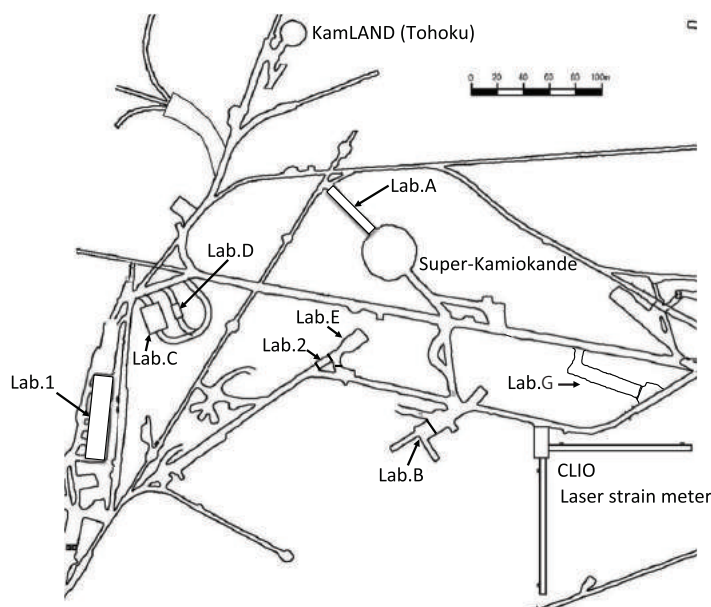


Fig. 1. Kamioka Underground Observatory.

KAGRA OBSERVATORY

KAGRA observatory is located in the Ikenoyama-mountain on the border between Gifu and Toyama prefecture, about 35 km south of Toyama city in Japan. The observatory was established in 2016 in order to operate Large-scale Cryogenic Gravitational Wave Telescope (nicknamed KAGRA). KAGRA itself has a L-shape tunnel facility, and it is located more than 200m under Mt.Ikeno-yama. The corner station of the L-shape tunnel is accessible through a 500-m horizontal access tunnel from Atotsu area. The observatory has its own surface research buildings and rental space in the community center of Hida city located about 5km away from the Atotsu entrance of KAGRA.

KAGRA aims to observe several gravitational waves (GWs) per a year with its designed sensitivity as one of observatories of the world GW detection network including Advanced-LOGO, Advanced-Virgo and planned LIGO-India. KAGRA project (formerly named LCGT) was partially approved in 2010 as one of Leading-edge Research Infrastructure Program, and also supported by Program for Promoting Large-scale Science Projects, Subsidy for Facilities Expense

and Grants-in-Aid for Scientific Research from Ministry of Education, Culture, Sports, Science and Technology (MEXT).

In KAGRA project, Institute for Cosmic Ray Research plays a role of a host promoting institute, and National Astronomical Observatory in Japan (NAOJ) and High Energy Accelerator Research Organization (KEK) are the main support organizations, then more than 280 researchers in 87 institutes and universities in the world are collaborating for construction and data analysis of KAGRA.

The tunnel excavation started in May 2012, and finished in March 2014. After that, the basic laboratory environment was prepared until September 2015. A Michelson interferometer with 3km arm (iKAGRA) was demonstrated in March 2016, and the first engineering run was performed until May 2016. At present (June 2017) all interferometer components are being installed to complete KAGRA observatory that adopts a power recycled Fabry-Perot Michelson type interferometer with resonant sideband extraction technique. We hope to start KAGRA observatory operation around March 2019.



Fig. 1. Surface Research Building.



Fig. 2. Atotsu Entrance of KAGRA.

RESEARCH CENTER FOR COSMIC NEUTRINOS

The Research Center for Cosmic Neutrinos (RCCN) was established in April 1999. The main mission of this center is to promote researches related to neutrinos based on data from various observations and experiments, and we have provided the occasion to discuss theoretical ideas and experimental results on neutrino physics. Members of this center have been involved in the Super-Kamiokande and T2K experiments, and contributing precise measurements of neutrino oscillations. Also, we have been involved in Hyper-Kamiokande project, and worked on the calculation of the atmospheric neutrino flux to have better predictions of the neutrino flux.

RCCN, together with the computer committee, oversees the operation of the central computer system in ICRR (Fig 1). The computer facility has high performance to analyze huge amount of data, and has been operated without any serious trouble since it was upgraded in 2014. Since 2004, RCCN has

been accepted inter-university programs related to activities in the low-background underground facility also (Fig 2). In FY2016, we accepted 8 programs related to these facilities.

RCCN has been organizing domestic neutrino-related workshop since it was established. On February 4, 2017, we hosted one neutrino workshop on Physics of Neutrino Interactions. Thirty-seven physicists participated in this meeting. We have also contributed holding public lectures. Since JFY2009, ICRR and the Kavli Institute for the Physics and Mathematics of the Universe (Kavli-IPMU) have co-sponsored two public lectures each year. The public lecture held in Spring is co-organized by RCCN and the Public Relation Office of ICRR. The Spring public lecture in FY2016 was held on April 16, 2016. Two scientists lectured on the latest neutrino physics and the cosmological observations.



Fig. 1. Photo of the central computer facility in ICRR upgraded in 2014.



Fig. 2. Photo of the low-background underground facility in ICRR.

APPENDICES

A. ICRR Workshops and Ceremonies

B. ICRR Seminars

C. List of Publications

- (a) **Papers Published in Journals**
- (b) **Conference Papers (Proceedings)**
- (c) **ICRR Report**

D. Doctoral Theses

E. Public Relations

- (a) **ICRR News**
- (b) **Public Lectures**
- (c) **Visitors**

F. Inter-University Research Activities

G. List of Committee Members

- (a) **Board of Councillors**
- (b) **Advisory Committee**
- (c) **User's Committee**

H. List of Personnel

A. ICRR Workshops and Ceremonies

Third International Meeting for Large Neutrino Infrastructures

Date: May 30 - June 1, 2016

Place: KEK

Outline: The Third International Meeting for Large Neutrino Infrastructures organized by KEK, ICRR, Fermilab, the Astroparticle Physics European Consortium (APPEC), the ICFA Neutrino Panel, the IUPAP Astroparticle Physics International Committee (APPIC) and several worldwide funding agencies took place at KEK on the 30th and 31st of May 2016.

The meeting was preceded by the meetings of the ICFA Neutrino Panel and ApPIC both of which reported in the Third International Meeting. This meeting followed the second International Meeting for Large Neutrino Infrastructures that took place in April 2015 at Fermilab, during which several agencies and laboratory directors issued a joint press release declaring that the elucidation of the neutrino sector is a worldwide priority that justifies the coherent distribution of tasks and infrastructures across the world. The press release went on to urge the international neutrino community to develop urgently the necessary coherent, international program that exploits and builds on existing infrastructures and to announce the Third International Meeting held in Japan, to evaluate the progress made with respect to the above goals.

This Third International Meeting aimed to gauge the progress that had made since last meeting in terms of the development of the scientific case and the organizational aspects of the worldwide collaboration in long baseline studies. The Meeting also charted the timeline of the decision process, examined the institutional forms that will support it and also passed in review the necessary programme of supporting measurements, prototyping and R&D. In the case of the programme of supporting measurements, prototyping and R&D, possible forms of worldwide cooperation and collaboration as well as a possible distribution of tasks at the scientific community level, as well as eventual institutional forms of common or parallel funding at the agency level, were examined.

The first day of the meeting addressed the accelerator-based programme. The second day of the meeting was devoted to the examination of the non-accelerator physics potential of the various large neutrino infrastructures and started the discussion of closer coordination in this domain.

The summary of discussions and conclusion has been announced and can be found here:
<https://www.kek.jp/en/NewsRoom/Release/2016/07/08/NuInfra2016-2.pdf>

Participants: 80 participants.

PhyStat- ν Workshop on Statistical Issues in Experimental Neutrino Physics

Date: May 30 - June 1, 2016

Place: Kavli Institute for the Physics and Mathematics of the Universe (Kavli IPMU), The University of Tokyo

Outline: Neutrino experiments are reaching exciting new levels of precision: percent-level systematic uncertainties in oscillation experiments, the eV scale in direct mass measurements, 10^{25} year half-lives in double beta decay experiments, and neutrino-nucleus cross section measurements at the 5% level. With this new precision comes an important focus on the statistical understanding of data from neutrino experiments, and techniques to ensure the quality of the results produced.

The PhyStat series of workshops has been a successful institution in the world of collider physics over the past 15 years, providing a forum for discussing topics such as setting upper limits on or discovering rare processes, and combining results from different experiments. We now aim to turn this success to the field of neutrino physics.

PhyStat- ν addressed statistical issues in the broad range of modern neutrino physics, including making measurements of model parameters, setting limits, discovery criteria, discrete choice of models, Bayesian vs. frequentist inference, and combining experiments. Two workshops were planned for 2016: this workshop at the Kavli Institute for the Physics and Mathematics of the Universe in Kashiwa, Japan in May, and a second workshop at Fermilab in the autumn. These workshops consisted of invited and contributed talks, and poster and discussion sessions, and brought together experts in the analysis of neutrino data with experts in statistics to explore the statistical issues in neutrino physics.

Participants: 90 participants.

CTA Consortium Meeting Kashiwa

Date: June 16-20, 2016

Place: Kashiwa-No-Ha Conference Center

Outline: CTA project is the worldwide and international collaborative project, conducting Very High Energy (VHE) gamma ray research. More than 1300 scientists from 32 countries are participating in this research.

170 members, such as the leaders from each working group in each country, gathered in Kashiwa, Chiba, Japan, and discussed about the future business plans and the key scientific projects for CTA.

Participants: 170 participants.



Fig. 1. CTA Consortium Meeting.

Symposium and Celebration to Commemorate the 20th anniversary of Super-Kamiokande

Date: June 17th, 2016

Place: Wohlfahrt Toyama and Oarks Canal Park Hotel Toyama, Toyama, Japan

Outline: On June 17th, 2016 a symposium to mark the 20th anniversary of Super-Kamiokande was held in Toyama. The symposium was followed by a celebration and both events were hosted by the Institute for Cosmic Ray Research, University of Tokyo. Around 250 guests composed of both collaborators and people who have supported the continuous observations of Super-Kamiokande attended.

The symposium opened with an address from Prof. Takaaki Kajita, the director of ICRR and was followed by congratulatory speeches from Ms. Yayoi Komatsu, director-general of Research Promotion Bureau, MEXT and Prof. James Stone on behalf of Dr. Alan Stone, High Energy Physics Budget and Planning, the US DOE. Super-Kamiokande collaborators then proceeded to present not only the results of Super-Kamiokandes research over the last 20 years, but also explained planned upgrades of the experiment and introduced the next generation project, Hyper-Kamiokande.

During the celebration following the symposium, Prof. Makoto Gonokami, president of University of Tokyo, delivered a speech of congratulations which was followed by congratulatory addresses from Mr. Tsuzuku, the Mayor of Hida City, and Prof. Yasuhiro Okada, the director of KEK. Throughout the evening guests and collaborators shared their memories of the early days of Super-Kamiokande and offered their congratulations.

Speaking on this occasion, Masayuki Nakahata, Spokesperson of Super-Kamiokande and Director of Kamioka Observatory, ICRR, University of Tokyo, noted that, Over the last 20 years Super-Kamiokandes numerous neutrino oscillation discoveries have contributed greatly to elementary particle physics. In addition to further contributions that will be made with more data from T2K, Super-Kamiokande can be expected to contribute to astrophysics as well, with observations of supernova neutrinos. Henry Sobel, Co-Spokesperson of Super-Kamiokande and Professor of Physics at the University of California, Irvine, followed by stating, Besides having world-leading results and prize-winning discoveries, Super-Kamiokande has led to the awarding of over 70 Ph.D. degrees to students who have gone on to become leaders in new generations of experiments.

Participants: 250 participants.



Fig. 2. The symposium to commemorate the 20th anniversary of Super-Kamiokande.



Fig. 3. Prof. Kajita expressed his gratitude for supporting the continuous observations of Super-Kamiokande.

B. ICRR Seminars

1. Apr 6, 2016: Dr. Florian Rodler, "Inspecting the atmospheres of giant exoplanets"
2. Apr 27, 2016: Dr. Fumitaka Sato
3. May 16, 2016: Dr. Basudeb Dasgupta (Tata institute), "Temporal Instability of Supernova Neutrinos"
4. May 25, 2016: Dr. Toshihiro Fujii (ICRR), "Future Perspectives on the UHECR Observatories and the FAST Project"
5. Jun 9, 2016: Dr. Elina Lindfors (Tuorla Observatory), "Very High Energy gamma-rays from Flat Spectrum Radio Quasars"
6. Jun 15, 2016: Dr. Tomoya Kinugawa (ICRR), "Gravitational Waves from Black Hole Binary (in Japanese)"
7. Jul 1, 2016: Dr. Mohammad Sajjad Athar (Aligarh Muslim University), "Neutrino-Nucleus Cross Sections At Atmospheric Neutrino Energies"
8. Aug 10, 2016: Dr. Hide-Kazu Tanaka (ICRR), "Latest results of the T2K experiment using the first anti-neutrino dataset"
9. Sep 28, 2016: Dr. Rene A. Ong (University of California, Los Angeles), "The Future of Very High Energy Astrophysics"
10. Dec 16, 2016: Dr. Satoshi Shirai (IPMU), "Search for Wino (ICRR & IPMU joint seminar)"
11. Jan 10, 2017: Dr. William Creus (Institute of Physics, Academia Sinica), "The First Five Years of the Alpha Magnetic Spectrometer on the International Space Station"
12. Jan 12, 2017: Dr. Shigeo Kimura (Pennsylvania State University), "Recycling Galactic Cosmic-Ray Nuclei by Shear Acceleration: A Radio Galaxy Model for Ultrahigh-Energy Cosmic Rays"
13. Mar 7, 2017: Dr. Hiro Ejiri (RCNP Osaka University), "Search for cold dark matter by measuring X and γ rays"
14. Mar 21, 2017: Dr. Masato Shiozawa (ICRR), "Hyper-Kamiokande project"
15. Mar 31, 2017: Dr. Hayato Shimabukuro (Observatoire de Paris), "Analysing the 21cm signal from epoch of reionization with artificial neural networks (ICRR & IPMU Joint seminar)"
16. Mar 31, 2017: Dr. Stefan Ritt (Paul Scherrer Institut (PSI), Switzerland), "Fast waveform digitizing for the search of the $\mu^+ \rightarrow e^+$ gamma decay"

C. List of Publications

(a) Papers Published in Journals

1. "Search for two-neutrino double electron capture on ^{124}Xe with the XMASS-I detector", K. Abe et al. [XMASS Collaboration], Phys. Lett. **B759** (2016) 64-68.
2. "Light yield of an undoped CsI crystal coupled directly to a photomultiplier tube at 77 Kelvin", Liu, J; Yamashita, M; Soma, AK, Journal of Instrumentation, Volume **11**, October 2016 .
3. "Measurement of Muon Antineutrino Oscillations with an Accelerator-Produced Off-Axis Beam", The T2K Collaboration, Phys. Rev. Lett, **116**, 181801 (2016).
4. "Real-Time Supernova Neutrino Burst Monitor at Super-Kamiokande", The Super-Kamiokande Collaboration, Astropart. Phys. **81** (2016) 39-48.
5. "Solar Neutrino Measurements in Super-Kamiokande-IV", K. Abe et al. (Super-Kamiokande Collaboration), Phys. Rev. D **94**, 052010.
6. "Search for Neutrinos in Super-Kamiokande Associated with Gravitational-wave Events GW150914 and GW151226", Super-Kamiokande Collaboration, The Astrophysical Journal Letters, Volume **830**, Number 1.

7. "Measurements of the atmospheric neutrino flux by Super-Kamiokande: Energy spectra, geomagnetic effects, and solar modulation", E. Richard et al. (Super-Kamiokande Collaboration), *Phys. Rev. D* **94**, 052001.
8. "Search for proton decay via $p \rightarrow e^+ \pi^0$ and $p \rightarrow \mu^+ \pi^0$ in 0.31 megaton years exposure of the Super-Kamiokande water Cherenkov detector", Super-Kamiokande Collaboration, *Phys. Rev. D* **95**, 012004 (2017).
9. "Testing charged current quasi-elastic and multinucleon interaction models in the NEUT neutrino interaction generator with published datasets from the MiniBooNE and MINERvA experiments", C. Wilkinson, R. Terri, C. Andreopoulos, A. Bercellie, C. Bronner, S. Cartwright, P. de Perio, J. Dobson, K. Duffy, A.P. Furmanski, L. Haegel, Y. Hayato, A. Kaboth, K. Mahn, K.S. McFarland, J. Nowak, A. Redij, P. Rodrigues, F. Sánchez, J.D. Schwehr, P. Sinclair, J.T. Sobczyk, P. Stamoulis, P. Stowell, R. Tacik, L. Thompson, S. Tobayama, M.O. Wascko, J. Żmuda, *Phys. Rev. D* **93**, 072010.
10. "NUISANCE: a neutrino cross-section generator tuning and comparison framework", P. Stowell, C. Wretb, C. Wilkinson, L. Pickering, S. Cartwright, Y. Hayato, K. Mahn, K.S. McFarland, J. Sobczyk, R. Terri, L. Thompson, M.O. Wascko and Y. Uchida, *JINST* **12** (2017) no.01, P01016.
11. "Direct dark matter search by annual modulation in XMASS-I", K. Abe et al. (XMASS Collaboration), *Phys. Lett. B* **759** (2016) 272-276.
12. "Detectability of galactic supernova neutrinos coherently scattered on xenon nuclei in XMASS", K. Abe et al. (XMASS Collaboration), *Astropart. Phys.* **89** (2017) 51-56.
13. "A measurement of the time profile of scintillation induced by low energy gamma-rays in liquid xenon with the XMASS-I detector", H. Takiya et al. (XMASS Collaboration), *Nucl. Instrum. Meth.* **A834** (2016) 192-196.
14. "Measurement of Coherent π^+ Production in Low Energy Neutrino-Carbon Scattering", The T2K Collaboration, *Phys. Rev. Lett.* **117**, 192501.
15. "First measurement of the muon neutrino charged current single pion production cross section on water with the T2K near detector", The T2K Collaboration, *Phys. Rev. D* **95**, 012010 (2017).
16. "Measurement of double-differential muon neutrino charged-current interactions on C_8H_8 without pions in the final state using the T2K off-axis beam", The T2K Collaboration, *Phys. Rev. D* **93** 112012 (2016).
17. "Minute-Timescale >100 MeV Gamma-Ray Variability during the Giant Outburst of Quasar 3C 279 Observed by Fermi-LAT in 2015 June", Ackermann, Anantua, Asano et al. (Corr. Authors: Hayashida, Madejski, Nalewajko), 2016APJL**824**:L20.
18. "MAGIC detection of very high energy γ -ray emission from the low-luminosity blazar 1ES 1741+196", M.L. Ahnen, H.Kubo, M.Teshima et al., *Monthly Notice of Royal Astronomical Society*, **468**,1534A(2017).
19. "Development of a composite large-size SiPM (assembled matrix) based modular detector cluster for MAGIC", A.Hahn, M.Teshima et al., *Nucl. Instr. Meth. A*, **845**(2016)89-92.
20. "Evaluation of Photo Multiplier Tube candidates for the Cherenkov Telescope Array", R. Mirzoyan, M.Teshima, T.Yamamoto et al., *Nucl. Instr. And Meth. Phys. Res. A*, **824**(2016)640-641.
21. "A Search for Spectral Hysteresis and Energy-dependent Time Lags from X-Ray and TeV Gamma-Ray Observations of Mrk 421", A.U. Abeysekera, M.Teshima et al., *Ap.J.* **834**(2017), no.1, 2.
22. "Detection of very high energy gamma-ray emission from the gravitationally lensed blazar QSO B0218+357 with the MAGIC telescopes", J.Ahnen, H. Kubo, M.Teshima et al., *Astronomy and Astrophysics*, **595**(2016), 98A.
23. "Long-term multi-wavelength variability and correlation study of Markarian 421 from 2007 to 2009", M.L.Ahnen, H. Kubo, M.Teshima et al., *Astronomy and Astrophysics*, **593**(2016), 91A.
24. "Investigating the peculiar emission from the new VHE gamma-ray source H1722+119", M.L. Ahnen, H.Kubo, M.Teshima et al., *Monthly Notice of Royal Astro. Soc.*, **459**(2016)3271A.
25. "Multiwavelength observations of the blazar 1ES 1011+496 in Spring 2008", M.L.Ahnen, H. Kubo, M.Teshima et al., *Monthly Notice of Royal Astro. Soc.*, **459**(2016)2286A.
26. "Search for VHE gamma-ray emission from Geminga pulsar and nebula with the MAGIC telescopes", M.L.Ahnen, H. Kubo, M.Teshima et al., *Astronomy and Astrophysics*, **591**(2016), 138A.

27. "Super-orbital variability of LS I +61° 303 at TeV energies", M.L.Ahnen, H. Kubo, M.Teshima et al., *Astronomy and Astrophysics*, **591**(2016), 76A.
28. "Insights into the emission of the blazar 1ES 1011+496 through unprecedented broadband observations during 2011 and 2012", J.Aleksic, H. Kubo, M.Teshima et al., *Astronomy and Astrophysics*, **591**(2016), 10A.
29. "MAGIC observations of the February 2014 flare of 1ES 1011+496 and ensuing constraint of the EBL density", M.L.Ahnen, H. Kubo, M.Teshima et al., *Astronomy and Astrophysics*, **590**(2016), 24A.
30. "Deep observation of the NGC 1275 region with MAGIC: search of diffuse γ -ray emission from cosmic rays in the Perseus cluster", M.L.Ahnen, H. Kubo, M.Teshima et al., *Astronomy and Astrophysics*, **589**(2016), 33A.
31. "Multiwavelength Study of Quiescent States of Mrk 421 with Unprecedented Hard X-Ray Coverage Provided by NuSTAR in 2013", M. Balokovic, H. Kubo, M.Teshima et al., *Ap.J.*, **819**(2016), 156B.
32. "The major upgrade of the MAGIC telescopes, Part II: A performance study using observations of the Crab Nebula", J. Aleksic, H. Kubo, M.Teshima et al., *Astroparticle Physics*, **72**(2016), 76A.
33. "Teraelectronvolt pulsed emission from the Crab Pulsar detected by MAGIC", J.Ansoldi, H. Kubo, M.Teshima et al., *Astronomy and Astrophysics*, **585**(2016), 133A.
34. "The energy spectrum of cosmic rays above 1017.2 eV measured by the fluorescence detectors of the Telescope Array experiment in seven years", R.U. Abbasi et al., *Astroparticle Physics* **80** (2016) pp131-140.
35. "First upper limits on the radar cross section of cosmic-ray induced extensive air showers", R.U. Abbasi et al., *Astroparticle Physics* **87** (2017) p1-17.
36. "Search for EeV protons of galactic origin", R.U. Abbasi et al., *Astropart. Phys.* **86** (2017) 21-26.
37. "Energy determination of gamma-ray induced air showers observed by an extensive air shower array", K. Kawata et al., *Experimental Astronomy*, online.
38. "Northern Sky Galactic Cosmic Ray Anisotropy between 10 and 1000 TeV with the Tibet Air Shower Array", M. Amenomori et al. (the Tibet AS γ collaboration), *Astrophysical Journal*, **836**: 153(7pp), 2017.
39. "Electromagnetic Afterglows Associated with Gamma-Ray Emission Coincident with Binary Black Hole Merger Event GW150914", Ryo Yamazaki, Katsuaki Asano, Yutaka Ohira,, *PTEP* 2016, **051E01**.
40. "Very Long Baseline Interferometry Experiment on Giant Radio Pulses of Crab Pulsar toward Fast Radio Burst Detection", K. Takefuji, T. Terasawa, T. Kondo, R. Mikami, H. Takeuchi, H. Misawa, F. Tsuchiya, H. Kita, M. Sekido, *The Astronomical Society of the Pacific*, **128**, 966.
41. "Gravitational Wave Quasinormal Mode from Population III Massive Black Hole Binaries in Various Models of Population Synthesis", Tomoya Kinugawa, Hiroyuki Nakano and Takashi Nakamura, *PTEP2016*, **103E01** .
42. "A Unified Model for GRB Prompt Emission from Optical to Gamma-rays; A New Type of Standard Candle", S. Guiriec, C. Kouveliotou, D. H. Hartmann, J. Granot, K. Asano, P. Meszaros, R. Gill, N. Gehrels, and J. McEnery, *2016APJL***831**:L8.
43. "CALET Upper Limits on X-ray and Gamma-ray Counterparts of GW 151226", O. Adriani, Y. Akaike, K. Asano, et al., *The Astrophysical Journal Letters*, Volume **829**, Number 1.
44. "Ultra High-Energy Cosmic Ray Production by Turbulence in Gamma-Ray Burst Jets and Cosmogenic Neutrinos", Katsuaki Asano and Peter Mészáros, *Phys. Rev. D* **94**, 023005.
45. "Pre-DECIGO can get the smoking gun to decide the astrophysical or cosmological origin of GW150914-like binary black holes", Takashi Nakamura, Masaki Ando, Tomoya Kinugawa, et al., *Prog Theor Exp Phys* (2016) 2016 (9): **093E01**.
46. "Electric Field Screening with Back-Flow at Pulsar Polar Cap", Shota Kisaka, Katsuaki Asano, Toshio Terasawa, *The Astrophysical Journal*, **829**:12.
47. "Wide-Band Spectra of Giant Radio Pulses from the Crab Pulsar", Ryo Mikami, Katsuaki Asano, Shota J. Tanaka, Shota Kisaka, Mamoru Sekido, Kazuhiro Takefuji, Hiroshi Takeuchi, Hiroaki Misawa, Fuminori Tsuchiya, Hajime Kita, Yoshinori Yonekura, Toshio Terasawa,, *The Astrophysical Journal*, Volume **832**, Number 2.

48. "The possible existence of Pop III NS-BH binary and its detectability", Tomoya Kinugawa, Takashi Nakamura, Hiroyuki Nakano, *Prog Theor Exp Phys* (2017) 2017 (2): **021E01**.
49. "High-Energy Non-Thermal and Thermal Emission from GRB141207A Detected by Fermi", Makoto Arimoto, Katsuaki Asano, Masanori Ohno, Peter Veres, Magnus Axelsson, Elisabetta Bissaldi, Yutaro Tachibana, Nobuyuki Kawai, *The Astrophysical Journal*, Volume **833**, Number 2.
50. "Formation Pathway of Population III Coalescing Binary Black Holes through Stable Mass Transfer", Kohei Inayoshi, Ryosuke Hirai, Tomoya Kinugawa and Kenta Hotokezaka, *MNRAS* **468**, 5020-5032 (2017).
51. "Circular Polarizations of Gravitational Waves from Core-Collapse Supernovae: A Clear Indication of Rapid Rotation", Kazuhiro Hayama, Takami Kuroda, Ko Nakamura, and Shoichi Yamada, *Phys. Rev. Lett.* **116**, 151102.
52. "Characterization of non-Gaussianity in gravitational wave detector noise", Takahiro Yamamoto, Kazuhiro Hayama, Shuhei Mano, Yousuke Itoh, and Nobuyuki Kanda, *Phys. Rev. D* **93**, 082005.
53. "Observation of reduction of radiation-pressure-induced rotational anti-spring effect on a 23 mg mirror in a Fabry-Perot cavity", Yutaro Enomoto, Koji Nagano, Masayuki Nakano, Akira Furusawa and Seiji Kawamura, *Class. Quantum Grav.*, **33** (2016) 145002.
54. "Standard quantum limit of angular motion of a suspended mirror and homodyne detection of ponderomotively squeezed vacuum field", Yutaro Enomoto, Koji Nagano, and Seiji Kawamura, *Phys. Rev. A* **94**, 012115 (2016).
55. "Unveiling linearly and nonlinearly correlated signals between gravitational wave detectors and environmental monitors", Hiroataka Yuzurihara, Kazuhiro Hayama, Shuhei Mano, Didier Verkindt, and Nobuyuki Kanda, *Phys. Rev. D* **94**, 042004.
56. "Mitigation of radiation-pressure-induced angular instability of a Fabry-Perot cavity consisting of suspended mirrors", Koji Nagano, Yutaro Enomoto, Masayuki Nakano, Akira Furusawa and Seiji Kawamura, *Phys. Lett. A* **380** (2016) 3871-3875.
57. "Morphologies of $\sim 190,000$ Galaxies at $z=0-10$ Revealed with HST Legacy Data II. Evolution of Clumpy Galaxies", Takatoshi Shibuya, Masami Ouchi, Mariko Kubo, Yuichi Harikane, 2016 *ApJ* **821** 72.
58. "Evolution of Stellar-to-Halo Mass Ratio at $z=0-7$ Identified by Clustering Analysis with the Hubble Legacy Imaging and Early Subaru/Hyper Suprime-Cam Survey Data", Yuichi Harikane, Masami Ouchi, Yoshiaki Ono, Surhud More, Shun Saito, Yen-Ting Lin, Jean Coupon, Kazuhiro Shimasaku, Takatoshi Shibuya, Paul A. Price, Lihwai Lin, Bau-Ching Hsieh, Masafumi Ishigaki, Yutaka Komiyama, John Silverman, Tadafumi Takata, Hiroko Tamazawa, Jun Toshikawa, 2016 *APJ* **821**:123.
59. "Bright and Faint Ends of $\text{Ly}\alpha$ Luminosity Functions at $z=2$ Determined by the Subaru Survey: Implications for AGN, Magnification Bias, and ISM HI Evolution", Akira Konno, Masami Ouchi, Kimihiko Nakajima, Florent Duval, Haruka Kusakabe, Yoshiaki Ono, Kazuhiro Shimasaku, 2016 *APJ* **823**:20.
60. "A Very Compact Dense Galaxy Overdensity with $\delta \simeq 130$ Identified at $z \sim 8$: Implications for Early Protocluster and Cluster Core Formation", Masafumi Ishigaki, Masami Ouchi, Yuichi Harikane, 2016 *ApJ* **822** 5.
61. "Subaru high- z exploration of low-luminosity quasars (SHELLQs). I. Discovery of 15 quasars and bright galaxies at 5.7", Matsuoka, Yoshiki; Onoue, Masafusa; Kashikawa, Nobunari; Iwasawa, Kazushi; Strauss, Michael A.; Nagao, Tohru; Imanishi, Masatoshi; Niida, Mana; Toba, Yoshiki; Akiyama, Masayuki; Asami, Naoko; Bosch, James; Foucaud, Sébastien; Furusawa, Hisanori; Goto, Tomotsugu; Gunn, James E.; Harikane, Yuichi; Ikeda, Hiroyuki; Kawaguchi, Toshihiro; Kikuta, Satoshi Komiyama, Yutaka; Lupton, Robert H.; Minezaki, Takeo; Miyazaki, Satoshi; Morokuma, Tomoki; Murayama, Hitoshi; Nishizawa, Atsushi J.; Ono, Yoshiaki; Ouchi, Masami; Price, Paul A.; Sameshima, Hiroaki; Silverman, John D.; Sugiyama, Naoshi; Tait, Philip J.; Takada, Masahiro; Takata, Tadafumi; Tanaka, Masayuki; Tang, Ji-Jia; Utsumi, Yousuke, 2016 *APJ* **828**:26.
62. "A New Constraint on the $\text{Ly}\alpha$ Fraction of UV Very Bright Galaxies at Redshift 7", Hisanori Furusawa et al., 2016 *APJ* **822**:46.
63. "Cosmic Galaxy-IGM HI Relation at $z \sim 2-3$ Probed in the COSMOS/UltraVISTA 1.6 deg² Field", Shiro Mukae, Masami Ouchi, Koki Kakiichi, Nao Suzuki, Yoshiaki Ono, Zheng Cai, Akio K. Inoue, Yi-Kuan Chiang, Takatoshi Shibuya, Yuichi Matsuda, 2017 *APJ* **835**:281.
64. "Detection of an oxygen emission line from a high redshift galaxy in the reionization epoch", Inoue, Akio K.; Tamura, Yoichi; Matsuo, Hiroshi; Mawatari, Ken; Shimizu, Ikkoh; Shibuya, Takatoshi; Ota, Kazuaki; Yoshida, Naoki; Zackrisson, Erik; Kashikawa, Nobunari; Kohno, Kotaro; Umehata, Hideki; Hatsukade, Bunyo; Iye, Masanori; Matsuda, Yuichi; Okamoto, Takashi; Yamaguchi, Yuki, 2016 *Science*, **352**, 1559.

65. "A Spectroscopically Confirmed Double Source Plane Lens System in the Hyper Suprime-Cam Subaru Strategic Program", Tanaka, Masayuki; Wong, Kenneth C.; More, Anupreeta; Dezuka, Arsha; Egami, Eiichi; Oguri, Masamune; Suyu, Sherry H.; Sonnenfeld, Alessandro; Higuchi, Ryo; Komiyama, Yutaka; Miyazaki, Satoshi; Onoue, Masafusa; Oyamada, Shuri; Utsumi, Yousuke, *The Astrophysical Journal Letters*, Volume **826**, Number 2 .
66. "Similarities and uniqueness of Ly α emitters among star-forming galaxies at z=2.5", Rhythm Shimakawa, Tadayuki Kodama, Takatoshi Shibuya et al., *MNRAS*, **468**, 1123-1141 (2017).
67. "A new quadruple gravitational lens from the Hyper Suprime-Cam Survey: the dilemma of HSC-J115252+004733", Anupreeta More., Masami Ouchi et al., *MNRAS* **465**, 2411-2419 (2017).
68. "A hard ionizing spectrum in z=3-4 Ly-alpha emitters with intense [OIII] emission: Analogs of galaxies in the reionization era?", Kimihiko Nakajima, Richard S. Ellis, Ikuru Iwata, Akio Inoue, Haruka Kusakabe, Masami Ouchi, Brant Robertson., 2016APJL, **831**:1.
69. "Imaging of diffuse HI absorption structure in the SSA22 proto-cluster region at z = 3.1", Ken Mawatari, Akio K. Inoue, Toru Yamada, Tomoki Hayashino, Takuya Otsuka, Yuichi Matsuda, Hideki Umehata, Masami Ouchi, Shiro Mukae, 2017MNRAS. **467**, 3951.
70. "Direct evidence for Ly α depletion in the protocluster core", Rhythm Shimakawa, Tadayuki Kodama, Masao Hayashi, Ichi Tanaka, Yuichi Matsuda, Nobunari Kashikawa, Takatoshi Shibuya, Ken-ichi Tadaki, Yusei Koyama, Tomoko L. Suzuki, Moegi Yamamoto, *MNRAS* **468**, L21-L25 (2017).
71. "ALMA Reveals Strong [C II] Emission in a Galaxy Embedded in a Giant Ly α Blob at z = 3.1", Umehata, Hideki; Matsuda, Yuichi; Tamura, Yoichi; Kohno, Kotaro; Smail, Ian; Ivison, R. J.; Steidel, Charles C.; Chapman, Scott C.; Geach, James E.; Hayes, Matthew; Nagao, Tooru; Ao, Yiping; Kawabe, Ryohei; Yun, Min S.; Hatsukade, Bunyo; Kubo, Mariko; Kato, Yuta; Saito, Tomoki; Ikarashi, Soh; Nakanishi, Kouichiro Lee, Minju; Izumi, Takuma; Mori, Masao; Ouchi, Masami, 2017ApJ...**834**L..16U.
72. "Affleck-Dine baryogenesis just after inflation", Masaki Yamada., *Phys. Rev. D* **93**, 083516.
73. "Can massive primordial black holes be produced in mild waterfall hybrid inflation?", Masahiro Kawasaki and Yuichiro Tada., *JCAP***08**(2016)041.
74. "High-scale SUSY from an R-invariant New Inflation in the Landscape", Masahiro Kawasaki, Masaki Yamada, Tsutomu T. Yanagida, Norimi Yokozaki., *PHYSICAL REVIEW D* **93**,055022 (2016).
75. "Cosmology with a Heavy Polonyi Field", Keisuke Harigaya, Taku Hayakawa, Masahiro Kawasaki, Masaki Yamada, *JCAP***06**(2016)015.
76. "Spontaneous Baryogenesis from Asymmetric Inflation", Fuminobu Takahashi and Masaki Yamada, *Phys. Lett. B* **756**(2016), 216-220.
77. "Cosmological Problems of the String Axion Alleviated by High Scale SUSY of $m_{3/2} \simeq 10$ -100 TeV", Masahiro Kawasaki, Tsutomu T. Yanagida and Norimi Yokozaki, *Phys. Lett. B* **753** 389-394.
78. "Can thermal inflation be consistent with baryogenesis in gauge-mediated SUSY breaking models?", Taku Hayakawa, Masahiro Kawasaki and Masaki Yamada, *PHYSICAL REVIEW D* **93**, 063529 (2016).
79. "Why three generations?", Masahiro Ibe., Alexander Kusenko, Tsutomu T. Yanagida, *Phys.Lett. B***758**(2016)365-369.
80. "750 GeV diphoton resonance in a visible heavy QCD axion model ", Cheng-Wei Chiang, Hajime Fukuda, Masahiro Ibe, Tsutomu T. Yanagida, *Phys. Rev. D* **93**, 095016.
81. "Dark matter annihilation and decay from non-spherical dark halos in the Galactic dwarf satellites", Kohei Hayashi, Koji Ichikawa, Shigeki Matsumoto, Masahiro Ibe, Miho N. Ishigaki, Hajime Sugai., *MNRAS* **461**, 2914-2928 (2016).
82. "Charged Q-ball Dark Matter from B and L direction", Jeong-Pyong Hong, Masahiro Kawasaki, and Masaki Yamada, *JCAP***08**(2016)053.
83. "Revisiting constraints on small scale perturbations from big-bang nucleosynthesis", Keisuke Inomata, Masahiro Kawasaki and Yuichiro Tada, *Phys. Rev. D* **94**, 043527.
84. "A Simple Cosmological Solution to the Higgs Instability Problem in the Chaotic Inflation and Formation of Primordial Black Holes", Masahiro Kawasaki, Kyohei Mukaida, Tsutomu T. Yanagida, *Phys. Rev. D* **94**, 063509 (2016).

85. "PBH Dark Matter in Supergravity Inflation Models", Masahiro Kawasaki, Alexander Kusenko, Yuichiro Tada, and Tsutomu T. Yanagida, *Phys. Rev. D* **94**, 083523 (2016).
86. "A map of the non-thermal WIMP", Hyungjin Kim, Jeong-Pyong Hong, and Chang Sub Shin, *Phys. Lett. B* **768**(2017), 292-298.
87. "Gravitino Problem in Minimal Supergravity Inflation", Fuminori Hasegawa, Kyohei Mukaida, Kazunori Nakayama, Takahiro Terada, and Yusuke Yamada, *Phys. Lett. B* **767** (2017) 392-397.
88. "Thermal Relic Dark Matter Beyond the Unitarity Limit ", Keisuke Harigaya, Wakutaka Nakano, Masahiro Ibe, Motoo Suzuki, *JHEP* **1608** (2016) 151 .
89. "Cracking down on fake photons: Cases of diphoton resonance imposters ", Hajime Fukuda, Masahiro Ibe, Osamu Jinnouchi, Mihoko Nojiri, *PTEP* **2017** (2017) no.3, 033B05.
90. "Lower limit on the gravitino mass in low-scale gauge mediation with $m_H \sim 125\text{GeV}$ ", Masahiro Ibe, Tsutomu Yanagida, *Phys.Lett. B* **764** (2017) 260-264 .
91. "Revisiting gravitino dark matter in thermal leptogenesis ", Masahiro Ibe, Motoo Suzuki, Tsutomu Yanagida, *JHEP* **1702** (2017) 063 .
92. "Constraints on $L_\mu - L_\tau$ gauge interactions from rare Kaon decay", Wakutaka Nakano, Masahiro Ibe, Motoo Suzuki, *Phys.Rev. D* **95** (2017) no.5, 055022 .

(b) Conference Papers (Proceedings)

1. "Neutrino Masses Discovered at Kamioka Underground", Masayuki Nakahata, The 44th symposium of the visualization society of Japan, Kogakuin University, Shijyuku, Tokyo, July 19, 20, 2016.
2. "Supernovae in SuperK-Gd and other experiments", Lluís Martí-Magro, NuPhys2016, Prospects in Neutrino Physics, London, 12-14 December, 2016, arXiv:1705.00675.
3. "New atmospheric and solar results from Super-Kamiokande", Shigetaka Moriyama, The XXVII International Conference on Neutrino Physics and Astrophysics (Neutrino 2016), London, United Kingdom, 4 July to 9 July 2016.
4. "Recent results of direct dark matter search with XMASS", Katsuki Hiraide, 38th International Conference on High Energy Physics (ICHEP2016), Chicago, USA, August 3-10, 2016, PoS ICHEP2016 (2016) 213.
5. "The Super-Kamiokande Gadolinium Project", Hiroyuki Sekiya, ICHEP 2016, Chicago, 2016 Aug3-10, PoS(ICHEP2016)982.
6. "Supernova neutrinos in SK-Gd and other experiments", Hiroyuki Sekiya, Neutrino 2016, London, 2016 July 4-9.
7. "Measurements of the atmospheric neutrino flux by Super-Kamiokande: energy spectra, geomagnetic effects, and solar modulation", Kimihiro Okumura, XXVII International Conference on Neutrino Physics and Astrophysics (Neutrino 2016), 4-9 July 2016, South Kensington, London.
8. "New 50 cm Photo-Detectors for Hyper-Kamiokande", Yasuhiro NISHIMURA, ICHEP2016, Chicago, USA, 6/August/2016, Pos(ICHEP2016)303.
9. "Development of Neutron Tagging Algorithm for Hyper-Kamiokande with Pure Water", Yuji Okajima, XXVII International Conference on Neutrino Physics and Astrophysics (Neutrino 2016), 4-9 July 2016, South Kensington, London.
10. "Direct Dark Matter Search with XMASS", Kobayashi, Kazuyoshi, XMASS Collaboration, 37th International Conference on High Energy Physics (ICHEP), Valencia, SPAIN, JUL 02-09, 2014.
11. "Solar neutrinos in Super-Kamiokande", Sekiya, Hiroyuki, 7th International Conference on High Energy Physics (ICHEP), Valencia, SPAIN, JUL 02-09, 2014.
12. "Development of a liquid scintillator containing a zirconium beta-keto ester complex for the ZICOS experiment", Fukuda, Yoshiyuki; Gunji, Takahiro; Moriyama, Shigetaka; et al., 37th International Conference on High Energy Physics (ICHEP), Valencia, SPAIN, JUL 02-09, 2014.
13. "Search for double electron capture on Xe-124 with the XMASS-I detector", Hiraide, Katsuki, XMASS Collaboration, 14th International Conference on Topics in Astroparticle and Underground Physics (TAUP), Torino, ITALY, SEP 07-11, 2015.

14. "Direct dark matter search with XMASS: modulation analysis", Kobayashi, Kazuyoshi, XMASS Collaboration, 14th International Conference on Topics in Astroparticle and Underground Physics(TAUP), Torino, ITALY, SEP 07-11, 2015.
15. "Low energy neutrinos in Super-Kamiokande", Sekiya, Hiroyuki, 4th International Conference on Topics in Astroparticle and Underground Physics (TAUP) , Torino, ITALY, SEP 07-11, 2015.
16. "Highlights from Super-Kamiokande", Okumura, Kimihiro, 4th International Conference on New Frontiers in Physics (ICNFP), Crete, GREECE, AUG 23-30, 2015.
17. "Atmospheric Neutrino Flux", Athar, M. Sajjad; Honda, M., 21st DAE-BRNS High Energy Physics (HEP) Symposium, Indian Inst Technol Guwahati, Guwahati, INDIA, DEC 08-12, 2014.
18. "XMASS experiment", Abe, Ko, XMASS Collaboration, 5th Workshop on Dark Matter, Neutrino Physics and Astrophysics (CETUP) / 9th International Conference on Interconnections between Particle Physics and Cosmology (PPC), Deadwood, SD, JUL 15-17, 2015.
19. "New DAQ System for the CANDLES Experiment", Suzuki, K.; Ajimura, S.; Chan, W. M.; et al, 19th Real Time Conference (RT), Nara, JAPAN, MAY 26-30, 2014.
20. "The CANDLES Trigger System for the Study of Double Beta Decay of Ca-48", Maeda, T.; Ajimura, S.; Chan, W. M.; et al., 19th Real Time Conference (RT) , Nara, JAPAN, MAY 26-30, 2014.
21. "The Beamline DAQ System for the T2K Experiment", Suzuki, S. Y.; Sakashita, K.; Kakuno, H.; et al., 19th Real Time Conference (RT), Nara, JAPAN, MAY 26-30, 2014.
22. "Micro-source development for XMASS experiment", Kim, N. Y.; Abe, K.; Hieda, K.; et al., 15th Symposium on Radiation Measurements and Applications (SORMA), Univ Michigan Campus, Ann Arbor, MI, JUN 09-12, 2014.
23. "Development of a composite large-size SiPM (assembled matrix) based modular detector cluster for MAGIC", Hahn, A.; Mazin, D.; Bangale, P.; et al., 4th Vienna Conference on Instrumentation, Vienna Univ Technol, Dept Elect Engn, Vienna, AUSTRIA, FEB 15-19, 2016.
24. "Evaluation of novel PMTs of worldwide best parameters for the CTA project", Mirzoyan, R.; Mueller, D.; Hose, J.; et al., 14th Vienna Conference on Instrumentation, Vienna Univ Technol, Dept Elect Engn, Vienna, AUSTRIA, FEB 15-19, 2016.
25. "MAGIC VHE Gamma-Ray Observations Of Binary Systems", Bednarek, W.; Blanch, O.; Cortina, J.; et al., MAGIC Collaboration, 6th International Meeting on High Energy Gamma-Ray Astronomy, Heidelberg, GERMANY, JUL 11-15, 2016.
26. "First minute-scale variability in Fermi-LAT blazar observations during the giant outburst of 3C279 in 2015 June", Hayashida, Masaaki; Madejski, Greg; Blandford, Roger; et al., Fermi-LAT Collaboration, 6th International Meeting on High Energy Gamma-Ray Astronomy, Heidelberg, GERMANY, JUL 11-15, 2016.
27. "Large Size Telescope Report", Mazin, D.; Cortina, J.; Teshima, M., CTA Consortium, 6th International Meeting on High Energy Gamma-Ray Astronomy, Heidelberg, GERMANY, JUL 11-15, 2016.
28. "EBL Constraints Using a Sample of TeV Gamma-Ray Emitters Measured with the MAGIC Telescopes", Mazin, D.; Dominguez, A.; Ramazani, V. Fallah; et al., CTA Consortium, 6th International Meeting on High Energy Gamma-Ray Astronomy, Heidelberg, GERMANY, JUL 11-15, 2016.
29. "Evaluation of the basic propertied of the novel 1.5 in. size PMTs from Hamamatsu Photonics and Electron Tubes Enterprises", Toyama, T.; Hanabata, Y.; Hose, J.; et al., 7th International Conference on New Developments in Photodetection (NDIP) ,Tours, FRANCE , JUL, 2014.
30. "Correlation between UHECRs measured by the Pierre Auger Observatory and Telescope Array and neutrino candidate events from IceCube", IceCube Collaboration; Pierre Auger Collaboration; Telescope Array Collaboration, 4th International Conference on Topics in Astroparticle and Underground Physics (TAUP), Torino, ITALY, SEP 07-11, 2015.
31. "Preliminary analysis of EUSO-TA data", Fenu, F.; Piotrowski, L. W.; Shin, H.; et al., 14th International Conference on Topics in Astroparticle and Underground Physics (TAUP), Torino, ITALY, SEP 07-11, 2015.
32. "Correlation between the UHECRs measured by the Pierre Auger Observatory and Telescope Array and neutrino candidate events from IceCube", IceCube Collaboration; Pierre Auger Collaboration; Telescope Array Collaboration, 7th Biannual Very Large Volume Neutrino Telescope Workshop (VLVnT), La Sapienza Univ, Dept Phys, Rome, ITALY, SEP 14-16, 2015.

33. "Measurement of Schumann Resonance at Kamioka", Atsuta.S, Ogawa.T, Yamaguchi.S, Hayama.K, Araya.A, Kanda.N, Miyakawa.O, Miyoki.S, Nishizawa.A, Ono.K, Saito.Y, Somiya.K, Uchiyama.T, Uyeshima.M, Yano.K, 11th Edoardo Amaldi Conference on Gravitational Waves (AMALDI), Gwangju, SOUTH KOREA, JUN 21-26, 2015.
34. "Determination of mass of an isolated neutron star using continuous gravitational waves with two frequency modes: an effect of a misalignment angle", Eda, Kazunari; Ono, Kenji; Itoh, Yousuke, 11th Edoardo Amaldi Conference on Gravitational Waves (AMALDI), Gwangju, SOUTH KOREA, JUN 21-26, 2015.
35. "Active damping performance of the KAGRA seismic attenuation system prototype", Fujiii, Yoshinori; Sekiguchi, Takanori; Takahashi, Ryutaro; et al., 11th Edoardo Amaldi Conference on Gravitational Waves (AMALDI) , Gwangju, SOUTH KOREA, JUN 21-26, 2015.
36. "Status of the cryogenic payload system for the KAGRA detector", Kumar, R.; Chen, D.; Hagiwara, A.; et al., 11th Edoardo Amaldi Conference on Gravitational Waves (AMALDI), Gwangju, SOUTH KOREA, JUN 21-26, 2015.
37. "An update on the Axion Helioscopes front: current activities at CAST and the IAXO project.", Dafni, T.; Arik, M.; Armengaud, E.; et al., 7th International Conference on High Energy Physics (ICHEP), Valencia, SPAIN, JUL 02-09, 2014.

(c) ICRR Reports

N/A

D. Doctoral Theses

1. "Experimental Search for Hidden-Photon Cold Dark Matter Signatures in the $O(10)$ keV mass range with XMASS-I", Osamu Takachio, Ph.D Thesis, Jun. 2016
2. "Curvature Perturbations and Primordial Black Hole Formation in the Inflationary Universe", Yuichiro Tada, Ph.D Thesis, Mar. 2017
3. "Study of muons from ultra-high energy cosmic ray air showers measured with the Telescope Array experiment", Ryuji Takeishi, Ph.D Thesis, Mar. 2017
4. "Galaxy Evolution and Cosmic Reionization History Studied by Subaru Lyman α Emitter Surveys", Akira Konno, Ph.D Thesis, Mar. 2017

E. Public Relations

(a) ICRR News

ICRR News is a quarterly publication written in Japanese about scientific and educational activities at ICRR. It includes:

1. reports on scientific activities of ICRR staff members and those conducted at one or more of its facilities,
2. reports of international conferences on topics relevant to ICRR's research activities,
3. reports on topics discussed at ICRR's Committees,
4. list of publications published by ICRR [ICRR-Report],
5. list of seminars held at ICRR,
6. announcements, and
7. other items of relevance.

Below lists the main topics in the issues published in FY 2016:

No.96 (2016 Spring)

- Report on the current status of SK-Gd project for Super-Kamiokande, Hiroyuki Sekiya
- Studies on the Earth: laser strainmeters in the Kamioka underground observatory, Akiteru Takamori
- Report of the ICRR Joint-Use Report Workshop, Shinji Miyoki
- ICRR Spring School 2016 Report
- Report of the 14th ICRR/IPMU joint public lecture
- Awards
- Staff reassignment
- ICRR-Seminar

No.97 (2016 Autumn)

- Report of the Symposium and Celebration to Commemorate the 20th anniversary of Super-Kamiokande, Masato Shiozawa
- Report on the current status of the CTA project, Masahiro Teshima
- Staff reassignment
- ICRR-Seminar

No.98 (2017 Winter)

- Gravitational waves from Pop III binary black holes, Tomoya Kinugawa
- Report of the ICRR Joint-Use Report Workshop, Shigetaka Moriyama
- Open Campus 2016 Report
- Launch of ICRR VR (Virtual Reality) website
- Awards
- Staff reassignment
- ICRR-Seminar

(b) Public Lectures

- "Open Lecture," May. 20, 2016, Keio MCC, Takaaki Kajita (ICRR, the University of Tokyo).
- "Memorial Symposium commemorating 130th anniversary of Chunichi Newspaper," Jun. 03, 2016, Nagoya-City, Aichi, Takaaki Kajita (ICRR, the University of Tokyo).
- "Science Cafe in Gifu," Jun. 04, 2016, Gifu-City, Gifu, Takaaki Kajita (ICRR, the University of Tokyo).
- "Nobel Prize Commemorative Lecture," Jul. 16, 2016, Tokai-Mura, Ibaraki, Takaaki Kajita (ICRR, the University of Tokyo).
- "Public Lecture," Aug. 02, 2016, Toyohashi-City, Aichi, Takaaki Kajita (ICRR, the University of Tokyo).
- "Special Lecture," Aug. 18, 2016, KEK Summer Challenge 2016, Takaaki Kajita (ICRR, the University of Tokyo).
- "The Yomiuri international forum with Nobel Laureates," Oct. 01, 2016, Toyama-City, Toyama, Takaaki Kajita (ICRR, the University of Tokyo).
- "Aichi Science Festival," Oct. 08, 2016, Nagoya-City, Aichi, Takaaki Kajita (ICRR, the University of Tokyo).
- "Public Lecture," Nov. 04, 2016, JST 20th Anniversary Forum, Takaaki Kajita (ICRR, the University of Tokyo).
- "The 33rd Hamamatsu Conference," Nov. 05, 2016, Act City, Hamamatsu-City, Shizuoka, Takaaki Kajita (ICRR, the University of Tokyo).
- "Public Lecture," Nov. 20, 2016, Tsukuba-City, Ibaraki, Takaaki Kajita (ICRR, the University of Tokyo).
- "Public Lecture," Nov. 25, 2016, Kyoto University, Kyoto-City, Kyoto, Takaaki Kajita (ICRR, the University of Tokyo).
- "JPS Public Lecture 2016," Nov. 26, 2016, Ito International Research Center, Bunkyo-Ku, Tokyo, Takaaki Kajita (ICRR, the University of Tokyo).
- "From Hiroshima University to The World," Nov. 29, 2016, Hiroshima-Univ., Higashi-Hiroshima City, Hiroshima, Takaaki Kajita (ICRR, the University of Tokyo).
- "Science Class," Dec. 11, 2016, Yonago-City, Tottori, Takaaki Kajita (ICRR, the University of Tokyo).
- "Nobel Prize Commemorative Lecture," Dec. 27, 2016, Kashiwa Shiminbunkakaikan, Kashiwa-City, Chiba, Takaaki Kajita (ICRR, the University of Tokyo).
- "Commemorative event of 50th anniversary of Fuji-City," Jan. 09, 2017, Fuji-City, Shizuoka, Takaaki Kajita (ICRR, the University of Tokyo).
- "Special Lecture commemorating conclusion of partnership agreement between ICRR and Hida-City," Jan. 22, 2017, Hida-City, Gifu, Takaaki Kajita (ICRR, the University of Tokyo).
- "Nambu Colloquium," Feb. 02, 2017, Osaka University, Osaka, Takaaki Kajita (ICRR, the University of Tokyo).
- "Sumisei Life Forum Kashiwa," Feb. 26, 2017, Kashiwa Shiminbunkakaikan, Kashiwa-City, Chiba, Takaaki Kajita (ICRR, the University of Tokyo).
- "Public Lecture in the 72nd Annual Meeting of Physical Society of Japan," Mar. 19, 2017, Ikeda-City, Osaka, Takaaki Kajita (ICRR, the University of Tokyo).
- "Public Lecture," Mar. 27, 2017, Kawagoe-City, Saitama, Takaaki Kajita (ICRR, the University of Tokyo).
- "Nobel Prize Commemorative Lecture," Mar. 29, 2017, Kobe University, Kobe-City, Hyogo, Takaaki Kajita (ICRR, the University of Tokyo).
- "Tokitsu Junior High School," Nov. 16, 2016, Toki-City, Gifu, Kimihiro Okumura (ICRR, the University of Tokyo).
- "Chiben Gakuen Wakayama Junior & Senior High School," Nov. 21, 2016, Wakayama-City, Wakayama, Kimihiro Okumura (ICRR, the University of Tokyo).
- "ICRR/IPMU joint public lecture," Apr. 16, 2016, Kashiwa-City, Chiba, Yoshinari, Hayato (Kamioka Observatory, ICRR, the University of Tokyo).

- "Kawasaki Public Academy," Apr. 19, 2016, Kawasaki-City, Kanagawa, Hiroyuki, Sekiya (Kamioka Observatory, ICRR, the University of Tokyo).
- "SSH, Shizuoka Kita High School," Apr. 21, 2016, Kamioka Observatory, ICRR, the University of Tokyo, Ko Abe (Kamioka Observatory, ICRR, the University of Tokyo).
- "Nobel Prize Commemorative Lecture," Apr. 24, 2016, Yasuda Auditorium, the University of Tokyo, Masayuki Nakahata (Kamioka Observatory, ICRR, the University of Tokyo).
- "Kawasaki Public Academy," Apr. 26, 2016, Kashiwa-City, Chiba, Hiroyuki Sekiya (Kamioka Observatory, ICRR, the University of Tokyo).
- "Public Lecture," Jun. 27, 2016, Toyama Science Museum, Masato Shiozawa (Kamioka Observatory, ICRR, the University of Tokyo).
- "Public Lecture," Jul. 2, 2016, Takayama-City, Gifu, Yasuhiro Kishimoto (Kamioka Observatory, ICRR, the University of Tokyo).
- "SSH, Yoshiki High School," Jul. 7, 2016, Kamioka Observatory, ICRR, the University of Tokyo, Makoto Miura (Kamioka Observatory, ICRR, the University of Tokyo).
- "Toyama High School," Jul. 13, 2016, Toyama-City, Toyama, Yumiko Takenaga, Osamu Takachio (Kamioka Observatory, ICRR, the University of Tokyo).
- "Geo Space Adventure," Jul. 16, 2016-Jul. 17, 2016, Super-Kamiokande, Yasuhiro Kishimoto, Hiroyuki Sekiya, Makoto Miura, Ko Abe, Atsushi Takeda, Yo Kato, Yumiko Takenaga (Kamioka Observatory, ICRR, the University of Tokyo).
- "Geo Space Adventure," Jul. 16, 2016, Hida-City, Gifu, Masayuki Nakahata (Kamioka Observatory, ICRR, the University of Tokyo).
- "SSH, Keio High School," Jul. 20, 2016, Kamioka Observatory, ICRR, the University of Tokyo, Shigetaka Moriyama (Kamioka Observatory, ICRR, the University of Tokyo).
- "Toyama High School," Jul. 21, 2016, Kamioka Observatory, ICRR, the University of Tokyo, Yasuhiro Kishimoto (Kamioka Observatory, ICRR, the University of Tokyo).
- "Aichi Shukutoku High School," Jul. 22, 2016, Kamioka Observatory, ICRR, the University of Tokyo, Makoto Miura (Kamioka Observatory, ICRR, the University of Tokyo).
- "SSH, Nanao High School," Jul. 27, 2016, Kamioka Observatory, ICRR, the University of Tokyo, Ko Abe (Kamioka Observatory, ICRR, the University of Tokyo).
- "SSH, Momoyama High School," Jul. 28, 2016, Kamioka Observatory, ICRR, the University of Tokyo, Motoyasu Ikeda (Kamioka Observatory, ICRR, the University of Tokyo).
- "Hirameki Tokimeki Science," Aug. 1, 2016, Kamioka Observatory, ICRR, the University of Tokyo, Ko Abe, Koichi Ichimura (Kamioka Observatory, ICRR, the University of Tokyo).
- "SSH, Ashikaga High School," Aug. 2, 2016, Kamioka Observatory, ICRR, the University of Tokyo, Jun Kameda (Kamioka Observatory, ICRR, the University of Tokyo).
- "SSH, Takada High School," Aug. 3, 2016, Kamioka Observatory, ICRR, the University of Tokyo, Jun Kameda (Kamioka Observatory, ICRR, the University of Tokyo).
- "Yume-no-Tamago-Juku," Aug. 5, 2016, Hida-City, Gifu, Jun Kameda (Kamioka Observatory, ICRR, the University of Tokyo).
- "Hirameki Tokimeki Science," Aug. 5, 2016, Kamioka Observatory, ICRR, the University of Tokyo, Atsushi Takeda, Hiroshi Ogawa (Kamioka Observatory, ICRR, the University of Tokyo).
- "SSH, Osaka Seiko High School," Aug. 9, 2016, Kamioka Observatory, ICRR, the University of Tokyo, Masato Shiozawa (Kamioka Observatory, ICRR, the University of Tokyo).
- "SSH, Sapporo Nishi High School," Aug. 10, 2016, Kamioka Observatory, ICRR, the University of Tokyo, Atsushi Takeda (Kamioka Observatory, ICRR, the University of Tokyo).

- "Matsumoto Fukashi High School," Aug. 17, 2016, Kamioka Observatory, ICRR, the University of Tokyo, Masayuki Nakahata (Kamioka Observatory, ICRR, the University of Tokyo).
- "SSH, Bandai High School," Aug. 17, 2016, Kamioka Observatory, ICRR, the University of Tokyo, Masayuki Nakahata (Kamioka Observatory, ICRR, the University of Tokyo).
- "SSH, Senior High School attached to Kyoto University of Education," Aug. 23, 2016, Kamioka Observatory, ICRR, the University of Tokyo, Motoyasu Ikeda (Kamioka Observatory, ICRR, the University of Tokyo).
- "SSH, Ochanomizu University Senior High School," Aug. 25, 2016, Kamioka Observatory, ICRR, the University of Tokyo, Hiroyuki Sekiya (Kamioka Observatory, ICRR, the University of Tokyo).
- "Public Lecture," Aug. 27, 2016, Toyama Science Museum, Yasuhiro Kishimoto (Kamioka Observatory, ICRR, the University of Tokyo).
- "SSH, Kariya High School," Aug. 30, 2016, Kamioka Observatory, ICRR, the University of Tokyo, Yoshinai Hayato (Kamioka Observatory, ICRR, the University of Tokyo).
- "SSH, Ikuno Senior High School," Sep. 12, 2016, Kamioka Observatory, ICRR, the University of Tokyo, Yasuhiro Nakajima (Kamioka Observatory, ICRR, the University of Tokyo).
- "Public Lecture," Oct. 15, 2016, Oita-City, Oita, Masato Shiozawa (Kamioka Observatory, ICRR, the University of Tokyo).
- "Yoshiki High School," Oct. 17, 2016, Hida-City, Gifu, Masato Shiozawa (Kamioka Observatory, ICRR, the University of Tokyo).
- "Kawasaki Public Academy," Oct. 25, 2016, Kawasaki-City, Kanagawa, Hiroyuki Sekiya (Kamioka Observatory, ICRR, the University of Tokyo).
- "Seisho Junior High School," Nov. 9, 2016, Kamioka Observatory, ICRR, the University of Tokyo, Shoei Nakayama (Kamioka Observatory, ICRR, the University of Tokyo).
- "Kamioka Junior High School," Nov. 16, 2016, Hida-City, Gifu, Ko Abe (Kamioka Observatory, ICRR, the University of Tokyo).
- "Public Lecture," Nov. 26, 2016, Tamarokuto Science Center, Hiroyuki Sekiya (Kamioka Observatory, ICRR, the University of Tokyo).
- "Public Lecture for Super-Kamiokande Open House," Nov. 26, 2016, Hida-City, Gifu, Masayuki Nakahata (Kamioka Observatory, ICRR, the University of Tokyo).
- "Super-Kamiokande Open House," Nov. 26, 2016, Super-Kamiokande, Masato Shiozawa, Shigetaka Moriyama, Yoshinari Hayato, Yasuhiro Kishimoto, Ko Abe, Yasuhiro Nakajima, Hidekazu Tanaka (Kamioka Observatory, ICRR, the University of Tokyo).
- "Super-Kamiokande Quiz event," Nov. 26, 2016, Hida-City, Gifu, Jun Kameda (Kamioka Observatory, ICRR, the University of Tokyo).
- "Keio Shonan Fujisawa Senior High School," Mar. 2, 2017, Kamioka Observatory, ICRR, the University of Tokyo, Motoyasu Ikeda (Kamioka Observatory, ICRR, the University of Tokyo).
- "ROKET Project," Mar. 6, 2017, Kamioka Observatory, ICRR, the University of Tokyo, Shoei Nakayama (Kamioka Observatory, ICRR, the University of Tokyo).
- "Public Lecture," Mar. 10, 2017, Japan Society of Civil Engineers, Hidekazu Tanaka (Kamioka Observatory, ICRR, the University of Tokyo).
- "Science Cafe for Open Campus," Oct. 22, 2016, ICRR, Kashiwa-City, Chiba, Daisuke Nakajima (ICRR, the University of Tokyo).
- "Exploring the Edge of the Universe," July 26, 2016, Omiya Sonic City Building, Masami Ouchi (ICRR, the University of Tokyo).
- "Exploring the 13.8 Billion-Year Cosmic History and the Future," September 17, 2016, NHK Culture Center Machida, Masami Ouchi (ICRR, the University of Tokyo).

- "Challenging the Edge of the Universe," November 2, 2016, Tokyo Metropolitan Hachioji Higashi High School, Masami Ouchi (ICRR, the University of Tokyo).
- "Three Things that We Want to Know," February 22, 2017, Tokyo Metropolitan Hachioji Higashi High School, Masami Ouchi (ICRR, the University of Tokyo).
- "Galaxy Formation and Evolution Studied with the Large Telescopes," November 27, 2016, Ito Hall, the University of Tokyo, Yoshiaki Ono (ICRR, the University of Tokyo).
- "Cosmic History Studied with the Large Telescopes," November 9, 2016, Tokyo Metropolitan Musashi High School, Yoshiaki Ono (ICRR, the University of Tokyo).
- "Cosmic Reionization and Galaxy Formation," April 16, 2016, Asahi Culture Center Yokohama, Yoshiaki Ono (ICRR, the University of Tokyo).
- "Public Lecture," Apr. 19, 2016, Hokuto-City, Yamanashi, Yoshio Saito (KAGRA Observatory, ICRR, the University of Tokyo).
- "SSH, Shizuoka Kita High School," Apr. 21, 2016, KAGRA Observatory, Keiko Kokeyama (KAGRA Observatory, ICRR, the University of Tokyo).
- "Public Lecture," May. 14, 2016, Hongo Campus, the University of Tokyo, Shinji Miyoki (KAGRA Observatory, ICRR, the University of Tokyo).
- "Public Lecture," May. 20, 2016, Minato-Ku, Tokyo, Yoshio Saito (KAGRA Observatory, ICRR, the University of Tokyo).
- "Public Lecture," Jun. 28, 2016, Toyonaka Campus, Osaka University, Keiko Kokeyama (KAGRA Observatory, ICRR, the University of Tokyo).
- "SSH, Yoshiki High School," Jul. 7, 2016, KAGRA Observatory, Kazuhiro Hayama (KAGRA Observatory, ICRR, the University of Tokyo).
- "KAGRA tour for Donators," Jul. 23, 2016, KAGRA Observatory, KAGRA Observatory members (KAGRA Observatory, ICRR, the University of Tokyo).
- "KAGRA Public Tour," Jul. 24, 2016, KAGRA Observatory, KAGRA Observatory members (KAGRA Observatory, ICRR, the University of Tokyo).
- "Hida Kamioka High School," Jul. 25, 2016, KAGRA Observatory, Osamu Miyakawa (KAGRA Observatory, ICRR, the University of Tokyo).
- "Workshop about Gravitational Wave," Jul. 27, 2016, Faculty of Science, Ochanomizu University, Seiji Kawamura (KAGRA Observatory, ICRR, the University of Tokyo).
- "Workshop about KAGRA," Jul. 27, 2016, Faculty of Science, Ochanomizu University, Keiko Kokeyama (KAGRA Observatory, ICRR, the University of Tokyo).
- "Kamioka High School," Jul. 28, 2016, Hida-City, Gifu, Osamu Miyakawa, Keiko Kokeyama, Kouseki Miyo, Yukitsugu Sasaki (KAGRA Observatory, ICRR, the University of Tokyo & Nagaoka University of Technology).
- "SSH, Momoyama High School," Jul. 28, 2016, KAGRA Observatory, Kazuhiro Hayama (KAGRA Observatory, ICRR, the University of Tokyo).
- "Public Lecture," Aug. 6, 2016, Toyama-City, Toyama, Osamu Miyakawa (KAGRA Observatory, ICRR, the University of Tokyo).
- "Public Lecture," Aug. 7, 2016, Amakubo Campus, Tsukuba University of Technology, Kazuhiro Hayama (KAGRA Observatory, ICRR, the University of Tokyo).
- "Public Lecture," Aug. 9, 2016, KAGRA Observatory, Shinji Miyoki (KAGRA Observatory, ICRR, the University of Tokyo).
- "The Vacuum Society of Japan," Aug. 9, 2016, KAGRA Observatory, Shinji Miyoki (KAGRA Observatory, ICRR, the University of Tokyo).

- "Matsumoto Fukashi High School," Aug. 17, 2016, KAGRA Observatory, Shinji Miyoki (KAGRA Observatory, ICRR, the University of Tokyo).
- "Science Cafe in Hida," Aug. 20, 2016, Hida-City, Gifu, Akira Ozeki, Masatake Ohashi, Osamu Miyakawa (Science Journalist and KAGRA Observatory, ICRR, the University of Tokyo).
- "Chunichi Culture Center," Aug. 20, 2016, Nagoya-City, Aichi, Seiji Kawamura (KAGRA Observatory, ICRR, the University of Tokyo).
- "College of Science and Engineering, Aoyama Gakuin University," Aug. 31, 2016, Shibuya-ku, Tokyo, Kazuhiro Hayama (KAGRA Observatory, ICRR, the University of Tokyo).
- "Public Lecture," Sep. 9, 2016, Pacifico Yokohama, Kanagawa, Yoshio Saito (KAGRA Observatory, ICRR, the University of Tokyo).
- "Chunichi Culture Center," Sep. 10, 2016, Nagoya-City, Aichi, Seiji Kawamura (KAGRA Observatory, ICRR, the University of Tokyo).
- "University of Toyama, Department of Physics," Sep. 26, 2016, KAGRA Observatory, Seiji Kawamura (KAGRA Observatory, ICRR, the University of Tokyo).
- "Public Lecture," Oct. 16, 2016, Samsung R&D Institute Japan, Seiji Kawamura (KAGRA Observatory, ICRR, the University of Tokyo).
- "Public Lecture," Oct. 21, 2016, Arcadia Ichigaya, Tokyo, Masatake Ohashi (KAGRA Observatory, ICRR, the University of Tokyo).
- "Public Lecture," Oct. 29, 2016, Sano-City, Tochigi, Shinji Miyoki (KAGRA Observatory, ICRR, the University of Tokyo).
- "Public Lecture," Oct. 29, 2016, Hida-City, Gifu, Masatake Ohashi, Hideaki Hayakawa, Osamu Miyakawa (KAGRA Observatory, ICRR, the University of Tokyo and National institute of Polar).
- "Public Lecture," Oct. 31, 2016, Chiyoda-Ku, Tokyo, Seiji Kawamura (KAGRA Observatory, ICRR, the University of Tokyo).
- "Somiya Laboratory, Department of Physics, Tokyo Institute of Technology," Nov. 4, 2016, Meguro-Ku, Tokyo, Kazuhiro Hayama (KAGRA Observatory, ICRR, the University of Tokyo).
- "The Vacuum Society of Japan," Nov. 8, 2016, KAGRA Observatory, Shinji Miyoki, Yoshio Saito, Takashi Uchiyama (KAGRA Observatory, ICRR, the University of Tokyo).
- "Public Lecture," Nov. 12, 2016, Chiyoda-ku, Tokyo, Shinji Miyoki (KAGRA Observatory, ICRR, the University of Tokyo).
- "College of Science and Technology, Nihon University," Nov. 26, 2016, Funabashi-City, Chiba, Seiji Kawamura (KAGRA Observatory, ICRR, the University of Tokyo).
- "Toyama High School," Jan. 23, 2017, Toyama High School, Osamu Miyakawa, Keiko kokeyama (KAGRA Observatory, ICRR, the University of Tokyo).
- "Toyama High School," Jan. 23, 2017, Toyama-City, Toyama, Osamu Miyakawa, Keiko Kokeyama (KAGRA Observatory, ICRR, the University of Tokyo).
- "ICEHAP Seminar," Jan. 26, 2017, Nishi-Chiba Campus, Chiba University, Keiko Kokeyama (KAGRA Observatory, ICRR, the University of Tokyo).
- "Science Cafe," Feb. 4, 2017, Tamarokuto Science Center, Seiji Kawamura (KAGRA Observatory, ICRR, the University of Tokyo).
- "Public Lecture," Mar. 15, 2017, Pacifico Yokohama, Kanagawa, Yoshio Saito, Takashi Uchiyama (KAGRA Observatory, ICRR, the University of Tokyo).
- "Department of Physics, University of Toyama," Nov. 1, 2016 - Feb. 9, 2017 Toyama-city, Toyama, Keiko Kokeyama (KAGRA Observatory, ICRR, the University of Tokyo).

- "Geo Space Adventure," Jul. 16-17, 2016, KAGRA Observatory, Takashi Uchiyama, Kazuhiro Yamamoto (KAGRA Observatory, ICRR, the University of Tokyo).
- "Department of Physics, University of Toyama," Sep. 1, 2016 - Mar. 31, 2017 Toyama-City, Toyama, Seiji Kawamura (KAGRA Observatory, ICRR, the University of Tokyo).

(c) Visitors

Kashiwa Campus (Total: 38 groups, 3,431 people)

- Elementary, Junior High and High schools: 11 groups
- Universities and Graduate schools: 3 groups
- Researchers: 0 group
- Inspections: 1 group
- Press: 16 groups
- Others: 7 groups

KAMIOKA Observatory (Total: 269 groups, 3,907 people)

- Elementary, Junior High and High schools: 29 groups
- Universities and Graduate schools: 29 groups
- Researchers: 47 groups
- Inspections: 45 groups
- Press: 18 groups
- Others: 101 groups

KAGRA Observatory (Total: 152 groups, 1,948 people)

- Junior High and High schools: 10 groups
- Universities and Graduate schools: 14 groups
- Researchers: 21 groups
- Inspections: 29 groups
- Press: 20 groups
- Others: 58 groups

F. Inter-University Research Activities

Numbers of Researchers

	Number of Applications	Number of Adoptions	Number of Researchers
Facility Usage			
Kamioka Observatory	39	39	876
Akeno Observatory	4	4	54
Norikura Observatory	12	12	104
Low-Level Radioisotope Measurement Facility	4	4	24
Cryogenic Laser Interferometer in Kashiwa	17	17	434
Laboratorial Facility in Kashiwa	3	3	27
Computer Facility in Kashiwa	12	12	280
Conference Facility in Kashiwa	11	11	443
Over Sea Facilities	23	23	366
Annual Sums	125	125	2,608
Joint Research			
Neutrino and Astroparticle Research	39	39	877
High Energy Cosmic Ray Research	55	55	1,138
Astrophysics and Gravity Research	23	23	514
Research Center for Cosmic neutrinos	8	8	79
Annual Sums	125	125	2,608

Research Project Titles

1. Study of simulation for atmospheric neutrino
2. Study of atmospheric neutrino flux and neutrino oscillations
3. Three-flavor oscillation study in atmospheric neutrinos
4. Study of flavor identification of atmospheric and beam neutrinos
5. Study of solar neutrino energy spectrum
6. Solar neutrino measurement at Super-Kamiokande
7. Precise measurement of Day/Night effect for B8 solar neutrinos
8. Study for Supernova monitor
9. Study of Supernova Relic Neutrinos
10. Search for proton decay via $e^+\pi^0$ mode
11. Study of proton decay $p \rightarrow \nu K^+$
12. Study in upward-going muons and high energy neutrinos
13. Sidereal daily variation of ~ 10 TeV galactic cosmic ray intensity observed by the Super-Kamiokande
14. Tokai to Kamioka Long Baseline Experiment T2K
15. Neutrino interaction study using accelerator data
16. Study of the electron neutrino appearance measurement in the T2K experiment
17. Joint Oscillation Analysis With the T2K and Super-Kamiokande Experiments

18. Energy calibration for Super-Kamiokande
19. Development of low concentration radon detection system
20. R&D of Megaton scale water Cherenkov Detector Hyper-Kamiokande
21. Development of the Hybrid Photodetector for a next-generation neutrino detector
22. A search for Dark Matter using Liquid Xenon Detector
23. Study of annual modulation for dark matter search with XMASS
24. Study for upgrade of XMASS detector
25. Development of calibration system for XMASS detector
26. Micro-analysis of gaseous contamination in Xe
27. R&D for low temperature rubber for XMASS
28. Radon emanation measurement from material using dark matter search experiment
29. A study on near-ultraviolet emission of liquid xenon scintillator
30. Study on surface background removal in the dark matter search
31. Study of double beta decay of ^{48}Ca
32. Direction-sensitive dark matter search experiment
33. Study for lowering backgrounds of radioisotopes in large volume detectors
34. Studies on the background evaluation using laser spectroscopy analysis
35. Development of a radioactivity assay system for underground experiments
36. Dark Matter Search with double-phase Argon detector
37. Integration of crustal activity observation around the Atotsugawa fault
38. Strain, tilt, seismic measurement in Kamioka-mine
39. Keeping nuclear emulsion plates in a box made of lead blocks at Kamioka Underground Lab
40. Precise calculation of the atmospheric neutrino flux
41. Neutrino Workshop
42. R&D for a Small Atmospheric Cherenkov Telescope in Akeno Observatory
43. Development of new surface detector for observation of ultra high energy cosmic ray at Telescope Array site
44. Observation of Galactic Cosmic Ray Intensities using Large Area Muon Telescopes
45. Multi-Color Imager for Transients, Survey and Monstrous Explosions
46. Observation of solar neutrons in solar cycle 24
47. Space weather observation using muon hodoscope at Mt. Norikura
48. Monitoring of secondary cosmic-ray neutrons at Norikura Observatory
49. Observation of cosmogenic nuclides concentrations at Mt. Norikura
50. Development of high energy proton irradiation technique for devices used in spaceship
51. Relativistic Electron Acceleration in Thunderstorm Electric Field
52. Study of secondary cosmic rays from Thundercloud at Mt. Norikura
53. Observation of total ozone and UV solar radiation with Brewer spectrophotometer on the Norikura mountains

54. Investigation of alpine plants on Mt. Norikura
55. Effect of forest fragmentation on the belowground microorganisms
56. Dynamics of *Abies mariesii* forests at forest line of Mt. Norikura
57. Observational study of electron acceleration mechanism in thunderclouds
58. R&D for the CTA Project
59. CTA-Japan Physics Research
60. Development of Foal Plane Instruments for the CTA Large Scale Telescope
61. Development of the readout system for the CTA large sized telescopes
62. Development of advanced photon counter for the future IACT
63. Installation and commissioning of the first Large Size Telescope of CTA in La Palma, Canary Islands, Spain
64. Intergration and Commissioning of the Slow Control Program for Camera of the first Large Size Telescope of CTA in La Palma, Spain
65. Development of the optical system for CTA Large size telescopes
66. Development of high bandwidth data acquisition system for the CTA Large Size Telescope
67. Development of camera for CTA small-sized telescopes
68. CTA Monte Carlo simulation
69. Study of High Energy Gamma-ray Objects with the MAGIC telescope
70. Study of Extremely-high Energy Cosmic Rays by Telescope Array
71. Observation of Ultra High Energy Cosmic-Ray with New Fluorescence Detector at the Telescope Array Site
72. Timing and position calibration of surface detectors of TAX4 and TALE experiment
73. Research and development of the surface detectors for the TALE experiment
74. Study of radio detection of highest energy cosmic rays
75. Calibration for TA FD with RC helicopter
76. The observation of abnormal shower event with lightning by TA surface particle detector
77. Atmospheric transparency measurement for calibration of air fluorescence telescope
78. Development and analysis of night cloud observation by CCD camera for automatic observation of air fluorescence detector
79. Study of absolute energy calibration of air shower by a compact electron linac
80. Observation of airshower fluorescence light at the TA FD site by using an Imaging UV telescope
81. Cosmic ray interactions in the knee and the highest energy regions
82. Characteristics of extensive air showers induced by ultra-high energy cosmic rays observed with AGASA
83. Experimental Study of High-energy Cosmic Rays in the Tibet AS γ Experiment
84. Study of High Energetic Radiation from Thundercloud in Tibet
85. Sidereal daily variation of ~ 10 TeV galactic cosmic ray intensity observed by the Tibet air shower array
86. Study of the composition of cosmic-rays at the Knee
87. A study on variation of interplanetary magnetic field with the cosmic-ray shadow by the sun
88. Air shower observation for high-energy gamma ray and cosmic ray detections at the Chacaltaya Cosmic Ray Observatory

89. Study on High Energy Cosmic Ray Sources by Observation in Space
90. Design study of a Compton camera for study of cosmic rays
91. Observation with Ashra
92. Integration of the optical fiber trigger system for Ashra
93. Development of a new code for cosmic-ray air shower simulation
94. Comparative study of astrophysical particle acceleration processes
95. YMAP symposium 2016
96. The extreme Universe viewed in very high energy gamma-rays 2016
97. Cosmic Reionization Probed with Large Optical Near-Infrared Telescope
98. Research of Large-scale Gravitational wave Telescope (VI)
99. Numerical simulation of electro-Magnetic Wave Propagation in Gravitational wave Detector IV
100. Development of Very Low Vibration CryoCooler System
101. Development of High Performance Cryogenic Mirror Control System
102. Research on cryogenic payload for KAGRA
103. Development of ultra-low loss coating for the KAGRA sapphire mirror
104. Improvement of cryogenic performance of sapphire by microwave heating
105. Development of precision profiler for mirrors of LCGT interferometer 6
106. Study for improving a curing time of silicate bonding by controlling gas environment
107. Research on ultra-low frequency anti-vibration system for KAGRA
108. R&D for the intensity stabilization of the laser system in KAGRA
109. Development of beam centering techniques for KAGRA Mode Cleaner
110. Development of the output mode-cleaner for KAGRA
111. Control and automatic operation for KAGRA
112. Rack Environmental Monitor System in KAGRA
113. Construction of KAGRA data transfer and storage system (2)
114. Data analysis of KAGRA detector (II)
115. Gravitational Wave Detector in Kamioka (XV)
116. Development of optical cavities for ultranarrow stable lasers
117. R&D of a free-fall type gravity gradiometer (II)
118. Application of geophysical observations in the Kamioka mine to the dynamics of snow and water
119. Evolution of the universe and particle physics
120. Frontier of the planetary material science
121. Detection of time variations for cosmogenic nucleid Be-7
122. Time profile of radioactive Cs concentration and its aerosol size distribution in local area
123. Continuous Measurement of Underground Laboratory Environment
124. Evaluation of the erupted radioactivities into the environment
125. CRC workshop for future plans in cosmic ray research (2)

G. List of Committee Members

(a) Board of Councillors

KAJITA, Takaaki	ICRR, the University of Tokyo
OHASHI, Masatake	ICRR, the University of Tokyo
TESHIMA, Masahiro	ICRR, the University of Tokyo
NAKAHATA, Masayuki	ICRR, the University of Tokyo
FUKUDA, Hiroo	The University of Tokyo
HOTATE, Kazuo	The University of Tokyo
TOKUSHUKU, Katsuo	KEK
SASAKI, Misao	Yukawa Institute for Theoretical Physics, Kyoto University
HAYASHI, Masahiko	National Astronomical Observatory of Japan
NAKAMURA, Takashi	Kyoto University
OKAMURA, Sadanori	Hosei University
TORII, Shoji	Research Institute for Science and Engineering, Waseda University
TSUNETTA, Saku	Institute of Space and Astronautical Science
MORI, Masaki	Ritsumeikan University
KOMAMIYA, Sachio	ICEPP, the University of Tokyo

(b) Advisory Committee

KAJITA, Takaaki	ICRR, the University of Tokyo
HISANO, Junji	Nagoya University
IOKA, Kunihito	Yukawa Institute for Theoretical Physics, Kyoto University
HAZUMI, Masashi	KEK
AOI, Nori	Osaka University
YOKOYAMA, Masashi	The University of Tokyo
KAWAI, Nobuyuki	Tokyo Institute of Technology
ITOW, Yoshitaka	Nagoya University
OGIO, Shoichi	Osaka City University
KANDA, Nobuyuki	Osaka City University
NISHIJIMA, Kyoshi	Tokai University
KAWASAKI, Masahiro	ICRR, the University of Tokyo
NAKAHATA, Masayuki	ICRR, the University of Tokyo
SHIOZAWA, Masato	ICRR, the University of Tokyo
KAWAMURA, Seiji	ICRR, the University of Tokyo
TESHIMA, Masahiro	ICRR, the University of Tokyo
OHASHI, Masatake	ICRR, the University of Tokyo
SAGAWA, Hiroyuki	ICRR, the University of Tokyo

(c) Inter-University Research Advisory Committee

KANDA, Nobuyuki	Osaka City University
MUNAKATA, Kazuoki	Shinshu University
MORI, Masaki	Ritsumeikan University
YOSHIDA, Shigeru	Chiba University
TAKEUCHI, Yasuo	Kobe University
SAKO, TAKASHI	Nagoya University
TOMARU, Takayuki	KEK
MASUDA, Kimiaki	Nagoya University
NAKAHATA, Masayuki	ICRR, the University of Tokyo
TAKITA, Masato	ICRR, the University of Tokyo
SAGAWA, Hiroyuki	ICRR, the University of Tokyo
UCHIYAMA, Takashi	ICRR, the University of Tokyo
MORIYAMA, Shigetaka	ICRR, the University of Tokyo

H. List of Personnel

Director	KAJITA, Takaaki,		
Vice-Director	KAWASAKI, Masahiro,	NAKAHATA, Masayuki,	
Kamioka Observatory (Neutrino and Astroparticle Division)			
Scientific Staff	ABE, Ko, ICHIMURA, Koichi, KATO, Yo, MARTI MAGRO, Lluís, NAKAHATA, Masayuki, OGAWA, Hiroshi, TAKEDA, Atsushi, YANG, Byeongsu,	HAYATO, Yoshinari, IKEDA, Motoyasu, KISHIMOTO, Yasuhiro, MIURA, Makoto, NAKAJIMA, Yasuhiro, SEKIYA, Hiroyuki, TANAKA, Hidekazu,	HIRAIDE, Katsuki, KAMEDA, Jun, KOBAYASHI, Kazuyoshi, MORIYAMA, Shigetaka, NAKAYAMA, Shoei, SHIOZAWA, Masato, YAMASHITA, Masaki,
Administrative Staff	OIDA, Yoshihito,		
Public Relations Staff	TAKENAGA, Yumiko,		
Technical Staff	FURUTA, Hajime, TAMORI, Yukio,	HIGASHI, Tetsuji,	ONOUE, Tatsuya,
Research Fellow	PRONOST, Guillaume Jean Francois, TASAKA, Shigeki,	SATO, Kazufumi,	TAKACHIO, Osamu,
Secretary	DOI, Kyoko, KAMIKAWATO, Rie,	EJIRI, Midori,	FUJIMURA, Yuko,
Research Center for Cosmic Neutrinos (Neutrino and Astroparticle Division)			
Scientific Staff	ATHAR, Mohammad Sajjad, NISHIMURA, Yasuhiro,	KAJITA, Takaaki, OKUMURA, Kimihiro,	MASUDA, Kimiaki,
Technical Staff	SHINOHARA, Masanobu,		
Research Fellow	OBAYASHI, Yoshihisa,		
Secretary	KITSUGI, Atsuko,	MASHIMA, Chieko,	WATANABE, Keiko,
High Energy Cosmic Ray Division			
Scientific Staff	ASANO, Katsuaki, IKEDA, Daisuke, KUBO, Hidetoshi, NAKAJIMA, Daisuke, OHNISHI, Munehiro, TAKEDA, Masahiro, YAMAMOTO, Tokonatsu	ENOMOTO, Ryoji, KAWATA, Kazumasa, LINDFORS, Elina Johanna, NONAKA, Toshiyuki, ONG, Rene Ashwin, TAKITA, Masato, YOSHIKOSHI, Takanori,	HAYASHIDA, Masaaki, KIDO, Eiji, MAZIN, Daniil Mihajlovic, OHISHI, Michiko SASAKI, Makoto, TESHIMA, Masahiro,
Technical Staff	AOKI, Toshifumi,		
Research Fellow	FUJII, Toshihiro, MIKAMI, Ryo, TERASAWA, Toshio,	HADASCH, Daniela, SAKAKI, Naoto,	KINUGAWA, Tomoya, SAKO, Takashi,
Secretary	IDOMURA, Takako,	SHIRAGA, Ryoko	SUGAHARA, Midori,
Akeno Observatory (High Energy Cosmic Ray Division)			
Scientific Staff	SAGAWA, Hiroyuki,		
Technical Staff	KOBAYASHI, Ryoichi,	OHOKA, Hideyuki,	
Norikura Observatory (High Energy Cosmic Ray Division)			
Technical Staff	AWAI, Kyosuke, SHIMODAIRA, Hideaki,	IMANISHI, Hidenori, TOMURA, Tomonobu,	OKAZAKI, Nao, USHIMARU, Tsukasa,

Astrophysics and Gravity Division

Scientific Staff	IBE, Masahiro, OUCHI, Masami,	KAWASAKI, Masahiro,	ONO, Yoshiaki,
Research Fellow	OHYAMA, Yoshihiko,	SHIBUYA, Takatoshi,	SHOJI, Yutaro,

KAGRA Observatory (Astrophysics and Gravity Division)

Scientific Staff	HAYAMA, Kazuhiro, KIMURA, Nobuhiro, MIYOKI, Shinji, SUZUKI, Toshikazu, YAMAMOTO, Kazuhiro,	HIROSE, Eiichi, KOKEYAMA, Keiko, OHASHI, Masatake, TOMARU, Takayuki,	KAWAMURA, Seiji, MIYAKAWA, Osamu, SAITO, Yoshio, UCHIYAMA, Takashi,
Administrative Staff	KAMIIZUMI, Masahiro,	OKINAKA, Mihoko,	TAKAYAMA, Kyoichi,
Technical Staff	FURUTA, Kiyoshi,	NAKADA, Kazuo,	SHIMODE, Katsuhiko,
Research Fellow	CRAIG, Kieran,	CREUS, William,	YAMAMOTO, Takahiro,
Secretary	AOTA, Akiko, KIKUCHI, Rie,	CHIDA, Ai, MAEDA, Yukari,	IWAMATSU, Miho,

Graduate Students

Doctor	AKUTSU, Ryosuke, HARIKANE, Yuichi, HIROSHIMA, Nagisa, ISHIZAKI, Wataru, KONNO, Akira, NAKANO, Masayuki, SHIN, Heungsu, TAKEISHI, Ryuji, TSUI, Kaming,	FUJIMOTO, Seiji, HASEGAWA, Fuminori, HONG, Jeong Pyong, IYOGI, Kazuki, LIU, Yingtao, ONO, Kenji, SUZUKI, Motoo, TANAKA, Hiroki, ZHANG, Haibin,	FUKAMI, Satoshi, HAYAKAWA, Taku, ISHIGAKI, Masafumi, KOBAYASHI, Masatoshi, MIYAMOTO, Takahiro, ORII, Asato, TAKAHASHI, Mitsunari, TO, Sho,
Master	ANDO, Kenta, HIGUCHI, Ryo, INADA, Tomohiro, IWAMURA, Yuki, KATO, Sho, KURODA, Hayato, MUKAE, Shiro, OCHI, Toshiro, SAKURAI, Shunsuke, SUGAHARA, Yuma, TAKENAKA, Akira, YAMAGUCHI, Soma,	ENOMOTO, Yutaro, HILMI, Miftahul, INOMATA, Keisuke, KATAOKA, Atsunori, KIRII, Shin, MIYO, Koseki, NAGANO, Koji, SAITO, Koki, SONODA, Yutaro, SUZUKI, Kazumine, TOKUNAGA, Kyosuke,	HASEGAWA, Kunihiko, HSIEH, Bin-Hua, ITO, Shungo, KATAYAMA, Junko, KOJIMA, Takashi, MOROZUMI, Tatsuhiko, NAKANO, Wakutaka, SAKAI, Yuzuru, SONOMOTO, Eisuke, SUZUKI, Takumi, YAMADA, Tomohiro,

Administrative Division

Administrative Staff	AKIYAMA, Makiko, KONDO, Hitomi, OHURA, Kiichi, SAITO, Akiko, YAMAGUCHI, Akiko,	FUKUHARA, Nana, MARUMORI, Yasuko, OKANO, Yuka, SATO, Yu,	KOBAYASHI, Toyoki, NAMATAME, Kaneo, OTSUKA, Koichi, YAJIMA, Yuki,
Research Administrator	SATO, Ritsuko,		
Public Relations Staff	FUKUDA, Hironobu,	ITO, Yoriko,	

